EXPERIMENTAL, PETROLOGIC, AND GEOCHEMICAL STUDIES ON THE ORIGINS OF ANDESITE

by

DAVID A. GUST

Thesis submitted for the degree of

DOCTOR OF PHILOSOPHY

THE AUSTRALIAN NATIONAL UNIVERSITY

November, 1981

STATEMENT

The data, arguements, and conclusions presented in this thesis are my own work unless otherwise acknowledged. Work which represents the joint efforts of myself and others is described in the INTRODUCTION and in the relevant portions of the text.

David Gust

DAVID A. GUST

ACKNOWLEDGEMENTS

There have been many people who have helped me during the research and preparation of this thesis. I would, in this section, like to formally acknowledge those people and thank them for their efforts.

I am grateful to A. Major and B. Hibberson for their time, helping hands, and wisdom in the preparation and execution of numerous high pressure experiments. I appreciate their skill and expertise in the essentials of experimental petrology. I also thank N. Ware and P. Oswald-Sealy for their assistance in their analytical specialities.

I acknowledge A.E. Ringwood and S.R. Taylor for their comments on the early phases of this research and for the use of the facilities which they have developed at R.S.E.S.. I would also like to thank R.W. Johnson (BMR) for involving me in the Boisa project and pushing it toward publishable form; B. Chappell for trace element analyses of 'MMVF' rocks; M.R. Perfit and T.M. Harrison for $^{87}Sr/^{86}Sr$ analyses of 'MMVF' rocks and T.M. Harrison for K/Ar dates of two 'MMVF' samples.

I would like to thank M.R. Perfit and R.J. Arculus for reading numerous drafts of the following chapters, criticizing and offering suggestions on ways in which improvements might be made. I am grateful for their friendship and advice throughout my course of study.

I give thanks to a 'corps' of typists who transposed my script into a presentable manuscript. Thank you, S. Kruck, B. Hall-Saha, P. Morton, L. Gust and R. Curtin. I would also like to acknowledge the Australian taxpayer who supported my research by providing an A.N.U. Ph.D scholarship. Finally, I would like to acknowledge the support and patience of my parents, and my wife, Linda.

ABSTRACT

Numerous petrogenetic hypotheses have been advanced to account for the origin of calc-alkaline andesites. On the balance, it appears that the majority of orogenic andesites (i.e. those which occur in volcanic arcs) result from the fractional crystallization of basaltic magmas, and are therefore not primary magma-types. The petrogenesis of orogenic andesites must therefore involve a detailed understanding of of the petrogenesis of basalt. Multi-stage hypotheses relate the following processes to arc magma genesis: 1) subduction of oceanic lithosphere (basalt + ultramafics); 2) transformation of basalt to eclogite; 3) partial melting of the eclogite or dehydration of a hydrous phase; 4) reaction of these products with the overlying mantle; and provide a conceptual framework to evaluate various aspects of arc volcanism.

Calc-alkaline andesites also occur in continental intra-plate environments where subduction-related processes are absent. These anorogenic andesites may be primary magmas resulting from crustal anatexis. Their petrogenesis is relevant to arc volcanism in arcs characterized by thick continental crust (e.g. Andes).

The experimental study of the phase relations of eclogite under anhydrous and hydrous conditions at high pressure (35 kbar) allow the equilibrium fusion paths of eclogite to be calculated. Liquids generated by small degrees of partial melting are quartz normative and enriched in calcium and alkalis. They are not equivalent to calc-alkaline andesites, dacites, or rhyolites. Under hydrous conditions, phengite is a subsolidus and possibly hypersolidus phase and its melting behaviour will affect the composition of liquids resulting from small degrees of melting of 'wet' eclogite. If the subducted slab

does melt, then the amount of melting will probably be <15% based on probable water contents of the slab and thermal characteristics of subduction zones. The residual eclogite is not totally depleted, and may be involved in further melting episodes of basaltic magma generation. Similarities between the calculated residual eclogites from the experiments of this study and some eclogite xenoliths in kimberlite hosts suggest that pieces of the subducted slab may reappear at the Earth's surface.

The presence of a fluid phase is an important component of multi-stage hypotheses and may be provided by the dehydration of hydrous minerals in the subducted oceanic crust. The results of high pressure experiments on one possible mineral, zoisite, in the pseudo-binary systems of diopside-zoisite and enstatite-zoisite, indicate that zoisite is stable to at least 60 kbar. Results from experimental studies on hydrous mafic compositions suggest that zoisite may be part of a 'wet' eclogite paragenesis, and as such, is likely to occur in the subducted lithosphere. The contribution of zoisite to arc volcanism however, remains obscure.

Phlogopite, as a hydrous phase and host for highly incompatible elements, may also be important in arc volcanism. Experiments on a phlogopite-rich 'model mantle' (phlogopite:enstatite = 1:5), indicate that phlogopite is stable to at least 60 kbar. The presence of phlogopite in the mantle is controlled by its thermal stability and the potassium content and temperature distribution of the mantle. Thermal models of subduction zones suggest that phlogopite may occur in the mantle wedge and possibly the subducted slab to depths of ~200 km. Phlogopite is important in arc volcanism as an intermediary, transporting water and incompatible elements from subduction zones into regions of magma generation in the mantle.

Petrologic and geochemical study of the products of arc

volcanism illustrate the complexities of petrogenetic models involving fractional crystallization of basaltic magma to produce andesite. As an example, the genesis of andesite on the Quaternary island of Boisa in the western Bismarck arc of Papua New Guinea has been studied. Boisa consists of an older cone made up of porphyritic, amphibole-free, mafic rocks, and two younger cumulodomes of hornblende-bearing, high-silica andesite. One of the cumulodomes contains coarse-grained plutonic inclusions consisting of amphibole, plagioclase, clinopyroxene, orthopyroxene, olivine, and spinel. Both cognate and xenocrystal components are present in the andesites. The anhydrous phenocryst assemblage in the basalts and the amphibole-bearing assemblage of the inclusions provide equally low residuals in least-squares linear-mixing calculations, suggesting that fractionation of either assemblage could have given rise to the andesites. However, this is not supported by the results of Rayleigh-fractionation calculations for several incompatible elements. Four possible interpretations are: (1) the Rayleigh-fractionation results are inappropriate and misleading; (2) the andesites were formed by crystal fractionation of a mafic parental magma not represented on Boisa Island; (3) mixing of a fractionated parental magma with an incompatible-element depleted mafic magma (also not represented on Boisa); (4) mixing of mafic crystal represented by the Boisa inclusions with a magma richer in SiO_2 than the most felsic rocks on Boisa. This last interpretation is supported by petrographic evidence, but the origin and nature of the postulated felsic magma remain unclear.

Anorogenic andesites, dacite, and rhyodacites of calc-alkaline affinities occur in the Mormon Mountain volcanic field situated on the Colorado Plateau, Arizona, U.S.A.. Although associated with alkali - transitional - subalkalic basalts, these silicic rocks are not produced by fractional crystallization. Petrologic and geochemical data and qualitative and quantitative petrochemical modelling indicate that the

origin of this silicic suite can be explained by the anatexis of lower crustal amphibolites. Comparison of the geochemistry of the andesites of Mormon Mountain with average 'Andean-type' orogenic andesite reveals many similarities, and suggests that crustal anatexis may be an important petrogenetic process in volcanic arcs characterized by thick continental crust.

TABLE OF CONTENTS

Page

CHAPTER 1

INTRODUCTION

The origin of calc-alkaline andesites remains a controversial subject despite more than a decade of intensive petrological, geochemical, and experimental research. The occurrence and petrogenesis of large volumes of andesitic magmas in island arcs has, since the advent of plate tectonic theory, been linked with the processes of subduction and orogeny. This association, in addition to the assumption that andesite is the dominant magma type in island arcs, has encouraged the development of numerous hypotheses linking subduction and the generation of primary andesitic magma. The concept of primary andesitic magma(s) has more recently been eclipsed by the realization that most andesites in island arcs are probably the products of fractional crystallization of parental basalts (Gill, 1980), perhaps rendered more complex by other processes (Arculus, 1981; Arculus and Johnson, 1981). The recognition of andesites as derivative and not primary magmas emphasizes the need to understand the petrogenesis of island arc basalts (IAB) and subsequent conditions of magmatic evolution which lead to the production of andesites.

Calc-alkaline andesites also occur in regions, such as intraplate continental environments, where subduction is not occurring The origin of these 'anorogenic' andesites (distinct from the 'anorogenic' subalkaline and alkaline 'andesites' of Thompson (1972)) probably involves the anatexis of the lower crust. In this respect, anorogenic andesites may truly represent primary magmas. Similarities between 'anorogenic' andesites and orogenic andesites from island arcs characterized by thick continental crust (e.g.

Andes) suggest that primary andesitic volcanism may also be important in regions of thick crust.

Understanding the character and petrogenesis of island arc volcanism is crucial to the interpretation of the evolution of the crust/mantle system. Most explanations for the growth of the continental crust are predicated on the assumption that the composition of the crust is approximately andesitic due to the peripheral accretion of island arcs throughout time (e.g. Taylor, 1967, 1977; Jakeš and White, 1971; Ringwood, 1977). Recently, the 'andesite' model has been modified such that island arc accretion is regarded as important for continental growth only in the post-Archean, after the major portion (70-80%) of the crust had evolved (Taylor and McLennan, 1981; Tarney and Windley, 1977). Although this modification somewhat lessens the relevance of the 'andesite' model to the evolution of the entire continental crust, the 'andesite' model remains the basis of estimating post-Archaen crustal additions.

Extensive sampling programs of the exposed upper crust indicate that its composition is approximately granodioritic (reviewed by McLennan, 1981). Numerous geochemical, thermal, and geophysical observations argue that this composition can not be representative of the total crust. Thus the division of the crust, into an upper 'granodioritic' crust and a lower, more mafic, crust is required if the total crust is approximately andesitic. However, criticism of the 'andesite' model, primarily on the basis that the average compositions of island arcs are not andesitic but basaltic to basaltic-andesite (Arculus, 1981), implies a lower crustal composition more mafic than that which has been previously proposed (Taylor and McLennan, 1981). The possible existence of large amounts of basaltic material in the lower crust, as inferred from geophysical studies and the occurrence of eclogite and mafic granulite nodules

in explosive volcanic hosts (e.g. Kay and Kay, 1981), is in broad agreement with this suggestion.

Recycling of crustal components via island arc volcanism (i.e. subduction and melting of sediments (Kay, 1980) or contamination with the lower crust (Arculus and Johnson, 1981) is also an important factor in models of crust/mantle evolution. The rate of continental growth (continuous or episodic) and the amount of mantle which has been involved in the crustal fractionation process are two which are affected by 'recycling'. Resolution of these issues is possible only by examining the details of island arc petrogenesis.

There have been many hypotheses advanced to explain the petrogenesis of andesite. Green and Ringwood (1968) and Boettcher (1973) present eloquent historical reviews of these hypotheses. Their reviews, along with more recent proposals are summarized in Table 1. Gill (1981) has compiled an extensive survey of andesite geochemistry, petrology and petrogenesis in a recently published book on orogenic andesites. For detailed arguments on the various petrogenetic hypotheses, the reader is referred to that text and the references therein.

The petrogenesis of andesite must be considered as part of a broader geochemical problem which is the nature of island arc volcanism. The recognition of basalt as the primary island arc magma type (see previous discussion) is a first step in this process. However, some distinctive geochemical patterns of IAB have led to the general acceptance of some type of multi-stage hypothesis (e.g. Ringwood, 1977; Kay, 1980) rather than single-stage melting of upper mantle peridotite beneath arcs. The multi-stage hypothesis reflects the realization that terrestrial evolution is a complex process and represents a conceptual framework within which research on the origin of island arc volcanism can be directed.

Table 1. Summary of Hypotheses for the Origin of Andesites

GENERAL HYPOTHESIS	SPECIFIC PROPOSAL
Partial melting of mantle peridotite.	Generation of 'andesitic liquids' with small degrees of partial melting at high f_{H_2O} (Poldervaart, 1955; Wilson, 1959; Yoder and Chinner, 1960; O'Hara, 1965; Kushiro, 1972; Yoder, 1969, Kushiro and Yoder, 1969; Kushiro et al., 1972; Green, 1973a,b,1976; Nicholls, 1974; Nicholls and Ringwood, 1972, 1973; Ringwood, 1974; Mysen and Boettcher, 1975a,b, 1976; Boettcher and Modreski, 1975).
Partial melting of subducted lithosphere.	Partial melting of quartz eclogite under anhydrous conditions (O'Hara, 1963; Green and Ringwood, 1968).
	Partial melting of amphibolitic slab (Boettcher, 1973, 1977; Allen and Boettcher, 1978).
	Partial melting of quartz eclogite under hydrous conditions (Ringwood, 1974; Stern and Wyllie, 1973, 1978; Stern, 1974).
	Partial melting of 'altered' oceanic lithosphere and influence of minor phases (sphene) in partial melting and fractionation (Green, 1981a).
	Partial melting of oceanic lithosphere with significant sediment contribution (Oxburgh and Turcotte, 1970; Armstrong, 1971; Hamilton, 1969; Gilluly, 1971).
Multi-stage hypothesis	Partial melting of 'wet' quartz eclogite, reaction with overlying pryolite, melting of rising 'altered' pyrolite diapirs to generate calc-alkaline lavas with proper chemical characteristics. These may be modified by crystal fractionation (Nicholls and Ringwood, 1973; Ringwood, 1974, 1975, 1977; Kay, 1977; Thorpe et al., 1976).

Table 1. continued

GENERAL HYPOTHESIS	SPECIFIC PROPOSAL
Fractional crystallization of basalt.	Simple fractional crystallization (Bowen, 1928).
	Magnetite fractionation from tholeiitic basalt under constant high fO_2 in addition to simple fractional crystallization; prohibits Fe-enrichment and produces calc-alkaline AFM trend (Osborn, 1959, 1962, 1969; Leeman et al., 1978; Osborn and Watson, 1977).
	Amphibole fractionation from hydrous basalt to generate calc-alkaline AFM trend (Daly, 1933; Tilley, 1950; Best and Mercy, 1967; Green and Ringwood, 1968; Allen and Boettcher, 1971, 1975, 1978; Allen et al., 1972; Holloway and Burnham, 1972; Arculus and Curran, 1972; Eggler and Burnham, 1973; Cawthorn and O'Hara, 1976).
	Eclogite fractionation from basalt to generate calc-alkaline AFM trend (Green and Ringwood, 1968, 1972; Green, 1972; Ringwood, 1974).
Anatexis of or contamination by sialic crust.	Fractional crystallization of basalt modified by crustal contamination (Daly, 1933; Tilley, 1950; Kuno, 1950; Waters, 1955; Wilcox, 1954).
	Magma mixing - basalt magma + rhyolite magma (Larsen et al., 1936; MacDonald and Katsura, 1965; Eichelberger, 1974, 1975).
	Anatexis of sialic crust (Holmes, 1932; Hess, 1960; Turner and Verhoogen, 1960).
	Hybridism and mixing of acidic magma with basic material to produce basic members (basalt, basaltic andesite) of calc-alkaline suites (Nockolds, 1934; Wilkinson, 1966).
Anatexis of lower crust	Partial melting of lower crustal granulites, amphibolites and eclogites (Helz, 1976).

Part of the research undertaken in this thesis was conceived to provide additional information on various aspects of the multi-stage hypothesis. This research, presented in Chapters 2 - 4, utilizes the techniques and approaches of high-pressure experimental petrology. Chapter 2 examines the effects of melting of anhydrous and hydrous eclogite to further refine our understanding of what the subducted slab's contribution to island arc volcanism might be. Chapters 3 and 4 report the results of studies on the stabilities of hydrous phases, zoisite and phlogopite at high-pressures and examines the implications of these results with respect to the subduction-zone environment.

The remaining chapters (Chapters 5 and 6) discuss the petrogenesis of andesite from two different tectonic environments. Chapter 5, written in conjunction with R. W. Johnson, presents the petrology and geochemistry of a calc-alkaline suite from a single volcano, Boisa, which is part of the western Bismarck (Papua New Guinea) volcanic arc. These data are used to evaluate the possible fractional crystallization paths which lead to the formation of the andesite of Boisa. Chapter 6 is a petrologic and geochemical study of an anorogenic calc-alkaline salic suite from the Mormon Mountain volcanic field located on the Colorado Plateau in Arizona, U.S.A.. The information obtained in this research suggests that this suite, which consists of andesites, dacites and rhyodacites, is the product of crustal anatexis.

In addition to these chapters, there are included in the thesis a number of appendices. Some of these, such as Appendices 2, 4 and 6 are compilations of the data used in a number of the preceeding chapters. Appendix 1 summarizes the experimental and analytical techniques used in the research presented in this thesis. Appendix 3 presents geochemical analysis of the zoisite used in the experi-

ments discussed in Chapter 3. Appendix 5 is a copy of a paper written in conjunction with M. R. Perfit, A. E. Bence, R. J. Arculus and S. R. Taylor. My contribution consisted of collecting the data base (1200 analyses of IAB from the literature), assisting in the interpretation of the 'processed' data, rewriting the initial draft and preparing the manuscript for publication. This paper summarizes and discusses the geochemistry of IAB. The 'anorogenic' andesites, described in Chapter 6, are part of a bimodal suite of which the other group is represented by a suite of alkalic-transitional - subalkalic basalts. The petrology, geochemistry and petrogenesis of this basaltic suite is examined in Appendix 7. Appendix 8 summarizes the petrology and geochemistry of a suite of lower crustal xenoliths from the Colorado Plateau. These xenoliths, which consist of pyroxene granulites, amphibolites and various 'granitoids', provide insight on the possible involvement of the crust in the petrogenesis of the basaltic and salic suites of the Mormon Mountain volcanic field. Finally, Appendix 9 is a collection of several abstracts on other aspects of island arc and continental intra-plate volcanism, research which represents the joint efforts of myself and colleagues.

CHAPTER 2

PARTIAL MELTING OF ECLOGITE: IMPLICATIONS FOR THE SUBDUCTED SLAB

INTRODUCTION

The subduction of lithospheric plates composed of basaltic and ultramafic rocks is an essential tenet of the plate tectonic hypothesis, providing a means by which lithosphere created at oceanic ridges is eliminated, thereby preserving a constant terrestrial surface area. The ultimate fate of the subducted slab, and in particular, its relatively thin (<5km) veneer of basaltic crust remains unclear, even though it is crucial to our understanding of the evolution of the Earth's mantle and crust. The association of volcanic arcs with these subduction (Benioff) zones, for example, has suggested to many, a petrogenetic link between the volcanism and the subducted slab. Less obviously, the origins of some eclogitic inclusions in kimberlites may be slab-related. These possibilities can be tested by examining the results of high-pressure experiments on basaltic compositions with respect to numerous intensive parameters (e.g. P/T/fO_2/ fH_2O). Although some data have been accumulated, the questions are far from being satisfactorily answered. This chapter reports the results of experiments at 35 kbar on a basaltic composition under hydrous and anhydrous conditions, and discusses the results with respect to the subduction of oceanic lithosphere.

Yoder and Tilley (1962) established that the high pressure equivalent of basalt is eclogite under anhydrous conditions and amphibolite under hydrous conditions. Further research has since shown that amphibolite transforms to eclogite at pressures above

amphibole stability (≈25 kbar) (Lambert and Wyllie, 1968, 1972; Allen and Boettcher, 1971, 1978; Hill and Boettcher, 1970; Allen, Boettcher, and Marland, 1975). A number of early studies were concerned with the anhydrous gabbro/eclogite transition with particular respect to the Moho controversy (reviewed by Wyllie, 1971a).

Work by Cohen, Ito and Kennedy (1967) and Green and Ringwood (1968) examined the melting and phase relations of anhydrous basalts to high pressures (50 kbar), and presented the first quantitative chemical analyses of garnets and clinopyroxenes. Green and Ringwood used their data, collected at near liquidus temperatures to calculate coexisting liquid compositions, and fractionation trends. They concluded that these trends would broadly follow the calc-alkaline trend and consequently, that the low melting fraction of eclogite would be andesitic.

Ito and Kennedy (1974) investigated the melting relations of an eclogite nodule from the Roberts Victor kimberlite pipe under anhydrous conditions. From analysis of the liquids, they concluded that at high pressures, small degrees of melting would produce nepheline normative basalts with hypersthene normative basalts resulting from larger degrees of melting.

The acceptance of plate tectonics as a unifying Earth science theory renewed interest in the partial melting products of hydrous basalt at high pressures. Lambert and Wyllie (1972) investigated the melting of gabbro (quartz eclogite) with excess H_2O, but concentrated on the subsolidus amphibolite/eclogite transition. Their conclusion that all H_2O in the subducted slab would be lost to

the overlying mantle wedge during this transition, and that the resulting eclogite would be essentially anhydrous apparently precluded the partial melting of eclogite deeper in the mantle. Nevertheless, Stern and Wyllie (1973; 1978) studied the melting of hydrous quartz eclogite; their work is, to date, the most comprehensive analysis of that problem. The results of their experiments and calculations suggest that calc-alkaline andesites are not produced by fusion of subducted oceanic crust (quartz eclogite). In summary, the effects of the partial melting of eclogite, hydrous or otherwise, are understood in only the most general terms. Additional quantitative data on liquid and solid compositions of eclogite during melting are needed.

METHOD

Starting Composition - In attempting to model the composition of the subducted oceanic lithosphere, it is necessary to make some simplifying assumptions. These are:

1) The overall gross structure of the lithosphere consists of a thin veneer, but of variable thickness, of sediments overlying a 5km thick crust of basaltic material. This crust is underlain by 80-100km of depleted pyrolite (Cann, 1970; Green, 1976).
2) Prior to subduction, the sedimentary cover is scraped off (Dewey and Bird, 1970; Karig and Sharman, 1975; Seeley, et al., 1974) and is not involved in partial melting at depth (cf. Kay, 1980; Perfit et al., 1981).
3) The depleted pyrolite which is subducted, is not involved in the melting episodes (cf. Kay 1980) except by supplying H_2O from the dehydration of serpeninites (Ringwood, 1975).

4) Seamounts, oceanic islands, and alkalic basalts may be subducted, forming heterogeneities within the slab, but their contribution is insignificant compared to the dominance of olivine tholeiite.

5) The composition of the oceanic crust is equivalent to an average basalt, calculated from only fresh basaltic samples. The extent and effects of low temperature alteration, either by seawater or circulating hydrothermal fluids (Humphris and Thompson 1978) and low pressure metamorphism (Cann, 1979)

are ignored.

While adhering to these assumptions introduces a degree of unrealism, the time and effort required to effectively treat more complicated situations is beyond present abilities.

A number of average ocean basalt compositions have been published (Engel, et al., 1965; Cann, 1971; Kay, et al., 1970; Frey, et al., 1974). The average of Cann (1971) (Table 1) was chosen for this study because a large number of unaltered samples (94) were included in the average. This composition is more primitive than the bulk of sampled MORB (Fig. 1) and may be more representative of the entire basaltic portion of the oceanic crust.

A synthetic mixture, DG-1, was prepared from 'spec-pure' oxides, ground for several hours under acetone in an agate mortar, sintered for 12 hours and reground. FeO was produced by the reaction of Fe_2O_3 and Fe metal (excess) during fusion in a Fe-saturated Pt crucible in an Ar atmosphere at 1350°C. The resulting glass was reground with excess Fe-metal being removed by a magnet and refused under similar conditions. The glass was analyzed by electron microprobe and found to be homogeneous. Fe^{2+}/Fe^{3+} was determined by microanalysis (E. Kiss, analyst). The composition of the mix is

is compared to Cann's average (Table 1) and although slight differences in SiO_2, Al_2O_3, CaO, and MgO are noted, the compositions are nearly identical with respect to normative mineralogy (Fig. 1).

Experimental Techniques - Runs using DG-1 were conducted under anhydrous and hydrous conditions (1.5 and 5.0 wt. % H_2O). To ensure reproducibility in experiments with low water contents, DG-1 was amphibolitized. 0.260g of DG-1 was loaded with 20 wt. percent H_2O into a $Ag_{75}Pd_{25}$ capsule, sealed, and heated to 700°C at 3kbar in a Tem-Press hydrothermal apparatus for 2 weeks. The resulting amphibolite, dominantly plagioclase and ferroan pargasite, contained 1.5 wt. percent H_2O. Runs with 5 wt. percent H_2O were prepared from DG-1 with required amounts of deionized-distilled H_2O being added by micro-syringe. Errors in this technique are estimated to be approximately 5 percent.

All hydrous runs were sealed in $Ag_{75}Pd_{25}$ capsules to minimize Fe loss during the experiment. The capsule weights were recorded at all times as a check on possible H_2O loss. The capsules were loaded into the 'wet' 5/32" solid-media assembly. Anhydrous experiments utilized graphite capsules with tight-fitting lids and the 'dry' 1/8" solid-media assembly. Both assemblies are described in detail in Appendix 1, as is the operation of the piston-cylinder apparatus. Analytical techniques consist of optical, x-ray diffraction, and electron microprobe analysis (Appendix 1).

Iron Complications - Experimental problems with iron-bearing systems are generally the result of a reaction between iron and the enclosing capsule material. These reactions, and their resulting effects on the attainment of equilibrium during experimental conditions often compromise the credibility of otherwise well-controlled investigations.

TABLE 1: Starting Composition of DG-1 Compared to Average Oceanic Olivine Tholeiite (Cann, 1971) and DW-1 (Stern and Wyllie, 1978)

	DG-1	Cann's Average	DW-1
SiO_2	49.00	49.19	45.91
TiO_2	1.37	1.42	.94
Al_2O_3	16.10	15.87	17.19
FeO	11.17	11.57	9.76
MgO	7.93	7.77	7.48
CaO	11.42	11.22	13.54
Na_2O	2.79	2.74	1.63
K_2O	.22	.22	.14
TOTAL	100.00	100.00	96.59+
CIPW			
Or	1.30	1.30	.86
Ab	23.61	23.19	14.28
An	30.76	30.35	40.56
Di	21.37	20.92	23.88
Hy	.71	3.81	2.34
Ol	19.65	17.73	16.24
Il	2.60	2.70	1.85
Mg #*	60.0	58.6	61.8
A	13.6	13.3	8.5
F	50.5	51.9	51.3
M	35.9	34.8	39.2
CaO	26.7	26.2	32.0
MgO + FeO	44.7	45.1	41.0
$SiO_2/4$	28.6	28.7	27.0

* Adjusted Fe^{2+} = .85 ΣFe

\+ Also contains MnO, P_2O_5 and H_2O. All iron as FeO.

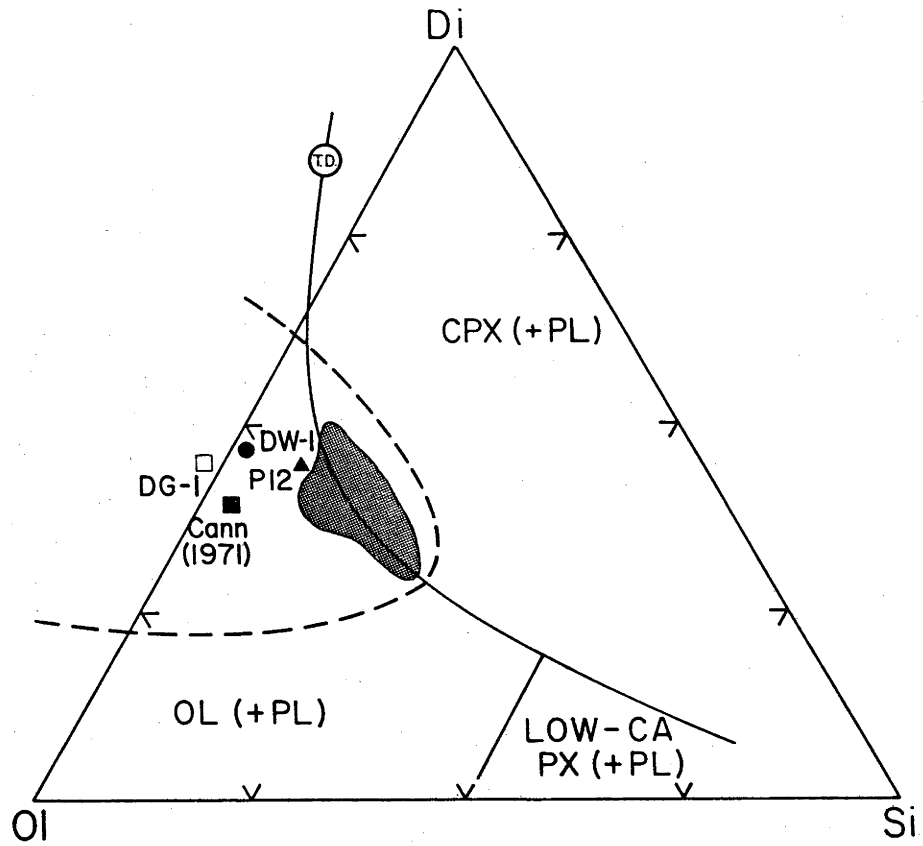

Figure 1: Compositions of starting mix DG-1 (□), average MORB of Cann (1971) (■), and gabbro DW-1 (●) (Stern and Wyllie, 1978) projected in molecular proportions of Diopside-Olivine-Quartz. The projected 1 bar plagioclase saturated liquidus of Walker et al. (1979) is also shown. Circled TD is the thermal divide. P12 (▲) is the primitive sample of MORB of Walker et al. (1979). The compositions of a majority of MORB lie within the shaded area. The dashed line encompasses all MORB. Data is taken from Bence et al. (1979).

Although some preventative and corrective measures have been proposed (Green, 1976; Stern and Wyllie, 1975), there still remains the possibility of significant error.

The present experiments suffer two distinctly different problems with regard to iron. Each is related to a particular capsule material. Anhydrous runs, done in graphite capsules, suffer from reduction of FeO to Fe-metal, as evidenced by small globules of Fe-metal near the capsule wall. Such effects have been reported elsewhere (Ito and Kennedy, 1974; Råheim and Green, 1974). Minimizing run times and analyzing only the central portions of the charge tends to obviate this problem. The second difficulty is observed in the hydrous charges, run in $Ag_{75}Pd_{25}$ capsules. Although the choice of this material does minimize Fe-loss from the charge, Stern and Wyllie (1975) demonstrate that in runs greater than 5 hours duration at 1200°C, up to 60 percent loss of FeO can occur. Less loss is experienced with shorter times and lower temperatures. They also show that the iron loss occurs initially from the liquid phase, then from clinopyroxene and finally from garnet. Circumvention of iron-loss thus reduces to a trade-off between system equilibrium, crystal growth, and iron diffusion.

An attempt was made with DG-1 + 1.5 wt. percent H_2O to evaluate experimental durations necessary for equilibration and a maximum in crystal size. A number of runs at 1000°C, ranging in duration from 1 to 14 hours, were analyzed for garnet and clinopyroxene compositions. No significant compositional differences were observed between runs of 4 and 14 hours. Runs less than 4 hours in duration lacked crystals large enough to probe. A similar assessment was made at 1100°C. Runs at 1200°C and 1260°C were not duplicated, but were of minimal duration (2 hours and 20 minutes, respectively).

Significant iron-loss occurred in the 1300°C run (30 minutes), and is evident in both the analyzed liquid and clinopyroxene compositions.

RESULTS

Phase Relations - The phase relations of DG-1 with 0, 1.5, and 5 wt. percent H_2O were determined at 35 kbar and are summarized in Table 2 and Figure 2. The anhydrous subsolidus assemblage consists of clinopyroxene, garnet and minor kyanite. Clinopyroxene comprises approximately 85 percent of the experimental charge (determined by point-counting and least squares fitting of clinopyroxene, garnet and kyanite analyses). This assemblage begins to melt about 1460 (±5)°C. These temperatures and phase relations are, in general, comparable with results of other anhydrous eclogite melting studies (Green and Ringwood, 1967; Ito and Kennedy, 1974; Cohen, Ito and Kennedy, 1967; O'Hara and Yoder, 1967), but differ significantly from the anhydrous solidus and liquidus temperatures of the quartz eclogite of Stern and Wyllie (1978).

Runs with 1.5 wt. percent H_2O illustrate the lower solidus temperatures and greatly expanded melting interval expected in water-deficient, vapor-present systems (Robertson and Wyllie, 1971). The subsolidus assemblage consists of clinopyroxene (~50%), garnet (~45%) with minor rutile, phengite, kyanite and quartz. The solidus temperature lies between 750°C and 780°C. The exact locations of the phengite and quartz-out boundaries are difficult to determine accurately; the curves in Figure 2 are suggested by results of Stern and Wyllie (1978) and Harris (unpublished data). The amount of liquid generated in the first 200 C is small, but increases rapidly with the disappearance of kyanite (~1040°C) and rutile (~1080°C). Garnet and clinopyroxene persist until liquidus

TABLE 2: Compilation of all Experiments on DG-1 Composition

RUN	P(kb)	T(°C)	t	H_2O content	Results					
8665	35	1350	6hr	-	Cpx	Gt		Ky		
8652	35	1440	1hr	-	Cpx	Gt		Ky		
8845	35	1450	10min	-	Cpx	Gt	Ky			
8864	35	1472	10min	-	Cpx	Gt	L	Ky (?)		
8650	35	1490	30min	-	Cpx	Gt	L			
8841	35	1500	10min	-	Cpx	Gt	L			
8880	35	1525	10min	-	Cpx	Gt	L			
8659	35	1535	1hr	-	Cpx	Gt	L			
8879	35	1550	5min	-	L	Cpx	Gt			
8656	35	1560	1hr	-	L	Cpx	Gt	(?)		
8653	35	1610	30min	-	L					
6923	35	700	8hr	1.5%	Cpx	Gt	Ph	Qtz	Rut	Ky
6944	35	700	54hr	1.5%	Cpx	Gt	Ph	Qtz	Rut	Ky
8010	35	700	168hr	1.5%	Cpx	Gt	Ph	Qtz	Rut	Ky
6880	35	750	12hr	1.5%	Cpx	Gt	Ph	Qtz	Rut	Ky
7373	35	800	3hr	1.5%	Cpx	Gt	Ph	Qtz	Rut	Ky L(?)
7372	35	850	3hr	1.5%	Cpx	Gt	Rut	L	Ky	
7549	35	1000	1hr	1.5%	Cpx	Gt	L	Rut	Ky	
7551	35	1000	2hr	1.5%	Cpx	Gt	L	Rut	Ky	
7550	35	1000	4hr	1.5%	Cpx	Gt	L	Rut	Ky	
8829	35	1000	13.5hr	1.5%	Cpx	Gt	L	Rut	Ky	
8866	35	1100	2hr	1.5%	Cpx	Gt	L	Rut	Ky(?)	
8818	35	1100	8hr	1.5%	Cpx	Gt	L	Rut	Ky(?)	
8808	35	1200	2hr	1.5%	Cpx	Gt	L			
8865	35	1260	20min	1.5%	L	Cpx	Gt			
8816	35	1300	30min	1.5%	L	Gt	Cpx			
8813	35	1400	15min	1.5%	L					
8020	25	1000	48hr	1.5%	Gt	Amph		L		
8869	35	1000	2hr	5.0%	Cpx	Gt	Rut	L	Ky	
8867	35	1100	2hr	5.0%	Cpx	Gt	L			
8868	35	1200	1hr	5.0%	L	Gt	Cpx			

Cpx - clinopyroxene, Gt - garnet, Ky - Kyanite, L - liquid, Rut - rutile
Ph - phengite, Qtz - quartz

Phases are listed in approximate abundancies from high to low.

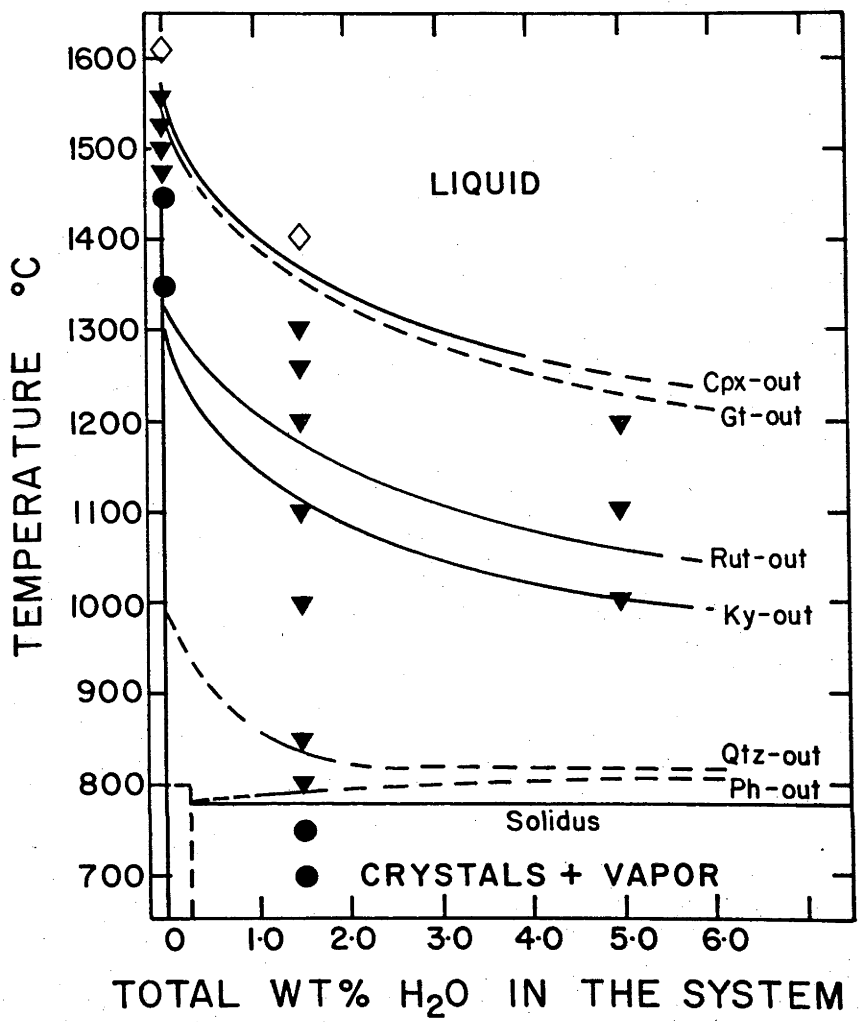

Figure 2: Phase relations of basalt DG-1 plus H_2O at 35 kbars. Phase boundaries which are estimated are indicated by dashed lines.

temperatures in excess of 1300°C. Only a few experiments with H_2O contents of 5 wt. percent were run and suggest a decrease in kyanite-out, rutile-out and liquidus temperatures.

Phase Compositions - A portion of each experimental charge was mounted and polished for analysis by the TPD electron microprobe (Reed and Ware, 1973; 1975). The energy spectrum data were reduced by the computer program OXIDE (Ware, 1981), with detection limits of approximately 0.1 wt. percent. A minimum of 5 garnet and clinopyroxene grains were analyzed per charge except in cases where grain size approached the beam dimensions (3μm). All mineral analyses with reasonable stoichiometry are tabulated in Appendix 2. Analysis of liquid compositions was moderately successful for anhydrous experiments, but unsuccessful for hydrous experiments. Unambiguous analyses of liquid and phengite in near-solidus experiments were unobtainable due to their small exposed area.

(a) Garnets - The garnets of the anhydrous and hydrous runs are euhedral grains up to 20μm in diameter. The compositions of the analyzed garnets exhibited little variation within each charge. Small amounts of Na_2O (0.2 wt. % or less) in the garnets are thought to be real, with higher abundances reflecting contamination by clinopyroxene or glass.

The garnets of the anhydrous runs vary systematically with respect to temperature, changing to more pyrope-rich compositions with increasing temperature (Fig. 3). Grossular content remains constant throughout the melting interval. These garnets resemble those analyzed by Cohen et al. (1967) and Råheim (1974) from experiments at comparable pressures and with starting compositions similar to DG-1. TiO_2 contents are fairly high (1.3 wt. %) at lower temperatures (1450°C) and decrease with increasing temperature.

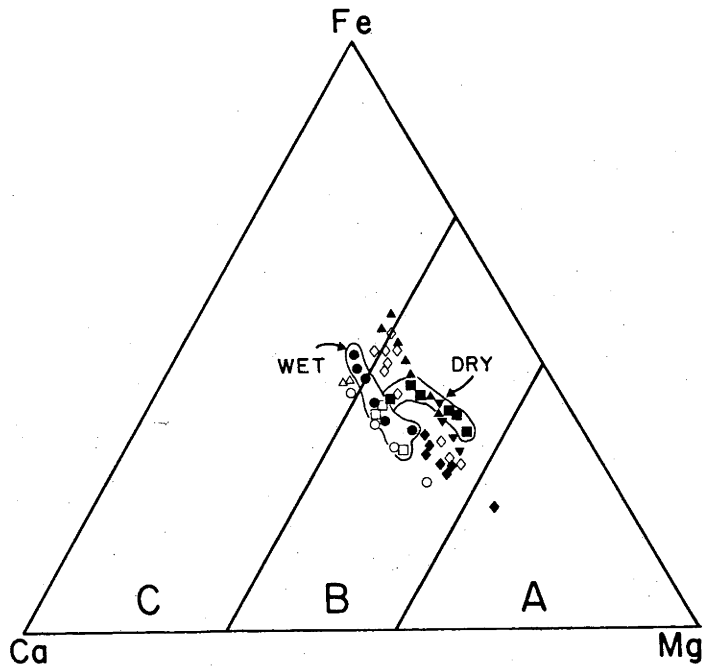

Figure 3: Average compositions of garnets from experiments at 35 kbar on DG-1 under anhydrous (■) and hydrous (●)(1.5 wt.% H_2O), (□)(5.0 wt.% H_2O) conditions projected in molecular proportions of Ca : Mg : Fe. DG-1 garnets are compared with garnets from other experimental studies (▲ Mg 55.4, ▼ Mg 69.4 (Råheim, 1974), ◇ (Cohen, et al. 1967); △ High-Al basalt (Green, 1967); ◆ (Green and Ringwood, 1968); ○ DW-1 (Stern and Wyllie, 1978). Fields A, B, C correspond to Group A, B, C eclogites (Coleman, et al., 1965).

The compositions of garnets from hydrous runs are distinctly different from those analyzed in the anhydrous experiments. They contain on average, 10 mole percent more grossular and do not become as pyropic at high degrees of melting. This shift in composition is observed in garnet compositions from other hydrous eclogite studies (Stern and Wyllie, 1978). In addition, the garnets from hydrous runs contain less TiO_2 than do anhydrous garnet compositions. Further, TiO_2 increases as temperature increases. These differences reflect the stabilization of rutile as a solidus and hypersolidus phase under hydrous conditions (noted in the frequent inclusions of rutile in large garnet grains). No obvious differences are observed between the 1.5 and 5 wt. percent H_2O addition experiments.

(b) Clinopyroxene - Clinopyroxene in the eclogite was frequently difficult to analyze due to the small grain size (max. 8 μm diameter) and intergrowths with pools of liquid. Many analyses were discarded on the basis of minor K_2O abundances or poor stoichiometry. The remainder of the compositions exhibit some variation which may be due to iron loss or quench phenomena (Green, 1976).

The compositions of the clinopyroxenes in the anhydrous experiments do however, exhibit a fairly systematic behaviour with respect to increasing temperature. Subsolidus clinopyroxene (1450°C) contains a 22-26 mole percent jadeite component with a Mg#(100 Mg/Mg + Fe ratio of 58 to 60. As temperature increases, the Mg # of the clinopyroxenes increases due to a significant decrease in the ferrosilite component (Fig. 4a). The jadeite component decreases only slightly. CaTs and wollastonite components remain approximately constant or increase slightly. TiO_2 contents, moderately high in the subsolidus clinopyroxene (1.3 wt. %) decrease

Figure 4:

(a) Mole percent of pyroxene end members versus 100 Mg/Mg + Fe for omphacites from experiments on DG-1 at 35 kbar under anhydrous conditions. Symbols refer to different temperature (^{o}C) experiments (▽ - 1350; ● - 1450; ◆ - 1472; X - 1490; ▲ - 1500; ■ - 1525; □ - 1535).

(b) Mole percent of pyroxene end member versus 100 Mg/Mg + Fe for omphacites from experiments on DG-1 at 35 kbar under hydrous conditions (1.5 wt.% H_2O). Symbols refer to different temperature (^{o}C) experiments (■ - 700; □ - 750; ▲ - 800; ◆ - 1000; △ - 1100; ▽ - 1200; ◇ - 1260; ● - 1300).

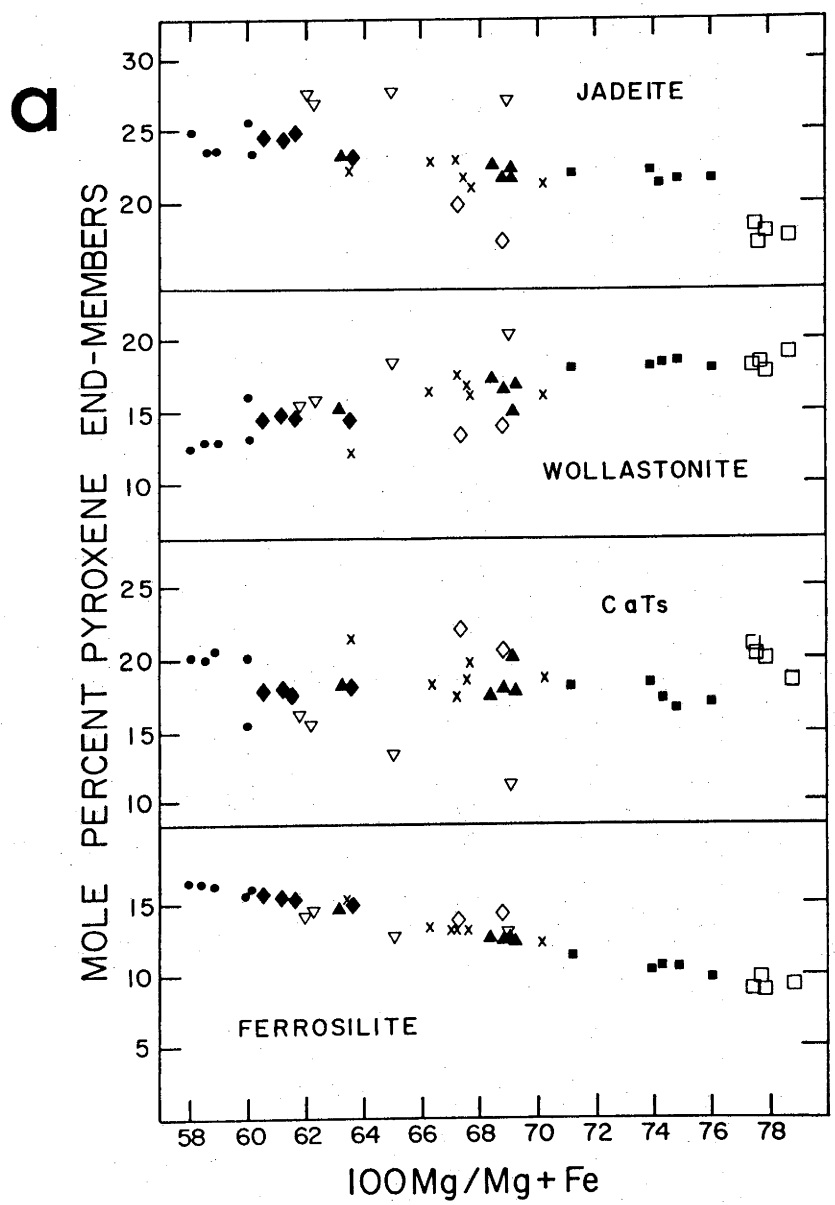
a
JADEITE
WOLLASTONITE
CaTs
FERROSILITE
MOLE PERCENT PYROXENE END-MEMBERS
100Mg/Mg+Fe
30
25
20
15
10
5
58
60
62
64
66
68
70
72
74
76
78

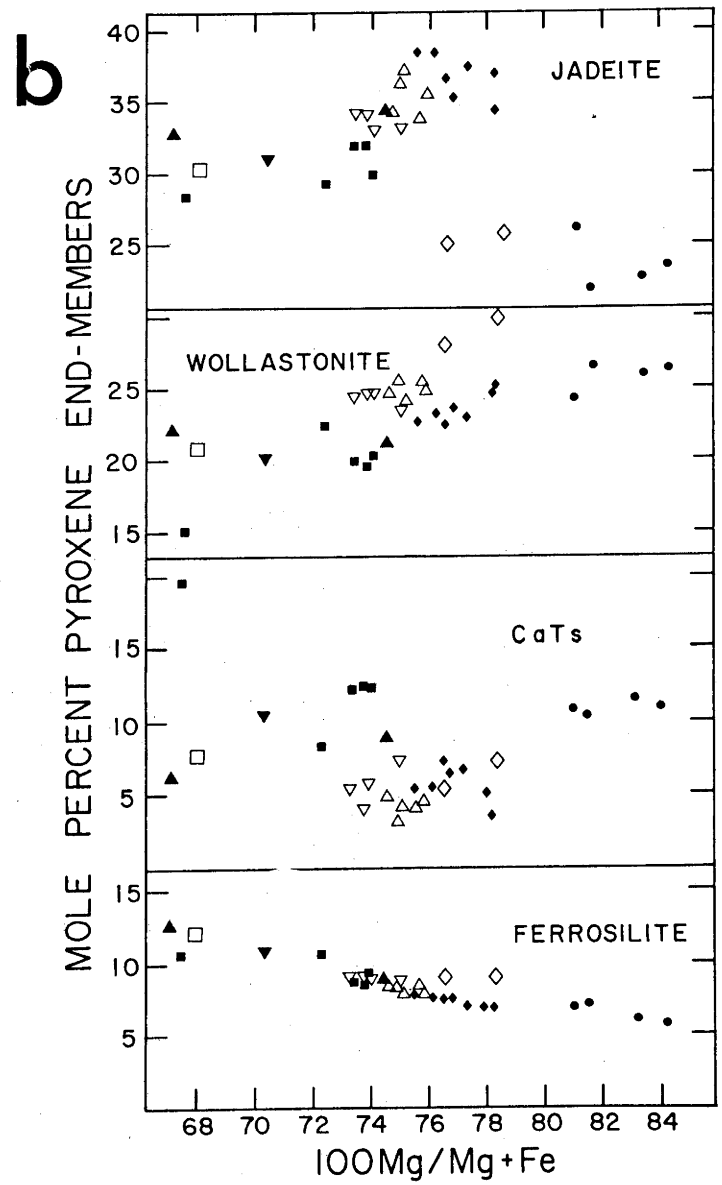
b
JADEITE
WOLLASTONITE
CaTs
FERROSILITE
MOLE PERCENT PYROXENE END-MEMBERS
100Mg/Mg+Fe
40
35
30
25
20
15
10
5
68
70
72
74
76
78
80
82
84

as melting proceeds. The $K_D^{Cpx/Gt}_{Ti}$ remains fairly constant (0.7-0.8) throughout the melting interval. Little information is available with which to compare these clinopyroxene compositions. However, a subsolidus clinopyroxene calculated from the garnet composition and modal percentages of Cohen et al. (1967) is in good agreement with the present data, as is that of Råheim (1974) for his Mg#55 composition.

The microprobe analyses of the clinopyroxenes from hydrous runs are much more variable than those from anhydrous experiments (Fig. 4b). This variability is the result of experimental (i.e. differential iron-loss) and analytical problems (inclusion of kyanite or liquid in the analysis due to the small grain size of the clinopyroxene). It is difficult to judge the quality of an analysis on the basis of stoichiometry, as omphacitic pyroxenes are notoriously non-stoichiometric (Cawthorn and Collerson, 1974; Smyth, 1980).

However, some systematic differences are evident between subsolidus and subliquidus compositions as well as between hydrous and anhydrous conditions. The differences are apparent in Figure 5a, in which Jadeite-CaTs-Quad (Σ wollastonite + enstatite + ferrosilite) pyroxene components are projected. The subsolidus clinopyroxenes from hydrous runs have highly variable compositions, but contain less jadeite and more CaTs component than do subliquidus runs. As melting begins, the jadeite component drastically increases at the expense of the CaTs component, then gradually decreases with increasing temperature. Throughout this process, Mg # increases only slightly (~70 to 78). TiO_2 abundances are generally low and increase as temperatures increase (opposite to the effects in the dry runs). As with the anhydrous melting runs, $K_D^{Cpx/Gt}_{Ti}$ remains fairly constant (0.45-0.66). Clinopyroxenes in the 5 wt. percent H_2O runs are only

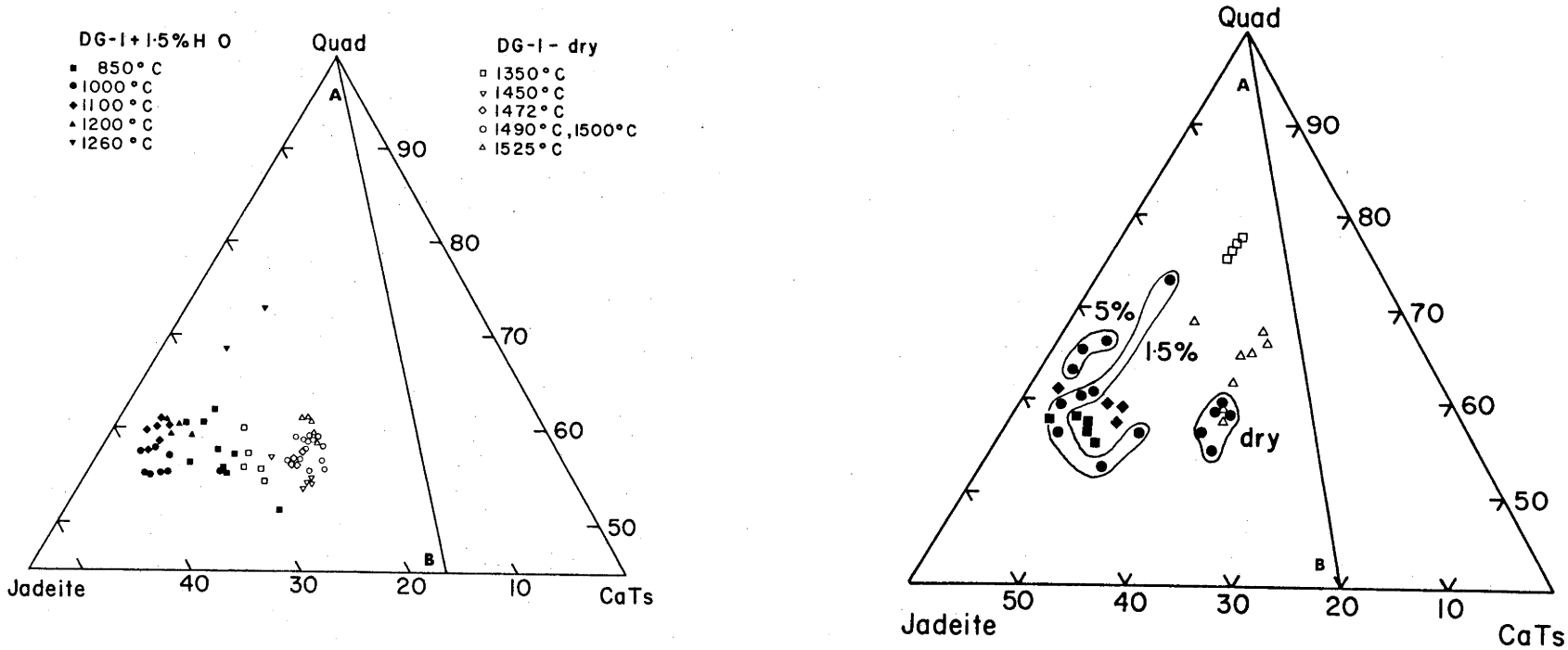

Figure 5. a) Omphacite compositions from experiments on DG-1 at 35kbar under anhydrous and hydrous (1.5 wt. %) conditions. Projection components are Jadeite - calcium tschermaks molecule (CaTs) - Wollastonite + enstatite + ferrosilite (QUAD). Line AB (Jd:CaTs = 1:2) is the proposed division of eclogite and granulite clinopyroxenes (White,1964). b) Average omphacite compositions from DG-1 experiments (Table 7) compared with omphacites from other experimental studies. Symbols are: △ - Green and Ringwood (1968); ■ - Mg 59.4, ◆ - Mg 69.4 - Råheim (1974); □ - DW-1 - Stern and Wyllie (1978).

slightly different in composition from the 1.5 wt. percent H_2O runs. Representative analyses are compared with other experimental clinopyroxenes in Figure 5b.

Comparison of the anhydrous clinopyroxene compositions with those resulting from hydrous experiments reveals several distinct features. Firstly, the anhydrous clinopyroxenes are less-jadeitic, containing more CaTs component. Secondly, their range in Mg # is greater during melting, but is lower overall (60-75 versus 70-78). Thirdly, they contain nearly twice as much TiO_2, and finally, $K_D^{Fe/Mg}_{Cpx/Gt}$ (Fig.6) is significantly lower due to the higher temperatures of equilibration (Ellis and Green, 1979).

(c) Minor Phases and Liquid Compositions - Good, unambiguous analyses of phengite, rutile, quartz, and kyanite were not obtained due to their small grain size. Their presence was inferred from 'contaminated' analyses which were high in Al_2O_3, K_2O and low in SiO_2 (phengite), high in TiO_2 (rutile), high in SiO_2(>80 wt. %, quartz), and high in Al_2O_3 (kyanite). Rutile, kyanite, and quartz were also identified by optical examination of grain mounts and polished surfaces.

Liquid compositions were successfully directly determined only in the anhydrous runs (Table 3). They exhibit a moderate degree of heterogeneity within each sample. In the most extreme case, two distinctly different liquids occur in one sample. Similar observations were made by Ito and Kennedy (1974) and attributed to the effect of minute quantities of H_2O near the capsule walls. The remainder of the analyzed liquids are not nearly so heterogeneous, but averages indicate general changes in liquid composition during melting. SiO_2 varies from 60 wt. percent in the initial melts to 49 wt. percent in near-liquidus experiments. A notable feature is the

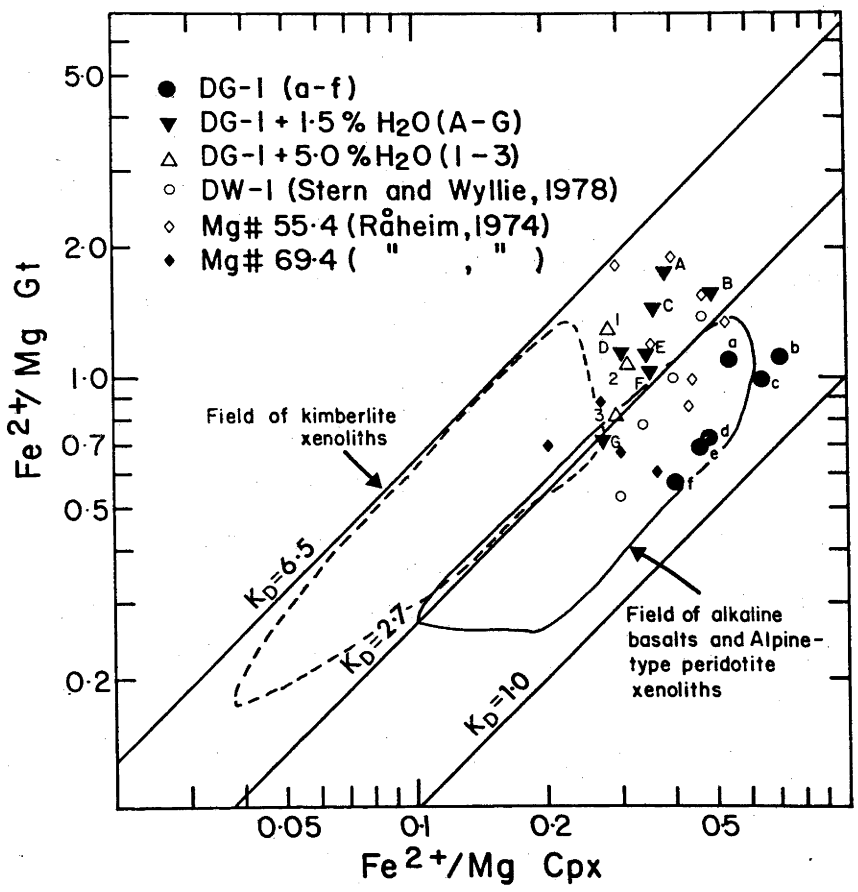

Figure 6: Distribution of Fe^{2+}/ Mg between coexisting garnet and clinopyroxene (after Banno and Matsui, 1965) for experimental eclogites. Symbols are identified in the figure. Fields of alkaline basalt and Alpine-type peridotite xenoliths (Irving, 1974) and eclogite xenoliths in Kimberlites (Lovering and White, 1969; Irving, 1974) are shown.

TABLE 3: Averages of Microprobe Analyses of Liquid Compositions
Anhydrous Conditions

Temperature	1440	1472	1490	1500	1525	1550A	1550B	1560
Run #	8652	8864	8650	8841	8880	8879	8879	8656
SiO_2	58.21	53.17	54.82	52.32	53.56	51.05	58.90	48.82
TiO_2	1.59	1.73	1.93	2.05	2.22	1.53	1.76	1.36
Al_2O_3	15.74	15.04	15.81	15.80	16.87	15.29	16.07	16.22
FeO	8.63	10.67	11.12	12.83	13.77	10.39	7.83	10.75
MgO	2.93	5.49	2.23	2.84	1.81	5.36	.48	8.27
CaO	6.94	9.63	7.01	7.00	6.04	9.00	3.36	11.39
Na_2O	3.43	3.33	3.43	3.58	3.98	2.98	2.68	3.01
K_2O	1.29	.68	1.12	.95	1.29	.58	1.74	.19
TOTAL	98.76	99.74	97.47	97.37	99.54	96.18	92.82	100.01

high FeO content (10-12 wt. %) which remains relatively constant throughout the melting interval. MgO and CaO contents increase while Na_2O and Al_2O_3 remain uniform. It must be emphasized that these liquid compositions have not been reversed and can not be established conclusively as equilibrium melts of DG-1.

Thermodynamic Considerations - Extensive efforts have been expended on the calibration of a geothermometer based on the equilibrium partitioning of Fe^{2+} and Mg between coexisting garnet and clinopyroxene (Råheim and Green, 1974; Ellis and Green, 1979). The results of these efforts can be used to assess the degree of equilibrium attained in the experiments of the present study by applying the geothermometer to analyzed garnet and clinopyroxene pairs and checking whether or not the known temperature of the experiment is reproduced. There are two important assumptions upon which the approach is based. Firstly, it is assumed that the only major impediment to the attainment of equilibrium is the loss of iron from the system (i.e. the system does not remain closed). Equilibrium may finally be achieved, but in a vastly different bulk composition, and consequently such data are of little direct use. Secondly, the rate of response to this change varies with respect to the coexisting phases. In this context, the melt phase is initially affected, followed by clinopyroxene, with garnet being the least affected. Thus, the composition of the garnet is the best representation of the initial equilibrium conditions in the compositionally pristine system. These compositions are the known variable in the geothermometry calculations against which different clinopyroxene compositions are evaluated.

Table 4 presents the results of these calculations on garnet/clinopyroxene pairs from anhydrous and hydrous runs of this study.

TABLE 4: Range of Temperatures Calculated from Co-existing Garnet/Clinopyroxene Pairs

DG1 Anhydrous Run T°C	MAX.	MIN.	OTHERS	MAX.	MIN.
1350	1422	1278	Ref. 1-Anhydrous		
1450	1525	1361	High-Al/Ol Tholeiite		
1472	1570	1275	1430	1315	1243
1490	1916	1426	1520	1370	--
1500	2169	1430	High-Al Qtz Tholeiite		
1525	1593	1301	1385	1234	--
1535	1941	1318	1400	1256	--
1550	1722	1311	1420	1191	--
			1490	1227	--
			1510	1232	--
Hydrous 1.5 wt%H_2O			Ref. 2 Hydrous		
700	1070	914	Qtz Tholeiite		
800	1106	963	900	1170	--
850	1085	945	1000	1244	--
1000	1247	996	1100	1285	--
1100	1402	1067	1200	1435	--
1200	1207	1111			
1260	1521	1199			
1300	1233	1045			
5wt%H_2O					
1000	1254	1016			
1100	1210	1089			
1200	1282	1177			

REFERENCES 1) Green and Ringwood, 1968
2) Stern and Wyllie, 1978

For comparison, temperatures calculated from garnet/clinopyroxene pairs of Green and Ringwood (1968) and Stern and Wyllie (1978) are also given. The relatively large ranges in the calculated temperatures of this study are a function of variable Fe/Mg ratios in the clinopyroxene as Fe/Mg ratios of the garnets are fairly uniform. Temperatures lower than the known experimental temperature are attributable to Fe-loss from the bulk chemical system, while those which are higher are the result of either poor analysis of the clinopyroxene (i.e. an aggregate of dominantly cpx, but with minor garnet) or in the hydrous runs, higher fO_2 and Fe^{3+}/Fe^{2+} ratios (Ryborn, et al., 1976). For example, the subsolidus experiments with 1.5 wt. percent H_2O (700°, 800°, 850°C) all produce calculated temperatures one to three hundred degrees in excess of the actual temperature. The presence of excess H_2O vapor in these assemblages may maintain, through its disassociation, a relatively high fO_2 inside the capsule. Although this effect will disappear as the furnace and capsule equilibrate via H_2 diffusion into the capsule, the short run times of these experiments may interrupt this process before it has gone to completion (as in the case of low T, hydrous runs of Råheim and Green, 1974). Runs at higher temperatures and involving a melt phase may also be affected initially by high fO_2's, but because of the higher temperatures, equilibrate quickly with the fO_2 of the furnace.

In an attempt to estimate the relative importance of Fe^{3+} to Fe^{2+} in the garnet and clinopyroxene, the analyses were recalculated by the following procedure:

(a) Garnet analyses are corrected in an iterative fashion such that in the structural formula ($X_3\ Y_2\ Z_3\ O_{12}$), enough Fe^{3+} was assigned to the Y position to make Y = 2.

(b) Clinopyroxene analyses are corrected in an iterative fashion such that the $K_D^{gt/cpx}_{Fe/Mg}$ using the new Fe^{2+}/Mg ratio of the corrected garnet reproduces the experimental temperature. Other clinopyroxene Fe^{3+}/Fe^{2+} recalculation schemes based upon cation totals of 4.00 do not work for cation deficient omphacite (Cawthorn and Collerson, 1974).

The results of these recalculations are given in Table 5. The Fe^{3+}/Fe^{2+} ratio in the garnets of both the anhydrous and hydrous experiments increases slightly with decreasing Fe/Mg value. The amount of Fe^{3+} in these garnets is small. The Fe^{3+}/Fe^{2+} ratios of the clinopyroxenes are less systematic than those of the co-existing garnets. The anhydrous clinopyroxenes require only small uniform adjustments of Fe^{2+}/Mg ratios to preserve their equilibrated temperatures. The hydrous clinopyroxenes especially those under subsolidus conditions require highly variable corrections. These observations are consistent with the suggestion that the hydrous experiments reflect higher fO_2 conditions than the anhydrous experiments.

In view of these problems, it is difficult to unambiguously identify the equilibrium composition of the clinopyroxene which coexists with the unaffected garnet. Within the range of calculated temperatures there are, however, numerous garnet/clinopyroxene pairs which reproduce the experimental temperature to within 30°C. These compositions have been averaged to produce a thermodynamically consistent garnet and clinopyroxene pair for each experiment (Tables 6 and 7). As observed above, subsolidus hydrous assemblages do not reproduce their experimental temperature. In these cases, clinopyroxenes which are stoichiometrically realistic are averaged. Together, these averages form the basis on which the composition of

Table 5a. Fe corrections – Garnets

	Hydrous							Anhydrous			
TEMP.	1260	1200	1100	1000	850	800	700	1525	1500	1472	1450
SiO_2	39.83	39.83	40.19	39.73	39.53	39.12	38.95	40.48	39.46	39.05	38.61
TiO_2	.62	1.47	1.20	1.07	.85	.89	.71	1.15	1.27	1.41	1.65
Al_2O_2	22.30	21.24	20.94	21.29	21.34	21.66	21.58	22.39	22.48	22.41	21.88
Fe_2O_3	1.50	1.15	1.25	1.25	1.10	.80	.90	.83	.98	.42	.97
FeO	12.95	15.83	16.84	17.59	19.28	19.41	20.97	12.91	14.62	18.25	18.95
MgO	11.36	9.40	8.70	8.74	7.87	7.25	7.00	13.31	12.58	10.38	9.88
CaO	11.34	10.77	10.42	10.13	10.04	10.04	9.75	8.63	8.53	7.97	7.88
Na_2O	.10	.31	.44	.20	--	.82	.15	.30	.08	.10	.17
Si	2.955	2.991	3.028	3.000	3.003	2.983	2.983	2.973	2.925	2.934	2.920
Ti	.034	.083	.067	.060	.048	.051	.041	1.919	1.945	1.965	1.931
Al	1.931	1.862	1.841	1.876	1.892	1.927	1.928	.063	.071	.079	.094
Fe^{3+}	.083	.064	.070	.070	.062	.045	.051	.045	.054	.023	.054
Fe^{2+}	.804	.994	1.061	1.111	1.225	1.237	1.343	.793	.906	1.147	1.199
Mg	1.256	1.052	.976	.983	.891	.824	.798	1.456	1.390	1.163	1.113
Ca	.901	.866	.841	.820	.817	.820	.800	.679	.677	.642	.639
Na	.014	.045	.064	.029	--	.120	.022	.043	.011	.015	.025
Fe^{2+}/Mg	.640	.945	1.087	1.130	1.375	1.501	1.683	.545	.652	.986	1.077
Fe^{3+}/Fe^{2+}	.103	.064	.070	.063	.051	.036	.038	.057	.060	.020	.045
$K_D^{gt\text{-}cpx}{}_{Fe^{3+}/Fe^{2+}}$	.660	2.21	1.40	.496	.070	.023	.023	1.27	1.176	.952	.484

Table 5b. Fe corrections – Clinopyroxenes

	Hydrous							Anhydrous			
TEMP	1260	1200	1100	1000	850	800	700	1525	1500	1472	1450
SiO_2	51.62	53.10	53.75	54.69	53.42	52.90	52.68	49.49	49.02	50.33	49.86
TiO_2	.41	.85	.79	.45	.32	.34	.24	.88	.90	1.17	1.30
Al_2O_3	8.59	11.53	11.22	11.93	13.79	10.90	13.18	14.52	14.81	14.77	15.72
Fe_2O_3	.92	.20	.32	.62	2.67	5.53	4.57	.72	.45	.24	.48
FeO	5.26	5.72	5.30	4.24	3.31	3.24	2.44	6.73	7.80	9.57	9.62
MgO	12.35	9.38	9.20	8.93	8.81	9.30	9.44	10.21	10.14	8.38	7.92
CaO	17.98	14.46	14.33	13.90	12.71	13.15	13.24	14.40	13.79	12.26	11.91
Na_2O	2.87	4.76	5.08	5.24	4.97	4.62	4.21	3.05	3.09	3.29	3.19
Si	1.878	1.908	1.927	1.945	1.896	1.901	1.875	1.789	1.777	1.823	1.805
Al	.365	.483	.470	.495	.571	.457	.547	.612	.627	.624	.664
Ti	.011	.023	.021	.012	.009	.009	.006	.024	.025	.032	.035
Fe^{3+}	.025	.005	.008	.016	.071	.148	.121	.019	.012	.006	.013
Fe^{2+}	.160	.172	.159	.126	.098	.097	.073	.203	.236	.290	.291
Mg	.670	.502	.491	.473	.466	.498	.500	.550	.548	.452	.427
Ca	.701	.557	.551	.530	.483	.506	.505	.557	.536	.476	.462
Na	.202	.331	.353	.361	.342	.322	.291	.214	.217	.231	.224
Fe^{2+}/Mg	.239	.342	.324	.266	.210	.195	.145	.369	.430	.641	.681
Fe^{3+}/Fe^{2+}	.156	.029	.050	.127	.724	1.524	1.657	.093	.051	.021	.045

TABLE 6: Representative 'Equilibrium' Garnets

	DRY						WET						
RUN TEMPERATURES	1350	1450	1472	1490	1500	1525	700	800	850	1000	1100	1200	1260
RUN #	8865	8845	8864	8650	8841	8880	6944	7373	7372	7550 8829	8818 8866	8808	8865
SiO_2	40.42	38.66	39.07	39.45	39.50	40.52	38.99	38.29	39.58	39.79	40.26	39.88	39.90
TiO_2	1.41	1.65	1.41	1.37	1.27	1.15	.71	.88	.85	1.07	1.20	1.47	.62
Al_2O_3	20.58	21.91	22.42	22.31	22.51	22.41	21.60	21.30	21.37	21.32	20.98	21.27	22.34
FeO	18.56	19.83	18.63	15.68	15.50	13.66	21.78	20.00	20.27	18.72	17.97	16.87	14.30
MgO	9.43	9.89	10.39	12.36	12.60	13.32	7.00	7.10	7.88	8.75	8.71	9.41	11.38
CaO	9.16	7.89	7.98	8.52	8.54	8.64	9.76	9.83	10.05	10.15	10.44	10.78	11.36
Na_2O	.74	.17	.10	.31	.08	.30	.15	.80	-	.20	.44	.31	.10
Cations/ 12 oxygens													
Si	3.042	2.927	2.937	2.933	2.932	2.979	2.990	3.014	3.012	3.010	3.037	2.999	2.966
Ti	.079	.094	.080	.077	.071	.064	.041	.052	.048	.061	.068	.083	.034
Al	1.807	1.936	1.967	1.936	1.950	1.923	1.933	1.865	1.898	1.901	1.847	1.867	1.938
Fe	1.168	1.255	1.171	.975	.962	.840	1.397	1.317	1.290	1.184	1.134	1.061	.889
Mg	1.058	1.116	1.164	1.369	1.393	1.459	.800	.833	.894	.987	.979	1.055	1.261
Ca	.739	.640	.643	.679	.679	.681	.802	.829	.819	.822	.844	.869	.906
Na	.108	.024	.015	.044	.011	.043	.022	.122	-	.029	.064	.045	0.14
TOTAL	8.001	7.992	7.997	8.013	7.998	7.989	7.985	8.032	7.961	7.994	7.973	7.970	8.008
Ratios													
Ca	24.9	21.2	21.6	22.4	22.3	22.8	26.7	27.8	27.2	27.5	28.5	29.1	29.6
Mg	35.8	37.0	39.1	45.2	45.9	48.9	26.6	27.9	29.7	33.0	33.1	35.3	41.2
Fe	39.3	41.8	39.3	32.4	31.8	28.3	46.5	44.2	42.9	39.6	38.3	35.5	29.0
A	2.6	.6	.3	1.1	.3	1.1	.5	2.9	-	.7	1.6	1.2	.4
F	64.6	66.3	63.9	55.3	55.0	50.0	75.3	71.7	72.0	67.6	66.3	63.4	55.5
M	32.8	33.1	35.8	43.6	44.7	48.9	24.2	25.4	28.0	31.7	32.1	35.3	44.1
Fe/Mg	1.104	1.124	1.006	.712	.690	.576	1.746	1.581	1.443	1.199	1.158	1.006	.705
$K_D \frac{gt/cpx}{Fe/Mg}$	2.037	1.572	1.534	1.477	1.519	1.422	4.512	3.207	3.986	3.972	3.396	3.028	2.554
Calculated T°C	1327	1454	1475	1518	1495	1552	970	1120	1022	1025	1100	1187	1251

TABLE 7. Representative 'Equilibrium' Cpx.

	Anhydrous						1.5% H_2O							5.0% H_2O	
Run Temps	1350	1450	1472	1490	1500	1525	700	800	850	1000	1100	1200	1260	1000	1100
Run #	8665	8845	8829	8650	8841	8880	6944	7373	7372	7550 8829	8818 8866	8808	8865	8869	8867
SiO_2	51.4	49.8	50.34	48.78	49.04	49.53	52.93	53.23	53.80	54.41	53.77	53.12	51.67	54.13	54.37
TiO_2	1.36	1.30	1.17	.94	.90	.88	.24	.34	.32	.48	.79	.85	.41	.39	.85
Al_2O_3	13.70	15.70	14.77	15.10	14.82	14.53	13.24	10.97	13.89	12.22	11.23	11.53	8.60	9.93	9.52
FeO	8.15	10.05	9.79	8.52	8.21	7.38	6.55	8.22	5.74	5.13	5.59	5.90	6.09	5.09	5.53
MgO	8.43	7.91	8.38	9.92	10.14	10.22	9.48	9.36	8.88	8.92	9.20	9.38	12.36	10.22	9.88
CaO	13.65	11.90	12.26	13.83	13.80	14.41	13.31	13.24	12.80	13.54	14.34	14.47	18.00	15.32	15.44
Na_2O	3.76	3.19	3.29	2.95	3.09	3.05	4.23	4.65	5.00	5.30	5.08	4.76	2.87	4.77	4.40
K_2O	--	--	--	--	--	--	--	--	--	--	--	--	--	--	--
Cation/6 oxygens															
Si	1.849	1.806	1.824	1.771	1.779	1.791	1.894	1.925	1.907	1.939	1.929	1.909	1.882	1.945	1.953
Ti	.037	.035	.032	.026	.024	.024	.006	.009	.008	.013	.021	.022	.011	.010	.023
Al	.575	.664	.625	.640	.627	.613	.553	.463	.575	.508	.470	.484	.365	.417	.403
Fe	.245	.305	.297	.259	.249	.223	.196	.249	.170	.153	.168	.177	.185	.153	.166
Mg	.452	.427	.453	.537	.548	.550	.506	.505	.469	.474	.492	.502	.671	.547	.529
Ca	.526	.462	.476	.538	.536	.558	.510	.513	.486	.517	.551	.557	.702	.590	.594
Na	.262	.224	.231	.206	.217	.213	.294	.326	.343	.366	.353	.332	.203	.332	.306
K	--	.007	--	--	--	--	--	--	--	--	--	--	--	--	--
TOTAL	3.941	3.923	3.938	3.977	3.980	3.972	3.959	3.990	3.958	3.970	3.984	3.983	4.019	3.944	3.975
Pyroxene Components															
Jadeite	27.5	24.1	24.5	21.0	22.0	21.7	30.5	32.8	35.6	37.6	35.7	33.6	19.8	33.2	31.4
CaTITs	3.9	3.8	3.4	2.6	2.4	2.4	.6	.9	.8	1.3	2.1	2.2	1.1	1.0	2.4
CaTs	12.6	19.9	17.5	19.5	18.3	18.0	12.8	5.9	11.2	5.9	3.8	5.4	6.8	3.2	2.6
Wo	19.4	13.0	14.8	16.4	16.8	18.3	19.7	22.3	19.2	22.9	24.9	24.3	30.4	27.4	28.0
En	23.7	22.9	24.0	27.3	27.8	28.1	26.2	25.4	24.3	24.3	24.9	25.4	32.8	27.3	27.1
Fs	12.9	16.4	15.7	13.2	12.6	11.4	10.1	12.5	8.8	7.8	8.5	8.9	9.0	7.7	8.5
Ratios															
%Jadeite	28.6	25.0	25.4	21.6	22.6	22.3	30.7	33.1	35.9	38.1	36.5	34.3	20.0	33.6	32.1
%CATS	13.1	20.6	18.1	20.0	18.8	18.4	12.9	6.0	11.3	6.0	3.8	5.6	6.9	3.3	2.7
%QUAD	58.3	54.4	56.5	58.4	58.6	59.2	56.4	60.9	52.8	55.8	59.7	60.1	73.0	63.1	65.2
Ca	43.0	38.7	38.8	40.3	40.2	41.9	42.0	40.6	43.2	45.2	45.5	45.0	45.0	45.7	46.0
Mg	37.0	35.7	36.9	40.2	41.1	41.3	41.7	39.8	41.7	41.4	40.6	40.6	43.0	42.4	41.0
Fe	20.0	25.6	24.3	19.5	18.7	16.8	16.3	19.6	15.1	13.3	13.9	14.4	12.0	11.9	12.9
A	18.5	15.7	23.5	13.8	14.4	14.7	20.8	20.9	25.5	27.4	25.5	23.7	13.5	23.8	22.2
F	40.0	47.1	30.4	39.8	38.3	35.7	32.3	37.0	29.2	26.5	28.1	29.5	28.6	25.3	27.9
M	41.4	37.1	46.1	46.3	47.3	49.5	46.8	42.1	45.2	46.1	46.3	46.8	57.9	50.9	47.9
Fe/Mg	.542	.714	.656	.482	.454	.405	.387	.493	.362	.322	.341	.352	.276	.229	.313

liquids formed by the equilibrium partial melting of eclogite are computed.

Finally, it is interesting to note that none of Green and Ringwood's (1968) coexisting garnet/clinopyroxene pairs produce calculated temperatures close to reported experimental temperatures. If the reasoning developed above based on the Ellis and Green (1979) calibration is correct, then these pairs do not reflect equilibrium conditions.

DISCUSSION

The primary purpose of these experiments on the partial melting of eclogite is to define the chemical characteristics of the melt phase in equilibrium with the co-existing crystalline phases. As indicated before, the determination of these characteristics by direct means (i.e. microprobe analysis) is complicated by a number of experimental problems. Consequently, the compositions of these melts are calculated by mass balance, and should be reversed to unequivocally establish that they are equilibrium products. The liquids calculated in this study have not been reversed, and therefore should not be considered as proven equilibrium melts. However, because of the many independent constraints built into their calculation, little difference is expected between the compositions presented and the reversed, equilibrium liquids. Complementary to the determination of the liquids, the bulk chemistry and phase equilibria of the residue is defined. Together, this information provides a basis on which to evaluate the role of eclogite in the upper mantle.

Calculation of Liquids - The composition of the liquid phase is calculated by mass balance where (X) Liquid composition + (1-X) Residue composition = Bulk composition. This approach requires

knowledge of the bulk and residue chemistries and the degree of melting (X), all of which can be subject to experimental and analytical errors. Although the bulk chemistry of the system may change because of Fe-loss to the capsule, this change need not be considered if the residual crystalline phases are corrected for no Fe-loss (see above). In this case, the bulk system equals the initial starting composition, DG-1 $\pm H_2O$ for the anhydrous or hydrous experiments. The bulk composition of the residue is dependant upon the Fe-correction procedure employed and on errors in estimating the relative weight proportions of the various crystalline phases. Abundances derived by point counting of crushed grain mounts or polished surfaces are valid only if it can be demonstrated that the sample is homogeneous. Errors are introduced if heterogeneous samples, resulting from gravitational settling of dense crystals (garnet) are examined. Similar problems are encountered in estimating the proportions of glass in the charge (i.e. degree of melting). These problems suggest that the calculation of liquids by mass balance can result in a variety of compositions for a particular temperature, even if the compositions of the residual phases are adequately described. Additional criteria are therefore required with which the calculations can be more rigorously constrained.

The distribution of particular elements between coexisting mineral/liquid pairs is one possible means of 'testing' the calculated composition. The partition coefficient of Fe/Mg between clinopyroxene and liquid ($K_D^{cpx/liq}_{Fe/Mg}$) ranges from $\sim$0.25 to 0.3 for anhydrous basaltic liquids (Nielson and Drake, 1979) and exhibits no apparent change with respect to variations in pressure or composition (Thompson, 1974). Similar information for hydrous systems is not so abdundant and the published $K_{D's}$ are more varied ($0.1 < K_D^{cpx/liq}_{Fe/Mg}$

< 0.4) (Helz, 1973; Green, 1976; Stern and Wyllie, 1978; Nicholls and Harris, 1980). These variations are possible functions of incorrect assessment of Fe^{3+}/Fe^{2+} ratios, or relate to considerable compositional variations in the host liquids (basalt-dacite). Liquids calculated in this study from equilibrium melting possess $K_D^{cpx/liq}_{Fe/Mg}$ of ∿ 0.25-0.30 (anhydrous) and 0.275-0.383 (hydrous). In comparison, $K_{D's}^{cpx/liq}_{Fe/Mg}$ for the calculated clinopyroxene/liquid pairs of Stern and Wyllie range from 0.341 (1200°C) to 0.073 (900°C).

$K_D^{cpx/liq}_{Ti}$ is another criterion by which the calculated liquids can be judged. Low pressure studies on anhydrous basaltic compositions indicate that this value will decrease with increasing termperature (∿0.8-0.13; Irving, 1978). Changes due to increasing pressure, hydration or compositional variations (Ito, 1973; Thompson, 1974; Nicholls and Harris, 1980) are obscured by the temperature effect. $K_{D's}^{cpx/liq}_{Ti}$ for the clinopyroxene/calculated liquid pairs are ∿ 0.5 for the anhydrous melts, and vary between 0.28 and 1.5 for the hydrous melts. The presence of even minor rutile in the hydrous 1000°C residue (K_D = 1.5) significantly alters the TiO_2 content of the calculated liquid and consequently the use of the $K_D^{cpx/liq}_{Ti}$ is restricted in these cases.

For a particular residual chemistry, the degree of partial melting is determined primarily by the $K_D^{cpx/liq}_{Fe/Mg}$ of the coexisting clinopyroxene/calculated liquid pair, with the $K_D^{cpx/liq}_{Ti}$ providing a secondary verification. The residues of near-solidus experiments are constrained by proportions of phases computed from point counting. However, for experiments in which large degrees of liquid are produced, these constraints are less rigid, and the residual chemistries are governed by two simple assumptions. Firstly, changes

in the proportions of phases which constitute the residue are systematic. For example, as melting proceeds, the garnet/clinopyroxene ratio must either continuously increase, decrease, or remain constant. Secondly, these changes are subject to minor adjustments necessary to produce a smooth continuuous variation in the composition of the liquid phase. This feature characterizes equilibrium fusion in which a phase does not disappear (Presnall, 1969).

The details of the liquid calculation involve the computation of a variety of possible melt compositions using several different residual chemistries for a particular temperature. In all calculations, K_2O and H_2O are totally incompatible with the residue, thus, their abundances in the liquid reflect only the degree of melting. Liquid compositions are examined relative to each other on two ternary projections, $CaO - MgO + FeO - \frac{1}{2}SiO_2$ and $Na_2O + K_2O - FeO - MgO$ (AFM). These projections are extremely useful as they include every major element except Al_2O_3. In addition, minor variations in composition create different effects on the two plots. Thus, only a limited number of liquids can be calculated which meet all of the aforementioned assumptions.

Figures 7a-d and 8a-d illustrate these graphical solutions for the hydrous case. Briefly, the liquid compositions for all degrees of melting for a particular residual chemistry are defined by a line which passes through the bulk and residue compositions. The required $K_D^{\text{cpx/liq}}_{\text{Fe/Mg}}$ occurs at only one position along that line and consequently sets the degree of melting and the liquid composition. The point which represents the residual chemistry must, if garnet and clinopyroxene are the only CaO, MgO, FeO, SiO_2 or alkali bearing residual phases, fall on the projected garnet/clinopyroxene tie-line

Figure 7:

(a) Shaded area in CaO - MgO - ¼ SiO_2 ternary is the area represented in figures b, c, and d. The dotted line is the calc-alkaline trend (basalt-rhyolite) of Stern and Wyllie (1978).

(b) Graphical solution for liquid compositions coexisting with different clinopyroxene/garnet ratios. Garnet and clinopyroxene compositions are those given in Tables 6 and 7. DG-1 is the composition of the initial starting mixture. Lines a-f represent liquid compositions calculated by subtracting from DG-1 a residual composition (% Cpx + % Gt). These lines pass through DG-1 and intersect the garnet - clinopyroxene tie line at the predetermined clinopyroxene/garnet ratio. Degrees of melting are given by lines approximately parallel to the garnet - clinopyroxene tie line, but on the liquid side of DG-1. The solid square is the preferred liquid for partial melting of DG-1 at 1000°C. See text for additional discussion on liquid calculation.

(c) As above, except for 1100°C.

(d) As above, except for 1200°C.

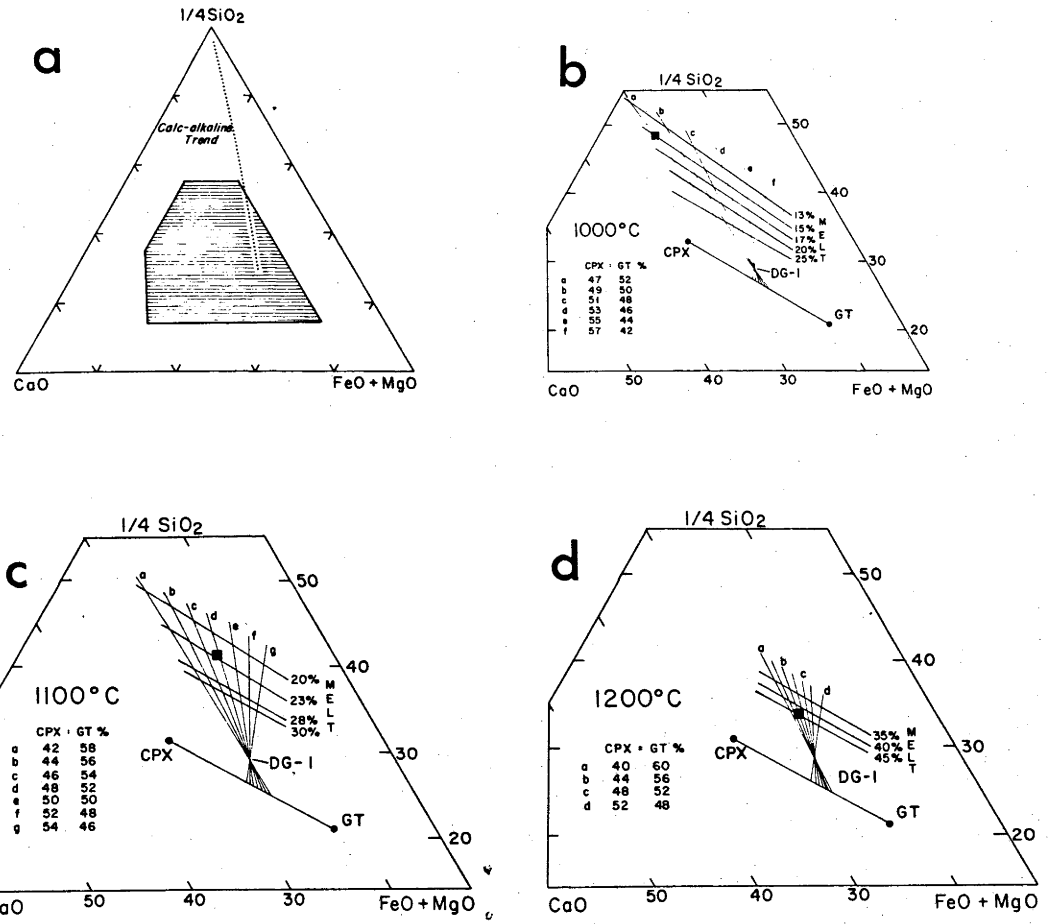
a
1/4SiO2
Calc-alkaline Trend
CaO
FeO + MgO
b
1/4 SiO2
1000°C
CPX
DG-1
GT
13% MELT
15% MELT
17% MELT
20% MELT
25% MELT
CPX : GT %
a 47 52
b 49 50
c 51 48
d 53 46
e 55 44
f 57 42
CaO
FeO + MgO
c
1/4 SiO2
1100°C
CPX
DG-1
GT
20% MELT
23% MELT
28% MELT
30% MELT
CPX : GT %
a 42 58
b 44 56
c 46 54
d 48 52
e 50 50
f 52 48
g 54 46
CaO
FeO + MgO
d
1/4 SiO2
1200°C
CPX
DG-1
GT
35% MELT
40% MELT
45% MELT
CPX : GT %
a 40 60
b 44 56
c 48 52
d 52 48
CaO
FeO + MgO

Figure 8:

(a) Shaded area in $Na_2O + K_2O$ (A) - FeO (F) - MgO (M) ternary is the area represented in figures b, c, and d. The dotted line is the calc-alkaline trend (basalt-rhyolite) of Stern and Wyllie (1978).

(b) Graphical solution for liquid compositions coexisting with different clinopyroxene/garnet ratios. See caption for Figure 7b for additional explanation. Liquid composition is for 1000°C.

(c) As above, except for 1100°C.

(d) As above, except for 1200°C.

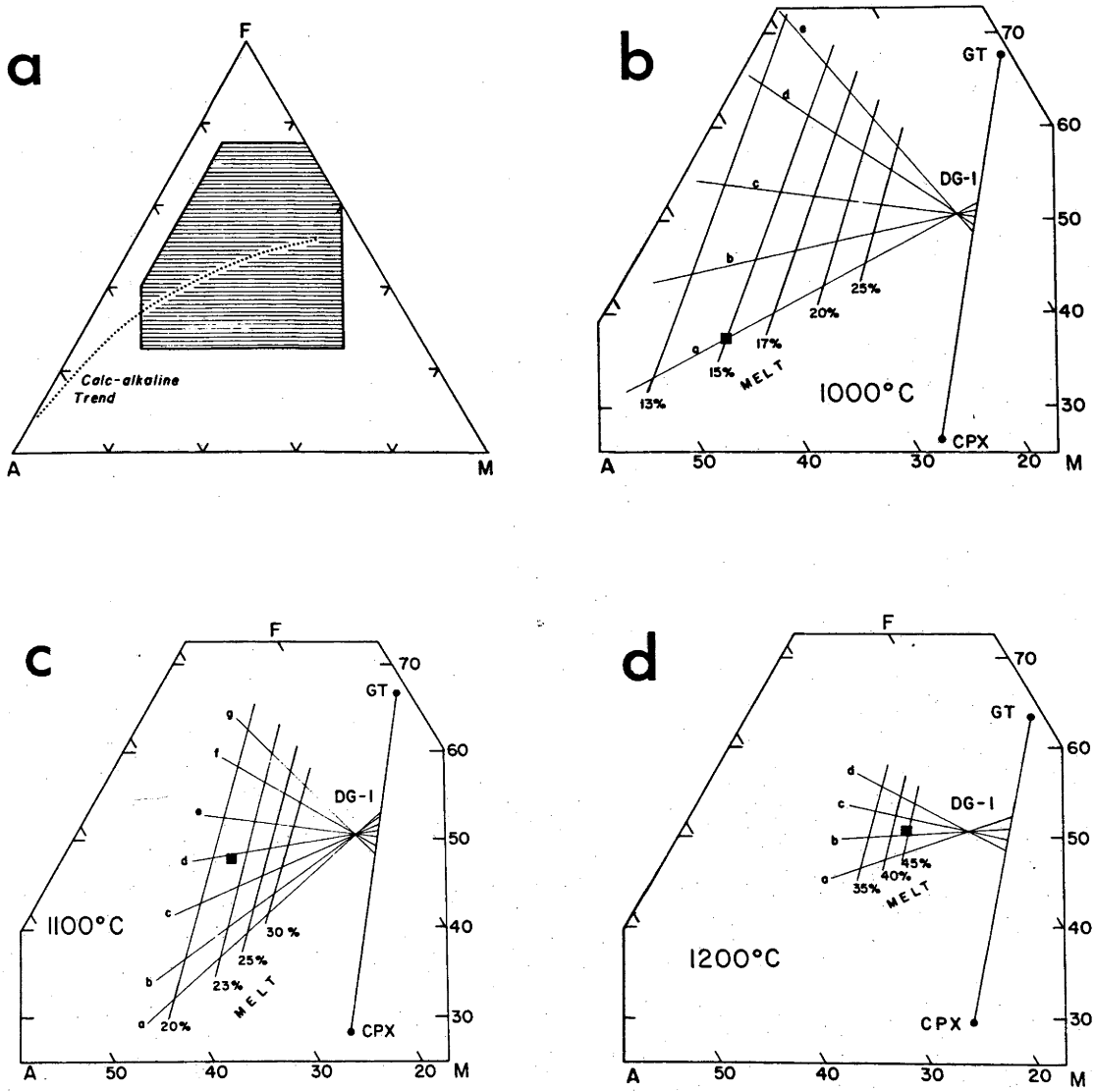
a
F
A
M
Calc-alkaline
Trend
b
F
70
GT
60
DG-1
50
40
30
A
50
40
30
20
M
CPX
1000°C
MELT
13%
15%
17%
20%
25%
c
1100°C
30%
25%
23%
20%
d
1200°C
45%
40%
35%

at a point corresponding to the assumed garnet/clinopyroxene ratio. With regard to these simple geometrical constraints, it should be noted that the calculated hydrous melts and crystalline residues of Stern and Wyllie (1978; table 8), are incompatible with the constraints of bulk composition and garnet/clinopyroxene tie-lines (Fig. 9).

Liquid Compositions - The compositions of the preferred liquids calculated for anhydrous and hydrous equilibrium melting of eclogite are given in Table 8, along with the coexisting residue chemistry. The trends of these liquids on the AFM and CaO - MgO + FeO - $\frac{1}{4}SiO_2$ diagrams are compared with an average calc-alkaline trend and the melting trend of Stern and Wyllie (1978) for a hydrous oceanic tholeiite (Fig. 10a and b). Even a brief glance at these figures reveals differences between this study and that of Stern and Wyllie's, although their major conclusion that the equilibrium fusion path of eclogite (olivine tholeiite composition) is not equivalent to a calc-alkaline trend of basalt-rhyolite, is not compromised. There is however, no petrogenetic requirement for eclogite fusion to produce the entire calc-alkaline suite, but only andesite. The critical observation is the composition of the liquid which marks the intersection of the fusion path and the calc-alkaline path .

Anhydrous Melting - The calculated liquids produced by the melting of eclogite under anhydrous conditions are model dependent. Three different melting pathways are presented in Figure 10a and b corresponding to three extremes in residual chemistry (i.e. melting mode). Trend A, in which the garnet/clinopyroxene ratio increases with melting is the preferred equilibrium fusion pathway and is the one presented in Table 8. This preference is based on similarities between model and observed weight proportions of the charges and the

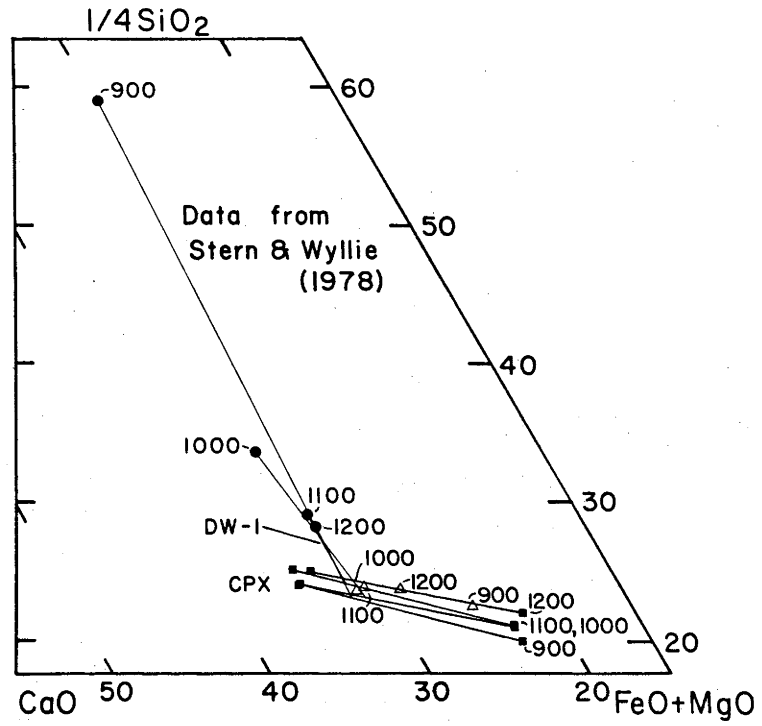

Figure 9: CaO - MgO + FeO - ¼ SiO_2 projection of calculated liquids, clinopyroxenes and garnets of Stern and Wyllie (1978) along with their residual chemistries at 900 C, 1000, 1100, and 1200 C (△). Note that the tie-lines joining the liquid composition and bulk composition (DW-1) do not intersect the relevant clinopyroxene - garnet tie line at the residue composition given by Stern and Wyllie.

TABLE 8: Anhydrous Liquids

	ANHYDROUS LIQUIDS						HYDROUS LIQUIDS							
							Water-Free				Water-Present			
TEMPERATURE	1525	1500	1490	1472	1464+	1458+	1260	1200	1100	1000	1260	1200	1100	1000
% MELT	50	42	38	12	8	6	90	45	22	15	90	45	22	15
SiO_2	51.18	52.50	53.19	56.54	58.17	61.79	49.51	53.09	58.47	65.71	48.68	51.32	54.49	59.14
TiO_2	1.78	1.88	1.89	2.38	2.28	2.15	1.46	1.59	1.63	.36	1.44	1.54	1.52	.32
Al_2O_3	15.31	15.01	14.80	14.46	12.40	9.11	16.02	15.04	15.29	10.49	15.75	14.54	14.25	9.44
FeO	13.07	12.55	12.58	8.48	7.30	5.64	11.19	10.13	7.71	5.01	11.00	9.79	7.19	4.51
MgO	4.71	3.96	3.69	1.75	1.60	1.12	7.49	6.07	4.17	2.80	7.37	5.87	3.89	2.52
CaO	10.16	10.09	9.66	10.83	11.83	12.45	11.13	10.16	8.27	10.03	10.94	9.82	7.71	9.03
Na_2O	3.35	3.49	3.61	3.75	3.70	4.00	2.97	3.42	3.41	4.03	2.92	3.31	3.18	3.63
K_2O	.44	.52	.58	1.81	2.72	3.73	.23	.49	1.03	1.56	.23	.47	.96	1.40
H_2O	-	-	-	-	-	-	-	-	-	-	1.67	3.33	6.82	10.00
Fe/Mg	1.55	1.76	1.90	2.69	2.54	2.807	.832	.930	1.03	.998	-	-	-	-
K_D cpx/liq Fe/Mg	.261	.258	.253	.239	.255	.249	.332	.378	.331	.322	-	-	-	-
K_D cpx/liq Ti	.49	.48	.49	.49	.59	.54	-	-	-	-	.28	.55	.52	1.5
A	17.6	19.5	20.4	35.2	41.9	53.3	14.6	19.4	27.2	41.7	-	-	-	-
F	60.6	61.3	61.6	53.6	47.6	38.9	51.2	50.4	25.6	37.4	-	-	-	-
M	21.8	19.2	18.0	11.2	10.5	7.8	34.2	30.2	47.2	20.9	-	-	-	-
CaO	24.9	25.4	24.7	30.8	33.5	35.9	26.4	25.6	23.8	29.3	-	-	-	-
MgO + FeO	43.6	41.6	41.5	29.0	25.2	19.5	44.3	40.9	34.1	22.8	-	-	-	-
$SiO_2/4$	31.4	33.0	33.8	40.2	41.2	44.6	29.6	33.5	42.0	47.9	-	-	-	-
CIPW Norm														
Qtz	-	-	.17	4.56	4.80	10.58	-	-	9.35	16.18	-	-	-	-
Or	2.60	3.07	3.43	10.70	16.07	22.04	1.36	2.90	6.09	9.22	-	-	-	-
Ab	28.35	29.53	30.55	31.73	31.31	26.10	25.13	28.94	28.86	34.10	-	-	-	-
An	25.44	23.75	22.47	17.28	9.19	-	29.70	24.24	23.38	5.93	-	-	-	-
Di	21.07	22.28	21.62	31.14	26.72	18.82	21.09	21.69	14.66	31.23	-	-	-	-
Hy	10.38	15.66	18.18	.08	-	-	2.07	16.06	14.57	-	-	-	-	-
Ol	8.79	2.13	-	-	-	-	17.87	3.15	-	-	-	-	-	-
Il	3.38	3.57	3.59	4.52	4.33	4.08	2.77	3.06	3.10	.68	-	-	-	-
Wo	-	-	-	-	7.57	16.57	-	-	-	2.66	-	-	-	-
Ns	-	-	-	-	-	1.80	-	-	-	-	-	-	-	-
Residue														
Cpx	70	73	75	80	83	84	40	44.5	47.2	47	-	-	-	-
Gt	30	27	25	20	17	16	60	55.5	52.5	52	-	-	-	-
Rut	-	-	-	-	-	-	-	-	.3	.75	-	-	-	-
Ky	-	-	-	-	-	-	-	-	-	.25	-	-	-	-

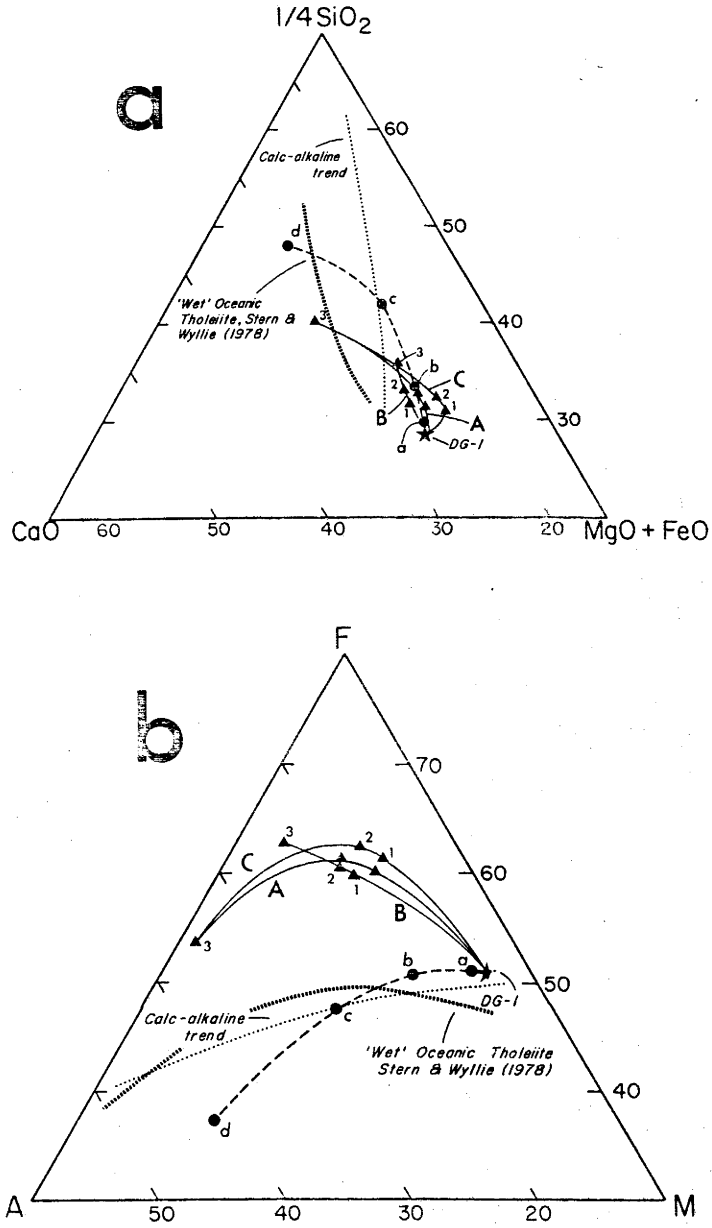

Figure 10. a) CaO - MgO + FeO - $\frac{1}{4}SiO_2$ projection of calculated liquid paths of DG-1 partial melts. The solid lines (A,B,C) are trends of anhydrous liquids with (A) being the preferred path. Numbers and solid triangles refer to (1) 1525, (2) 1500, (3) 1472°C liquids. The dashed line is the trend of hydrous (1.5 wt. %) liquids. Lower-case letters and solid circles refer to (a) 1260, (b) 1200, (c) 1100, (d) 1000°C liquids. Also shown are the hydrous melting trend of DW-1 and calc-alkaline path from Stern and Wyllie (1978).
b) AFM projection of calculated liquid paths of DG-1 partial melts. Explanation of symbols as above.

compositions of calculated melts and analyzed glasses (Table 3). Trends B and C, in which the garnet/clinopyroxene ratio drastically increases, or remains constant with melting, are also shown to illustrate the effects of two different assumptions on the liquid composition. The most striking observation concerns the curvature of the trends on the CaO - MgO + FeO - ¼ SiO_2 diagram. In contrast to the predicted liquid trends of Stern and Wyllie (1978), in which the curvature is concave towards the CaO apex, the calculated fusion path of DG-1 is convex toward CaO for melting models in which the garnet/clinopyroxene ratio increases with larger degrees of melting (Trends A and B). Only if this ratio remains constant (Trend C) or decreases, is the curvature similar to that predicted by Stern and Wyllie. In all cases, the calculated pathways do not resemble those of average calc-alkaline rocks.

Trends, A,B, and C, plotted on the AFM diagram, exhibit substantial Fe-enrichment in liquids derived during intermediate degrees of melting. Lesser degrees of melting produce liquids more enriched in alkalies and depleted in MgO and FeO only for those models in which the garnet/clinopyroxene ratio increases with greater degrees of melting. Alternately, liquids produced from constant or decreasing garnet/clinopyroxene ratios exhibit continuous Fe-enrichment with no turnover to more alkalic compositions.

As stated above, the preferred melting model (Trend A) is calculated on the basis of slight increases in the garnet/clinopyroxene ratio with increasing degree of melting. The calculated liquids from large degrees of melting (50% (1525°), 42% (1500°)) are similar, but differ from each other and the bulk composition, DG-1, in SiO_2, FeO, MgO, and Na_2O contents. These differences are manifested in terms of CIPW norms by a decrease in normative olivine

from 1525° to 1500°. Both liquids are, roughly, olivine tholeiites. The liquid calculated at 1472°C (12% melt) is roughly icelanditic in character. It is more enriched in SiO_2 and Na_2O and depleted in FeO and MgO than the liquids of greater degrees of melting. CaO contents are approximately constant throughout this melting interval (50% to 12%). The liquid generated at 1472°C contains minor normative quartz with plagioclase (∿ 60%) and diopside (∿ 30%) constituting the remainder of the normative mineralogy.

The equilibrium fusion path represented by the liquids calculated at 1525°, 1500°, and 1472° can with reservation, be extrapolated to lower temperatures and degrees of melting. Assuming that no minor phase, such as quartz, appears between 1472° and 1450° (solidus), liquids are calculated for 1465° (8% melting) and 1458° (6% melting) (Table 8). They continue the same trends to SiO_2 and alkali enrichment and FeO and MgO depletion previously noted. The major differences are an increase in CaO and a decrease in Al_2O_3. These liquids are quartz normative with substantial contents of normative wollastonite. They do not resemble any observed erupted magma type.

The shape of the preferred equilibrium fusion path for DG-1 (olivine tholeiite) is noticeably different from that calculated by Stern and Wyllie (1978) for another anhydrous olivine tholeiite (DW-1). This difference may be due in part to the data assumptions employed by Stern and Wyllie in their calculations, but it could also reflect intrinsic differences in the melting of eclogite. There are two important differences observed between DG-1 and DW-1 eclogites. Firstly, the presence of quartz in DW-1 and its absence or near absence in DG-1 is consistent with the second: the lower solidus temperature of DW-1 (~1325° vs1450°C for DG-1). Investigation of

the CIPW norms of these two compositions reveals less normative hypersthene in DG-1 than DW-1, and if both are plotted in the basalt tetrahedron (Yoder and Tilley, 1962), DG-1 is located closer to the critical plane of silica saturation. The different fusion paths of DW-1 and DG-1 thus may be an effect of their relative positions in this multicomponent space, enhanced by differences in a variety of minor elements (e.g. TiO_2, MnO, K_2O, P_2O_5).

Hydrous Liquids - The major effects of H_2O on eclogite are threefold: (1) solidus temperatures are lowered by several hundreds of degrees; (2) the melting interval (solidus to liquidus) is expanded; and (3) several minor (some hydrous) phases are stabilized in the subsolidus assemblage. The lower temperatures cause considerable adjustments in the composition of garnet and co-existing clinopyroxene and their relative modal proportions. Consequently, it is difficult to ascertain the exact role which H_2O plays in determining the character of the melt phase (e.g. modification of structural sites in the silicate liquid (Burnham, 1979)) by direct comparison with results from anhydrous melting.

The presence of several minor phases (phengite, rutile and quartz) and their largely unknown melting behaviours in the complex eclogite system, restrict the amount of possible extrapolation of liquid trends from high to low degrees of melting. The path of equilibrium fusion for DG-1 + 1.5 wt. percent H_2O is therefore calculated only for the temperature interval 1260° - 1000°C in which garnet and clinopyroxene are the major components of the residue. Extension of the path below 1000° without additional data is tenuous and depends upon the location of the quartz-in boundary

and character of the melting (probably incongruent) of phengite.

Before proceeding to a detailed examination of the chemistry of these liquids, it is important to reiterate some of the assumptions made in their calculation:

(A) The melting modes are not as well constrained as those used in the anhydrous calculations, partly because the small crystal size of the garnets and clinopyroxenes prohibits accurate point counting. Least squares solutions for the subsolidus assemblage of DG-1+1.5 wt. percent H_2O at 700°C, indicates that the relative proportion of garnet to clinopyroxene is significantly higher than for anhydrous DG-1 (40% vs. 15% garnet, respectively). The reasons for the increase of modal garnet in the hydrous eclogite are not clear, but must reflect the combined effects of lower temperatures and presence of H_2O. The subsolidus proportions provide an endpoint on which the amounts of garnet and clinopyroxene in the 'wet' eclogite residues are based. In accordance with most experimental data on eclogite fusion (see introduction), the ratio of garnet to clinopyroxe increases with increasing degree of melting. The residues for the 1000°-1260°C liquids have slightly higher proportions of garnet to clinopyroxene.

(B) The liquid trend, because it represents equilibrium fusion through the temperature interval of 1000° to 1260°C and is uninterrupted by the disappearance of a phase (e.g. quartz or phengite), must be continuous (Presnall, 1969). The degree of melting is set by the partioning of Fe and Mg between clinopyroxene and liquid. Unlike the anhydrous calculation where it is approximately constant (0.25) the hydrous values vary from 0.378 (1260°C) to 0.275(1000°C). If the geometric constructions of Figures 7 and 8 are carefully examined, it is apparent that very few

fusion paths can be devised which yield realistic liquids and yet fulfill all of these assumptions.

The calculated liquids are presented with H_2O included (the true calculated 'equilibrium' compositions), and normalized to H_2O free compositions (Table 8). Which liquid one considers depends upon the purpose to which that composition is applied. For example, if processes occurring immediately above the subduction zone are considered, the hydrous liquids are used, but if the melts are to be compared to erupted volcanic rocks, the anhydrous compositions are the better choice. Obviously, whether normalized or not, the compositional trends based upon ratios of elements are unaffected. Figure 10a presents the preferred calculated path of equilibrium fusion of DG-1 + 1.5 wt. percent H_2O on the CaO - MgO + FeO - SiO_2¼ ternary plot compared to the preferred anhydrous trend and the average calc-alkaline trend. The model path resembles that of the dry eclogite, but is displaced more towards the SiO_2 apex. Liquids derived from similar low degrees of melting contain more SiO_2 and less CaO for hydrous versus anhydrous fusion. They are also considerably less enriched in FeO as evident from the trace of the fusion path on an AFM plot (Fig. 10b), although the absolute contents of alkalis are similar. The path is grossly comparable with the average calc-alkaline path in both plots at moderate and high degrees of melting, but diverges significantly at lower degrees of melting. The liquid composition which marks the intersection of the two curves is broadly andesitic (∿ 25% melting), but is lower in Al_2O_3 and higher in MgO and CaO than most calc-alkaline andesites. Lower degrees of melting produce liquids which, when normalized, are high in SiO_2 (∿ 65 wt. %) and Cao (∿ 9.5 wt. %) and low in Al_2O_3 (10 wt.%)

and total alkalis (5.5 wt %). The presence of quartz in the subsolidus assemblage of the wet eclogite, suggests that the silica contents of melts from even lower degrees of melting will not exceed approximately 65 wt. percent, although the ratio of Si/(Ca + Mg + Fe) will continue to increase (Stern and Wyllie, 1978). Total alkalis increase until the liquid precipitates phengite near the solidus. The equilibrium fusion path for these low degrees of melting will be altered by the appearances of these minor phases.

The displacement of the equilibrium fusion curve of eclogite towards the silica apex for hydrous versus anhydrous conditions is also observed by Stern and Wyllie (1978). This difference is attributed to a shift in the position of quartz precipitation (i.e. silica over-saturation) to more siliceous liquids with increasing water content. This explanation suggests that because quartz precipitation effectively limits the maximum contents of SiO_2 in a melt, more siliceous liquids will be derived by melting under hydrous versus anhydrous conditions. Comparison of the calculated liquids representing similar degrees of melting from the two different conditions, strengthens this hypothesis. It is important however, to stress that this reasoning is based upon observations made on the calc-alkaline basalt-andesite-rhyolite system, which may be inappropriate for the system represented by the equilibrium fusion curve of eclogite. Until additional information is available, predictions on what the maximum SiO_2 contents of melts from eclogite would be, are at best, tenuous estimates. In a similar sense, the presence of phengite and rutile in hydrous eclogite poses severe problems in the estimation of initial melts from liquid trends observed at higher temperatures.

In general, the calculated liquids from the melting of DG-1 + 1.5 wt. percent H_2O (normalized to H_2O - free compositions) are similar to those calculated by Stern and Wyllie (1978) for 'wet' DW-1. Differences are observed in absolute contents of FeO, MgO, and Na_2O at particular SiO_2 values, and may be related to differences in bulk composition, phase compositions or melting model. The variations in the abundances of these elements with degree of melting are comparable. CaO contents are high in both sets of liquids at all degrees of melting. A major discrepancy is the abundance of Al_2O_3 in all liquids. Al_2O_3 is extremely high ($\sim$ 22 wt. %) in Stern and Wyllie's model and low (11-15 wt %) in this model. Differences in the assessment of kyanite and CaTs component of the clinopyroxene are possible causes for the discrepancy.

In summary, the equilibrium melting of hydrous eclogite results in liquids which deviate significantly from the calc-alkaline basalt-andesite-rhyolite association. Liquids from high degrees of melting are approximately olivine tholeiites and at low degrees, calcium enriched 'dacites'. Andesitic compositions, higher in CaO, FeO and MgO than typical calc-alkaline andesites, are generated by approximately 20 percent partial melting of DG-1 + 1.5 wt. percent H_2O. These liquids are part of a continuous melting curve, and do not mark any change in the fusion of eclogite. The presence of H_2O lowers the temperature of melting, expands the melting interval and stabilizes minor phases. The composition of liquids formed at low degrees of melting depends upon the, as yet, unquantified behaviour of these phases.

Fractional Fusion of Eclogite - Helz (1976) studied the melting relations of amphibolite and carefully considered the differences between equilibrium fusion and fractional fusion. These differences

were quantified with respect to fractional fusion, by calculating a series of melt increments using the relationship:

$$\Delta \text{ element} = A_1X_1 - A_2X_2.$$

A_1 and A_2 are the weight percentages of glass (i.e. % melt) and X_1 and X_2 are the weight percentages of a particular element in the liquid. The subscripts 1 and 2 refer to high and low temperatures respectively. These melt increments are positive in sign, and when normalized, are equivalent to the liquids generated by fractional fusion. This procedure can also be applied to observe changes in mineral composition and detect possible reaction relationships. A more detailed discussion of this treatment and its implications is given by Helz (1976).

The results of fractional fusion of eclogite can be treated in a similar fashion. Melt increments are calculated for both anhydrous and hydrous melting, and are presented, along with their normalized liquid compositions and corresponding CIPW norms in Table 9. The first episode of fractional fusion is equivalent to the equilibrium liquid calculated for the same temperature interval. Successive fractional fusion events are presented only for the smallest temperature increase (i.e. anhydrous, 1458° - 1464°; 1464° - 1472°; 1472° - 1500°; 1500° - 1525°) and not for larger temperature increases (e.g. 1472° - 1525°).

The variations observed in the liquid derived by fractional fusion of dry eclogite are extremely discontinuous, changing from olivine, hypersthene normative, to quartz normative and then to nepheline normative compositions with increasing degree of melting. This amount of change is unexpected and perhaps unrealistic. Examination of the mineral increments for clinopyroxene and garnet (not tabulated) does not indicate any reaction relationship between

TABLE 9: Fractional Fusion - melt increments normalized to 100% and CIPW norms for Anhydrous and Hydrous Partial Melting

	ANHYDROUS				HYDROUS		
	1525-1500	1500-1472	1472-1464	1464-1458	1260-1200	1200-1100	1100-1000
SiO_2	43.43	50.88	53.14	48.54	45.91	47.93	42.85
TiO_2	1.27	1.67	2.56	2.59	1.33	1.56	4.28
Al_2O_3	17.14	15.24	18.71	21.22	17.0	14.82	25.57
FeO	16.04	14.17	10.92	11.75	12.24	12.43	13.57
MgO	8.77	4.83	2.05	2.87	8.91	7.87	7.14
CaO	10.69	9.8	8.77	10.15	12.08	11.95	4.42
Na_2O	2.65	3.4	3.84	2.87	2.51	3.43	2.14
CIPW NORMS							
Qtz	-	-	3.84	-	-	-	2.16
Ab	10.0	28.77	32.50	24.29	14.36	19.41	18.11
An	34.88	26.32	33.82	45.02	35.13	25.04	21.93
Ne	6.73	-	-	-	3.73	5.21	-
Di	15.14	18.86	8.32	4.55	20.47	28.37	-
Hy	-	14.34	16.66	18.48	-	-	35.64
Ol	30.84	8.53	-	2.74	23.79	19.01	-
Il	2.41	3.17	4.86	4.92	2.53	2.96	8.13
C	-	-	-	-	-	-	14.02

these phases and the liquid, thus eliminating this solution as a possible explanation. These changes can be explained if a small amount of quartz is present in the residue of the 1458° liquid. Less than 1 percent quartz would reduce the SiO_2 content of this liquid such that the melt increment between 1458° and 1464° would become quartz normative. The progression of liquid composition with increasing fractional fusion would be quartz normative to hypersthene, olivine normative to nepheline normative. This trend, while systematic, would still be discontinuous.

A similar treatment of the equilibrium liquids calculated from the hydrous data is valid only if H_2O is present. The anhydrous melting of these residues will be different from the hydrous melting. The initial (equilibrium) melt of 'wet' DG-1 is highly quartz normative and its removal from the bulk, makes the residue more alkalic. Melts from these new bulk compositions (fractional fusion) are silica-undersaturated, nepheline normative compositions similar to alkali olivine basalt (1100° - 1200°; 1200° - 1260°). The quartz, corundum normative composition of the melting interval 1000° - 1100° is, as discussed previously, an effect of kyanite. The mineral increments calculated for the garnet and clinopyroxene do not suggest reaction relationships with the liquid. These conclusions are, of course, not applicable to temperatures below 1000°C where such reactions may be expected with the melting of phengite.

GEOLOGICAL APPLICATIONS

These data and their interpretation can be used to examine the consequences of eclogite melting with respect to several geological phenomena. Foremost among these is the identification of the contribution via partial melting, of the subducted oceanic lithosphere

to the growth of an island arc. Another concerns the fate of the residual eclogite, its possible relation to eclogite nodules in kimberlite hosts and implications for the evolution of the crust and mantle. Finally, and much more speculative, is the possibility of eclogite melting at low pressures typical of the lower crust with respect to the origin of some anorogenic silicic magmas.

The results of this study confirm and extend the basic conclusion of Stern and Wyllie (1973, 1978) that the equilibrium partial melting of hydrous eclogite (olivine tholeiite composition) does not produce calc-alkaline basalts - andesites - dacites. Implicit in this conclusion is the refutation of the single-stage eclogite melting hypothesis for the generation of primary andesite. This hypothesis has been replaced by more complicated multi-stage scenarios in which melts from the subducted oceanic lithosphere react with the overlying peridotitic mantle which is then remelted (Nicholls and Ringwood, 1973; Ringwood, 1975, 1977; Kay, 1977; Thorpe et al., 1976). As shown by Green (1976) and Takahashi et al., (1981) melts from 'wet' peridotite are basaltic or boninitic and not andesitic in composition.

As a consequence of these complexities, the contribution of the subducted slab to island arc volcanism is difficult to identify from examination of the chemical characteristics of the erupted magmas. It is important therefore to examine what the possible products of eclogite fusion are at high pressure as one constraint on these multi-stage hypotheses.

Subduction and Eclogite Fusion - There are numerous models of the thermal characteristics of subduction zones which vary with respect to their different boundary conditions. Angle and rate of subduction, age and temperature of the subducted slab, initial geothermal gradient of the mantle, frictional heating and dehydration reactions of the

slab are some of these parameters (Anderson et al., 1978; Sydora et al., 1978; DeLong et al., 1979). A common characteristic of all of these models is their exclusion of eclogite and peridotite fusion under anhydrous conditions. The solidi of these rocks are considerably higher than the temperatures encountered in the subduction environment (Fig. 11). It is also noted that the various thermal models differ on whether or not eclogite partial melting is possible under hydrous conditions. For the sake of this discussion, it is assumed that the thermal gradient of the subduction zone is such that partial melting of 'wet' eclogite does occur.

The amount of water present in the eclogite is critical to its melting behaviour. Robertson and Wyllie (1971) defined four types of subsolidus assemblages in silicate-water systems ranging from hydrous to water-excess conditions. Their terminology for these four types (Type I - IV) is used in the following discussion on the partial melting of 'wet' eclogite and is summarized in Table 10 and Figure 12.

DG-1 + 1.5 wt. percent H_2O, which contains subsolidus phengite and vapor represents a Type III water-deficient/vapor-present system. The solidus temperature reported for these conditions is not lowered by the addition of more water, however the melting interval is reduced. Most realistic models of hydrous melting are Type III or Type II (water deficient/vapor absent) with H_2O contents similar to the present experiments being maximum values. A Type II system would contain a hydrous phase in the subsolidus and because vapor is absent, would begin to melt only when that phase reached its maximum thermal stability. The hydrous phase in a Type II system may dehydrate at a temperature above the solidus of Type III, thus raising the solidus temperature compared to 'wet' rock. The phase relations of hydrous DG-1 possibly represent such a system if phengite is stable in H_2O-

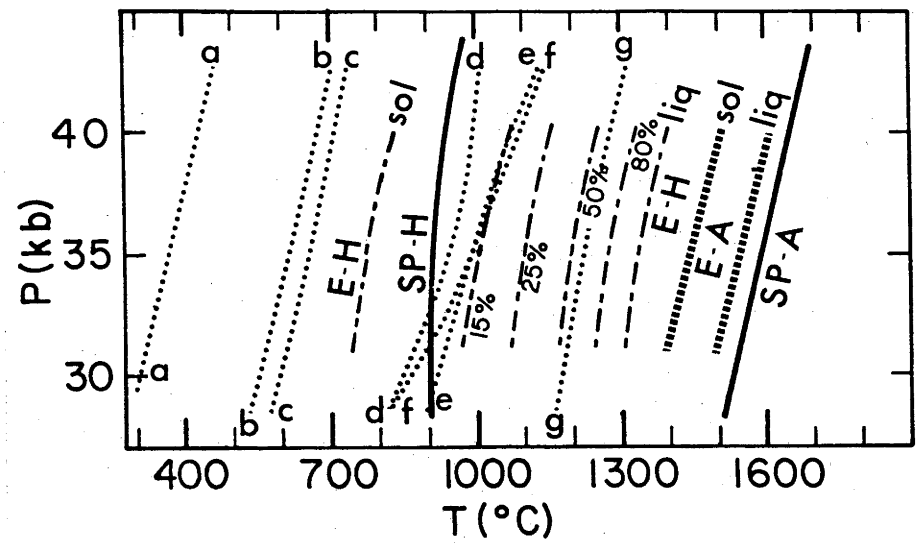

Figure 11: P/T projection of the solidus of spinel (garnet) peridotite under anhydrous (SP-A) and hydrous (SP-H) conditions compared with solidus and liquidus of eclogite, DG-1, under hydrous (1.5 wt. % H_2O) (E-H) and anhydrous (E-A) conditions. Percentages of melting (dot-dash lines) are given for the eclogite. Lines a-g are various mantle geotherms:

(a) Subduction, leading edge (Anderson et al., 1978),

(b) Subduction, leading edge (Schubert et al., 1975),

(c) Subduction, leading edge (Toksöz et al., 1971),

(d) Subduction, leading edge (Hasebe et al., 1970),

(e) Lesotho, continental (Carswell and Gibb, 1980),

(f) Subduction, leading edge (Toksöz et al., 1971), and

(g) Oceanic (Clark and Ringwood, 1964).

Spinel peridotite data from Kushiro et al., (1968).

Table 10. Summary of Robertson and Wyllie (1971) Terminology for Silicate-Water Systems

Type I - water absent. An assemblage of anhydrous silicate minerals with no vapor phase.

Type II - water-deficient and vapor-absent. An assemblage of silicate minerals which must include hydrous minerals but no vapor phase.

Type III - water-deficient and vapor-present. An assemblage of silicate minerals with or without hydrous minerals and with vapor phase. There is insufficient water present to saturate the liquid when the crystalline assemblage is completely melted at the existing pressure.

Type IV - water-excess. An assemblage of silicate minerals with or without hydrous minerals and with at least enough water to saturate the liquid when the crystalline assemblage is completely melted at the existing pressure. A vapor phase is present.

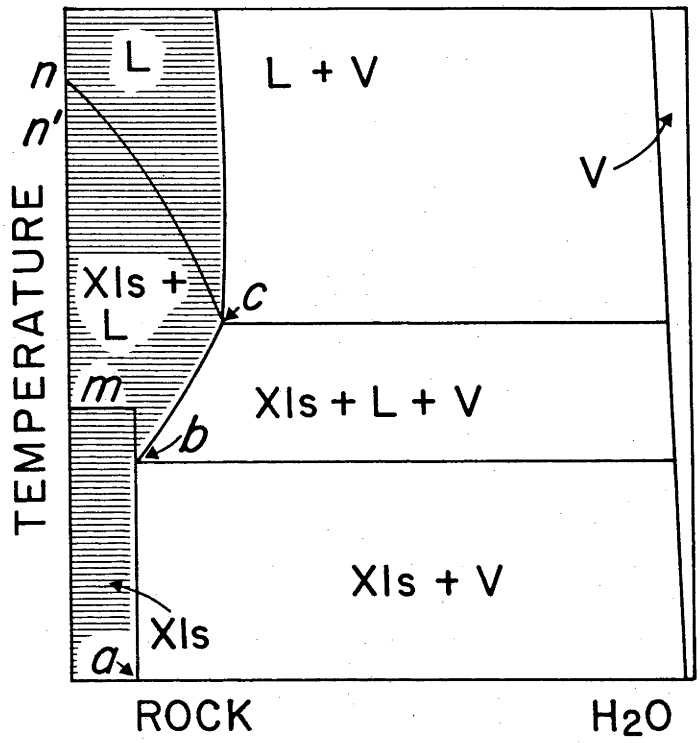

Figure 12: Schematic isobaric temperature-composition sections for silicate-water systems, in weight percent. Shaded areas are vapor-absent. System shown is one in which a hydrous mineral dehydrates at a temperature (m) above that of the solidus (b). Type II assemblages contain less water than a. Type IV assemblages contain more water than c, and Type III assemblages are intermediate between a and c. The anhydrous (Type I assemblage) solidus and liquidus are n' and n. (Diagram and explanation after Robertson and Wyllie, 1971).

deficient/vapor-absent conditions to temperatures in excess of 800° (at 35 kbar).

The initial liquids produced upon partial melting of this variation of a Type II system and that of a Type III system will be different. A Type II liquid will be H_2O-undersaturated while a Type III will be H_2O-saturated. A hydrous phase, such as phengite may be present above the solidus in a Type III system, and consequently influence the composition of that liquid. There is no 'a-priori' reason to choose one system over the other as the most likely representation of the subducted slab. The availability of H_2O in the subducted lithosphere at pressures beyond the stability of amphibole has been and is the subject of much study (see Chapter 3 for a discussion of this problem). No definite conclusion has been reached on the presence of H_2O let alone on the actual amounts in the eclogite slab.

The amount of H_2O is also critical because it directly affects the degree of partial melting which can occur at a particular temperature. The experiments on DG-1+1.5 wt. percent H_2O indicate that the amount of liquid produced in the first 200°C increase in temperature is approximately 15 percent. In systems which contain less H_2O, there is a reduction in the amount of melting which occurs. With regards to the thermal characteristics of even the most favorable subduction zone models, it appears that only small degrees of melting, probably < 15 percent are likely (Fig 11). The inability of the present experimental and analytical techniques to unambiguously define the chemical compositions of liquids generated by such small degrees of melting precludes an accurate and realistic assessment of the contribution from the slab.

The details of the equilibrium melting products of hydrous DG-1 and their limited extrapolation to lower degrees of melting has already been discussed. Liquids generated between the quartz-out and phengite-out phase boundaries will be enriched in CaO, SiO_2, the alkalis and H_2O, but depleted in FeO, MgO and TiO_2. The injection of this melt into the overlying hotter peridotitic mantle results in the formation of clinopyroxene and phlogopite at the expense of olivine and orthopyroxene (Sekine, 1981). The scale of this reaction is dependant upon the relative amounts of melt and mantle involved. Moderate degrees of partial melting from this mantle would produce silica-saturated basalts with slightly higher Na_2O and K_2O contents than melts resulting from similar degrees of melting of unaltered mantle. The experimental documentation of these reactions and their effect on the partial melting of peridotite is a complex problem and beyond the scope of this research.

The trace element characteristics of melts from the subducted slab are important in assessing the contribution of the slab to island arc volcanism. In particular, emphasis is placed on the highly incompatible elements, K, Ba, Rb, Cs, Sr, and especially the rare earth elements (REE's). Calculation of these characteristics using partial melting models is dependant upon many different factors (Gill, 1978; Apted, 1981) however, some general patterns are apparent. K, Ba, Rb, and Cs will be highly enriched in the melt unless mica is a residual phase. REE's will exhibit a LREE-enriched, HREE-depleted chondrite-normalized pattern due primarily to the partitioning behaviour of garnet.

Apted (1981) evaluated some of the effects which differences in initial composition, modal proportions and melting mode might have on these REE characteristics. His results, in which the LREE/HREE ratio

is decreased by an arbitrary choice of partition coefficients and garnet/clinopyroxene ratio, are used to support the derivation of 'proto-andesite' (?) by partial melting of the subducted slab. This conclusion is not consistent with the results of the present study which demonstrates that andesites can not be partial melts of eclogite. It is important that any solution on the contribution of the slab to island arc volcanism be consistent with all geochemical parameters.

The effects of low-temperature hydrothermal alteration and low-pressure metamorphism of the oceanic crust (Humphris and Thompson, 1978; Cann, 1979) on the high-pressure phase equilibria of the subducted slab can not be assessed from the present data. Green (1981a,b) suggests that many minor phases, such as sphene, zoisite, rutile, and mica will be present in the eclogite paragenesis of altered oceanic crust (see also Chapters 3 and 4). Apted (1981) also speculates on the effects of alteration at high pressures, suggesting that Na-enrichment (spilitization) will result in a higher omphacite/garnet ratio. These ideas can only be evaluated by additional research.

So far this discussion has emphasized the potential relationship of eclogite partial melting to the genesis of the calc-alkaline island arc volcanic association. This relationship, if it exists, is difficult to identify. Are partial melts from hydrous eclogite observed anywhere in the island arc environment? Table 11 compares the compositions of some eclogites from Hispaniola with the calculated melts from DG-1 + 1.5 wt. percent H_2O. These eclogites occur as discrete bodies within a serpentinite mass. Although they show signs of retrograde metamorphism, cores of garnet and omphacite indicate high pressure, moderate temperature origins. REE data from these

TABLE 11: Hispaniola Eclogites (Perfit et al., in prep.)

	R548	R746	R750	R751
SiO_2	53.21	48.91	58.04	53.06
TiO_2	1.24	2.57	.54	.53
Al_2O_3	11.04	17.42	14.88	15.77
FeO	7.02	14.37	6.94	8.49
MnO	.13	.32	--	--
MgO	7.33	4.47	7.57	8.99
CaO	14.70	7.77	6.26	7.30
Na_2O	5.41	1.95	3.45	5.23
K_2O	--	1.62	2.32	.64
P_2O_5	--	.61	--	--
CIPW NORMS				
Qtz	--	--	1.76	--
Or	--	9.57	13.71	3.72
Ab	22.85	16.49	29.19	36.69
An	5.83	33.98	18.26	17.69
Ne	12.40	--	--	4.10
Di	54.48	.48	10.43	15.12
Hy	--	31.79	25.62	--
Ol	1.98	1.36	--	21.67
Il	2.35	4.88	1.03	1.01
Ap	--	1.44	--	--

eclogites show strongly LREE fractionated patterns, which in addition to other geochemical data, makes their origins problematical (Perfit et al., in prep.) The striking resemblance of the major element compositions of these eclogites to the calculated melts of hydrous eclogite and their REE abundances, suggest that these eclogites may be melts from the subducted slab. These melts subsequently crystallized at high pressures and were brought to the surface relatively rapidly in serpentinite diapirs. Much more data, experimental and geochemical,are needed to support these speculations.

Eclogites, Kimberlites, Crust-Mantle Evolution - Assuming that the subducted oceanic lithosphere does melt (even if these melts are not observed), it is worthwhile to examine the effects of melt removal on the bulk chemistry of the residual eclogite. The composition of this residue is important in evaluating the role of eclogite in the mantle. It has implications for the origins of some eclogites in kimberlites and on a larger scale, the evolution of the crust-mantle system.

The compositions of the calculated residues from the hydrous melting of DG-1 and their CIPW norms are presented in Table 12. Also given in this table are the compositions and norms of several eclogitic nodules from kimberlite intrusions which are chemically similar to these residues. The similarities in composition between the residues and these eclogites may be coincidental, but alternatively may reflect a genetic relationship between the two. The suggestion that such bimineralic eclogites may be crystalline residues developed in contact with a liquid is not new (O'Hara et al., 1975, Ringwood, 1975) however it has not been pursued with respect to slab subduction. Differences are noted between the compositions of the omphacites and garnets (Figs. 13 and 14). These may be an effect of

TABLE 12: Comparison of DG-1 Calculated Eclogitic Residues with Eclogite Nodules From Kimberlites

	1260	1200	1100	1000	O-166[1]	M-180[1]	M-52[1]	M-33[1]	VP37079[2]
SiO_2	44.61	45.78	46.52	46.35	44.51	46.64	46.27	44.19	45.62
TiO_2	.54	1.19	1.30	1.53	.15	.10	.75	.49	.72
Al_2O_3	16.84	16.94	16.31	16.99	15.43	15.21	11.13	16.27	13.45
FeO	11.01	11.99	12.07	12.14	19.00	12.21	9.49	10.03	12.03
MgO	11.77	9.39	8.92	8.74	14.68	11.25	13.66	13.96	10.23
CaO	14.03	12.42	12.25	11.64	11.96	8.70	11.02	10.96	15.52
Na_2O	1.21	2.29	2.63	2.59	1.46	1.92	2.67	1.61	1.14
K_2O	--	--	--	--	.08	1.56	.28	.32	.09
CIPW NORMS									
Cor	--	--	--	--	.49	9.45	1.74	1.13	.54
Ab	4.73	12.95	15.27	17.15	8.28	14.44	15.11	8.71	5.21
An	40.51	35.94	32.70	34.74	36.30	28.97	18.44	37.03	31.70
Ne	2.98	3.48	3.79	2.59	2.39	1.19	4.67	2.83	2.47
Di	23.78	21.13	23.15	18.98	19.93	12.52	31.52	15.03	38.00
Ol	27.01	24.23	22.63	23.64	32.31	33.22	27.02	33.53	20.70
Il	1.03	2.26	2.47	2.91	.29	.19	1.50	.95	1.38
Hy	--	--	--	--	--	--	--	--	--

(1) Sobolev, N.V. (1977)
(2) O'Hara et al. (1975)

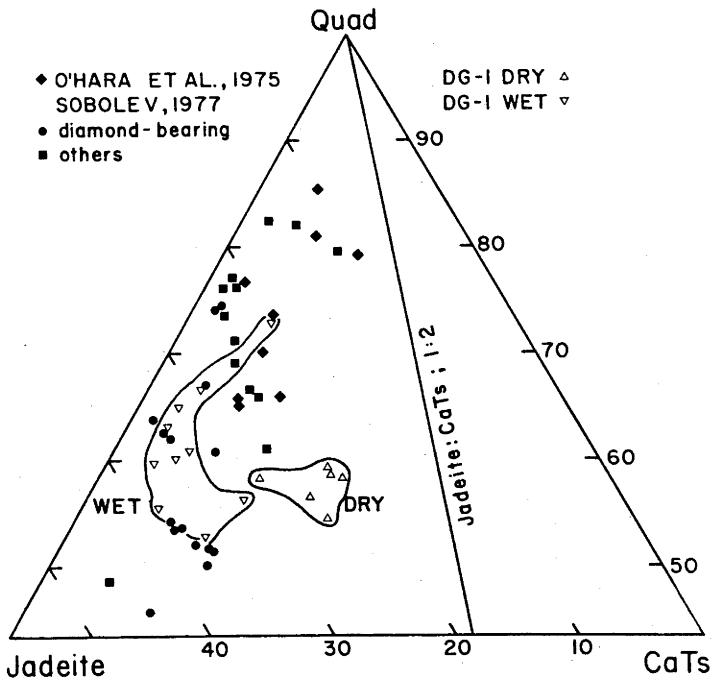

Figure 13: Omphacites from DG-1 experiments compared with omphacites from eclogite xenoliths in kimberlite hosts. Jadeite : CaTs (1:2) is proposed division of eclogite and mafic granulite clinopyroxene (White, 1964).

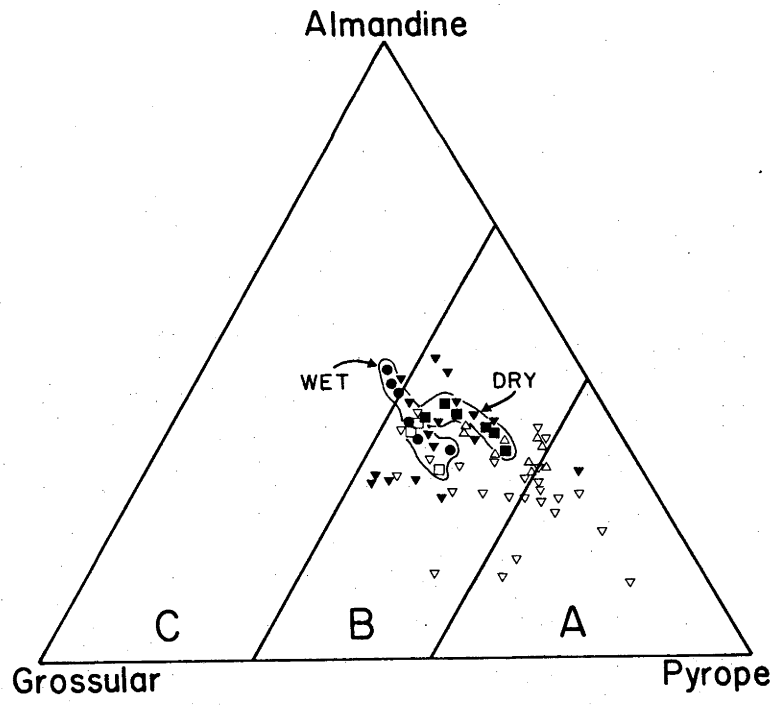

Figure 14: Garnets from DG-1 experiments (● ; ■) compared with garnets from eclogite xenoliths in kimberlite hosts. (▽); (▼) - diamond-bearing, Sobolev (1977), (△), O'Hara et al., (1975).

higher pressure. Further high pressure experiments (50 to 100 kbar) are needed to evaluate this suggestion in detail.

Most models for the evolution of the crust-mantle system assume that the subducted lithosphere melts extensively and provides a significant contribution to the crust via island arc volcanism (e.g. Ringwood, 1975). The resulting eclogitic residue is irreversibly differentiated and sinks to great depths ($\leq$ 700 km) in the mantle. Because of its residual character and high solidus temperatures, it can not be involved in any additional magmatic process. This process continually depletes the mantle in a multitude of incompatible elements.

The melting experiments on DG-1 + 1.5 wt. percent H_2O indicate that for geologically reasonable fluid contents, the amount of melting which will occur in the slab during subduction is quite small. The anhydrous, eclogitic residue will consequently be left with significant contents of SiO_2, Na_2O, TiO_2 and FeO. This residue will not melt again in the subduction regime unless a fluid phase is reintroduced, a possibility limited to pressures < 40 kbar (Delany and Helgeson, 1978). Thus, subduction may represent a mechanism by which the mantle is continually supplied with fertile material.

The involvement of this material (i.e. residual eclogite) in other magmatic processes not related to subduction is a complex issue. The solidi of these residual eclogites with respect to the solidus of peridotite is a crucial factor in assessing this problem. Comparison of the anhydrous solidus and liquidus of DG-1 with the peridotite solidus indicates that the eclogite will be completely melted before the peridotite begins to melt (Fig. 11). The extrapolation of these data to interpret the melting behaviour of eclogites depleted by a previous hydrous melting event is highly speculative, but nonetheless,

suggests that for eclogites which are only mildly depleted (e.g. < 15% previous melting), they too will begin to melt before the peridotite does (cf. O'Hara and Yoder, 1967). The results of the fractional fusion calculations (Table 9) suggest that the partial melts of the residual eclogites will be basaltic in composition. Such melting may be important in the generation of some basalts.

Eclogite Fusion At Low Pressure - Anorogenic 'Andesites' - An entirely different and more tenuous application of the results from this experimental study to geological phenomena concerns the origins of anorogenic calc-alkaline to alkaline silicic magmas. Petrologic and geochemical investigations of these magmas are not numerous possibly because of their limited occurrence (see Chapter 6), compared to the voluminous quantities of orogenic magmas. However, they may be the best candidates of primary 'andesitic' melts because of their tectonic setting in regions of thick continental crust. The partial melting of eclogite may be significant in the derivation of these magmas.

The extrapolation of the high pressure (35 kbar) data of this study to the lower pressures (15-20 kbar) typical of the continental lower crust is complicated by many unknown factors. The most important of these is amount of H_2O present in the crust prior to and during a melting event. Amphibolite is stable relative to eclogite at these pressures in Type III and IV systems (H_2O-deficient/vapor-present and H_2O-excess) (Essene, et al., 1970; Lambert and Wyllie, 1972). Decreases in fH_2O causes a reduction in the stability field of amphibole in basalt (Allen and Boettcher, 1978) such that hydrous eclogite may be stable at pressures as low as 15kbar. If the conditions correspond to a Type II system (H_2O-deficient/vapor absent), the resulting rock will be an amphibole-bearing eclogite. As discussed previously, the solidus temperatures

of Type II versus Type III and Type IV may be different with the Type II being greater and corresponding to the breakdown of amphibole. This difference may be significant (200°?) although the data necessary to document it is unavailable. The solidus temperatures of Type III and Type IV systems are identical and for basaltic composition are at approximately 700°C (15 kbar; Essene et al., 1970). These temperatures are easily exceeded in the lower crust in regions of moderate to high heat flow. Thus, the potential for melting may be realized, but whether the source is amphibolite or eclogite depends upon the water content.

Assuming that the source is eclogite, what are the characteristics of its partial melts? Decreasing pressure on a closed system, readjusts the Fe/Mg values of garnet and clinopyroxene, increases the amount of clinopyroxene to garnet and decreases the jadeite content of the clinopyroxene (Råheim and Green, 1974; Green 1972). The effects of these changes on the compositions of melts and the resulting equilibrium fusion path are unknown. It is suggested that these liquids will not be significantly different from those produced at higher pressures, except that the CaO content may be reduced as a result of the higher clinopyroxene/garnet ratio. Calc-alkaline magmas will not be produced, however their alkalic equivalents (trachyandesite, latite) may be (Arculus and Smith, 1979; Appendix 9).

SUMMARY

The equilibrium fusion paths for anhydrous and hydrous eclogite are calculated by mass balance using analyzed garnet and clinopyroxene from experiments at 35 kbar on an olivine tholeiite. These results

indicate that calc-alkaline andesites and dacites are not derived by the partial melting of eclogite.

Liquids generated by small degrees of melting are quartz normative and enriched in calcium, sodium, and potassium. Phengite is identified as a subsolidus and possibly a hypersolidus phase in hydrous eclogite and is important in determining the composition of the initial melts. Bulk composition of the eclogite has a significant effect on the subsolidus mineralogy of the eclogite and on the character of the melts.

Fractional fusion of hydrous eclogite is investigated using the melt interval approach developed by Helz (1976). The compositions of the melts generated by this process are hypersthene to nepheline normative basalts. If current thermal models of subduction zones are correct, then the likely water contents of the subducted slab restrict the degree of melting of hydrous subducted oceanic crust to < 15 percent. These melts may either react with the peridotite mantle or crystallize at depth. Because melting is limited, the residual eclogite is capable of producing additional melts (basalts) if rehydrated. The subduction process, instead of representing an irreversible differentiation of the mantle, may enrich the mantle directly via melts, or indirectly via fertile eclogite.

Similarities between the calculated eclogitic residues of this study and some eclogite nodules in kimberlite hosts suggests that pieces of the subducted slab may reappear at the surface. More information is required to understand the ultimate fate of subducted lithosphere in the mantle.

Partial melting of eclogite at low pressures may also be important in the petrogenesis of anorogenic trachyandesite-latite silicic suites which occur in areas characterized by thick continental crust.

CHAPTER 3

THE HIGH PRESSURE STABILITY OF ZOISITE: RESULTS FROM EXPERIMENTS ON THE JOINS DIOPSIDE-ZOISITE AND ENSTATITE-ZOISITE

INTRODUCTION

The presence of a fluid phase, consisting primarily of water, is an important component of contemporary hypotheses relating the genesis of the 'orogenic volcanic series' to subduction. Present concepts of the thermal characteristics of subduction zones (e.g. Anderson et al., 1978) preclude partial melting of peridotite or eclogite, unless their solidi are lowered by the addition of water, as likely sources for the magmas of this series. Also important are the properties of water as a solvent at high pressures and temperatures and its reputed mobility within the mantle. These properties have been utilized to explain a variety of geochemical anomalies associated with the 'orogenic volcanic series' (Kay, 1980; Mysen, 1979; Hawkesworth et al., 1979). The ultimate origin of this water, whether it is juvenile or 'recycled' seawater carried down to great depths by hydrous phases in the subducted oceanic lithosphere, is open to question (Arculus, 1981). Many candidates have been nominated as potential sources of water in the subducted slab and include talc, zoisite or other epidote minerals, serpentines (Nicholls and Ringwood, 1973), amphiboles (Allen and Boettcher, 1978) humites (McGetchin et al., 1970), biotites (Allen et al., 1972; Beswick, 1976a) initially present in the oceanic crust (Cann; 1979, Humphris and Thompson, 1978) or at higher pressures, dense hydrated magnesium silicates (Ringwood, 1977; Akimoto, 1977). It is desirable to know, therefore, the stabilities of these various

hydrous phases with respect to the pressure and temperature gradients found in subduction zone regimes.

This chapter presents the results of an experimental study on the stability of one of these hydrous phases, zoisite, at high pressures and temperatures, in the simple systems of diopside-zoisite and enstatite-zoisite. These joins constitute a portion of the boundaries of the simple basaltic system represented by the components CaO-MgO-Al_2O_3-SiO_2-H_2O (CMASH) (Fig. 1).

There exists a body of experimental data on zoisite in the CaO-Al_2O_3-SiO_2-H_2O (CASH) system applicable to low pressure metamorphic reactions. Pistorius (1961) and Fyfe (1960) synthesized zoisite at moderate temperatures (500-700°C) up to pressures of 35 kbar to study the zoisite-clinozoisite phase boundary. This boundary, because of only slight density differences between these phases, is sensitive to very small changes in amounts of impurities in the system (e.g. iron). Newton (1965, 1966), Newton and Kennedy (1963), Pistorius et al., (1962), Winkler and Nitsch (1962), and Nitsch and Winkler (1965) investigated a number of univariant reactions within the CASH system. These studies established the locations of reactions involving zoisite, grossular, anorthite, quartz, lawsonite and wollastonite among others in pressure/temperature space. Their work, done primarily at pressures less than 20 kbar, was extended to higher pressures by Boettcher (1970). His work defined the maximum thermal stability of zoisite as represented by the reaction of zoisite $\rightleftharpoons$ anorthite + grossular + corundum + liquid at ~26kbar, 1185°C. At higher pressures in this system, this reaction is replaced by zoisite $\rightleftharpoons$ grossular + corundum + kyanite + liquid, although no experimental data were collected on this high-pressure reaction. Boettcher (1970) also

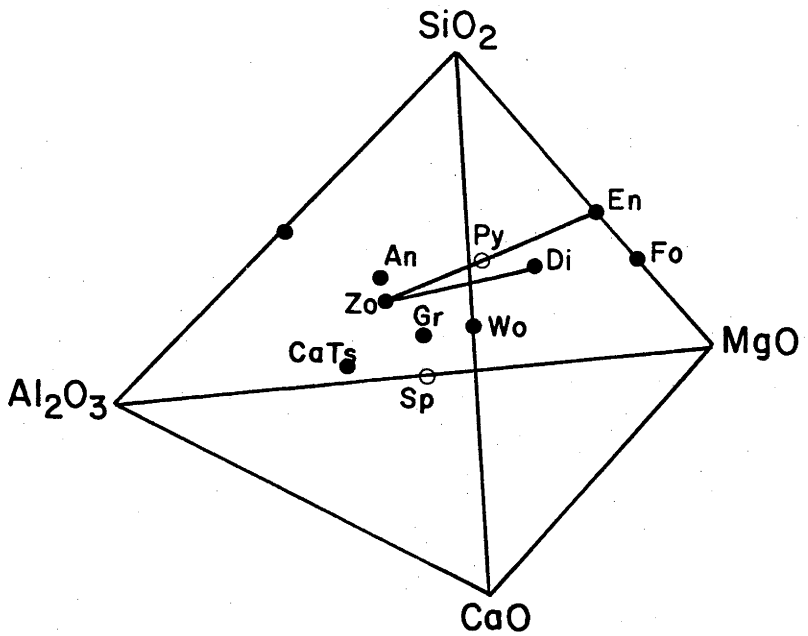

Figure 1: Zoisite - diopside and zoisite - enstatite joins projected in CMAS tetrahedron. Open circles are on the back face.

noted that in the presence of other phases, such as water, the solidus of zoisite is lowered by up to a maximum of ~400°C. Boettcher's results suggest that zoisite may have a considerable stability field at high pressure and temperatures in the CASH system.

Addition of iron to the CASH system was investigated by Holdaway (1972) who studied the stabilities of Al-Fe epidotes as a function of iron content and oxygen fugacity (fO_2). His work, at 3 kbars, indicates that the clinozoisite-epidote solid solution series ($Ca_2Al_3Si_3O_{12}OH$ - $Ca_2(Al,Fe^{3+})Al_2Si_3O_{12}OH$) is pseudo-binary and dependent upon bulk composition and fO_2 of the system. Low fO_2's, which lower the Fe^{3+}/Fe^{2+} ratio, favor the formation of aluminous epidotes (i.e. clinozoisite). Clinozoisite will invert to orthorhombic zoisite at temperatures >635±75°C and 3±1kbar (Holdaway, 1972).

Preliminary data on a model basaltic composition in the CMASH system identify zoisite as a hypersolidus phase at 30 kbar (Sekine, 1981). It coexists with liquid, garnet, clinopyroxene and coesite at temperatures 150°C above the solidus in a system containing 7.5 wt.% H_2O.

Zoisite has been observed as a hypersolidus phase (<800°C) over a range of pressures in experiments on hydrous mafic compositions (Lambert and Wyllie, 1972, Hellman and Green, 1979, K.L. Harris, unpublished data). Green (1981a) suggests that the maximum pressure stability of zoisite in these compositions is <25 kbar, although other researchers have reported the presence of zoisite in experiments at 30 kbar. Millhollen and Wyllie (1974) identified zoisite (solely on the basis of X-ray diffraction patterns), as a near-liquidus phase in experiments on a hornblende mylonite from St Paul's Rocks. In this highly undersaturated composition, equivalent to some basanites and nephelinites, zoisite is stable to 1100° - 1200°C and at least 30 kbar.

The common occurrence of zoisite in rocks of different compositions within a variety of metamorphic terranes (Game, 1954; Tilley, 1937, 1936; Harpum, 1954; Misch, 1964; Watson, 1942; Kushev, 1977; Liou and Ernst, 1979; Ernst, 1973; Ernst and Dal Piaz, 1978) illustrates the extent of zoisite stability in natural multicomponent systems.

METHODS

Starting Materials - The starting materials in these experiments were mixtures (molecular proportions) of synthetic diopside ($CaMgSi_2O_6$ or enstatite ($MgSiO_3$) and natural zoisite. Diopside and enstatite were made from 'spec-pure' oxides, sintered, fused and crystallized at one atmosphere. The purities of the synthesized minerals were checked by electron microprobe analysis and X-ray diffraction. Zoisite was separated from a zoisite amphibolite from Tanzania (courtesy of the Bureau of Mineral Resources, Canberra, A.C.T., Australia) by crushing and heavy liquid separation. It was handpicked to >99.9 percent purity and gently crushed to <20 μ-sized particles. The major element analysis of the zoisite, (Table 1) indicates that it is a low-ferrian variety (Fe_2O_3 < 2.5 wt.%) with a small Cr_2O_3 content.

Experimental Technique. Approximately 15 mg of the starting mixtures were sealed in Pt or AgPd capsules, after being dried in a 110°C oven to allow evaporation of absorbed water. All experiments were run under vapor-free conditions. The capsules, once sealed, were weighed to allow comparison with post-run weights as a check for capsule leakage. Experiments with significant deviations were repeated. The experiments at pressures <45 kbar were done in solid media piston-cylinder apparatus using the 'wet' 5/32" graphite furnace assembly (Essene et al., 1970). Experiments at higher pressures (45-60 kbar)

Table 1, Composition of Zoisite

SiO_2	39.38
Al_2O_3	32.50
Cr_2O_3	0.38
Fe_2O_3	1.56
CaO	24.46
H_2O[1]	1.72
TOTAL	100.00

Number of Ions per 13 (0,OH)

Si	3.002	
Al	2.920	
Cr^{3+}	0.023	3.032
Fe^{3+}	0.089	
Ca	1.998	
OH	0.874	

[1] Determination by LOI

were done using a high-pressure girdle device (Stromberg and Stephens, 1964). Additional details of experimental techniques are described in Appendix 1.

Run products were examined optically and by X-ray powder diffraction. Small chips of each sample were mounted and polished for electron microprobe analysis. An energy dispersive, Si(Li) detector (Reed and Ware, 1973, 1975) allowed accurate determination of garnet, zoisite, clinopyroxene, orthopyroxene, kyanite and glass compositions. Some results, especially those from the enstatite-zoisite experiments, were obtained primarily by microprobe analysis.

Optical Description of Phases -

Zoisite - stubby crystals, 10-20 μ in width, generally colourless to light blue, low birefringence, parallel extinction, R.I. > 1.70.

Diopside - stubby crystals, colourless, 10-50 μ, low birefringence, symmetrical extinction, R.I. <1.70.

Garnet - euhedral crystals, pale green, 5-10 μ, isotropic, inclusions of corundum and/or kyanite.

Enstatite - stubby crystals, colourless, 20-50 μ, low birefringence, parallel extinction, R.I. < 1.70.

Corundum - euhedral crystals, opaque, 1-3 μ, usually clumped together as inclusions in garnet.

Kyanite - prismatic needles, colourless, .5 μ in width, high birefringence, parallel extinction.

Glass - colourless R.I. < 1.6 vapour bubbles absent, quench clinopyroxene absent save for very high temperature near-liquidus runs, generally just 'wets' grain boundaries, but occasionally pools, 3-5 μ in diameter are observed.

RESULTS

The primary purpose of this study is to investigate the stability of zoisite at high pressure in the CMASH system as an indication of its behaviour in more complex basaltic compositions. In essence, this means locating the negative portion of its dP/dT stability curve - a phenomena exhibited by hydrous phases in response to changes in the volumetric properties of H_2O (Delany and Helgeson, 1978). During the course of this study it became apparent that the impurities in the natural zoisite used as a starting material (i.e. Fe_2O_3 and Cr_2O_3) had a more profound effect on the phase relations of the diopside-zoisite and enstatite-zoisite systems than anticipated. Univariant and divariant reactions become multivariant and invariant points become univariant lines. Although natural systems are more closely approximated, the 'simple' systems studied represent psuedo-binary joins within a more complex multi-component system. Results from a series of experiments on the diopside-zoisite join illustrate some of this complexity. Similar studies were not attempted for the enstatite-zoisite join. A summary of the experiments and the results for both systems is given in Table 2.

The results reported here were obtained from synthesis runs which varied in duration from 15 minutes to several days. Reversal runs were attempted, and were successful only at near-liquidus temperatures. Other experiments were not successfully reversed, possibly due to 1) existence of meta-stable phases (corundum), 2) slow reaction rates, 3) armouring of two or more phases (e.g. kyanite, corundum) by garnet, thus removing them from reaction, and 4) clino-pyroxene nucleation problems.

TABLE 2: Summary of Experiments on Diopside - Zoisite and Enstatite - Zoisite Systems

RUN	COMPOSITION			T(°C)	P(kb)	t(hr)	RESULTS
7333	Di	Zo	9:1	1150	35	6.5	Cpx, Gt^+, Ky, Co, L
7374	"	"	"	1000	35	92.5	Cpx^+, Gt, Co, L, Ky (?)
7411	Di:	Zo	6:4	1190	15	8.5	Cpx^+, Gt^+, Co, An, L^+
6920	"	"	"	1110	15	6.5	Cpx^+, Gt^+, Co, An, L
6882	"	"	"	1175	20	3.5	Cpx^+, Gt^+, Co, Ky, L
7381	"	"	"	1150	20	5	Cpx, Zo, Gt, Co, Ky, L
7287	"	"	"	1200	25	3.75	Cpx^+, Gt^+, Co, Ky, L
7289	"	"	"	1150	25	8.75	Cpx^+, Zo^+, Gt^+, Co, Ky, L^+
7288	"	"	"	1100	25	11.5	Cpx^+, Zo^+, Gt^+, Co, Ky, L
7292	"	"	"	1000	25	71	Cpx^+, Zo^+, Gt^+, Co
6910	"	"	"	1240	30	1	Cpx, Gt^+, Co, Ky, L
7403	"	"	"	1225	30	1	Cpx^+, Zo, Gt^+, Co, Ky, L^+
7297	"	"	"	1185	30	6	Cpx^+, Zo^+, Gt^+, Co, Ky, L
7318	"	"	"	1350	35	1	Cpx^+, Gt^+, Co, Ky, L^+
7298	"	"	"	1250	35	3	Cpx^+, Gt^+, Co, Ky, L^+
6912	"	"	"	1230	35	1.5	Cpx^+, Zo, Gt^+, Co, Ky, L^+
7291	"	"	"	1200	35	4	Cpx, Zo, Gt^+, Co, Ky, L
7293	"	"	"	1150	35	4	Cpx^+, Zo^+, Gt^+, Co, Ky, L
7375	"	"	"	1100	35	84	Cpx^+, Zo^+, Gt^+, Co, Ky, L
7384	"	"	"	1175	37.5	.5	Cpx^+, Zo, Gt^+, Co, Ky, L^+
8381	"	"	"	1250	40	1	Cpx, Gt^+, Co, Ky, L
7408	"	"	"	1235	40	.5	Cpx^+, Zo^+, Gt^+, Co, Ky, L^+
7393	"	"	"	1175	40	.25	Cpx^+, Zo^+, Gt^+, Co, Ky, L^+
HPG - 138	"	"	"	1205	45	1	Cpx^+, Gt^+, Co, Ky, L
7394	"	"	"	1200	45	.25	Cpx^+, Zo^+, Gt^+, Co, Ky, L^+
8384	"	"	"	1200	45	1	Cpx^+, Gt^+, Co, Ky, L
7385	"	"	"	1175	45	.25	Cpx^+, Zo^+, Gt^+, Co, Ky, L^+
HPG - 134	"	"	"	1200	49	1	Cpx^+, Gt^+, Co, Ky, L
HPG - 135	"	"	"	1100	49	1	Cpx^+, Zo^+, Gt^+, Co, Ky, L
HPG - 136	"	"	"	1150	51	1	Cpx^+, Zo^+, Gt^+, Co, Ky, L
HPG - 133	"	"	"	1200	52.5	1	Cpx^+, Gt^+, Co, Ky, L^+
HPG - 137	"	"	"	1150	56	1	Cpx^+, Gt^+, Co, Ky, L^+
HPG - 139	"	"	"	1075	56	1	Cpx^+, Zo, Gt^+, Co, Ky, L
HPG - 140	"	"	"	1075	59.5	1	Cpx, Gt, Co, Ky, L
7414	Di:	Zo	5.5: 4.5	1150	35	8.25	Cpx, Zo, Gt, Co, Ky, L

TABLE 2: Continued

RUN	COMPOSITION	T(°C)	P(kb)	t(hr)	RESULTS
7338	Di: Zo 5:5	1350	35	1	Gt^+, Co, Ky, L^+
7339	" " "	1250	35	2.5	Gt^+, Co, Ky, L^+
7341	" " "	1230	35	5	Gt^+, Zo^+, Co, Ky, L^+
7342	" " "	1150	35	7.5	Cpx^+, Zo^+, Gt^+, Co, Ky, L
7371	" " "	1000	35	102	Cpx^+, Zo^+, Gt^+, Co, Ky, L
7320	Di: Zo 4:6	1350	35	1	Gt, Co, Ky, L, Q
7319	" " "	1275	35	2	Gt^+, Zo^+, Co, Ky, L^+
7321	" " "	1225	35	3	Gt^+, Zo^+, Co, Ky, L^+
7332	" " "	1150	35	9.5	Cpx, Zo^+, Gt^+, Co, Ky, L^+
7312	Di: Zo 2:8	1425	35	1	Gt^+, Co, Ky, L^+, Q
7343	" " "	1350	35	2	Gt^+, Co, Ky, L^+
7303	" " "	1250	35	3	Gt^+, Zo^+, Co, Ky, L^+
7325	" " "	1200	35	3	Gt^+, Zo^+, Co, Ky, L^+
6866	" " "	1100	35	77	Gt^+, Zo^+, Co, Ky, L^+
7316	zoisite	1475	35	.75	Gt , Co, Ky, L, Q
7307	"	1400	35	1.5	Gt^+, Co, Ky, L
7305	"	1300	35	1	Gt^+, Co, Ky, L
7301	"	1250	35	2	Zo, Gt, Co, Ky, L
7299	"	1200	35	6	Zo, Gt^+, Co, Ky, L^+
7469	En: Zo 65:35	1100	15	4.5	Gt^+, L^+
8537	" " "	1050	15	6	Gt^+, L
7512	" " "	900	15	23	Gt, Cpx, Zo, Ky, L
7613	" " "	850	15	24	En, Zo^+, Gt(?)
7449	" " "	800	15	91	En^+, Zo^+
8210	" " "	650	15	91	En, Zo
7468	" " "	1200	25	5	Gt^+, L^+
8328	" " "	1100	25	9.5	Gt, Cpx, Zo, L
7445	" " "	1000	25	29	Gt^+, Cpx^+, Zo^+, L
7450	" " "	800	25	44	En^+, Zo^+
8618	" " "	900	30	7.5	Gt^+, Cpx^+, Zo^+, Ky,
7446	" " "	1000	35	24	Gt^+, Cpx^+, Zo^+, L
8623	" " "	850	35	12	Gt^+, Cpx^+, Zo^+, Ky,

+ analyzed by microprobe
Gt - garnet, Cpx - clinopyroxene, Zo - zoisite, En - enstatite, Co - corundum, Ky - kyanite, L - liquid, Q - quench

Diopside-Zoisite - The psuedo-binary phase diagram of the diopside-zoisite join (Fig. 2) represents one of the possible interpretations of the limited amount of data. Phase boundaries which are the most tightly constrained are indicated by solid lines. The solidus is difficult to determine and may be lower than indicated. It is marked by the appearance of liquid, grossular-rich garnet, and corundum. Zoisite and diopside coexist with this assemblage over a considerable temperature interval as a result of the multivariant nature of the reaction. Slight compositional changes in the garnet and liquid phases, (Table 3 and 4) support this interpretation. The maximum thermal stability of zoisite coexisting with diopside is marked by the point labeled A (Fig. 2) and is not expected to change with increasing amounts of diopside until the point (B) is reached at which all zoisite is consumed in the initial reaction. Thus, any composition between points A and B can be used to evaluate the maximum stability of zoisite with respect to pressure and temperature variations in a system which contains diopside.

The composition of 60 mole percent diopside - 40 mole percent zoisite was selected to investigate the effect of pressure on the stability of zoisite for two reasons. Firstly, the relatively large amount of zoisite aids in its detection after a majority of it has been consumed by the garnet-corundum-liquid reaction. Secondly, although the stability of zoisite in basaltic compositions is more realistically modeled by diopside-rich compositions such as between points B and C (Fig. 2), the presence of a liquid phase greatly enhances the attainment of equilibrium (Boettcher, 1970). This feature is much more important in the high pressure experiments where run times are limited by equipment constraints, than in the lower pressure experiments.

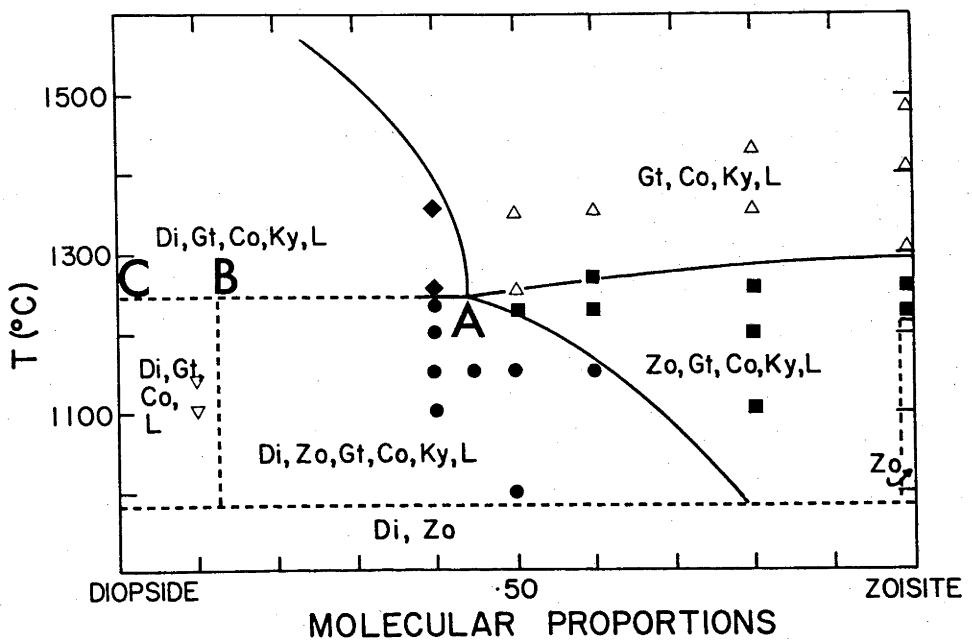

Figure 2: Phase diagram for the psuedo-binary zoisite - diopside join at 35 kbar. Phase boundaries which are most tightly constrained by the data are indicated by solid lines. The significance of points A, B, C are discussed in the text.

TABLE 3. Garnet Compositions: Averages of Microprobe Analyses.

	Di:Zo 9:1							Di:Zo 6:4							
RUN:	7333	7411	6920	6882	7287	7289	7288	7292	6910	7403	7297	7318	7298	6912	7291	7293
SiO_2	40.81	39.71	40.73	40.51	40.34	40.85	40.67	40.50	40.62	40.56	40.71	40.55	40.54	40.81	41.02	40.45
Al_2O_3	22.26	25.90	22.50	22.89	22.82	23.12	22.77	22.33	23.06	22.92	23.13	23.05	23.83	22.03	23.83	22.79
Cr_2O_3	0.38	0.33	0.39	0.23	0.30	0.36	0.35	0.64	0.35	0.21	0.32	0.29	0.25	0.18	0.23	0.27
FeO	0.65	0.94	1.00	1.41	1.31	0.95	1.08	0.62	1.47	1.40	1.15	1.33	0.96	1.13	1.03	1.35
MgO	4.47	7.47	2.89	3.51	4.79	4.33	3.95	2.75	5.86	5.91	6.07	6.16	6.02	6.55	6.99	5.88
CaO	31.39	25.61	32.51	31.46	30.33	30.83	31.67	33.32	28.33	28.59	28.93	28.91	28.69	28.28	27.48	29.00
Total	99.96	99.96	100.02	100.00	99.89	100.44	100.49	100.16	99.70	99.59	100.31	100.29	99.29	99.98	99.58	99.74

	Di:Zo 6:4														
RUN:	7375	7384	8381	7408	7393	HDG-138	7394	8384	7385	HPG-134	HPG-135	HPG-136	HPG-133	HPG-137	HPG-139
SiO_2	40.66	41.52	40.88	40.72	41.04	41.75	40.60	40.74	40.72	40.60	41.41	41.18	40.66	40.94	41.02
Al_2O_3	23.15	23.03	22.89	22.78	23.16	22.32	22.93	23.20	23.35	23.14	25.54	22.88	27.82	23.61	23.15
Cr_2O_3	0.26	-	-	0.23	0.20	-	0.25	-	0.27	-	-	-	-	-	-
FeO	1.56	1.05	1.28	1.32	1.10	1.06	1.28	1.06	1.33	1.24	1.41	1.28	1.20	1.17	1.09
MgO	6.16	7.52	6.39	6.68	7.33	7.34	6.54	7.55	5.97	7.06	3.78	6.44	3.75	6.95	6.93
CaO	28.52	26.56	28.57	27.79	27.08	27.53	28.02	27.45	27.92	27.88	26.69	28.60	26.54	27.58	27.82
Tot.	100.31	99.67	100.01	99.52	99.91	100.00	99.62	100.00	99.56	100.00	98.84	100.38	99.97	100.25	100.00

TABLE 3. cont'd.

	Di:Zo 5:5				Di:Zo 4:6					Di:Zo 2:8				Zoisite		
RUN:	7338	7339	7341	7342	7371	7319	7321	7332	7312	7343	7303	7325	6866	7307	7305	7299
SiO_2	41.03	40.91	40.73	40.63	40.97	40.70	40.79	40.96	39.78	40.31	40.80	40.63	40.17	40.25	39.21	39.52
Al_2O_3	23.04	23.28	23.38	23.16	23.09	23.12	23.32	23.21	22.84	23.02	23.18	23.52	22.81	22.76	22.37	33.76
Cr_2O_3	0.23	0.26	0.21	0.28	0.30	0.31	0.31	0.44	0.34	0.31	0.34	0.32	0.42	0.28	0.45	0.80
FeO	0.75	0.98	0.59	1.34	1.34	1.27	1.50	1.00	0.76	0.44	1.81	2.44	2.82	1.99	5.99	2.31
MgO	7.04	7.13	7.38	6.32	6.91	6.73	6.45	6.28	3.05	4.75	6.75	5.98	6.16	4.65	0.15	0.79
CaO	27.55	27.30	27.56	28.08	27.80	28.22	28.05	28.61	33.35	31.12	27.95	27.53	27.31	30.37	31.26	33.47
Total	99.69	99.86	99.85	99.81	100.41	100.35	100.42	100.50	100.12	99.95	100.83	100.42	99.69	100.30	99.43	99.64

	En:Zo 6.5:3.5						
RUN:	7469	8537	7468	7445	8618	7446	8623
SiO_2	40.44	43.78	42.49	43.43	43.69	44.06	42.74
Al_2O_3	50.35	21.88	24.16	23.79	23.42	22.51	24.22
Cr_2O_3	-	-	0.12	0.18	0.15	0.26	-
FeO	2.30	2.67	1.02	1.73	1.53	1.37	1.84
MgO	20.83	18.66	17.35	19.34	15.00	18.09	20.37
CaO	8.15	12.94	14.93	11.64	16.20	13.82	10.48
Tot.	100.00	99.93	100.07	100.11	99.99	100.11	99.65

TABLE 4. Liquid Compositions: Averages of Microprobe Analyses.

	Di:Zo 6:4										Di:Zo 5:5		
RUN:	7411	7403	7318	6912	7393	7384	7408	7394	7385	HPG-133	7388	7339	7341
SiO_2	49.59	55.40	60.24	62.53	61.11	61.23	61.51	62.40	58.21	63.15	55.97	60.53	60.90
Al_2O_3	20.08	16.60	13.97	12.34	11.83	12.02	11.94	10.78	12.25	9.42	17.57	15.53	14.35
Cr_2O_3	-	-	-	-	-	-	-	-	-	-	-	-	-
FeO	-	0.15	-	-	0.09	-	-	-	-	0.25	-	-	-
MgO	0.70	0.39	0.59	0.31	1.10	0.71	0.43	0.69	0.37	1.35	0.59	0.59	0.67
CaO	23.34	12.60	10.95	8.14	9.24	9.04	8.46	7.65	9.04	8.68	11.50	8.96	8.50
Total	93.71	85.14	85.75	83.32	83.37	83.00	82.34	81.52	79.87	82.85	85.63	85.61	84.42

	Di:Zo 4:6		Di:Zo 2:8					Zo	En:Zo 6.5:3.5	
RUN:	7319	7321	7312	7343	7303	7325	6866	7299	7469	7468
SiO_2	60.58	63.00	51.26	53.00	61.35	65.62	56.65	56.01	55.85	52.93
Al_2O_3	16.39	13.94	23.33	18.40	10.92	9.77	13.36	8.95	23.62	20.21
Cr_2O_3	-	-	-	-	-	-	-	-	-	-
FeO	-	-	-	-	-	0.10	0.72	0.57	-	-
MgO	0.62	0.77	0.42	1.79	1.37	0.98	1.53	-	3.53	3.79
CaO	9.63	8.89	12.44	14.40	9.16	7.74	11.21	13.54	9.49	14.11
Total	87.22	86.60	87.45	87.59	82.80	84.21	83.47	76.07	92.49	91.04

The results of this set of experiments indicate that zoisite is stable to pressure in excess of 60 kbar up to temperatures of approximately 1200°C (curve A, Fig. 3) in the paragenesis of zoisite, diopside, garnet, corundum, kyanite and liquid. As noted previously, the solidus of this system is difficult to detect, consequently its shape is suggested by analogy with other systems which involve a hydrous phase (e.g. amphibole/basalt). The solidus must intersect the zoisite-out boundary (curve A) at low and high pressures. Although no experiments were done to document the precise locations of these intersections, the presence of only minor amounts of liquid in the experiment at 59.5 kbar, 1075°C suggests that this run is near-solidus.

Enstatite-Zoisite - The stability of zoisite in the enstatite-zoisite system was briefly examined over a range of pressure and temperature in a series of reconnaissance experiments on a single enstatite-rich composition (65% En 35% Zo (molecular)). The detailed phase relations of the enstatite-zoisite were not determined, however it is assumed that they are broadly similar to the psuedo-binary diopside-zoisite join. The results of these experiments are schematically illustrated in Figure 4.Enstatite and zoisite coexist together as a stable sub-solidus assemblage to pressures of at least 35 kbar. The maximum thermal stability of zoisite in an enstatite-rich composition similar to basaltic compositions is coincident with the solidus of this system at which enstatite and zoisite react to produce garnet (60 - 80 mole % pyrope) and clinopyroxene (5-10 wt. % Al_2O_3 in solid solution kyanite and liquid. The solidus, approximately 850°C at 15 kbar, is essentially isothermal over the pressure range that was investigated and suggests the maximum pressure stability of zoisite in this system may be comparable to that observed in the diopside-zoisite system.

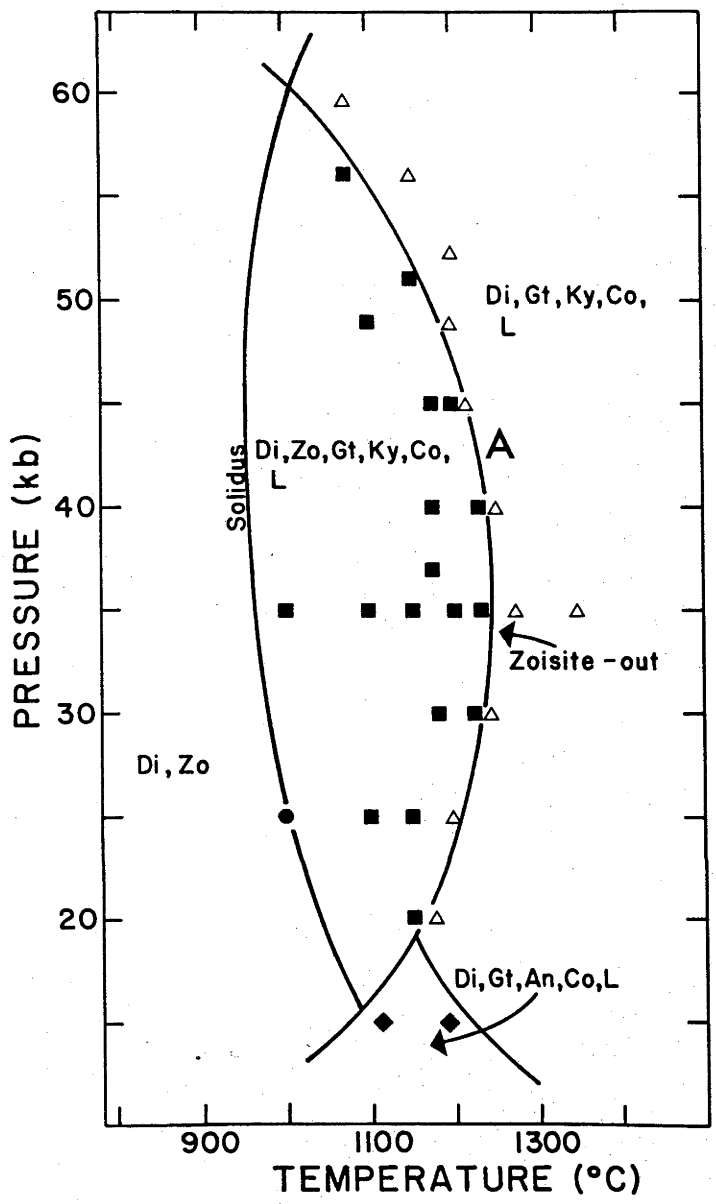

Figure 3: P/T projection of the phase relations Zoisite : Diopside (4:6, mole proportions). Curve A is the maximum stability of zoisite in a zoisite-rich system (see text for discussion).

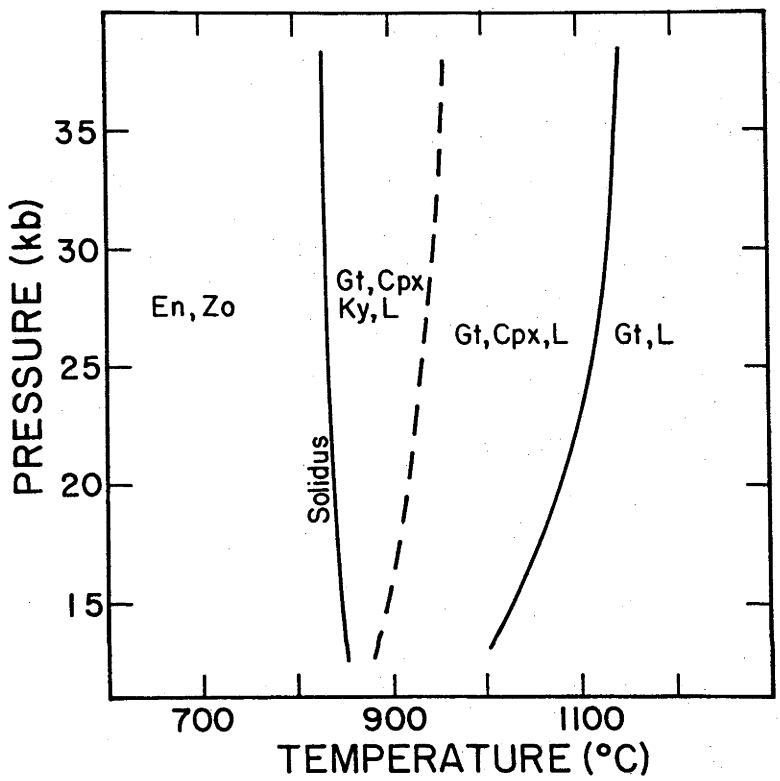

Figure 4: Schematic P/T projection of the phase relations and stability of zoisite in the Zoisite : Enstatite system for enstatite-rich compositions.

DISCUSSION

Occurrence of Zoisite in Subducted Lithosphere - The results of these experiments indicate that zoisite, a dense (3.36 g/cc) hydrated calcium aluminosilicate is stable to pressures approaching 60 kbar. These results also show that the maximum thermal stability of zoisite is dependent upon the bulk composition of the system. In diopside - or enstatite-rich systems whose compositions closely approximate a basalt, zoisite is stable only to the solidus where it dehydrates and reacts to form primarily garnet and liquid. This type of behaviour corresponds to Type II-water deficient and vapor-absent systems in which a hydrous phase is stable to the solidus (Robertson and Wyllie, 1971). The thermal stability of zoisite may be extended above the solidus in Type III and IV systems (water-deficient, vapor-present and water-excess respectively). The observations of zoisite as a hyper-solidus phase in hydrous mafic compositions is consistent with this interpretation. However, the present results on the maximum pressure stability of zoisite are in contrast to the only published complete zoisite dP/dT curve (Green, 1981a). There is no readily apparent reason why the addition of FeO, Na_2O, K_2O and TiO_2 should drastically reduce the stability of zoisite as observed in the present set of experiments by approximately 35 kbars.

The occurrence of zoisite as an accessory hydrous phase in the subducted oceanic lithosphere is dependant not only on its stability with respect to pressure and temperature, but also upon the bulk chemical composition of the system. The diversity of the oceanic crust has been established by numerous studies of drill holes, dredge hauls and samples obtained by submersibles. It consists of various

types of basalts (Bence, et al., 1979), gabbroic and noritic cumulates (Prinz et al., 1976; Hodges and Papike, 1976), chlorite, talc, and amphibolite schists (Bonatti, et al., 1975) and a host of ultramafic rocks (Prinz et al., 1976). Sediments, which also may be subducted, include clay oozes, cherts, sandstones and limestones (Hall and Robinson, 1979). It is not the intention of this discussion to examine the details of this diversity with respect to zoisite stability, but to merely indicate the range of possible compositions in any subducted lithosphere.

The occurrence of zoisite in high pressure experiments on hydrous mafic compositions suggests that it will be stable in eclogites which correspond compositionally to unaltered oceanic tholeiites. There are however, other experimental studies on similar compositions which do not report the presence of zoisite (Stern and Wyllie, 1978, Gust, Chapter 2). This discrepancy could easily be attributed to the failure of these investigators to observe small abundances of minor phases (Green, 1981a). It may also reflect the slight variations in bulk chemistry and H_2O contents which exist between these experiments. Alternatively, the appearance of zoisite as a hypersolidus phase may be due to some iron loss during the experiment, thus enriching the charge in CaO and Al_2O_3 and promoting the growth of zoisite (K.L. Harris, pers. comm.). In short, the experiments on hydrous mafic compositions do not conclusively establish or deny the possible occurrence of zoisite in a hydrous eclogite paragenesis.

Additional insight on this question of the occurrence of zoisite in the subducted slab can be gained by examining samples of the oceanic crust. The effects of hydrothermal alteration and low-pressure metamorphism of oceanic basalts commonly leads to the

formation of albite-actinolite-chlorite-epidote assemblages (Humphris and Thompson, 1978; Liou and Ernst, 1979; Cann, 1979). Prehnite, which decomposes to zoisite + grossular + quartz + vapor (Liou, 1971) is also observed with actinolite and chlorite as a characteristic assemblage of low pressure, low temperature metamorphism (Watson, 1942, Liou and Ernst, 1979). Epidote-rich assemblages have higher CaO and lower MgO contents than chlorite-rich assemblages (Humphris and Thompson, 1978). The progressively higher pressures and temperatures encountered by these mafic greenschists during the process of subduction metamorphoses them to andesine/oligioclase amphibolites and then to labradorite/bytownite amphibolites (Winkler, 1976) before the final transformation to eclogite. These changes are schematically illustrated on a series of ACF diagrams (Fig. 5a-d) which also includes a compositional field typical of oceaaic basalts and gabbros. If water is in excess after the formation of amphibole, zoisite may form from the reaction anorthite + vapor $\rightleftharpoons$ zoisite + quartz + kyanite (Boettcher, 1970). Alternatively it may be present during the entire metamorphic process as a result of the decomposition of prehnite or, if fO_2 decreases, the change from epidote to clinozoisite to zoisite (Holdaway, 1972).

Finally, the possible subduction of sediments, which form the top layer of the oceaaic crust is a potentially important mechanism by which zoisite may be stabilized to the high pressures and temperatures of the deep subduction zone. Calcareous clay oozes form zoisite in the lowest grades of metamorphism, with it remaining stable to high pressures at moderate temperatures (Winkler, 1976).

In summary, the possibility that zoisite is a component of the subducted oceanic crust can not be dismissed. It may occur in a

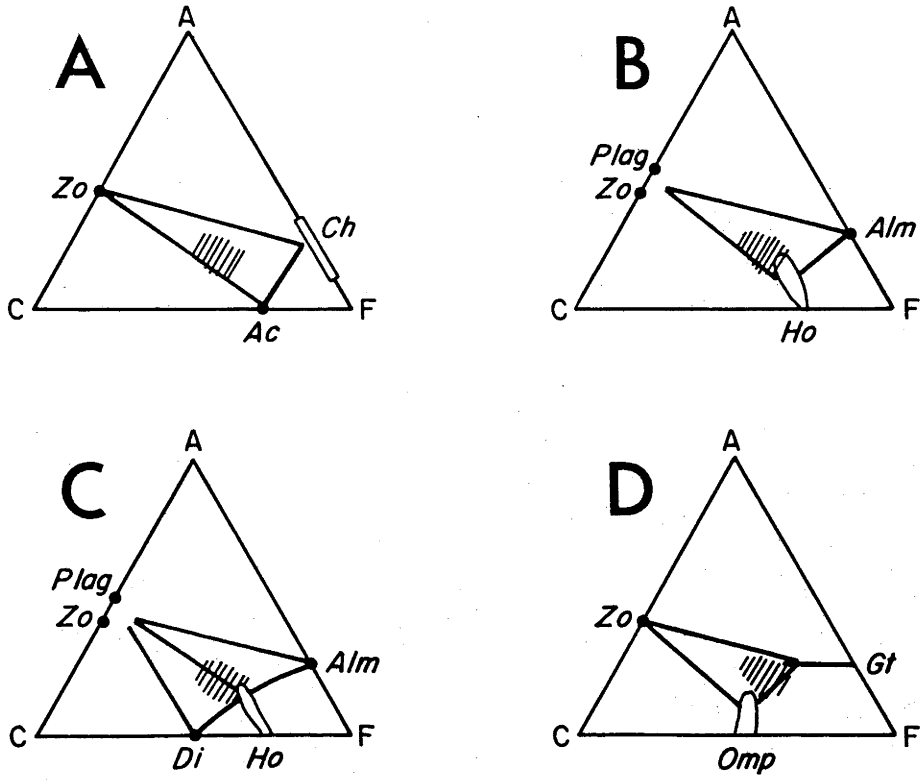

Figure 5: Schematic illustration on ACF of the changes in mineral compositions (e.g. MORB) with increasing grade of metamorphism. These changes may be similar to those encountered by a subducting slab. The ruled area is the location of olivine tholeiites in ACF component space.

A) Mafic greenschist; actinolite (Ac), chlorite (Ch), zoisite (Zo). Low grade.

B) Andesine - and oligoclase amphibolite; hornblende (Ho), garnet (Alm), plagioclase (Plag), zoisite (Zo). Medium grade.

C) Labradorite/bytownite - amphibolite; diopside (Di), hornblende (Ho), garnet (Alm), plagioclase (Plag), zoisite (Zo). High grade.

D) Eclogite; omphacite (Omp), garnet (Gt), zoisite (Zo). Very high grade.

A, B, and C are modified from Winkler (1976).

variety of rock types, ranging from pristine oceanic tholeiites to calcareous clay oozes. These possibilities in addition to its documented high-pressure stability requires the inclusion of zoisite as a possible H_2O-bearing phase for consideration in interpreting subduction-related processes. The consequences of the involvement of zoisite in these processes are twofold. Firstly, if the lithosphere melts, zoisite may be important as an accessory phase in the generation of magmas. If on the other hand, the lithosphere does not melt, water may be transported by zoisite deep into the subduction zone and released at high pressures.

Green (1981a) suggests that zoisite "could markedly affect trace element distribution in melts derived ... from mafic compositions in the deep crust". He acknowledges that this conclusion is unsupported by analytical data. However, Myer (1966) presented trace element data for five zoisites, which showed them to be depleted in almost all trace elements (except Ba and perhaps Y). The zoisite used in this study was analyzed for a number of trace elements including REE's by spark source mass spectrometry. The data (Appendix 3) indicate that this zoisite contains only minimal amounts of the incompatible elements. The shape of the chondrite-normalized REE pattern is similar to that of plagioclase. Although these abundances are not equivalent to partition coefficients, by analogy with the known partitioning characteristics of plagioclase, it is likely that the only significant effect that zoisite will have on a co-existing melt will be the creation of a slight negative Eu anomaly. As such anomalies are uncommon in volcanic rocks of the orogenic arc association (McLennan and Taylor, 1981), the possibility of substantial zoisite involvement in the generation of arc magmas can be dismissed.

The stability of zoisite to pressures in excess of 50 kbars at subsolidus temperatures (~800°C) suggests that the subsolidus dehydration of zoisite may be a mechanism of releasing water deep in the upper mantle (~200 km). This possibility is highly dependant upon the degree to which the cool subducted slab depresses a normal mantle geothermal gradient. Thermal models of subduction zones (Anderson et al., 1978; Hasebe et al., 1970) indicate that the middle of the slab will be cooler than either the leading or trailing edges, and may be only 800-900°C at 60 kbars. Zoisite, which initially forms in the lower part of the basaltic crust, such as the gabbros, could, according to these models, be stable to the pressure (~60 kbars) at which it dehydrates without melting.

SUMMARY

The results of high pressure experiments on the diopside-zoisite and enstatite-zoisite psuedobinary join in the CMASH system indicate that zoisite is stable to at least 60 kbar. The formation and stability of zoisite in more complex multi-component systems depends on the bulk composition, water content and possibly fO_2. Results from various experimental studies on hydrous mafic compositions, such as MORB, suggest that zoisite may be part of a 'wet' eclogite paragenesis. The occurrence of zoisite eclogites (e.g. Tilley, 1937; 1939) supports this suggestion.

Suitable compositions in which zoisite may form and be stable to high pressures are found amongst the variety of rocks which compose the oceanic crust (gabbroic cumulates, anorthosites, altered basalts, greenschists, and sediments). It is likely that zoisite does occur in the subducted lithosphere, however its contribution to subduction-related processes (magma generation, volatile release) remains poorly defined.

CHAPTER 4

THE HIGH PRESSURE STABILITY OF PHLOGOPITE: APPLICATION TO THE SUBDUCTION ENVIRONMENT

INTRODUCTION

The stabilities of hydrous phases in the Earth's upper mantle are of considerable importance with respect to the petrogenesis of mantle-derived magmas. The occurence of phlogopite, a tri-octahedral mica, in peridotitic nodules of upper mantle origin (e.g. Dawson and Smith, 1977; Aoki, 1975), suggests that it is a stable phase under the pressures and temperatures that exist in the upper mantle. This suggestion has been confirmed by numerous experimental studies on the stability of phlogopite in simple and complex systems (Markov et al., 1966; Kushiro et al., 1967; Yoder and Kushiro, 1969; Modreski and Boettcher, 1972, 1973; Forbes and Flower, 1974; Wendlandt and Eggler, 1980a). Wendlandt and Eggler (1980a) have discussed the petrogenetic implications of phlogopite stability with respect to potassic magmas, carbonatites and kimberlites.

Phlogopite is also an important host for large cations such as potassium, rubidium, and barium (Beswick, 1976a). These highly incompatible elements are not hosted to any degree by other mantle phases. The controversy of Beswick (1976 a,b) and Menzies (1976) illustrate some of the complexities involved in deciphering the possible geochemical role of phlogopite in magma genesis. Mantle metasomatism, by which incompatible elements may be transported in a fluid phase, may result in regions enriched in phlogopite, and may be important in the genesis of alkalic magmas (Boettcher et al., 1979).

This chapter presents the results of high pressure experiments on a mixture of phlogopite and enstatite, undertaken to define the

stability limits of phlogopite with pressure, and the nature of the subsolidus decomposition products of phlogopite. Although these goals were only partially achieved, the results indicate that the stability of phlogopite in the subsolidus is slightly higher than previously suggested by Wendlandt and Eggler (1980a). These conclusions are used to evaluate the role of phlogopite and related micas in the subduction environment.

EXPERIMENTAL AND ANALYTICAL METHODS

A mixture of phlogopite ($K_2Mg_6Al_2Si_6O_{20}(OH)_4$) and enstatite ($MgSiO_3$) in the molecular proportions of 1 to 5 was used. Reagents used in this mixture were analytical-grade MgO and SiO_2 (enstatite) and phlogopite previously synthesized by Dr. R.J. Arculus. This mixture was homogenized by grinding in acetone in an agate mortar and pestle for approximately three hours. For each experiment, approximately 10 mg of the mix was loaded into a Pt capsule, dried for 30 minutes in a 110°C oven, and then sealed by arc-welding. Experiments below 50 kbars were run in a solid media piston-cylinder device while those above 50 kbar were done using a modified high pressure girdle apparatus. Details of this equipment and general run procedures are given in Appendix 1.

The run products were identified by optical, x-ray diffraction and electron microprobe analysis. Stable and quench phlogopite were distinguished by their different morphological characteristics (Yoder and Kushiro, 1969).

RESULTS AND DISCUSSION

The results of the high pressure experiments on the composition (1)phlogopite:(5)enstatite under vapor-absent conditions are given in Table 1. The experiments at low pressures (30-40 kbar) agree well with those of Modreski and Boettcher (1972) on a 50/50 phlogopite-enstatite mix (Fig. 1). At higher pressures the solidus and phlogopite-

TABLE 1: Experimental Results on the Composition
1 Phlogopite: 5 Enstatite

RUN	P(kb)	T(°C)	t(min)	RESULTS
7208	30	1275	135	En, Ph, L(?)
7203	30	1300	120	En, Ph, Fo, L
7210	30	1325	125	En, Ph, Fo, L
7212	30	1325	140	En, Ph, Fo, L
7205	30	1350	135	En, Fo, L, Ph(?), Q
6797	40	1300	90	En, Ph
8898	40	1310	45	En, Ph
6791	40	1350	135	En, Ph, Fo, L
6794	40	1400	135	En, Ph, Fo, L, Q
8896	40	1425	30	En, Fo, L, Q
6795	40	1450	135	En, Fo, L, Q
8883	45	1425	30	En, Py, L, Q
G2-41	55	1250	30	En, Ph, Py
G2-46	55	1315	30	En, Ph, Py
G2-45	55	1340	30	En, Ph, Fo(?), Py(?), L(?)
G2-42	60	1350	15	En, Py, Fo, L, Ph, Q
G2-43	60	1400	15	En, Fo, Py, L, Q

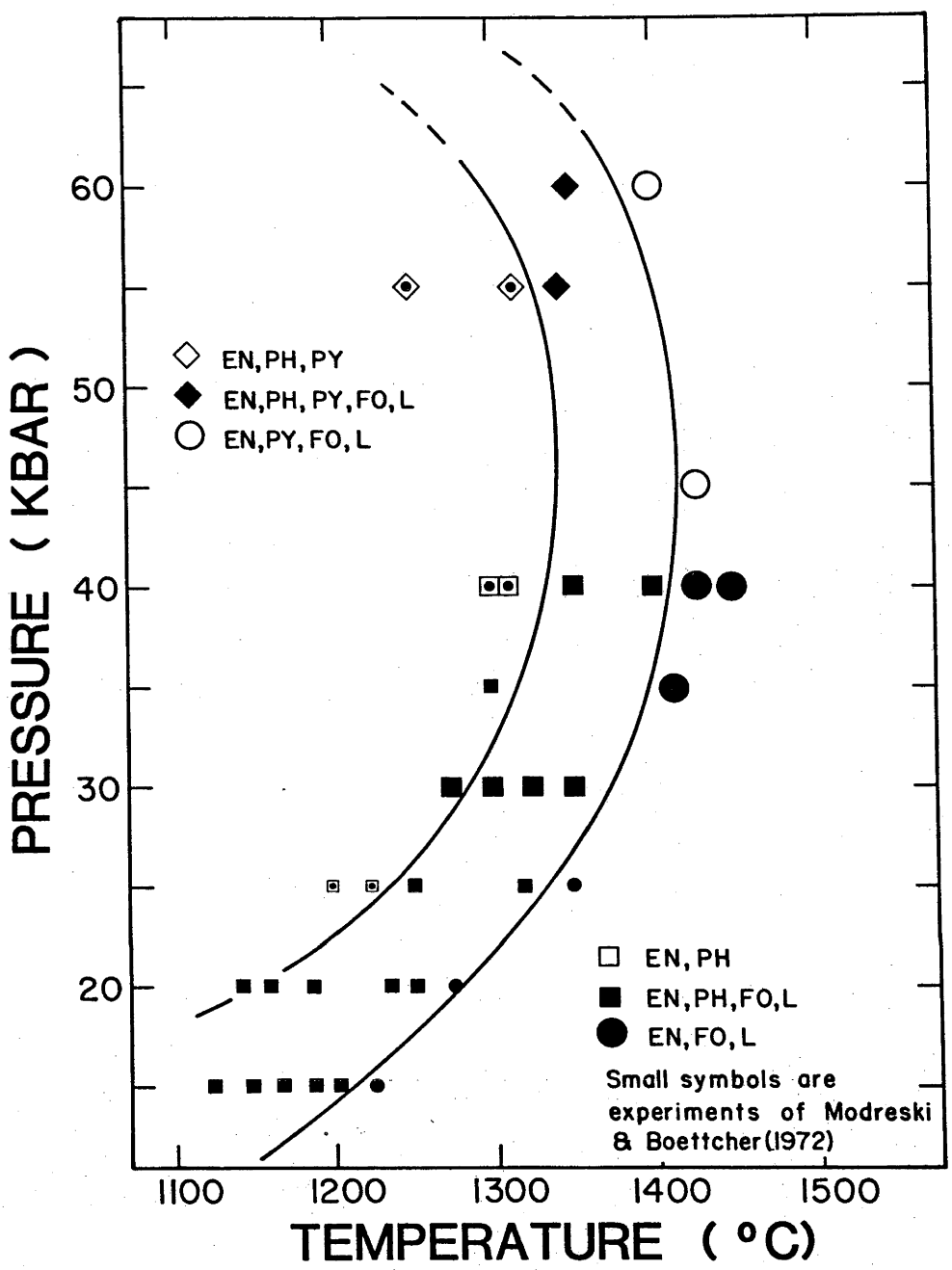

Figure 1. Pressure - temperature projection of experimental runs on phlogopite:enstatite (1:5) composition in the absence of a vapor phase (large symbols). The small symbols are runs by Modreski and Boettcher (1972) on phlogopite:enstatite (5:5) composition. The results of the present set of experiments agree with those of Modreski and Boettcher and indicate that phlogopite is stable to at least 60 kbar.

out curves steepen (∿45 kbars) and acquire negative slopes between 55 and 60 kbars. The subsolidus decomposition of phlogopite was not observed under the conditions of the experiments presented here.

The decomposition of phlogopite as it melts in the enstatite-phlogopite system is not a univariant reaction due to the slight solubility of alumina in enstatite (Modreski and Boettcher, 1972). At low pressures the univariant reaction for the breakdown of phlogopite is:

$$\text{phlogopite} + \text{enstatite} \rightleftarrows \text{forsterite} + \text{liquid}$$

but because of the enstatite solid solution, the reaction becomes:

$$\text{phlogopite} + \text{enstatite} \rightleftarrows \text{forsterite} + \text{liquid} + \text{enstatite}_{ss} +$$
$$\text{phlogopite} \rightleftarrows \text{forsterite} + \text{liquid}.$$

Consequently, the melting interval of phlogopite is expanded over a temperature range of approximately 80°C (Fig. 1).

The appearance of pyrope, first as a hypersolidus phase at 45 kbars and then as a subsolidus phase at higher pressures, coexisting with phlogopite and enstatite (± forsterite) results from the (idealized) reaction of spinel + enstatite $\rightleftarrows$ pyrope + forsterite (MacGregor, 1964). In actuality, the reaction is aluminous enstatite $\rightleftarrows$ pyrope + less aluminous enstatite (Modreski and Boettcher, 1972). The large field of coexisting phlogopite, aluminous enstatite, pyrope and forsterite shown in Figure 1, contrasts with the suggestion of Wendlandt and Eggler (1980a) that phlogopite will cease to be a subsolidus phase somewhere between 50 and 55 kbars at 1200°C. However, this requires, for stoichiometric reasons, that the composition of the phlogopite becomes less aluminous with increasing pressure. Electron microprobe analyses of hypersolidus phlogopites from experiments at 30,40, and 60 kbar (Table 2), suggest that phlogopites do become less aluminous at higher pressures. The preferential partitioning of Al_2O_3 from phlogopite into enstatite (and pyrope) was also sugges-

TABLE 2: Average Analyses of Hypersolidus Phlogopites from 30, 40, and 60 kbar Experiments

Run No.	7212	6791	G2-42
P (kbar)	30	40	60
T (^{o}C)	1325	1350	1350
SiO_2	41.74	40.75	41.18
Al_2O_3	15.26	14.42	13.21
MgO	26.50	26.34	26.71
K_2O	11.38	10.47	9.60
Total	94.89	91.98	90.71

ted by Modreski and Boettcher (1972) to account for the occurrence of subsolidus aluminous enstatite. Variation in the composition of phlogopite could reflect crystalline solid solution toward $KMg_{2.5}Si_4O_{10}(OH)_2$ or $KMg_3Si_{3.5}Mg_{.5}O_{10}(OH)_2$ (Siefert and Schreyer, 1971). The x-ray diffraction and electron microprobe data are inconclusive with respect to this possibility.

The composition used in the experiment consists of a 1:5 molecular mix of phlogopite:enstatite designed to model the subsolidus decomposition of phlogopite to form "Si-wadeite", by the reaction:

$$\underset{\text{(phlogopite)}}{K_2Mg_6Al_2Si_6O_{20}(OH)_4} + \underset{\text{(enstatite)}}{5MgSiO_3} \rightleftarrows \underset{\text{("wadeite")}}{K_2Si_4O_9} + \underset{\text{(forsterite)}}{4Mg_2SiO_4} + \underset{\text{(pyrope)}}{Mg_3Al_2Si_3O_{12}} + 2H_2O.$$

"Si-wadeite" is known to be a stable K-bearing phase at pressures of 90 kbar (Kinomura et al., 1975; W.J. Sinclair, pers. comm.). No "Si-wadeite" is observed in any of the experimental runs although subsolidus pyrope is observed. With regard to the hypothesized change in phlogopite composition discussed above, "Si-wadeite" will not be stable until the limit of Al deficiency in the phlogopite solid solution is reached and 'phlogopite' decomposes.

Other possible K-bearing phases which may result from the subsolidus decomposition of phlogopite if "Si-wadeite" is not stable at pressures <90 kbar are sanidine ($KAlSi_3O_8$) and kalsilite ($KAlSiO_4$). These phases are produced by the reactions:

$$\underset{\text{(phlogopite)}}{K_2Mg_6Al_2Si_6O_{20}(OH)_4} + \underset{\text{(enstatite)}}{6MgSiO_3} \rightleftarrows \underset{\text{(sanidine)}}{2KAlSi_3O_8} + \underset{\text{(forsterite)}}{6Mg_2SiO_4} + \underset{\text{(vapor)}}{V} \quad \text{and}$$

$$\underset{\text{(phlogopite)}}{K_2Mg_6Al_2Si_6O_{20}(OH)_4} \rightleftarrows \underset{\text{(kalsilite)}}{2KAlSiO_4} + \underset{\text{(forsterite)}}{2Mg_2SiO_4} + \underset{\text{(enstatite)}}{2MgSiO_3} + \underset{\text{(vapor)}}{V}.$$

The assemblage of sanidine + forsterite reacts to form kalsilite and enstatite at pressures >35 kbar (Wendlandt and Eggler, 1980 b). Because phlogopite decomposes at approximately 60 kbar, sanidine will not be produced if the system contains forsterite (i.e. upper mantle).

Thus, the only reasonable alternative to "Si-wadeite" as the decomposition product of phlogopite at subsolidus temperatures, is kalsilite.

GEOLOGICAL APPLICATIONS : SUBDUCTION ZONES

Modreski and Boettcher (1972) suggested that the stability of phlogopite in the upper mantle may be modeled by the assemblage of phlogopite and enstatite. Wendlandt and Eggler (1980a) studied the stability of phlogopite in a spinel lherzolite (anhydrous and hydrous conditions) and noted that its stability is reduced from the 'model system' by the relatively small temperature drop of 100°C at high pressures. Their experiments on this 'natural' composition did not exceed 30 kbars, although, from other experiments on the assemblage of phlogopite + enstatite + magnesite ($MgCO_3$), they concluded that phlogopite ceases to be a solidus phase between 50-55 kbar at 1200°C. The solidus of this system is nearly coincident with an extrapolation of the hypersolidus stability of phlogopite in a hydrous garnet (spinel) lherzolite. Wendlandt and Eggler (1980a) also observed that the geothermal gradient of the mantle is a determining factor controlling the presence or absence of phlogopite in the upper mantle. In regions with high gradients, for example, in ocean basins, phlogopite will be limited to lower pressures than in regions with lower gradients (i.e. continental interiors). Areas where these 'normal' geothermal gradients are altered, such as subduction zones, may be suitable environments where the stability field of phlogopite in the mantle is maximized.

There are numerous thermal models that portray the effects of subducting a relatively cold slab of oceanic lithosphere into a hot upper mantle. These models vary because of their different boundary conditions (e.g. initial mantle gradient, angle and rate of subduction, age and temperature of the oceanic plate, frictional heating and dehydration reactions) (reviewed in Anderson et al., 1978; in

addition, DeLong et al., 1979; Sydora et al., 1978). The model of Anderson et al. (1978), which incorporates the effects of frictional heating and dehydration as a function of time, is selected to represent the subduction environment in this discussion. Adoption of different models (see Fig. 11 Chpt. 2) may alter the following conclusions.

The dehydration of various hydrous minerals which occur in the oceanic crust (chlorite, talc, serpentine, amphibole) is an essential component of the Anderson et al. (1978) model. Apart from the thermal consequences resulting from these endothermic reactions, the release of a fluid phase capable of transporting incompatible elements (e.g. Mysen, 1978) and promoting partial melting (or diapiric uprise) of the overlying peridotitic mantle (Ringwood, 1974) links subduction and arc volcanism. This process, of which the details are poorly understood, may account for both the generation and the distinctive geochemistry of island arc basalts.

The nature of the dehydration of amphibole is especially important as it signals the transition of the slab to an eclogitic assemblage. Amphibole is the major reservoir of potassium and other incompatible elements in the subducted crust (Arth, 1976), and its decomposition at pressures <25 kbar (Allen et al., 1972), provides a substantial flux of these elements. These elements are either dissolved into the fluid phase and transported into the mantle or they are accommodated in new phases in the subducted slab (garnet, clinopyroxene and mica, if fluid is present in the slab).

High pressure experimental studies on hydrous eclogites, similar in composition to MORB, indicate that mica is a subsolidus/hypersolidus phase coexisting with garnet, amphibole, kyanite $\pm$ rutile $\pm$ quartz $\pm$ liquid (Råheim and Green, 1974; Green, 1981b; Chapter 2). Information on the composition of these micas is difficult to obtain, but they appear to be phengitic ($\sim K_2Al_2Mg_3Si_7AlO_{20}(OH)_4$). Green (1981b) suggests that the composition changes from subsolidus phengite

to hypersolidus phlogopite (~800°C to 1100°C). The maximum thermal stability of phlogopite is governed by the fH_2O of the system. The presence of phengite-phlogopite in the subducted oceanic lithosphere provides a mechanism by which water, potassium, barium, rubidium, and to a lesser extent, REE's, may be transported deep into the upper mantle.

Anderson et al. (1978) concluded that in mature arcs (>30 m.y. old), the subducted oceanic crust would not melt until it reached depths of at least 200 km. This conclusion, in conjunction with the results of this study and those discussed above, suggest that phlogopite could be stable in the subducted slab to 55-60 kbars (180-200 km). At these pressures, if the eclogitic portion of the slab has not melted, phlogopite will decompose under subsolidus conditions. The products of this decomposition in an eclogitic system are not known, but could be "Si-wadeite", sanidine, or kalsilite. Alternatively the fluid released by the decomposition of phlogopite may a) initiate melting in the slab or b) equilibrate with and transport K, Ba, and other incompatible elements into the mantle wedge above the slab.

The thermal characteristics which govern the stability of phlogopite in the subducted slab, also control its occurrence in the mantle wedge above the slab. The geothermal gradient of a region just prior to subduction is commonly considered to resemble the oceanic gradient. These conditions limit phlogopite in a hydrous peridotite, to pressures of <30 kbars (hypersolidus). Subduction depresses this gradient over time to the extent that phlogopite could be stabilized to its maximum depth (~200 km) in a small zone above the slab (Fig. 2).

Reaction of the peridotite with melts or fluids from the subducted slab results in the formation of phlogopite (Sekine, 1981). The addition of phlogopite (ρ = 2.76 - 2.9 g/cc) to peridotite decreases the average density of the peridotite, making it gravitationally unstable relative to other 'non-phlogopitized' perido-

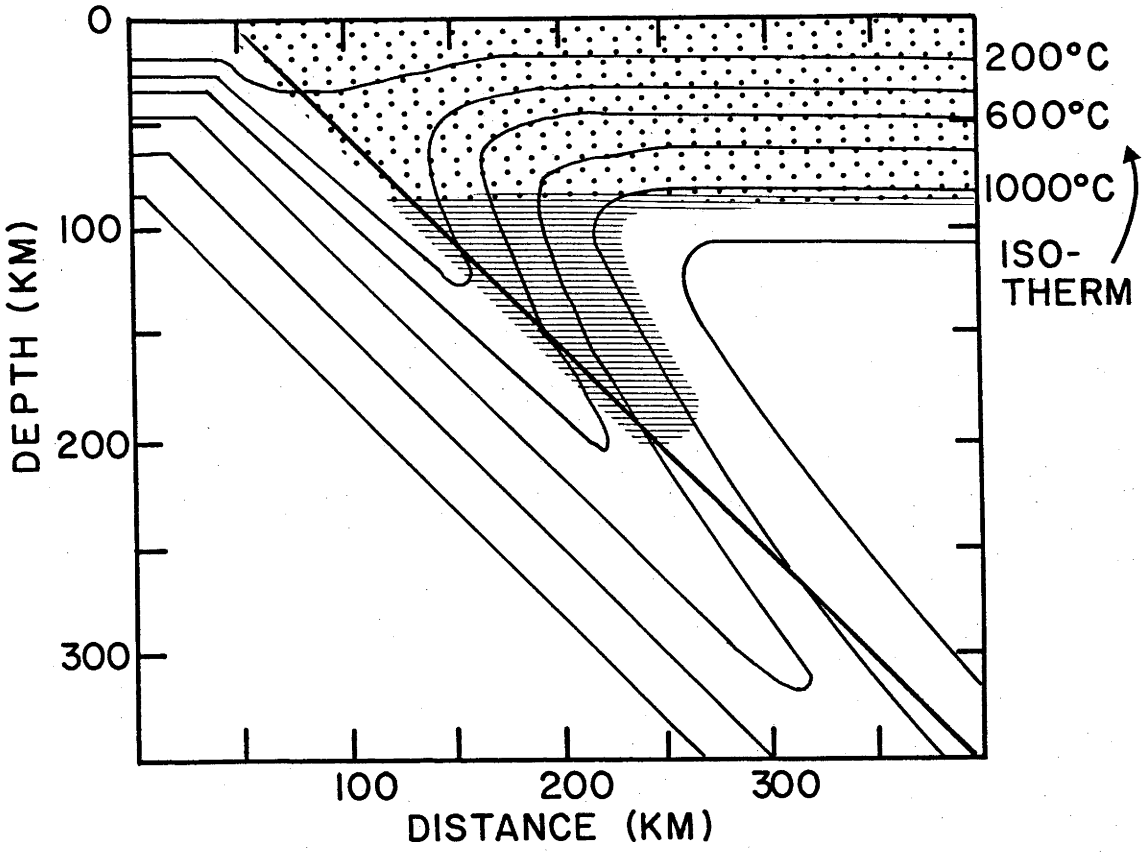

Figure 2. Stabilities of phlogopite (ruled area) and amphibole (dotted area) in a model subduction zone. Isotherms are from the thermal model of Anderson et al. (1978) for a 50m.y. old subduction zone. Phlogopite is also stable at lower pressures, but amphibole is more likely to occur as the H_2O, K- bearing phase in the mantle (Wendlandt and Eggler, 1980a).

tite. Aided by the presence of a fluid phase, this instability is relieved by the diapiric ascent of the less dense, phlogopite-rich material (Wyllie, 1971b; Ringwood, 1974). As the diapirs rise, they encounter progressively higher temperatures and consequently melt. The stability of phlogopite as a hypersolidus phase in the partially molten diapir will depend upon the maximum temperature attained and the amount of water in the system (Roberston and Wyllie, 1971).

The major element chemistry of most primary island arc basalts (IAB) resembles that of MORB except for slightly higher contents of K_2O in IAB (Perfit et al., 1980). Despite these similarities, the petrogenesis of IAB is fundamentally different from the petrogenesis of MORB due to the different thermal characteristics of their source environments. Because of the high geothermal gradient of ocean ridges, MORB are thought to result from the melting of anhydrous peridotite at pressures <20 kbar (Green et al., 1979; Presnall et al., 1979) whereas the perturbed geothermal gradient of the subduction zone (Anderson, et al., 1978) restricts the generation of IAB to the lower temperature fusion of hydrous peridotite (Wyllie, 1971a; Green, 1976; Ringwood, 1974). Green (1976) demonstrated that olivine tholeiites would be produced by approximately 30% partial melting of 'wet' peridotite ≤20 kbar, thus the segregation of magma (IAB) from subduction-related, 'wet' mantle diapirs can not occur at pressures >20 kbar. Green (1976) and Wendlandt and Eggler (1980a)demonstrated that at such pressures, amphibole, not phlogopite, buffers the fluid phase and K_2O content in the peridotite.

The relatively low K_2O of IAB olivine tholeiites (∿1.0 wt. %) also precludes the direct involvement of phlogopite in their genesis (i.e. as a fractionating phase or residual phase in the source). Edgar et al (1976) suggest that phlogopite could only be a liquidus phase in basaltic compositions for liquids with K_2O contents >5.0 wt. percent. Melting of model mantle systems with phlogopite (phlogo-

pite-enstatite) show that liquids generated within the hypersolidus stability of phlogopite are leucite-normative (Modreski and Boettcher, 1973). Wendlandt and Eggler (1980a) also indicate that liquids in equilibrium with a phlogopite-bearing lherzolite are leucite normative.

In summary, the origins of IAB are not compatible with a petrogenetic model in which phlogopite, as a residual phase in the partial melting of 'wet' peridotite, buffers H_2O, K, Ba, Rb (Beswick, 1976a) or Ti (Forbes and Flower, 1974). Regardless of this exclusion from a direct participation in IAB genesis, phlogopite is important in that it serves both as a source (eclogite slab) and a host (peridotite wedge) for H_2O and various incompatible elements in the mantle beneath island arcs.

The phlogopite content of a mantle which is ultimately the source of IAB is constrained by the K_2O contents of these basalts and the degree of partial melting which they represent, providing that no other K_2O-bearing phase, such as amphibole is stabilized. For an average IAB (K_2O = 1 wt. % : Perfit et al., 1980) derived by 30% partial melting of hydrous peridotite (Green, 1976) the amount of allowable subsolidus phlogopite is approximately 3% (% phlogopite= $\frac{(K_2O \text{ magma} \times \% \text{ melt})}{K_2O \text{ phlogopite}}$). IAB which are more alkalic (i.e. higher K_2O contents) are possibly derived from a) sources which are more enriched in phlogopite or b) lesser degrees of partial melting of sources with similar (3%) enrichments of phlogopite.

The formation of phlogopite in the mantle probably results from the reaction of an anhydrous mantle assemblage with an incompatible element enriched fluid phase. Due to our limited knowledge of the composition of this 'metasomatic' fluid phase, it is difficult to quantify the possible enrichments in various trace elements in the mantle which would accompany phlogopite formation. Relatively high

phlogopite/matrix and phlogopite/fluid partition coefficients for Ba and Rb (Philpotts and Schnetzler, 1970; Beswick, 1973) and low phlogopite/matrix partition coefficients for REE's (Schnetzler and Philpotts 1970) suggest that the formation of phlogopite could decouple these two groups of incompatible elements. Metasomatic enrichment of mantle material in phlogopite thus may result in enrichments in Ba and Rb relative to the REE's. Magmas derived from such sources would retain the high Ba (Rb) contents relative to the REE's characteristics of the source. The origin of Ba/La 'spikes' in IAB, as well as basalts from other tectonic environments (Perfit et al., 1980; Arculus and Johnson, 1981), may be, in part, a function of a mantle enriched in phlogopite.

CONCLUSIONS

The results of this experimental study demonstrate that phlogopite is stable in a model mantle composition (i.e. phlogopite + enstatite) to pressures of 55-60 kbar. The products of the subsolidus decomposition of phlogopite at high pressure were not observed, but are thought to include either "Si-wadeite" or kalsilite. The extension of this data on the stability of phlogopite to more complex systems, such as peridotite and eclogite, is possible by analogy with results from appropriate studies (Wendlandt and Eggler, 1980a; Chapter 2). The thermal stability of phlogopite in these natural systems is reduced by $\sim 100^{\circ}C$ (peridotite) to $\sim 500^{\circ}C$ (eclogite).

The presence or absence of phlogopite in the mantle is controlled primarily by its thermal stability and the temperature distribution in the mantle. Thermal models of subduction zones suggest that phlogopite may be stable in both the eclogitic slab and overlying peridotite wedge to $\sim$200 km ($\sim$60 kbar). At these pressures, phlogopite decomposes, possibly releasing H_2O, K_2O and other incompatible elements which react with the overlying peridotite to form phlogopite. The 'wet' phlogopite-bearing peridotite diapirically rises and melts

to produce IAB. Phlogopite does not remain as a residual phase in the partially melted peridotite and consequently is not a direct participant in IAB genesis. Phlogopite is possibly important as an intermediary, transporting H_2O, K_2O, and other incompatible elements into the mantle via subduction and then to the zone of magma genesis via diapiric ascent.

CHAPTER 5

AMPHIBOLE-BEARING INCLUSIONS FROM BOISA ISLAND, PAPUA NEW GUINEA: EVALUATION OF THE ROLE OF FRACTIONAL CRYSTALLIZATION IN AN ANDESITIC VOLCANO

PREFACE

This chapter is co-authored by R.W. Johnson (Bureau of Mineral Resources) and has been published in the Journal of Geology, 1981, vol. 89, p.219-232. R.W. Johnson and R.W. Davies collected the samples from Boisa Island. R.W. Johnson also described the geology of Boisa Island and its relations with the volcanism and tectonics of Papua New Guinea. B.W. Chappell provided the whole rock trace element data (X-ray Fluorescence).

My contribution consisted of collecting data (electron microprobe) on the phase chemistry of the Boisa samples, processing all of the petrologic and geochemical data and finally, writing the paper.

This chapter is presented in the form in which it was published, except that the References Cited section has been combined with the References Cited at the end of the thesis. The data catalogue mentioned in this chapter (BMR Rpt. 227, BMR Microform MF 147), is included in this thesis as Appendix 4.

INTRODUCTION

Fractionation of hornblende from hydrous mafic magmas may be an effective means of generating the large volumes of andesite commonly found in arc-trench systems (e.g. Bowen 1928; Green and Ringwood 1967; Boettcher 1973; Cawthorn and O'Hara 1976). Hornblende from arc-trench rocks is poor in SiO_2 and low in Mg/Fe, and its separation from a parental magma may produce the trends of strong silica enrichment and mild iron enrichment that characterise the rock associations of many andesitic provinces. Coarse-grained, hornblende-bearing inclusions in andesitic volcanoes may therefore represent the material extracted from mafic magmas parental to the andesites. However, these amphibole-bearing inclusions are not common in the volcanoes of island arcs and continental margins, although some from the Lesser Antilles island arc have recently received a great deal of attention (Lewis 1973; Rea 1974; Arculus 1978; Powell 1978; Arculus and Wills 1980; see also Sigurdsson and Shepherd 1974), and some are known for example from Japan (Yamazaki et al. 1966). Thus, their discovery on a Papua New Guinea andesitic volcano is of considerable interest.

Andesite is the most common rock in the Bismarck volcanic arc, a 1000 km-long chain of late Cainozoic volcanoes along the southern margin of the Bismarck Sea in northwestern Papua New Guinea (fig. 1; Johnson 1977). There are about 50 major volcanoes in the arc, but only one of them - Boisa (or Aris) Island, near the mouth of the Sepik River in northern New Guinea - has lavas containing coarse-grained, amphibole-bearing inclusions. A scarcity of amphibole is also a general feature of the lavas of the Bismarck volcanic arc. Amphibole phenocrysts are surprisingly rare, particular in New Britain where they seem to be restricted to dacites and rhyolites. Amphibole phenocrysts are found in andesites in the western part of the arc, but they are not common, and Boisa is one of only two exceptions (Sakar Island is the other) where hornblende andesites are present in significant amounts. In

contrast to the Bismarck volcanic arc, many rocks in other Papua New Guinea volcanic provinces, such as the Highlands and eastern Papua, contain amphibole and in general are also richer in incompatible elements (Johnson in press).

This paper is a documentation of the mineralogy and geochemistry of the Boisa inclusions and their host lavas. Analytical data are used to assess whether younger andesites on Boisa could have been produced from parental magmas represented by the older, more mafic lavas, by fractionation of the minerals in the inclusions. Whole-rock, major-element relationships are tested using least-squares mixing modelling and microprobe-determined mineral compositions, and differences in trace-element contents are examined using the Rayleigh-fractionation equation. This approach is particularly applicable to the Boisa Island rocks because they are all from one part of a single volcano, and their stratigraphic relationships are well established.

All analytical data obtained for this study, as well as notes on analytical technique and the results of the petrogenetic calculations, are given in 14 tables in a companion report by Gust et. al. (1980). The report is in microfiche form and may be obtained for $1.00 Australian (postage included) by writing to the Director, Bureau of Mineral Resources, Canberra.

GEOLOGY

Boisa Island lies about 20 km off the north coast of New Guinea (fig. 1). It is up to 1.7 km across, about 1.35 km^2 in area, 215 m above sea level, and rises from sea floor about 1000 m deep. Boisa is 10 km northwest of the much larger island of Manam, which is one of the most active volcanoes in Papua New Guinea (Palfreyman and Cooke 1976). In contrast, there are no known records of observed activity from Boisa, nor any present-day thermal activity, although the last eruption may have been quite recent judging by the youthful morphology of the island. Neither are there any previously published accounts of

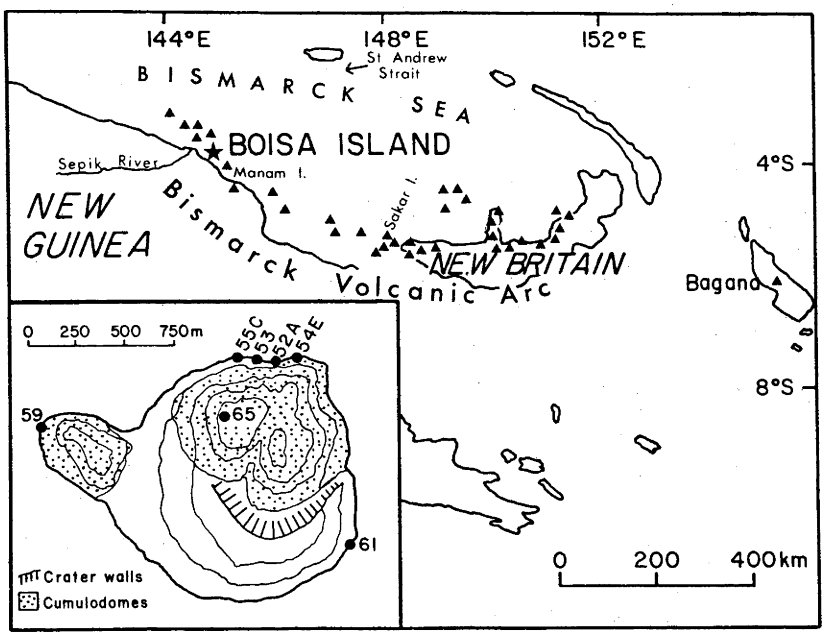

Figure 1. Papua New Guinea locality map, showing Boisa Island (star) and other volcanoes of the Bismarck volcanic arc and Bagana volcano (triangles). Inset map of Boisa Island, showing localities (filled circles) of analysed samples whose analyses are listed in table 1. Form lines are at intervals of about 40 m.

the petrology and geology of Boisa Island.

Boisa consists of a larger, more-or-less circular, eastern part, and a northwest-trending western peninsula (fig. 1). The eastern part is an andesitic cumulodome occupying, and overlapping the northern part of, the crater of an older, more mafic composite cone. A smaller andesitic cumulodome makes up the western peninsula. The coarse-grained inclusions are common in the eastern cumulodome, and are especially conspicuous in boulders along the northern shore.

MINERALOGY AND PETROGRAPHY

The rocks of Boisa Island may be divided into three groups (table 1): (1) mafic, clinopyroxene-rich basalts of the older cone; (2) amphibole bearing andesites of the cumulodomes; and (3) the coarse-grained inclusions. Most of the lavas are highly porphyritic, containing more than 30 percent phenocrysts, but the western-cumulodome lava contains only a few percent phenocrysts.

Group 1 - The mafic rocks contain phenocrysts of mainly Cr-rich clinopyroxene (mainly augite; fig. 2), and concentrically zoned, complexly twinned bytownite (An_{78}-An_{72}; fig. 3) that forms aggregates with ferromagnesium crystals. Orthopyroxene, olivine, and Fe-Ti oxides are relatively minor phenocryst minerals, and amphibole is absent. The groundmass appears to be made up of all these minerals, except for olivine (and amphibole).

Pyroxene phenocrysts are found as euhedral crystals and in aggregates of the following assemblages: clinopyroxene $\pm$ orthopyroxene $\pm$ plagioclase + Fe-Ti oxides. The clinopyroxene is concentrically zoned from (fig. 2) Ca-rich cores ($Ca_{43.5}Mg_{47.5}Fe_{9.0}$) to Fe-rich rims ($Ca_{37.4}Mg_{48.2}Fe_{14.4}$), and both Ti and Mn contents increase from core to rim. Orthopyroxene has a compositional range of En_{79} to En_{73} (bronzite) and some phenocrysts are rimmed by clinopyroxene. Both clinopyroxene and orthopyroxene have moderate Al_2O_3 contents, (1.3 to 3.6 weight percent) and high 100 Mg/(Mg+Fe) values (85-73). Olivine

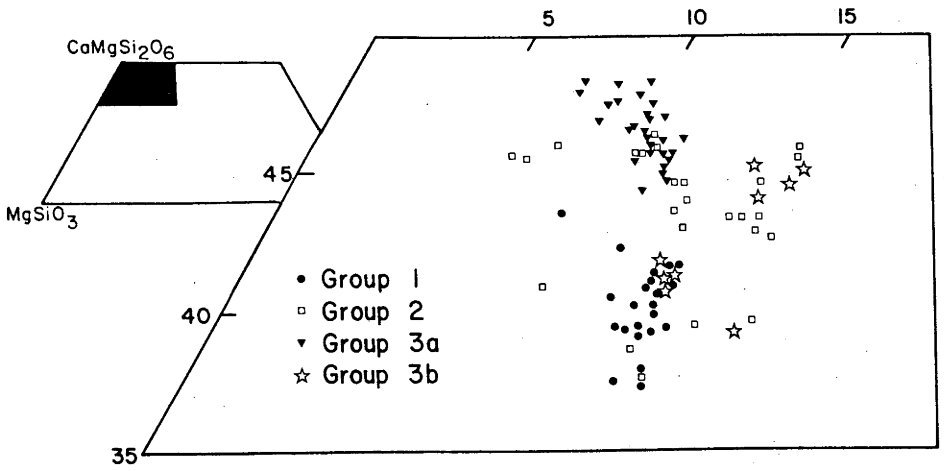

Figure 2. Pyroxene-phenocryst compositions.

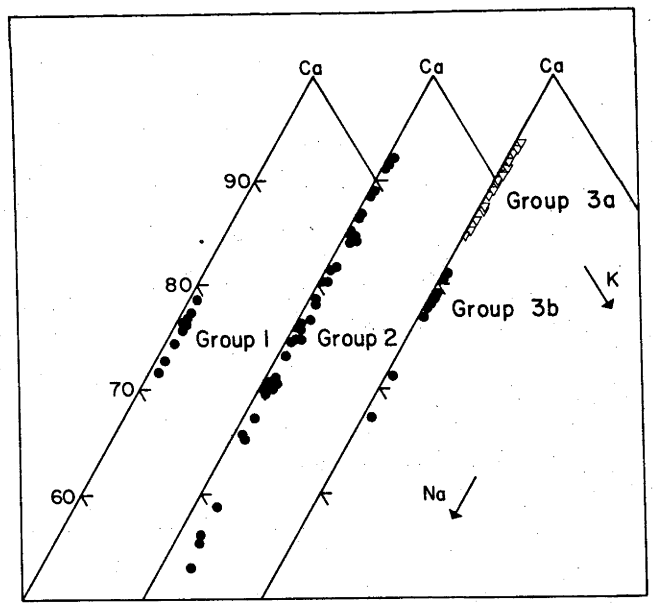

Figure 3. Plagioclase-phenocryst compositions.

phenocrysts are generally embayed and rimmed by clinopyroxene.

The Fe-Ti oxides (fig. 4) are present as individual phenocrysts, in aggregates, and as inclusions in pyroxene. The inclusions have higher Cr, Al, and Mg and lower V and Ti contents than do the phenocrysts.

Group 2 - The lavas of group 2 are less porphyritic than those of group 1, and are easily distinguished in hand specimen by their lighter colour and the presence of brown amphibole phenocrysts. The groundmass consists mainly of plagioclase and lesser amounts of clinopyroxene, orthopyroxene, amphibole, and Fe-Ti oxides. Laths of low refractive index are probably high-temperature silica polymorphs.

Two types of large crystals can be distinguished in the group-2 lavas - one representing cognate phenocrysts, the other representing fragments of disaggregated, coarse-grained, group-3-type inclusions. Many of the inclusion-type crystals have disequilibrium textures and are rimmed by the cognate component. The minerals of the inclusion-type group resemble those found in both group-3a and group-3b inclusions (see below). They are present as subhedral to anhedral fragments, or collectively in small clots having textures similar to the larger inclusions.

Plagioclases in the inclusion-type group are large, rounded, Ca-rich grains (An_{92}-An_{70}; fig. 3) containing 'dusty' cores, sieve textures, and inclusions of light brown glass. Many are rimmed by a more sodic plagioclase, similar in composition to groundmass plagioclase. Clinopyroxene has a wide range of compositions, from aluminous Cr-diopside to augite (fig. 2) and contains moderate amounts of Ti, and is present as fairly large subhedral crystals. Bronzite (En_{77}-$En_{71.5}$) contains different amounts of Al_2O_3 (up to 3 weight percent) and is similar in habit to the clinopyroxene. Olivine is very rare, ranges from Fo_{92} to Fo_{82}, and is commonly in the cores of diopsidic clinopyroxene where it is deeply embayed. Individual

grains of olivine have extensive reaction rims of orthopyroxene. Pseudomorphs of amphibole of inclusion origin are present only as anhedral patches of fine-grained Fe-Ti oxides, pyroxene, and plagioclase. Inclusions of Fe-Ti oxides in clinopyroxene grains are compositionally indistinguishable from those in the groundmass of the lavas.

The cognate phenocrysts consist of plagioclase and minor clinopyroxene, orthopyroxene and amphibole. Plagioclase is seen as small, concentrically zoned equant crystals (An_{75}-An_{53}; fig. 3). Clinopyroxene (salite: fig. 2) and bronzite are present as small euhedral grains. Amphibole phenocrysts are pleochroic in shades of brown (γ - dark chestnut brown >β - dark brown >α - pale yellowish brown) and are oxyhornblende ($Ca_{27.5-27.0}{}^{Mg}{}_{53.3-49.6}{}^{Fe}{}_{19.2-23.4}$). They contain 1.0 weight percent or less TiO_2 and are unzoned. K/Na and 100 Mg/(Mg + Fe) (all Fe as Fe^{2+}) range from 0.11 to 0.20 and 73.6 to 67.4 respectively. Most amphibole grains are euhedral crystals and are rimmed with fine-grained aggregates of pyroxene and Fe-Ti oxides. Fe-Ti oxides are large anhedral patches in the groundmass.

Rare quartz and apatite crystals, probably of xenocrystal origin, are also found in the group-2 lavas. The quartz is commonly rounded, but not embayed; reaction rims of pyroxene are absent. Apatite is present as small, euhedral prisms with a dusty-red tint.

Group 3a - The coarse-grained inclusions of the eastern cumulodome may be divided into two types - group 3a, and a less mafic group, 3b.

Plagioclase in the group 3a inclusions has a range of An_{94}- An_{85}, is typically unzoned and complexly twinned, and some crystals contain small spinel inclusions. Chrome-diopside, salite, and augite ($Ca_{48.3-44.3}{}^{Mg}{}_{44.6-42.2}{}^{Fe}{}_{7.4-11.7}$), and bronzite-hypersthene (En_{78} - En_{69}) are present in the group 3a samples. The diopside is generally euhedral, large poikilitic crystals containing plagioclase, spinel,

orthopyroxene and olivine. Orthopyroxene contains few inclusions, lacks pleochroism, and is occasionally rimmed by augite. Olivine (Fo_{84-78}) is rare, mostly fresh, but deeply embayed and rimmed by clinopyroxene.

Amphibole has an irregular, patchy appearance and commonly rims other ferromagnesian minerals. It is oxyhornblende, and chemically similar to the amphibole in the group-2 lavas, but generally has slightly lower TiO_2 and Na_2O contents. Reaction rims of Fe-Ti oxides and pyroxene are present, and where the inclusion has been invaded by the host lava the amphibole is extensively pseudomorphed to patches of sub-calcic augite, Fe-Ti oxides, and plagioclase. Spinels are abundant in all the minerals of the group-3a inclusions. They have a wide compositional range, but are generally distinct from the spinels in lavas of groups 1 and 2 (fig. 4). Group-3a spinels are Cr-rich hercynites (up to 20 weight percent Cr_2O_3) containing large amounts of MgO.

Estimates of the temperature, pressure, and oxygen fugacity at which group-3a inclusions equilibrated may be calculated thermodynamically (Appendix 1). These calculations require an appropriate mineralogic assemblage of olivine, plagioclase, clinopyroxene, orthopyroxene and spinel. Only one inclusion -sample 52B - fulfills this criterion; it contains all these minerals in addition to oxyhornblende. Equilibration temperatures (using co-existing clinopyroxene-orthopyroxene pairs; Wood and Banno 1973) range from 870°C to 970°C. Pressures, calculated from the reaction forsterite + anorthite = diopside + enstatite + spinel (Powell 1978; Arculus and Wills 1980), are estimated to be 1 kb to 1.5 kb, and aO_2 obtained from the reaction forsterite + fayalite + O_2 = enstatite + magnetite (Powell 1978) is slightly above that defined by the NNO buffer. The pressure and temperature estimates are consistent with experimental results on amphibole stability in basalt-water systems (Holloway and

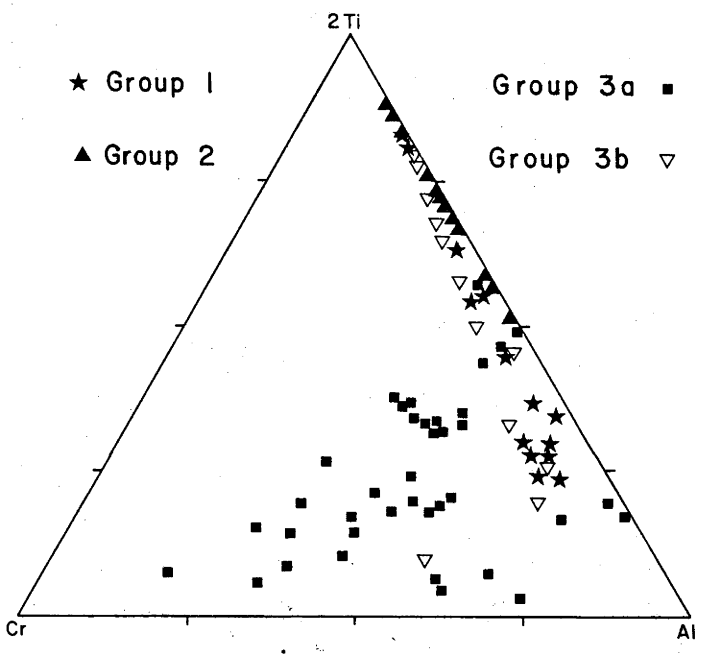

Figure 4. Spinel compositions.

Burnham 1972; Helz 1973; Cawthorn 1976). Amphibole in these experiments is shown to form from reaction of liquidus phases (olivine, clinopyroxene, orthopyroxene, or plagioclase) which, under the water-saturated conditions of the experiment, runs to completion with the loss of one or more liquidus phases. Preservation of the mineral assemblage in sample 52B may be evidence that the amphibole reaction is incomplete because the parental Boisa magma was water-undersaturated.

Group 3b - Group-3b inclusions are represented by sample 54E, which is compositionally distinct from those of group 3a. It is characterized by plagioclase (An_{81}-An_{67}), augite and salite ($Ca_{45.3-39.3}$ $Mg_{45.7-39.1}Fe_{12.9-16.5}$), orthopyroxene ($En_{75}$-$En_{68}$), and titanomagnetite. Secondary amphibole was probably produced by late-stage alteration of augite. It is compositionally distinct from amphiboles of group 2 and group 3a having higher TiO_2 (1.35-1.55 weight percent). Glass inclusions observed in some plagioclase grains are rhyolitic in composition. The compositions of these minerals are similar to those of the basalts of group 1 (figs. 2-4), and the inclusion therefore probably represents a fragment of group-1 magma which crystallized on the conduit walls and was accidentally included in the andesite.

GEOCHEMISTRY

Mafic Rocks of Groups 1 and 3 - Samples 53, 61 and 54E are chemically similar (table 1) and have many of the familiar features of island-arc tholeiitic basalts. TiO_2 is particularly low (less than 0.45 weight percent). Total-Fe values are low relative to MgO, and abundances of incompatible elements are moderately high compared to, say, the group-1 mid-ocean-ridge tholeiitic basalts of Bryan et al. (1976). The Boisa basalts are also moderately light-rare-earth-element (REE) enriched, and Ba/La values are high, resulting in a positive Ba anomaly in the chrondrite-normalized pattern for sample 53 (fig. 5), a feature considered by Sun and Hanson (1976) to be

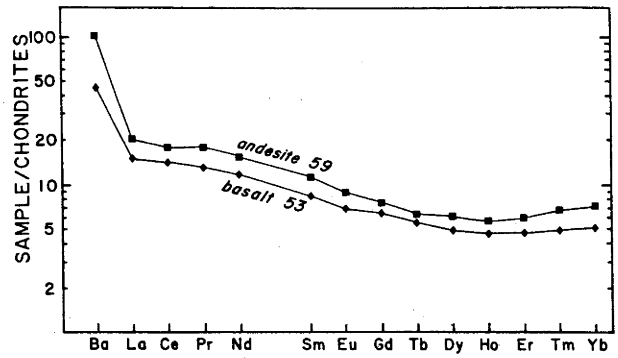

Figure 5. Chondrite-normalized REE patterns (normalizing values are those of Taylor and Gorton, 1977).

TABLE 1
Major and Trace-Element Analyses Seven Rocks from Boisa Island

	Group 1		Group 2			Group 3a	Group 3b
	No. 53	No. 61	No. 52A	No. 65	No. 59	No. 55C	No. 54E
SiO_2	53.0	53.2	58.8	60.2	61.7	48.9	51.1
TiO_2	.42	.35	.28	.29	.27	.35	.43
Al_2O_3	14.5	14.5	17.4	17.4	17.2	11.8	14.9
Fe_2O_3	3.95	5.30	4.75	3.90	3.30	4.85	6.00
FeO	5.10	3.70	2.00	2.40	2.45	4.65	4.60
MnO	.17	.15	.14	.14	.13	.17	.17
MgO	8.20	8.40	3.90	3.45	3.20	13.8	8.50
CaO	11.0	11.2	8.00	7.55	6.80	13.5	11.4
Na_2O	2.0	2.10	3.15	3.05	3.35	.93	1.78
K_2O	.55	.62	1.18	1.16	1.20	.13	.43
P_2O_5	.14	.11	.16	.16	.16	.09	.09
H_2O^+	.79	.21	.28	.07	.15	.28	.41
H_2O^-	.11	.07	.08	.09	.05	.18	.03
CO_2	.04	.13	.05	.08	.09	.09	.12
rest	.21	.21	.18	.18	.20	.24	.22
Total	100.18	100.25	100.35	100.12	100.25	99.96	100.18
$\frac{100Mg^a}{Mg + Fe^2}$	74 (67)	80 (68)	77 (57)	72 (55)	70 (55)	84 (76)	77 (64)
K	4600	5100	9800	9630	9960	1100	3600
Rb	10.6	7.4	14.4	18.2	15.8	.6	5.2
Ba	160	170	255	295	355	300	105
Pb	4.3[b]	3	7	5	6.8[b]	< 1	4
Sr	605	555	675	690	740	336	570
K/Rb	430	690	681	529	630	...	690
K/Ba	29	30	38.5	32.5	28.0	35	34
Ba/Rb	15.0	23	17.5	16.0	22.5	...	20
Sr/Ba	3.80	3.25	2.65	2.35	2.10	10	5.45
Rb/Sr	.0175	.013	.0215	.0265	.0215	...	.0091
La	4.7[b]	5	7	8	6.4[b]	3	5
Ce	11[b]	10	18	20	14[b]	9	12
Nd	7.0[b]	6	8	8	9.1[b]	5	5
Y	10	10	11	10	10	9	10
Ba/La	34	30	40	40	55	10	20
Sr/Nd	86	90	80	90	81	70	100
Zr	20	19	31	34	37	9	16
Nb	< 1	< 1	< 1	< 1	< 1	< 1	< 1
Zn	67	65	50	48	48	66	74
Cu	128	111	107	61	99	150	99
Ni	45	52	11	9	9	135	50
Sc	36	38	18	15	16	69	41
V	266	272	177	151	161	324	374
Cr	190	237	31	21	22	535	221
Ga	12.5	12.5	15.0	14.5	13.5	9.0	13.5
Cr/V	.714	.871	.18	.14	.14	1.65	.591

[a] Numbers in parenthesis are those obtained after adjusting $Fe^2 = 0.85\Sigma Fe$ (Nicholls and Whitford 1976).
[b] Values determined by spark-source mass spectrography (La and Ce in sample 53 by interpolation).

characteristic of arc basalts. Sr/Nd and Zr/Nb are also high - other characteristics of many island-arc basalts (DePaolo and Johnson 1979; Sun et al. 1979). Al_2O_3 contents, however, are low, though not anomalously so as many arc basalts have similar values.

100 $Mg/(Mg+Fe^{2+})$ values are 74-80, but this range is lowered to 64-68 after adjustment of the oxidation state of Fe (see Table 1). These adjusted values correspond to equilibrium olivine compositions of Fo_{86-87} (using the Roeder-and-Emslie (1970) Mg-Fe/olivine-liquid distribution coefficient of 0.3) - values which may be too low for the compositions of mantle olivine remaining after a partial-melting episode (e.g. Clarke and O'Hara 1979). The Ni contents of all three samples are also low (45-52 ppm). These samples therefore seem to represent magmas that have undergone olivine fractionation. If samples 53, 61, and 54E are the derivatives of primary magmas that were in equilibrium with mantle olivine of, say, Fo_{91} composition, then the primary magmas have lost 12.6, 11.1, and 16.9 percent olivine, respectively (results obtained from an iterative calculation similar to the one described by Nicholls and Whitford 1976).

The Cr-spinel-rich inclusion 55C is the most magnesian of the analysed rocks. Its incompatible-element contents are notably low, and its high Cr content and high 100 $Mg/(Mg+Fe^{2+})$ are more appropriate (than those of the other three basalts) to a mantle-derived composition. However, its Ni content is fairly low, and there is considerable doubt if this coarse-grained, possibly cumulative sample is representative of a true liquid composition.

Group-2 Andesites - The three analysed Boisa andesites are chemically similar, and have about 5-10 percent more SiO_2 than the basalts (table 1). The western-cumulodome samples, having higher SiO_2, Na_2O, K_2O and lower total-Fe, MgO, and CaO, but 100 $Mg/(Mg+Fe^{2+})$ values and transition-element abundances are more-or-less the same.

The Boisa andesites have 3-6 percent more SiO_2 than does a reference Papua New Guinea andesite composition from Bagana volcano (Bultitude et al. 1978), but nevertheless have lower contents of most incompatible elements (values for Ba, Pb and U are the same or slightly higher). Also, the chondrite-normalized REE pattern of sample 59 (fig. 5) is less fractionated than those of Bagana samples.

Boisa andesites contain 2-3 times the K_2O, Rb, Ba, Pb, Th, U, Zr, and Hf in the basalts, implying derivation from basaltic parents by about 33-50 percent fractionation if the bulk-distribution coefficient of the minerals is close to zero. REE enrichment in the andesites is about 1.3 greater than in the basalts, and there is no Eu anomaly in sample 59 or any detectable difference between La/Yb of samples 53 (basalt) and 59 (fig. 5). Cr and Ni contents are 5-10 times higher in the basalts than in the andesites, whereas Zn, Cu, Sc and Va re 1.5-2 times more abundant. There is a 3-6 fold decrease in Cr/V from the basalts to the andesites. Sr is only slightly higher in the andesites, thus accounting for the consistently higher Rb/Sr and lower Sr/Ba compared to the basalts. Ba/La values are 1.5-2.5 times higher in the andesites.

CRYSTAL FRACTIONATION MODELLING

Least-Squares-Mixing - A fractional-crystallization relationship between the basalts and andesites seems likely on the basis of the qualitative comparisons made above. Two possibilities may be evaluated: (1) an anhydrous fractionation sequence involving the phenocryst minerals in the basalt; (2) a hydrous one dominated by amphibole, as in the group-3a inclusions.

Samples 53 and 59 were chosen as a parent → derivative-magma pair. Sample 59, from the western cumulodome, was selected as the derivative composition because it is the least porphyritic of the

Boisa andesites and the least contaminated by group-3a-type crystal fragments, and is therefore the most likely to represent a liquid composition. Mineral compositions used in matching the two whole-rock, major-element analyses were averages of near-rim microprobe analyses, and were chosen to establish petrological continuity between the minerals separating from the parent and the composition of the residual liquid.

Results of the least-squares calculations are set out in Table 13 of Gust et al. (1980). (The calculations are based on the program of Wright and Doherty (1970), but the program we used is more flexible in that input mineral compositions may be excluded during the computation if this results in a significantly better least-squares fit). Calculations of this nature are subject to several uncertainties (e.g. Banks 1979), but the main conclusion is that either set of fractionating minerals - basaltic phenocrysts or those in the coarse-grained inclusions - provide a satisfactory (low ΣR^2) least-squares solution. Olivine, a minor constituent of only one amphibole-bearing assemblage (sample 52B) was excluded during the computation, and is therefore not in the list of final minerals, suggesting that it was not a major fractionating phase.

ΣR^2 values are similar for both solutions, but the calculated abundances for TiO_2 and K_2O using the amphibole-bearing assemblage are in poor agreement with the actual abundances, compared to those obtained using the phenocryst assemblage. Amphibole is the main host for Ti and K in the inclusions, and therefore provides the greatest error in the calculation. A similar result was obtained in the least-squares calculations involving amphibole for Lesser Antilles rocks (Arculus 1976; Arculus and Wills 1980).

A fractional-crystallization relationship between the basalts and andesites therefore seems to be a reasonable hypothesis for the Boisa lavas, although which of the two assemblages was responsible

cannot be deduced from the least-squares results.

Trace-element Modelling - Fractionation of about 52-57 weight-percent crystals from the basalts is indicated by the least-squares results, an amount only slightly higher than the 33-50 percent estimated on the basis of incompatible-element-enrichment factors of 2-3 in the andesites. However, a more detailed assessment using three sets of published partition coefficients for Rb, Ba, K, Sr and six REE has revealed important discrepancies that do not support a simple crystal-fractionation model. One set of partition coefficients consists mainly of average values for mineral-host pairs, whereas the other two are mainly for specific mineral-host pairs (Gust et al. 1980).

Four sets of results plotted in figure 6 were obtained by using the three partition-coefficient sets in conjuction with both sets of least-squares mineral proportions. ΔD in figure 6 is obtained from the relationship:

$$\Delta D = D \text{ (ideal)} - \Sigma d.$$

where D (ideal) is the bulk-distribution coefficient that must be used to obtain a perfect fit between trace-element contents in basalt 53 and andesite 59, and where Σd is the sum of individual mineral distribution coefficients obtained by using the individual mineral proportions from the least-squares results, and their corresponding distribution coefficients.

The ΔD values for Sr, Rb, and the six REE in all four sets of results are positive (except for Yb in model B'), indicating that the Boisa andesites are too poor in these elements to have been derived by closed-system Rayleigh-fractionation. In contrast, the values for K and Ba are negative for models A and A' indicating that the andesites are enriched in these elements relative to a fractionation scheme involving amphibole. Models B and B' provide reasonable

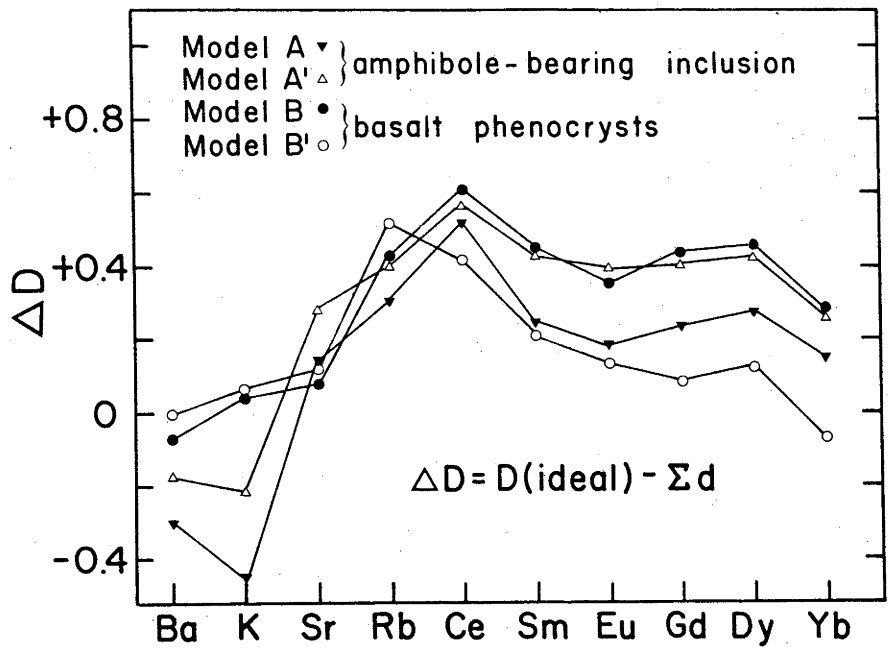

Figure 6. Differences (ΔD) between 'ideal' bulk-rock distribution coefficients (D) and those (Σd) calculated using least-squares mineral proportions and partition coefficients.

solutions for a simple fractionation model for K and Ba in that the ΔD values are close to zero. In addition, model B' (basalt phenocrysts with specific mineral/host partition coefficients) consistently has the lowest ΔD values for the six REE. If, however, these values are translated into calculated trace-element abundances and compared with observed abundances, the differences are significantly greater than analytical error.

In general, therefore, use of the amphibole-bearing assemblage (models A and A') is at best no more successful in obtaining an ideal fit ($D = 0$) than is the basalt-phenocryst assemblage (B and B'). Gill (1978) suggested that significant hornblende fractionation ought to be detected by a marked decrease of K/Rb, Ba/Rb and Ba/La and an increase in Cr/V in derivative andesites, and that heavy REE and Y remain constant or decrease during fractionation. None of these features are detectable in the Boisa suite. However, the [Yb/Ho] e.f. value of andesite 59 is slightly greater than that in the basalt, causing the slight negative anomaly in the REE pattern around Dy and Ho to be enhanced (fig. 5). If this is a real feature, then amphibole fractionation may have caused it, but this is the only evidence in favour of amphibole having been in the fractionating mineral assemblage.

DISCUSSION

Simple crystal fractionation - Disparities between observed trace-element abundances and those calculated on the basis of least-squares results and fractionation equations, have been noted in rock suites from several areas, particularly on oceanic islands and the ocean floor; fractionated rocks have greater amounts of several incompatible-elements that would otherwise be expected (e.g. Peck et al. 1966; Jackson and Wright 1970; Bryan and Moore 1977; White and Bryan 1977).

This effect has also been noted in island-arc and back-arc volcanoes (Johnson and Arculus 1978; Stern 1979). Explanations for the enrichments have included diffusion of certain elements to the peripheries of magma cupolas, and vapour-phase transport of elements within reservoirs, on the assumption that low-residual least-squares calculations are not coincidental, but reflect actual petrogenetic processes. The alternative is to reject low ΣR^2 least-squares results and explain the petrogenesis by some other means.

Several interpretations may be proposed to account for the ambiguities present in a simple crystal-fractionation relationship between the basalts and andesites of Boisa Island. The good fits for both least-squares calculations are evidence that crystal fractionation is a viable hypothesis, but these calculations do not establish either mineralogic assemblage as a unique or even a preferred solution. The disparities observed between 'ideal' fractionation and that required using the least-squares results in Rayleigh-fractionation calculations (for incompatible trace elements) do not clarify the problem. However, our results may be evidence that petrogenetic processes involving simple fractionation cannot be evaluated successfully using only least-squares calculations and the Rayleigh-fractionation equation. Certainly our results have not demonstrated the importance of amphibole in the fractionation of Boisa magmas, and this may be significant for the Bismarck volcanic arc as a whole where amphibole phenocrysts are absent from basalts and uncommon in andesites. Amphibole may not necessarily have played an important role in the fractionation of these mafic magmas.

There must also be concern that simple Rayleigh-type fractionation does not accurately represent the real life behaviour of the trace elements involved in the Boisa calculations. Albarede and Bottinga (1972) suggested that such might be the case for the REE, large alkali metals, and the large alkali earth metals, due to their low diffusion

rates in silicate liquids. A non-Rayleigh distillation model, such as their model B-3, would result in crystals with real partition coefficients significantly less than the average 'apparent' coefficients used in the Boisa calculations. Unfortunately, this result would cause an even greater disparity between calculated trace element abundances and those observed in the andesite.

Modifications of simple crystal-fractionation - Two more complex interpretaions may be proposed to account for the disparity between 'ideal' fractionation and the fractionation required using the least-squares results. First, the andesites may be related to a batch of basaltic parental magma different in incompatible-element content from the basalts found on Boisa. The concept of magma batches was also proposed recently for another Papua New Guinea volcano, Bagana, on Bougainville Island (fig. 1) where three andesite batches were recognized (Bultitude et al.,1978).

The second interpretation is that magmas may have mixed in the Boisa reservoir by a process analogous to the one proposed for ocean-floor basalts (O'Hara 1977; Dungan and Rhodes 1978; Rhodes et al. 1979). This involves a magma chamber being periodically refilled with liquid of uniform composition, and mixing with a pre-existing magma that has undergone some crystal fractionation. This process accounts for the enrichment of incompatible elements in some ocean-floor basalts, and a variation of it must be made for the case of apparent depletion in several incompatible elements in the Boisa andesites. Parental magmas that refill the Boisa chamber must contain lower abundances of the incompatible elements than the magmas that formed the older cone of Boisa Island.

Neither of these models can be tested, mainly because the obviously complex petrogenetic relationships are difficult to quantify. Furthermore, the possible supplementary roles of element

migration within magmas and by vapor-phase diffusion are unknown.

Magma mixing - An alternative hypothesis that does not require crystal fractionation involves the mixing and partial assimilation of group-3a inclusions by a silica-rich magma. This process embodies some of the 'classical' ideas of magma mixing (e.g. Eichelberger 1975, 1978; Anderson 1976), and accounts for many of the disequilibrium petrographic features observed in the andesites. In addition, the low abundances of incompatible trace elements can be accounted for by linear mixing.

Group-2 andesites, as stated above, contain two distinct types of crystals. One type consists of fragments of disaggregated group-3a inclusions, and the other type of cognate phenocrysts. The inclusion component has numerous disequilibrium-type textures (e.g. dusty and corroded Ca-rich plagioclase, pseudomorphed amphibole patches, forsteritic olivine rimmed by orthopyroxene, and highly magnesian and Al-rich diopsidic clinopyroxenes). These textures are evidence that the fragments reacted with, and were partially assimilated by, the host lava. A correlation between phenocryst content and chemical composition adds additional support to the mixing concept: andesites containing greater amounts of phenocrysts and crystal fragments are less siliceous than aphyric ones.

Objections have been raised to mixing and assimilation-type petrogenetic schemes. One of these - a thermal argument against assimilation (see discussion by McBirney 1979) - can be dismissed for the case of Boisa by stressing that our interpretation involves primarily mechanical disaggregation of solid inclusions. A more important objection concerns the nature and generation of the silica-rich magma responsible for the actual mixing event.

Rocks richer in SiO_2 than the most SiO_2-rich Boisa sample 59 (61.7 percent SiO_2; table 1) are rare in the western part of the

Bismarck volcanic arc (that is, as far east as the western tip of New Britain; fig. 1). Only six of 124 chemical analyses of western rocks tabulated by Johnson (1977) contain more than 61.7 percent SiO_2, and none contains more than 65.9 percent SiO_2. Dacites therefore appear to be extremely rare, and rhyolites completely absent. Dacites and rhyolites are much more common in central-north and east New Britain (Johnson, 1977), and are abundant in the St. Andrew Strait area (fig. 1) where rhyolitic volcanism has been attributed to partial melting of basaltic crust (Johnson et al. 1978). The rarity of silica-rich rocks in the western Bismarck volcanic arc relative to other parts of the Bismarck Sea region, is therefore a notable feature and remains a problem for a felsic-melt/mafic-inclusions mixing model for the Boisa andesites. Perhaps dacitic and rhyolitic magmas tend to be intruded rather than extruded in this part of the Bismarck volcanic arc. Perhaps also the presence of rhyolitic glasses as inclusions in the plagioclase crystals of the Boisa group-3b sample is evidence that more voluminous silica-rich magma once existed beneath Boisa.

CONCLUSION

The problem of the petrogenesis of Boisa Island basalts and andesites has no unique solution at present. Arguments can be advanced for a crystal-fractionation relationship, and these include as their mainstay the low-residual least-squares fits. However, ambiguity in the choice of the fractionating mineral assemblage, and disparities between the trace-element modelling results and the actual values, weakens this hypothesis. The disparities may be explained, however, by different parental magmas for the basalts and andesites, or by mixing of a fractionated parental magma with an incompatible-element-depleted mafic melt.

Another interpretation, involving mixing of mafic crystals with a silica-rich magma, apparently accounts for many of the petrographic

features and chemical features observed in the andesites. However, a cogenetic relationship between basalts and andesites is not required by this model, the least-squares fits must be regarded as coincidence, and the nature and origin of the postulated silica-rich magmas remain unclear.

ACKNOWLEDGEMENTS

R.A. Davies is thanked for the assistance he gave one of us (RWJ) in collecting the samples from Boisa, B.W. Chappel is thanked for providing most of the whole-rock trace-element data (X-ray fluorescence), and R.J. Arculus is thanked for helpful comments, especially concerning the thermodynamic calculations. We are also indebted to S.E. DeLong and A.L. Boettcher for their reviews of the manuscript. RWJ publishes with the permission of the Director of the Bureau of Mineral Resources, Canberra.

APPENDIX: THERMODYNAMIC CALCULATIONS OF T, P, aO_2 FOR EQUILIBRATION OF SAMPLE 52B

The activities of the end members used in these calculations were derived assuming ideal mixing on site and encompass a range of values. The components, definition of activity and range in values are, respectively: $aCaMgSi_2O_6$, $X_{M_1}^{Mg} \cdot X_{M_2}^{Ca} \cdot (X_{tet}^{Si})^2$, .637-.723; $a_{Mg_2Si_2O_6}^{cpx}$, $X_{M_1}^{Mg} \cdot X_{M_2}^{Mg^*}$, .04-.06; $aMg_2Si_2O_6$, $X_{M_1}^{Mg} \cdot X_{M_2}^{Mg^*}$, .502-.598; aMg_2SiO_4, $(XMg)^2$, .614-.695; aFe_2SiO_4, $(XFe)^2$, .027-.047; $aCaAl_2Si_2O_8$, XCa, .854-.912; $aMgAl_2O_4$, $X_{Mg}^{A} \cdot (X_{Al}^{B})^{2**}$, .112-.119; aFe_3O_4, $\frac{1}{2}nFe^{3+}$, .642-.756. $X_{M_2}^{Mg*}$ is defined by $\frac{nFe}{nMg}^{M_1} = \frac{nFe}{nMg}^{M_2} = \frac{nFe}{nMg}$ mineral and

$$(X_{Al}^{B})^{**} = \frac{n\ Al}{\text{Sites remaining after subtraction of charge balanced magnetite + ulvöspinel}}$$

Temperatures (T) were determined using the Wood and Banno (1973) two-pyroxene geothermometer:

$$\frac{-10202}{T} = \ln \left(\frac{a_{Mg_2Si_2O_6}^{cpx}}{a_{Mg_2Si_2O_6}^{opx}} \right) - 7.65\ X_{Fe}^{opx} + 3.88\ (X_{Fe}^{opx}) - 4.6 .$$

Pressures were determined using the reaction:

$$2Mg_2SiO_4 + CaAl_2Si_2O_8 = Mg_2Si_2O_6 + CaMgSi_2O_6 + MgAl_2O_4$$

as outlined by Powell (1978), but with important revisions in (1) the use of orthopyroxene-bearing assemblages, instead of fictive clinoenstatite in clinopyroxene, and (2) deletion of a rather arbitrarily assumed Henry's Law constant in $a_{MgAl_2O_4}$. The ΔG^{o}_{1} calculated for this reaction by Powell (1978) is only applicable to systems with

orthopyroxene, not clinoenstatite. Hence, pressure is given by:

$$0 = \Delta G^{o}_{1} + RT \ \ln \frac{aMg_2Si_2O_6 \cdot aCaMgSi_2O_6 \cdot aMgAl_2O_4}{a^2Mg_2Si_2O_4 - aCaAl_2Si_2O_8}$$

where $\Delta G^{o}_{1} = -16.5 + 0.0336\ T - 1.969\ P$ (P in kbars, T in ^{o}K; Powell 1978, Appendix 1).

aO_2 was calculated by the method of Powell (1978) but using orthopyroxene instead of clinoenstatite in clinopyroxene. The reaction is:

$$3Mg_2SiO_4 + 3Fe_2SiO_4 + O_2 = 3Mg_2Si_2O_6 + 2Fe_3O_4$$

where the aO_2 is given by $0 = \Delta G^{o}_{2} + RT \ln K' - RT \ln aO_2$ where $\Delta G^{o}_{2} = -534.8 + 0.1964T + 0.682P$ (P in kbar, T in ^{o}K; Powell 1978) and $\ln K'$ in $\ln \frac{a^2Fe_3O_4 \cdot a^3Mg_2Si_2O_6}{a^3Mg_2SiO_4 \cdot a^3Fe_2SiO_4}$.

CHAPTER 6

THE PETROLOGY, GEOCHEMISTRY AND PETROGENESIS OF ANORGENIC ANDESITES, DACITES AND RHYODACITES OF THE MORMON MOUNTAIN VOLCANIC FIELD, ARIZONA , U.S.A.

INTRODUCTION

The acceptance of the plate tectonic hypothesis constituted a major revolution in the Earth sciences and provided geologists with a theory by which many geological phenomena could be explained. Among the first applications of the hypothesis was the association of subduction zone processes with the origin of the 'calc-alkaline' island arc series, and in particular, the genesis of andesite. Numerous petrologic, geochemical and experimental investigations of these 'orogenic volcanic series' (Ringwood, 1975) over the past two decades have to date, nevertheless failed to establish the exact nature of this relationship. Many of these studies have shown that some andesites and dacites are derived by fractional crystallization from basaltic parents. The key to understanding island arc petrogenesis may therefore lie with the genesis of island arc basalts. Although these studies have substantially reduced the importance of primary andesitic magmas within the 'orogenic volcanic series' (excluding the boninite - high Mg andesite sequences), the generation of primary andesitic magmas remains viable for some volcanic suites of continental volcanic arcs such as the Andes (e.g. Bruhn et al., 1978). Anatexis of the continental crust as a means to produce primary andesitic magma is an important, but poorly understood process. The study of anorogenic volcanic suites from continental intra-plate

environments which may result in part, from crustal anatexis, may provide valuable insight on this process.

Anorogenic volcanic suites, which by definition are not related to subduction, are present in a number of continental intra-plate environments (e.g. Turkey - Lambert et al., 1974; Peccerillo and Taylor, 1976; Australia - Ewart et al., 1976; U.S.A. - Lipman et al., 1972; Christiansen and Lipman 1972; Elston, 1976; France - Girod and Lefèvre, 1972). These suites include mafic and silicic varieties which range from sub-alkalic to highly alkalic compositions. This study examines the petrology and geochemistry of the silicic members of a bimodal suite consisting of basalts (Appendix 7) and 'calc-alkaline' high-Si andesite, dacite and rhyodacite from the Mormon Mountain volcanic field ('MMVF') Arizona. This field occurs near the edge of the Colorado Plateau where the continental crust thins from ~ 40 km to 20 km, typical of the Basin and Range Province. Plate tectonic reconstructions (Atwater, 1970; Snyder and Dickinson, 1976) suggest that subducted lithosphere has been absent beneath this area for the last 15 m.y. This evidence, combined with the lack of intermediate and deep earthquakes and absence of an offshore trench indicate that this suite is not related to subduction, contrary to the hypothesis advanced by Lipman et al. (1972).

The petrology and geochemistry of the entire basalt to rhyodacite suite suggests that the silicic rocks are not derived from the basalts by crystal fractionation, simple crustal contamination of basalt magmas or magma-mixing. The petrogenesis of the silicic suite is evaluated with respect to crustal anatexis using major element, trace element, and isotopic data. These studies suggest that amphibolite or garnet amphibolite when partially melted at pressures typical of the lower crust, could produce magmas corresponding to the observed volcanic rocks.

Geology - The Mormon Mountain volcanic field is located just south of Flagstaff, Arizona (Fig. 1). The field covers approximately 7000 square kilometers and consists of a relatively thin, flat plateau of basalt with numerous cinder cones and localized silicic centers of andesite, dacite and rhyodacite. These centers form prominent local relief up to 460 meters higher than the surrounding basalt plateau. The exposed amount of basalt exceeds that of the silicic rocks, but precise estimates of volumes of total volcanic material are difficult to calculate. The detailed field relations of many of the rock types remain obscure as contacts are not well exposed.

The silicic volcanic rocks consist of coalescing high-silica andesite and dacite flows, and dacite or rhyodacite domes and plugs. Mormon Mountain is the largest silicic center in the field, and is composed of hornblende andesite flows overlain by dacite flows. A rhyodacite dome occurs near the southern flank of Mormon Mountain and is topographically set off from the mountain. A similar rhyodacite dome (sample MMT-18) of lesser extent outcrops approximately six miles south of Mormon Mountain (Fig. 2) and is situated in the middle of a basaltic cinder cone. Additional andesite domes occur sporadically throughout the field (samples MMT-21, MMT-22, MMT-25), but are of minimal extent.

The volcanic field directly overlies the Coconino sandstone of Permian age. Although not exposed locally, the entire Paleozoic sedimentary section can be observed at the Grand Canyon. It is assumed that this sedimentary strata as well as Precambrian granites, schists and gneisses similar to those which are exposed in the Grand Canyon, comprise the upper crust of this section of the Colorado Plateau. The nature of the lower crust can only be inferred from combined geophysical (Prodehl, 1970) and petrologic studies of high

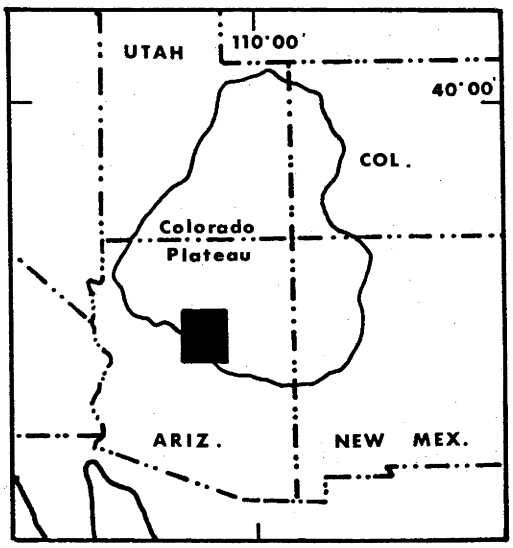

Figure 1. Location map of the 'MMVF' study area (dark square) with respect to the physiographic boundary of the Colorado Plateau.

Figure 2. Geologic map of the Mormon Mt. complex and surrounding area. Locations of samples MMT-1 to MMT-18 are shown.(NEXT PAGE)

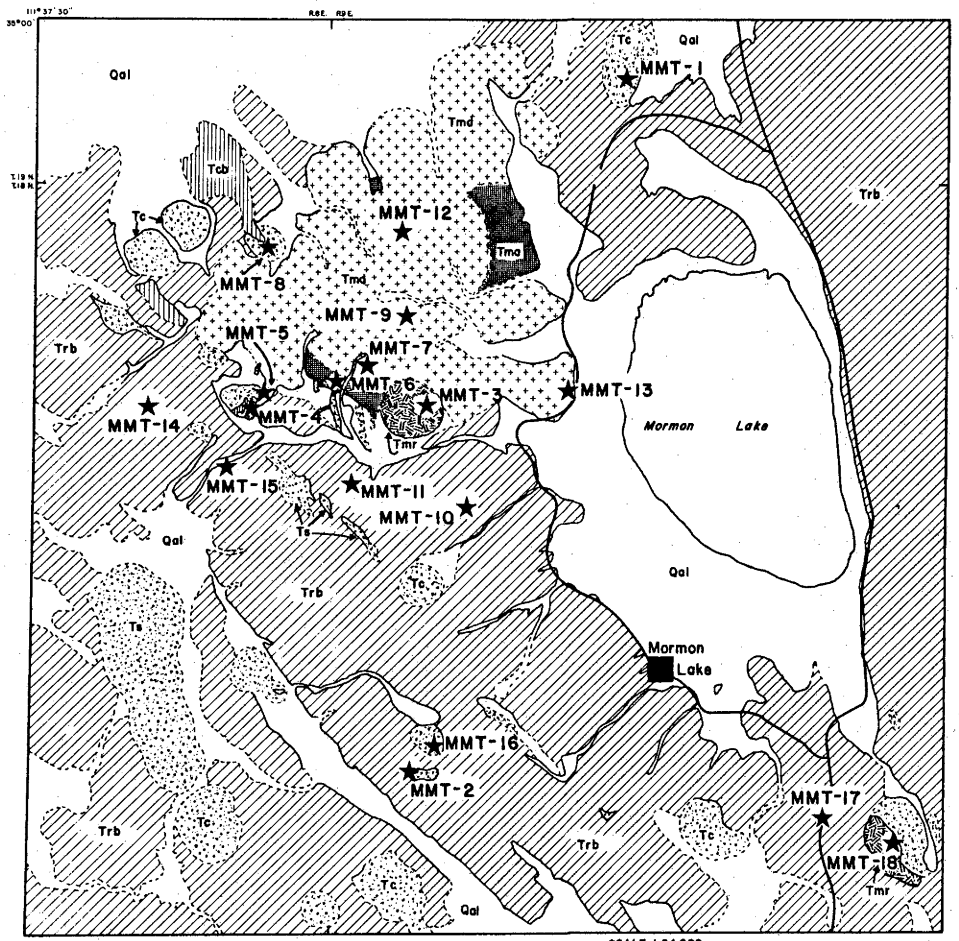

GEOLOGIC MAP OF THE MORMON MOUNTAIN VOLCANIC COMPLEX, ARIZONA

D.A. Gust
1981

EXPLANATION

Alluvial and Colluvial Deposits (Quaternary)

Qal — Alluvium and colluvium; sand, silt, gravel and boulders, mostly of basalt except near Mormon Mountain where andesite, dacite and rhyodacite prevail.

Mormon Mountain Volcanic Center (Pliocene)

Tmr — Rhyodacite domes of Mormon Mountain area, porphyritic with phenocrysts of hornblende and plagioclase.

Tmd — Pyroxene dacite flows of Mormon Mountain, porphyritic with phenocrysts of clinopyroxene and orthopyroxene ± hornblende. Occassionally contains xenoliths of plagioclase and hornblende. Dated at 3.1 m.y. (Moore, personal communication).

Tma — Andesite flows of Mormon Mountain, porphyritic with phenocrysts of hornblende and clinopyroxene. Probably overlain by the dacite flows.

Basaltic Rocks (Pliocene and Miocene)

Trb — Rim basalts, predominantly alkali olivine basalt with phenocrysts of olivine and clinopyroxene. Flows, erupted from NW-trending fissures, are subdued by weathering and mantled with a well developed soil.

Tcb — Small flows and dikes of alkali olivine basalt associated with cinder cones.

Ts — Spatter deposits of highly oxidized basalt commonly associated with fissure vents and cinder cones.

Tc — Cinder cones of red and brown basaltic cinders, generally deeply weathered to form a dark brown soil. Cones are subdued but not deeply dissected. Bombs of basalt occur on the slopes of the cones. Rims and dikes of basaltic spatter are common. Most cones are not associated with lava flows.

Map Symbols

— — — Contact, dashed where inferred

★ Sample location of geochemically analyzed samples.

——— Paved road

pressure nodules in explosive volcanics (Arculus and Smith, 1979; Ehrenberg and Griffin, 1979; Appendix 8).

Sampling - Several hundred samples of basaltic and silicic rocks, were collected and examined in hand specimen and thin section. From this group 71 samples were analyzed for major elements, with 34 being selected for trace element analysis. The locations of all 34 of these samples are given in Figures 2 and 3. The silicic samples (10) are MMT-6, 21, 22, 25, 7, 9, 12, 13, 3 and 18. The area around Mormon Mountain was examined in more detail (Fig. 2) with predominant sample selection obtained from that area. Almost all samples geochemically analyzed, were also examined using the electron microprobe. Phase chemical information was obtained for mineral phases and glasses.

Past Research - Past research in the region has concentrated on the extensive San Francisco volcanic field located due north of the Mormon Mountain volcanic field. Robinson (1913) spent one day in the vicinity of Mormon Mountain, completing a traverse to its summit on the eastern flank. He noted the dacite dome on the southern flank of the mountain and concluded 'that the mountain is made of coalescing latitic flows'. His memoir on the San Francisco volcanic field (Robinson, 1913) includes major element analyses of the dacite, a latite and a basalt from Mormon Mountain. No other petrologic or geochemical work has been conducted in the area.

Age Relations - Moore (pers. comm., 1977) obtained a sample of chilled dacite from the top of Mormon Mounain for K/Ar radiometric dating. This sample has been dated at 3.1 ± .06 m.y. (McKee, unpublished data). Harrison (pers. comm., 1980) dated an andesite (MMT-21) obtaining an age of 3.6 ± .04 m.y. (K/Ar). Damon et al. (1974) dated basalts from Anderson Mesa and Oak Creek Canyon, which mark the northern and western extent of 'MMVF'. These basalts yield K/Ar ages

Figure 3: Location of all samples from 'MMVF' which have been analyzed for major and trace elements. Silicic samples are MMT-3, 6, 7, 9, 12, 13 (from the Mormon Mt. complex, enclosed area) and MMT-18, 21, 22,25. MMT-18 is also within the enclosed area, which is the location of the geologic map shown in Figure 2 .

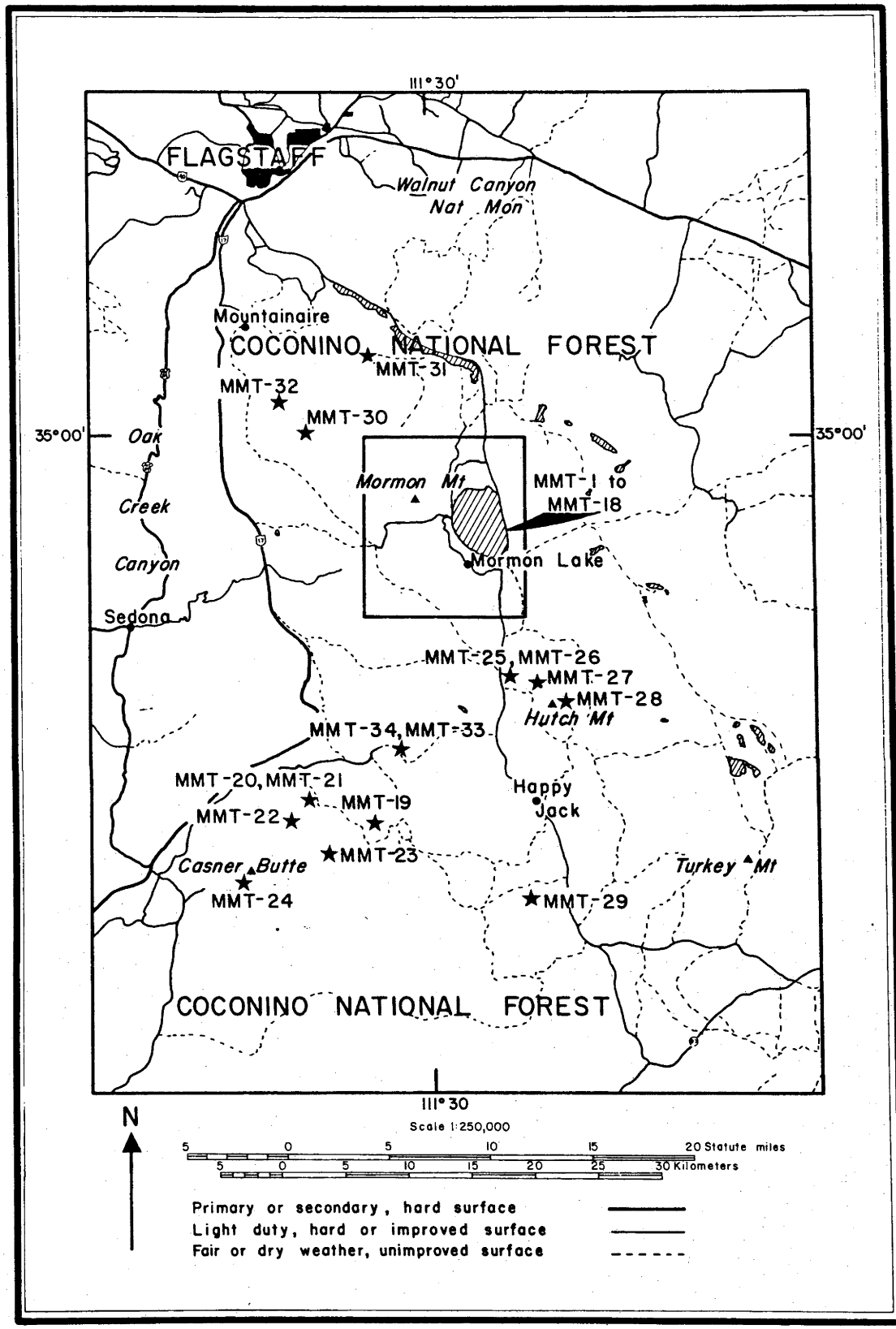
111°30'
FLAGSTAFF
Walnut Canyon
Nat Mon
Mountainaire
COCONINO NATIONAL FOREST
MMT-31
MMT-32
MMT-30
35°00'
Oak
Creek
Canyon
Sedona
Mormon Mt
MMT-1 to
MMT-18
Mormon Lake
MMT-25, MMT-26
MMT-27
MMT-28
Hutch Mt
MMT-34, MMT-33
MMT-20, MMT-21
MMT-19
MMT-22
MMT-23
Happy
Jack
Casner Butte
MMT-24
MMT-29
Turkey Mt
COCONINO NATIONAL FOREST
111°30
N
Scale 1:250,000
5 0 5 10 15 20 Statute miles
5 0 5 10 15 20 25 30 Kilometers
Primary or secondary, hard surface
Light duty, hard or improved surface
Fair or dry weather, unimproved surface

of 5.88 ± .91 m.y. and 6.00 ± .30 m.y., respectively. Recent data on basalts from the southern edge of the field near Casner Butte and Pine, indicate that the basaltic volcanism there is older (9 - 15 m.y.) (Peirce, et al., 1979).

PETROLOGY AND PHASE CHEMISTRY

General - The silicic volcanic rocks of 'MMVF' are hypocrystalline, mildly porphyritic with hyalopilitic textures. The classification of the suite into andesites, dacites and rhyodacites is based on geochemistry because the rocks are predominantly fine-grained and glassy. The classification of Middlemost (1973) in which total alkalis ($Na_2O + K_2O$) are plotted against SiO_2 is used (Fig. 4). Descriptive terms, such as hornblende andesite, reflect the dominant phenocryst mineralogy of the rock. The silicic suite consists of hornblende andesites, two-pyroxene dacites and hornblende rhyodacites.

Mineral analyses for the various rocks were determined by TPD electron microprobe (Reed and Ware, 1973; 1975) and with data reduction program 'OXIDE' (Ware, 1981). Representative mineral analyses are given in Appendix 6.

Groundmass Phases - The groundmasses of the silicic volcanic rocks are composed predominantly of plagioclase and glass with subordinate opaques, clinopyroxene, quartz, alkali feldspar, and apatite. Plagioclase occurs as small laths and has compositional ranges of An_{65-37} (andesites), An_{51-42} (dacites), and An_{40-25} (rhyodacites) (Fig. 5). Light to dark brown glass is fresh and exhibits only minor devitrification. Representative glass analyses from the andesites, dacites, and rhyodacites are given in Table 1. Opaque phases consist of either titanomagnetite alone, or with coexisting ilmenite. Titanomagnetite, which coexists with the ilmenite,

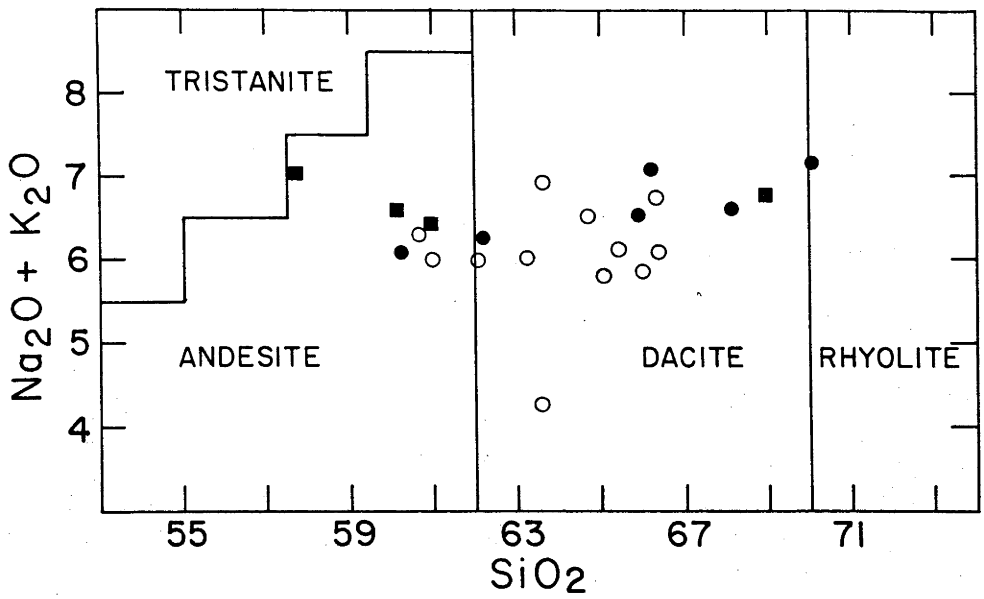

Figure 4. $Na_2O + K_2O$ vs. SiO_2 variation diagram for 'MMVF' silicic rocks. Open circles are analyses from Appendix 6. Filled circles are analyses from the Mormon Mt. complex, and filled squares are analyses from other areas. Classification is that of Middlemost (1973).

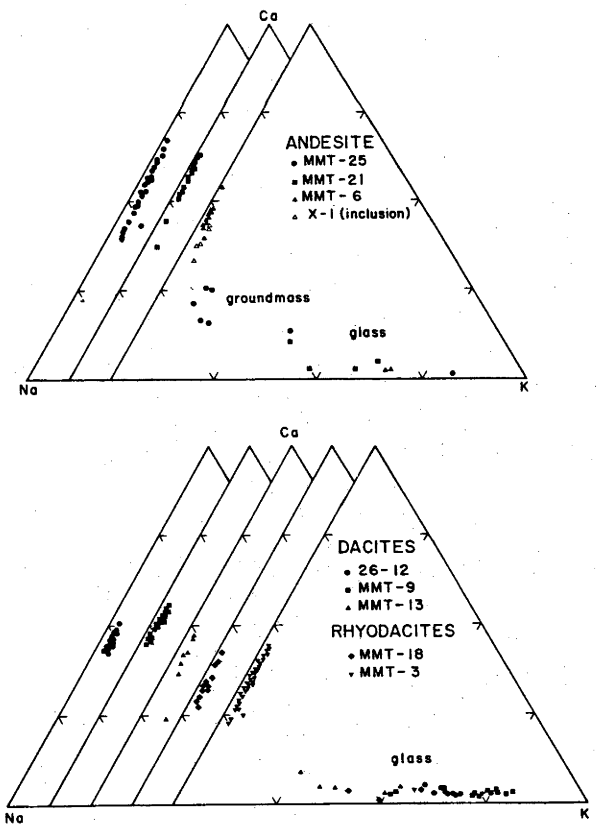

Figure 5. Plagioclase analyses of 'MMVF' silicic rocks.

TABLE 1: Representative Glass Analysis

	Andesites			Dacites			Rhyodacite
	MMT-6	MMT-21	MMT-25	MMT-9	MMT-13	26-12	MMT-18
SiO_2	72.8	73.2	73.2	75.5	71.1	72.3	76.9
TiO_2	.9	.8	.6	.8	.1	.6	.2
Al_2O_3	11.6	11.9	10.0	11.9	17.3	11.3	12.0
FeO	1.6	1.6	.4	1.3	.5	1.5	.5
MgO	.2	.5	--	.2	--	.2	.2
CaO	.2	.6	.2	.3	2.0	.4	.3
K_2O	5.0	4.6	6.3	4.3	2.9	5.3	3.6
Na_2O	1.7	2.7	.8	2.4	6.2	1.8	2.8
TOTAL	94.0	95.9	91.5	96.7	100.1	93.4	96.5

contains less ulvöspinel component than does titanomagnetite which occurs alone.

Phenocryst Phases -

(a) Plagioclase - Plagioclase phenocrysts occur abundantly in one andesite (Hutch Mt.) and both rhyodacites (MMT-3, MMT-18). It is rare in two other andesites (Round and Table Mts.) and absent in the andesite (MMT-6, 7) and dacites (MMT-9, 12, 13) at Mormon Mountain. The lack of significant phenocrystal plagioclase in rocks with these compositions is unusual (Ewart, 1976; 1979).

Euhedral plagioclase phenocrysts are present in the Hutch Mountain andesite with the crystals displaying strong reverse zoning (cores - An_{39}; rims - An_{64}). Rare phenocrysts (xenocrysts?) of albite are present and are associated with quartz fragments and large magnetite grains. The plagioclase phenocrysts of the other andesites from Round and Table Mountains, in contrast to the Hutch Mountain andesite are sparsely distributed, normally zoned (An_{63}- An_{56}), subhedral, fragmented grains. There are two generations of plagioclase phenocrysts in the rhyodacites, distinguishable by morphology and compositional range. The first generation of phenocrysts consist of large (up to 1 cm) rectangular grains with oscillatory zoning in contrast to the small (3 mm), normally zoned, equant crystals of the second generation. Core-rim analysis reveals variations from An_{45} to An_{30} and An_{33} to An_{24} (Fig. 5) in the first and second generations respectively.

(b) Amphibole - Amphibole is the second most abundant phenocryst phase occurring in variable proportions in the andesites and rhyodacites. The phenocrysts are generally large, subhedral to euhedral, prismatic grains with reaction rims dominated by magnetite. A few grains are totally replaced by microcrystalline aggregates of magnetite and

pyroxene ('black' type; Garcia and Jacobson, 1979). Medium-grained aggregates of anhedral orthopyroxene, clinopyroxene, plagioclase and magnetite ('gabbroic' type; Garcia and Jacobson, 1979) are not observed. Estimates of Fe^{3+}/Fe^{2+} ratios suggest these amphibole phenocrysts range from ferroan pargasitic hornblende (andesites) to ferroan pargasite (rhyodacite) (Leake, 1978).

(c) Clinopyroxene - Phenocrysts of clinopyroxene occur abundantly in the andesites and dacites of Mormon Mountain and infrequently in the andesite of Hutch Mountain. They are subhedral to euhedral, moderately-sized grains (0.5 cm) which commonly exhibit sector twining and concentric zoning. The phenocrysts are augitic with only minor compositional zoning from core to rim (Fig. 6). Augites in the andesites contain approximately twice as much TiO_2 and Al_2O_3 (0.71 wt.%; 4.5 wt.%) as augites in the dacites.

(d) Orthopyroxene - Orthopyroxene phenocrysts, ranging in composition from bronzite to hypersthene, occur only in the pyroxene dacite. They are commonly associated with clinopyroxene as two pyroxene glomerocrysts.

Inclusions - Occasional coarse-grained inclusions consisting of amphibole and skeletal plagioclase are found in the pyroxene dacite flows near Mormon Lake. The plagioclase of these inclusions is often altered, by both reaction and weathering. Compositions range from cores of An_{52} to rims of An_{47}. The amphibole is compositionally similar to the amphibole phenocrysts of the Mormon Mountain andesite. The similarities between these phases of the inclusion and those observed as phenocrysts in the andesite, suggest that these inclusions may represent andesitic cumulates, entrapped by the ascending dacitic magma.

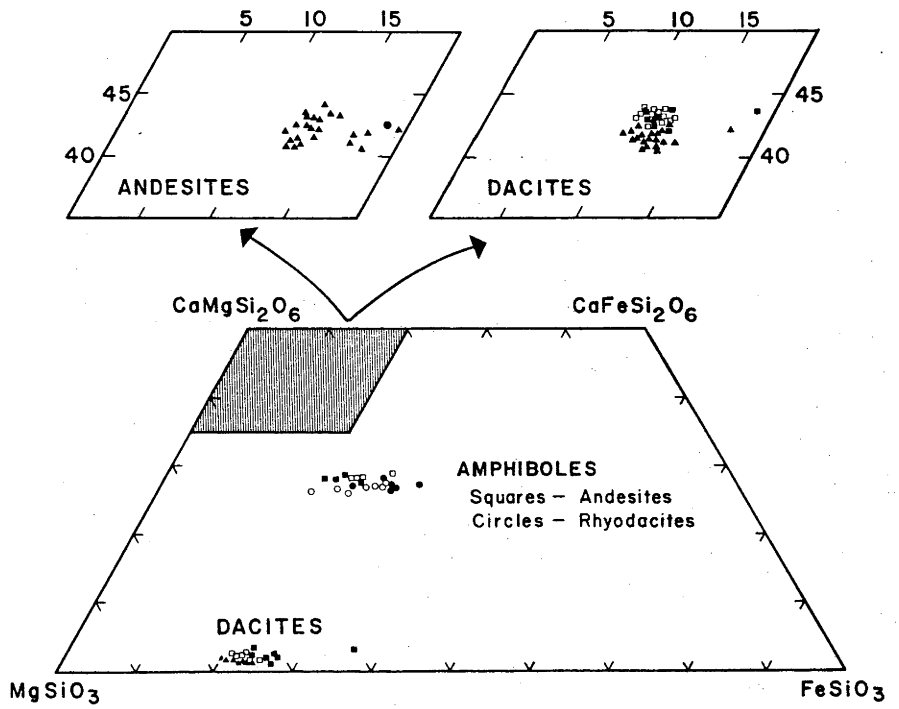

Figure 6. Clinopyroxene, orthopyroxene, and amphibole compositions of 'MMVF' silicic rocks. Clinopyroxene symbols are: andesites- (▲ - MMT-6); (● - MMT-25); dacites-(▲ - MMT-13); (□ - MMT-9); (■ - 26-12). Amphibole symbols are: andesite- (■ - MMT-6); (□ - MMT-21); rhyodacites- (● - MMT-3); (○ - MMT-18). Orthopyroxene symbols are: dacites- (▲ - 26-12); (□ - MMT-9); (■ - MMT-13).

Discussion -

(a) Geothermometry - The chemical compositions of the various groundmass and phenocryst phases are used to evaluate the temperatures of eruption and crystallization of the andesite, dacite and rhyodacite magmas. Several different geothermometers on coexisting pairs of Fe-Ti oxides (Buddington and Lindsley, 1964; Powell and Powell, 1977), plagioclase-glass (Mathez, 1973), plagioclase-alkali feldspar (Powell and Powell, 1977), amphibole-glass (Helz, 1979) and clinopyroxene-orthopyroxene (Wells, 1977) provide a check on the internal consistency of the calculated temperatures. The results of these geothermometry calculations are presented in Table 2.

Temperatures calculated from plagioclase-glass pairs (Mathez, 1973) range from 910° to 1100°C for the andesites, dacites and rhyodacites, with no apparent correlation with rock type. The use of this geothermometer is dependent upon the assumption that (a) the quenched glass was in equilibrium with the plagioclase composition chosen and (b) extension of activity coefficients ($\gamma AB/\gamma AN$) for plagioclase solid solutions to high-silica, alkali rich compositions is permissible. The occurrence of alkali feldspar in one dacite sample (Fig. 5) and the application of the alkali feldspar/plagioclase geothermometer (Powell and Powell, 1977) produces temperatures consistent with the results obtained from the plagioclase/glass geothermometer (Table 2).

Temperatures obtained from using the magnetite/ilmenite geothermometer (Powell and Powell, 1977) are 200° to 300°C lower than temperatures calculated from other geothermometers (Table 2). These disparities in estimated temperatures of crystallization from the different geothermometers can be explained by the re-equilibration of the oxide phases below solidus temperatures. In this light, it is interesting to note that oxygen fugacities obtained for these

TABLE 2. Geothermometry of silicic rocks from Mormon Mountain volcanic field.

Sample #	Rock Type	A Magnetite/ Ilmenite	B Plagioclase/ Glass	C Alkali feldspar/ Plagioclase	D Amphibole/ Glass	E Clinopyroxene/ Orthopyroxene
MMT - 6	Andesite	-	1056^{o}-1080^{o} [1,2] 988^{o}-1010^{o} [2]	-	873-925^{o} [1]	-
MMT - 25	Andesite	728^{o}-794^{o} -14.9- -13.7	986^{o}-1044^{o} [1,2] 1037^{o}-1067^{o} [2]	-	-	-
MMT - 21	Andesite	734^{o}-828^{o} -15.6- -12.6	932^{o}-1048^{o} [1,2] 997^{o}-1054^{o} [2]	-	566 -584	-
MMT - 13	Dacite	647^{o}-741^{o} -16.9- -15.6	900^{o}-1030^{o} [1,2] 892^{o}-971^{o} [2]	910^{o}-985^{o}	-	935^{o}-983^{o} [1,2] 981^{o}-982^{o} [2]
MMT - 9	Dacite	-	1096^{o}-1133^{o} [1,2] 938^{o}- 977^{o} [2]	-	-	998^{o} [1] 1011^{o} [2]
26 - 12	Dacite	-	974^{o}-1003^{o} [1,2] 1033^{o}-1046^{o} [2]	-	-	975^{o}-1020^{o} [1,2] 973^{o}-1015^{o} [2]
MMT - 18	Rhyodacite	1006^{o} -11.7	976^{o}-1040^{o} [1,2] 1021^{o}-1054^{o} [2]	-	573^{o}-635^{o} [1]	-

A. Magnetite/Ilmenite geothermometer (Powell and Powell, 1977). Temperatures are for groundmass phases except MMT-18 which is for magnetite and ilmenite inclusions in amphibole phenocrysts. fO_2 are indicated below each temperature.

B. Plagioclase/Glass geothermometer (Mathez, 1973). Temperatures are (1) dry conditions, .6 = $\gamma AB/\gamma AN$ and (2) 'wet' conditions, ½kb, .78 = $\gamma AB/\gamma AN$.

C. Alkali feldspar/Plagioclase geothermometer (Powell and Powell, 1977). Temperature range is for extremes of groundmass compositions.

D. Amphibole/Glass (Helz, 1979). Temperatures are for amphibole phenocrysts/glass.

E. Clinopyroxene/Orthopyroxene geothermometer for clinopyroxene and orthopyroxene phenocrysts. (1) Wood and Banno (1973),. (2) Wells (1977).

coexisting pairs are just slightly above the NNO buffer. This suggests that although the Fe-Ti oxide may re-equilibrate at lower temperatures, this process is not accompanied by extensive oxidation.

The distribution of alkalis between melt and amphibole has been proposed as a basis of an amphibole-glass geothermometer (Helz, 1979). Given the broad assumption that Helz's proposal may be extrapolated to high-silica volcanic rocks similar to those of 'MMVF', temperatures can be calculated for some andesites and rhyodacites. These temperatures are lower than those temperatures suggested by other geothermometers and indicates that (a) the amphibole phenocrysts are not in equilibrium with the groundmass glass or (b) the assumption given above is incorrect.

The existence of two-pyroxene glomerocrysts provide an opportunity to evaluate the crystallization temperatures of the dacite. Pairs of cpx-opx from three different dacite samples were examined, yielding temperatures 935° - 1020°C (Wood and Banno, 1973) or 973° - 1011°C (Wells, 1977) (Table 2). These temperatures agree well with those calculated from plagioclase/glass pairs.

(b) Crystallization Histories - It was noted in the previous section that the absence of significant amounts of plagioclase as a phenocryst phase was unusual in rocks of andesitic and dacitic composition. This characteristic, in conjunction with other petrographic observations can be explained by examining possible crystallization histories for the various magma types.

The crystallization of andesite under hydrous conditions has been explored over a range of pressures (Eggler, 1972; Eggler and Burnham, 1973; Allen and Boettcher, 1978). These experimental studies show that amphibole is the liquidus phase in andesite only above ~ 8 kbar at high H_2O fugacities (fH_2O). At lower fH_2O or

lower pressure, amphibole is replaced by an anhydrous assemblage of clinopyroxene, orthopyroxene and plagioclase (Fig. 7). Slight differences in bulk composition affect the relative positions of the clinopyroxene, orthopyroxene and plagioclase phase boundaries (e.g. Eggler and Burnham, 1973). The results of these experimental studies provide the same constraints upon which the discussion of possible crystallization histories of the 'MMVF' andesites and dacites.

The unusual phenocryst assemblage of the andesites (i.e. amphibole + clinopyroxene without plagioclase or orthopyroxene) is explained in part, by the rapid eruption of these magmas from depths exceeding 12 km under H_2O-saturated conditions. At these pressures, amphibole, clinopyroxene, and orthopyroxene crystallize before plagioclase (Eggler, 1972). Orthopyroxene may be replaced by an Fe-Ti oxide at fO_2's > NNO (Allen and Boettcher, 1978). The presence of other volatiles, such as CO_2 and F, in a dominantly H_2O-saturated fluid, may affect the stability of amphibole relative to the other phases in conflicting ways (e.g. CO_2 slightly decreases its thermal stability (Allen and Boettcher, 1978) while F increases it (Gilbert and Briggs, 1974; Holloway and Ford, 1975).

The anhydrous phenocryst association of the two-pyroxene dacite (i.e. clinopyroxene and orthopyroxene) is explained by its crystallization under conditions at which amphibole and plagioclase are unstable. A glance at Fig. 7, the H_2O-saturated andesite phase diagram, shows that for these conditions, clinopyroxene and orthopyroxene crystallize as liquidus phases without plagioclase or amphibole at pressures less than 8 kb and greater than 1 kb. Decreasing the amount of water and thereby the vapor fH_2O further restricts the thermal stability of amphibole, but increases the thermal stability of plagioclase (Eggler, 1972, Allen and Boettcher, 1978).

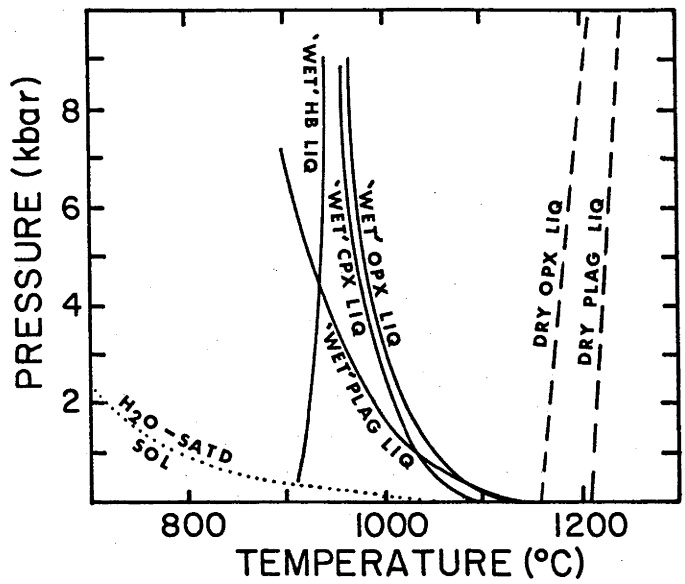

Figure 7. Phase relations of Paricutin andesite under water-saturated (solid lines) and anhydrous (dashed lines) conditions (after Eggler, 1972). Under water-saturated conditions, amphibole becomes the liquidus phase only above ∿ 8 kbar. The plagioclase-free andesites of 'MMVF' must be erupted from pressures in excess of 4 kbar (i.e. beyond the intersection of the amphibole (HB) liquidus and plagioclase (PLAG) liquidus). The plagioclase-free, two-pyroxene dacites must evolve under water-undersaturated conditions or at higher temperatures (H_2O-saturated) to prevent either amphibole or plagioclase from crystallizing.

The postulated crystallization models for the andesites and dacites suggest that they were probably erupted from magma chambers situated at least 10 to 15 km below the surface. These depths are comparable to estimated depths of andesitic magma chambers from other localities (e.g. Arculus and Wills, 1980). The rapid ascent of magma from this depth may have been aided by the presence of zones of weakness in the crust associated with the tectonics of the Colorado Plateau.

GEOCHEMISTRY

General - The volcanic suite of the Mormon Mountain field is distinctly bimodal with a silica gap of approximately 5 percent separating the most evolved basalt (SiO_2 = 52.6%) from the least silicic andesite (SiO_2 = 57.6%). The basalts, discussed in detail in Appendix 7, range from olivine nephelinites to high-alumina olivine tholeiites, but the majority are alkali olivine basalts and basanites. As noted before, the silicic volcanic rocks are classified on the basis of total alkalis ($\Sigma Na_2O + K_2O$) versus SiO_2 (Fig. 4) (Middlemost, 1973). Reflecting their different petrographies, the high-Si dacites are designated as rhyodacites.

The silicic suite as a whole, is 'calc-alkaline' as defined by several different criteria; normative plagioclase vs. Al_2O_3 content (Irvine and Barager, 1971; K_2O vs. SiO_2 (Peccerillo and Taylor, 1976) (Fig. 8 a,b). The Hutch Mountain andesite (MMT-25) is however, slightly more alkalic than the other andesites. The alkalic nature of this particular andesite is also apparent in other geochemical characteristics.

Major Elements - Representative major element analyses and CIPW normative mineralogies of the silicic suite are given in Table 3. Additional major element analyses may be found in Appendix 6. Harker-

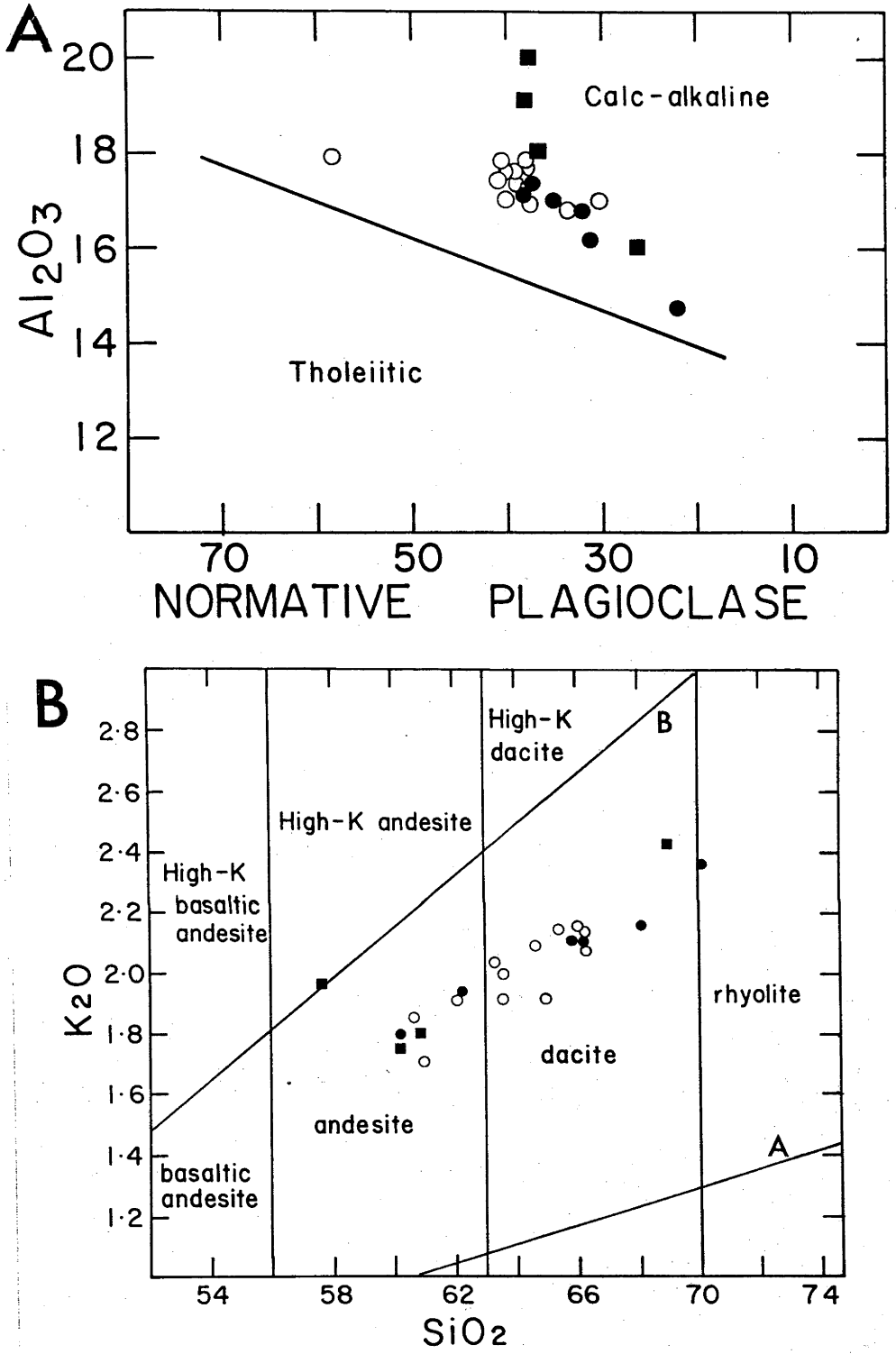

Figure 8. Criteria for designation of 'MMVF' silicic suite as 'calc-alkaline'. Explanation of the symbols is the same as in Figure 4.

A) Al_2O_3 (wt. percent) vs. normative plagioclase content (Irvine and Barager, 1971)

B) K_2O vs. SiO_2 (wt. percent) (Peccerillo and Taylor, 1976).

Table 3. Major Element Analyses of the Silicic Suite from the Mormon Mountain Volcanic Field

	ANDESITES				DACITES				RHYODACITES	
Sample	MMT-6	MMT-21	MMT-22	MMT-25	MMT-7	MMT-9	MMT-12	MMT-13	MMT-3	MMT-18
SiO_2	59.82	59.61	60.65	57.59	62.11	66.05	65.40	67.62	69.92	68.04
TiO_2	1.00	.68	.74	.86	.70	.33	.63	.53	.26	.43
Al_2O_3	17.26	18.97	17.99	19.94	17.15	16.02	16.84	16.62	14.65	15.96
FeO	5.57	5.00	4.90	6.35	5.40	4.29	3.64	3.07	3.30	2.69
MnO	-	-	-	-	.10	.05	-	-	-	-
MgO	3.68	2.08	2.95	1.79	2.63	2.02	2.09	1.11	1.33	1.58
CaO	5.86	6.20	5.93	6.30	5.42	3.98	4.08	3.67	3.16	3.35
K_2O	1.78	1.74	1.79	1.97	1.94	2.09	2.09	2.16	2.35	2.41
Na_2O	4.36	4.81	4.61	5.04	4.33	4.98	4.41	4.44	4.81	4.29
P_2O_5	.27	.38	.35	.56	.29	.19	.19	.17	.14	.15
LOI	.32	.76	.53	.07	.76	.09	1.06	.58	.85	1.80
Total	99.92	100.23	100.44	100.47	100.83	100.09	100.43	99.97	100.77	100.70
Mg#	58.1	46.6	55.8	37.2	50.6	49.7	54.7	43.2	45.8	55.21
CaO/Al_2O_3	.341	.327	.330	.316	.316	.248	.242	.221	.215	.210
K_2O/Na_2O	.41	.36	.39	.39	.45	.42	.47	.49	.49	.56
CIPW NORM										
Diop	5.58	4.79	5.19	4.44	4.35	3.78	.20	-	3.53	-
Hyp	12.80	8.88	10.59	9.84	11.12	8.81	9.31	6.30	5.83	7.14
Oliv	-	-	-	-	-	-	-	-	-	-
Or	10.58	10.37	10.61	11.65	11.48	12.36	12.44	12.86	13.91	14.41
Ab	37.09	41.02	39.13	42.65	36.67	42.17	37.58	37.83	40.75	36.73
An	21.77	24.35	22.40	24.69	21.00	14.81	19.74	18.00	11.14	16.50
Ne	-	-	-	-	-	-	-	-	-	-
Leu	-	-	-	-	-	-	-	-	-	-
Mt	1.35	1.22	1.19	1.54	1.31	1.04	.89	.75	.80	.66
Ilm	1.91	1.30	1.41	1.63	1.33	.63	1.21	1.01	.49	.83
Ap	.19	.27	.25	.40	.20	.13	.13	.11	.09	.10
Qtz	8.29	7.18	8.68	2.27	12.08	16.00	18.22	22.61	23.23	23.21
Cor	-	-	-	-	-	-	-	.31	-	.21

type variation diagrams using SiO_2 as the abscissa (Fig. 9) exhibit a fairly systematic change in the major elements as SiO_2 increases. MgO, FeO, CaO, Al_2O_3 and TiO_2 decrease with increasing SiO_2 with Na_2O remaining fairly constant. K_2O increases slightly, but does not exceed 2.5 wt. percent. P_2O_5 decreases with increasing SiO_2 (Fig. 10).

The 100 [Mg/Mg + Fe^{2+}] (Mg#) decreases from 58 to 43 for the andesite through rhyodacites from Mormon Mountain, with more random values for the other silicic volcanic rocks (MMT-25 = 37; MMT-21 = 47; MMT-22 = 56; MMT-18 = 55). K_2O/Na_2O ratios range from .39 to .56 for andesites through rhyodacites respectively. No outstanding differences are observed in either CaO/Al_2O_3 or K_2O/Na_2O between the Mormon Mountain rocks and those from outlying areas.

The andesite (MMT-25), which is mildly alkalic, differs from the other andesites not only in its total alkali content, but also in Al_2O_3 and Mg#. Al_2O_3 content is high (~ 20 wt.%) and Mg# is low (37).

Trace Elements - Ten samples have been analyzed for the trace elements Ba, Rb, Sr, Pb, La, Y, Zr, Nb, Ga, Cr, Ni, Sc, V, Cu, and Zn by XRF (Norrish and Chappell, 1977). The analyses are given in Table 4. Rare earth element (REE) abundances were determined for an andesite, dacite and rhyodacite of the Mormon Mountain complex by spark source mass spectrometry (Taylor and Gorton, 1977). These analyses are presented in Table 5.

All samples are high in Ba (1300 to 2200 ppm) and Sr (715-1530 ppm) but low in Rb (14-23 ppm) and Y (4-17 ppm). Zr and Nb contents are approximately constant at 125 and 20 ppm respectively. Ba, Rb, Pb and Zr (slightly) increase and La, Y, Nb and Sr (slightly) decrease with increasing SiO_2 contents (Fig. 11). The Hutch Mountain

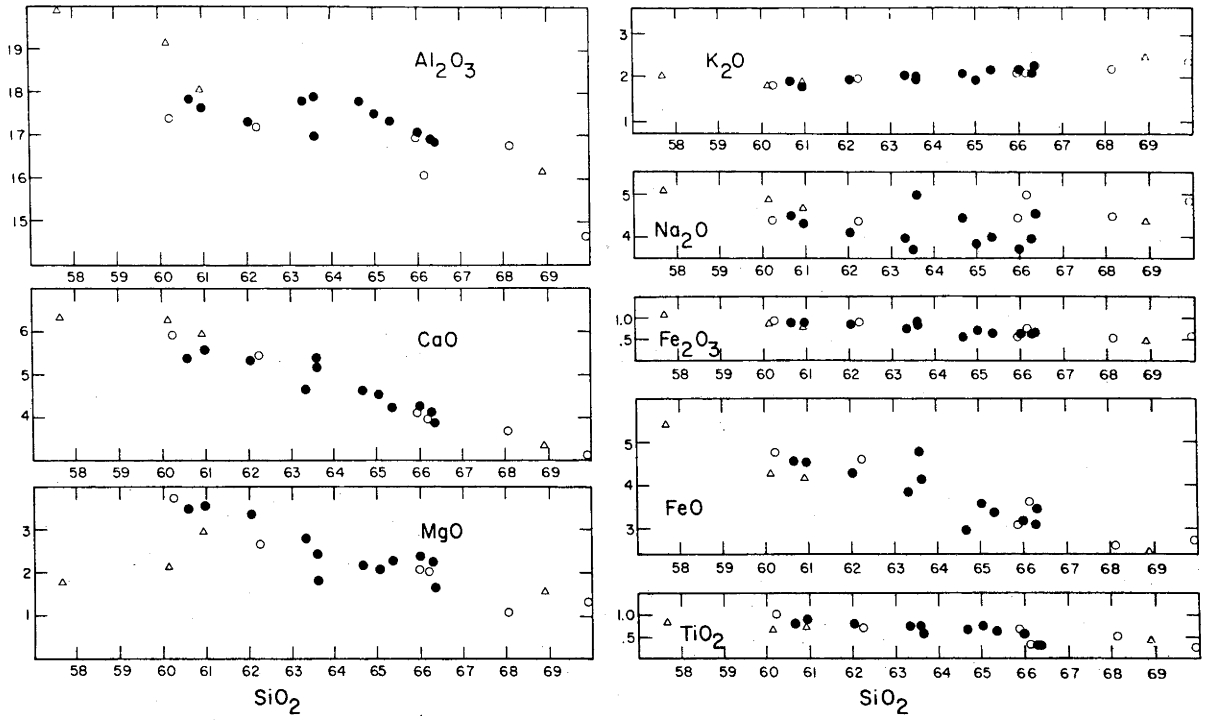

Figure 9. Harker-variation diagram for the 'MMVF' silicic rocks with SiO_2 as the abscissa. All oxides are in weight percent. Filled circles are analyses listed in Appendix 6. Open circles are analyses from the Mormon Mt. complex and open triangles are other localities.

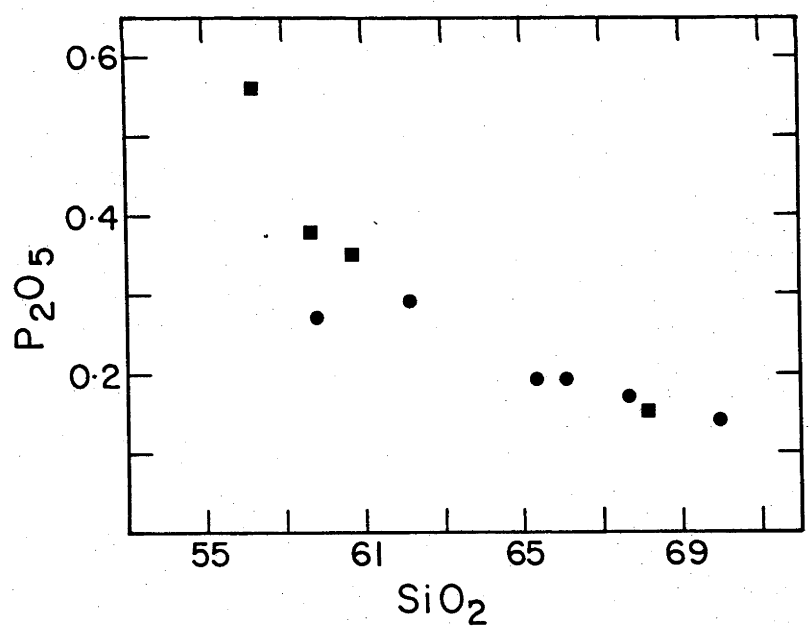

Figure 10. P_2O_5 vs. SiO_2 for silicic rocks of 'MMVF'. Closed circles - Mormon Mt. dacites; closed squares - Mormon Mt. andesite, rhyodacite; open circles - other andesites, rhyodacite.

Table 4. Trace element abundances of the silicic suite from Mormon Mountain volcanic field

	MMT 6	MMT 21	MMT 22	MMT 25	MMT 7	MMT 9	MMT 12	MMT 13	MMT 3	MMT 18
Rb	16	14	16	18	19	21	21	23	21	16
Ba	1310	1300	1520	2200	1440	1445	1440	1570	1525	1565
Sr	1145	1530	1520	1390	1220	1110	1120	1065	985	715
Pb	17	17	18	23	18	21	21	22	20	20
La	32	47	51	70	39	30	32	29	23	21
Y	11	13	11	17	12	8	9	7	6	4
Zr	111	145	146	175	124	122	120	121	107	126
Nb	25	28	33	69	29	21	21	19	12	12
Ga	18	20	20	20	18	18	17	18	17	15
Cr	34	3	21	21	26	27	20	23	17	17
Ni	34	8	23	4	30	26	23	21	14	14
V	121	69	74	83	102	64	69	49	41	44
Sc	15	10	10	8	13	9	9	8	6	6
Cu	36	14	12	12	22	26	29	24	14	12
Zn	66	74	73	75	66	59	57	65	46	48

TABLE 5: Additional Trace Elements of Andesite, Dacite and Rhyodacite of Mormon Mountain

	MMT-6	MMT-9	MMT-3
La	42.0	44.0	23.0
Ce	73.1	82.2	44.4
Pr	7.7	7.0	5.1
Nd	27.3	24.1	18.7
Sm	4.3	2.6	2.7
Eu	1.20	0.76	0.88
Gd	3.0	1.4	1.8
Tb	0.49	0.23	0.21
Ho	0.38	0.19	0.22
Er	0.93	0.37	0.48
Yb	0.75	0.20	0.32
Zr[1]	111	122	107
Hf	2.2	1.9	2.3
Y	17.0	11.3	8.1
Nb	33.2	38.0	17.0
Ba[1]	1310	1445	1525
Cs	0.43	0.79	0.58
U	1.47	1.56	0.95
Th	5.0	5.6	2.7
Sn	0.85	0.7	0.7
Mo	1.3	1.7	1.3
SiO_2	59%	62%	68%

[1] XRF values

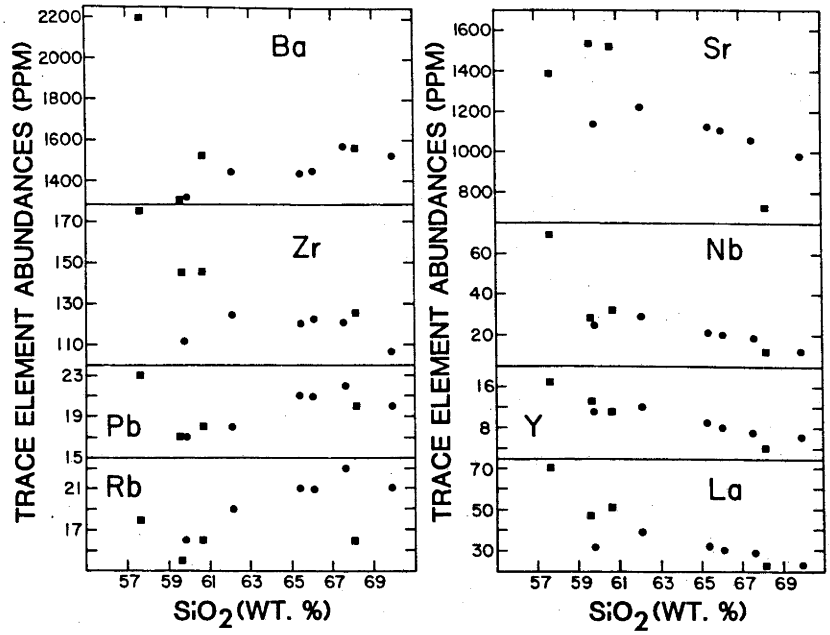

Figure 11. Abundances of Ba, Zr, Pb, Rb, Sr, Nb, Y, and La vs. SiO_2 for 'MMVF' silicic suite. Circles are samples from the Mormon Mt. complex and squares are samples from other localities.

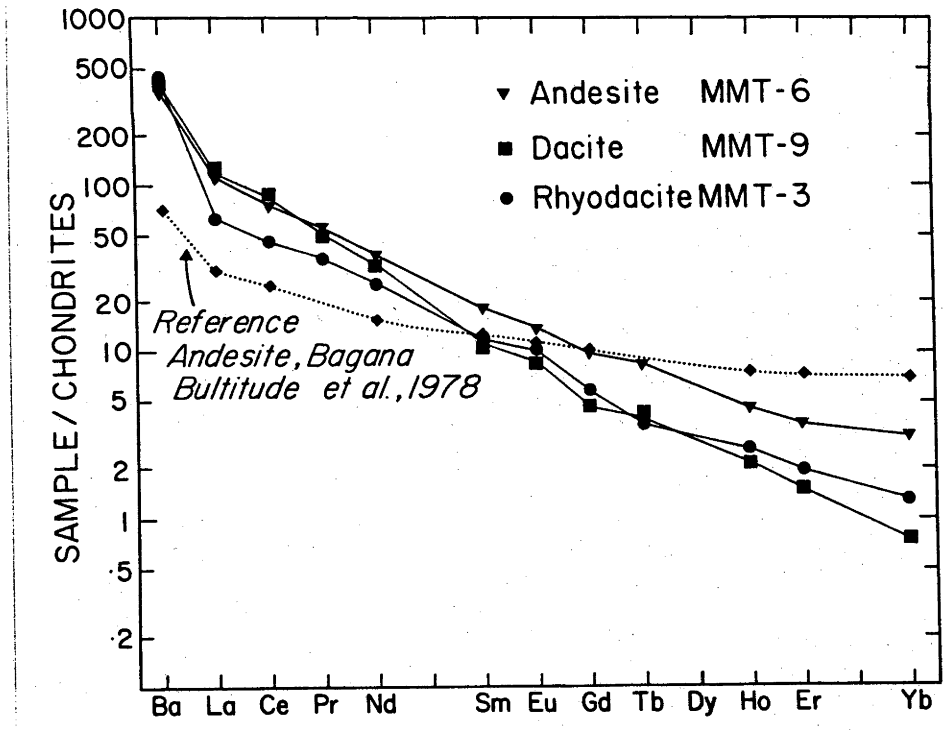

Figure 12. Chondrite-normalized rare earth element abundances of andesite (MMT-6), dacite (MMT-9), and rhyodacite (MMT-3) from the Mormon Mt. complex. The reference island-arc andesite from Bagana (Bultitude et al.(1978))is shown for comparison. Normalization factors are those of Taylor and Gorton (1977).

andesite (MMT-25) is distinctive from the other andesites by having the highest Ba, Pb, La, Y and Nb of the entire suite.

The REE abundances of the Mormon Mountain andesite and rhyodacite appear as steeply fractionated patterns in chondrite-normalized diagrams. These rocks are LREE-enriched (La/Yb = 55-73) with a flattening in the HREE (Fig. 12). The rhyodacite contains less total REE than does the andesite. The REE pattern of the dacite from Mormon Mountain, is distinct from the patterns of the andesite and rhyodacite. It is significantly more fractionated (La/Yb = 220) and cuts across both the andesite and rhyodacite patterns (Fig. 12). Only small positive Eu anomalies are observed in the dacite and rhyodacite patterns and no Eu anomaly is present in the andesite pattern.

The abundances of Ni, Cr, Sc, V, Cu and Zn decrease with increasing SiO_2 content. Andesites from Mormon Mountain are enriched in these elements relative to the andesites of Hutch, Round and Table Mountains. Inter-element correlations for the Mormon Mountain andesite-dacite-rhyodacite suite are high (Fig. 13).

Sr Isotopes - $^{87}Sr/^{86}Sr$ isotopic ratios were determined for an andesite from Table Mountain (MMT-22) and an andesite (MMT-6), dacite (MMT-7) and rhyodacite (MMT-3) from Mormon Mountain. These values are reported in Table 6 along with $^{87}Sr/^{86}Sr$ ratios of three 'MMVF' basalts and a pyroxene granulite nodule (SW-6) from nearby Williams, Arizona. All values fall within the limited range of .7033 to .7040.

The $^{87}Sr/^{86}Sr$ ratio of the Mormon Mountain dacite (.70400 ± 8) is different from those of the andesite (.70332 ± 2) and rhyodacite (.70363 ± 5) of Mormon Mountain. The $^{87}Sr/^{86}Sr$ value of the Table Mountain andesite (MMT-22) is .70378 ± 4, just slightly greater than the value of the Mormon Mountain andesite. The Sr isotopic ratios of the basalts are similar to each other (~ 7036) and slightly less than the granulite (.70372 ± 1).

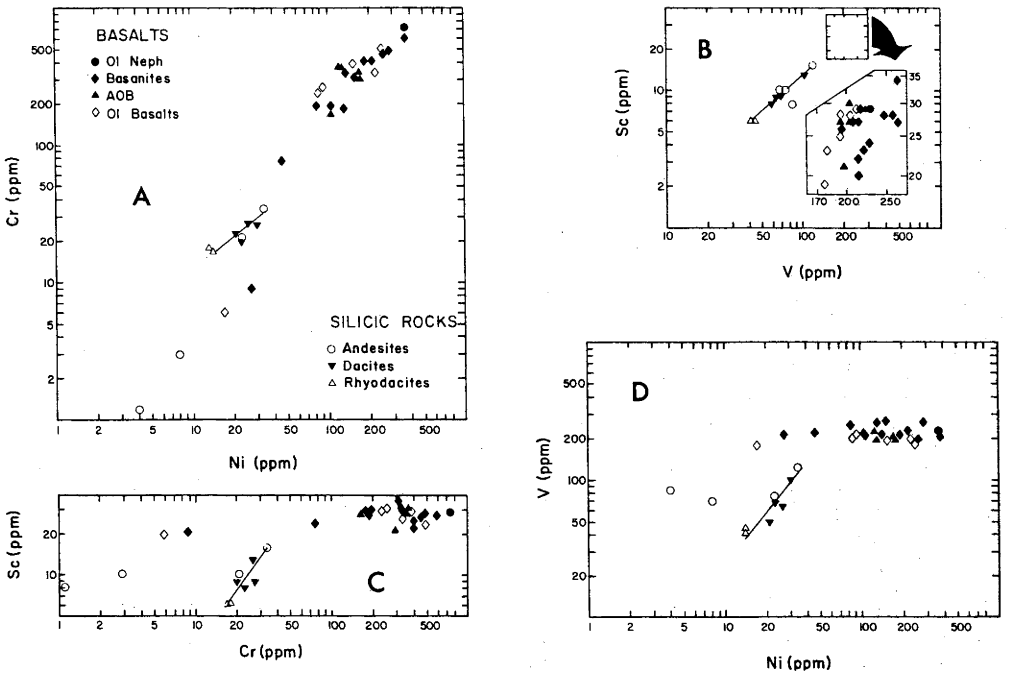

Figure 13. Log-Log variation diagrams of highly compatible elements Ni, Cr, Sc, and V for the 'MMVF' silicic rocks. Also shown are the abundances of these elements in the 'MMVF' basaltic suite, described in detail in Appendix 7. The symbols are explained in the figures. The two andesites which plot considerably away from the majority of the suite are from Hutch Mt. (MMT-25) and Table Mt. (MMT-21).

A) Cr vs. Ni

B) Sc vs. V

C) Sc vs. Cr

D) V vs. Ni

TABLE 6: $^{87}Sr/^{86}Sr$ Isotopic Ratios of Samples from the Mormon Mountain Volcanic Field

SAMPLE	ROCK TYPE	$^{87}Sr/^{86}Sr$	σ	Sr(ppm)	Rb(ppm)
MMT-6	hb. andesite	0.70332	±2	1145	16
MMT-7	pyx. dacite	0.70400	±8	1220	19
MMT-3	rhyodacite	0.70363	±5	985	21
MMT-22	hb andesite	0.70378	±4	1520	16
MMT-2	a.o.b.	0.7036	±3	1040	11
MMT-5	high-Al basalt	0.70367	±7	1120	16
MMT-24	ol. nephelenite	0.70361	±8	1065	24
SW-6	pyx. granulite	0.70372	±1	1013	0.5
Standard	NBS 987	0.71033		--	--

M. R. Perfit, analyst

DISCUSSION

Qualitative Interpretation of Trace Element Abundances - Minster and Allègre (1978) have discussed in detail the use of the qualitative character of trace element behaviour as a preliminary step in the identification of petrogenetic processes. In their discussion, they developed the concept of different degrees of element incompatibility (i.e. preference of an element for a melt phase vs. a mineral phase) as the basis of any petrogenetic interpretation. Elements were divided in those of a) high solid-liquid partition coefficients (K_D) (e.g. Ni, Cr, V) b) low partition coefficients (C^H) and c) intermediate partition coefficients (C^M). Figure 14, from Minster and Allègre (1978) summarizes the various possible combinations of these different groups of elements and their behaviour with respect to various petrogenetic processes.

The use of Minster and Allègre-type plots in the identification of petrogenetic processes in silicic suites, such as 'MMVF', requires a division of the trace elements into the three categories. Partition coefficients are, in part, a function of the composition of the melt phase; for example, REE mineral/melt partition coefficients in granitic melts are equal or greater than those for similar minerals in basaltic systems (Hanson, 1978). In addition, the increased stability of minor residual phases in silicic magmas (e.g. apatite, zircon (Watson, 1979a, 1979b)) affects the bulk solid (Σ minerals)/melt partition coefficient. These factors, compositional dependance of K_D mineral/melt and occurrence of minor phases, complicate the division of trace elements into the three Minster and Allègre categories. With respect to the 'MMVF' suite, those elements which exhbit positive correlations with SiO_2 (Ba, K, Rb, Pb) are highly

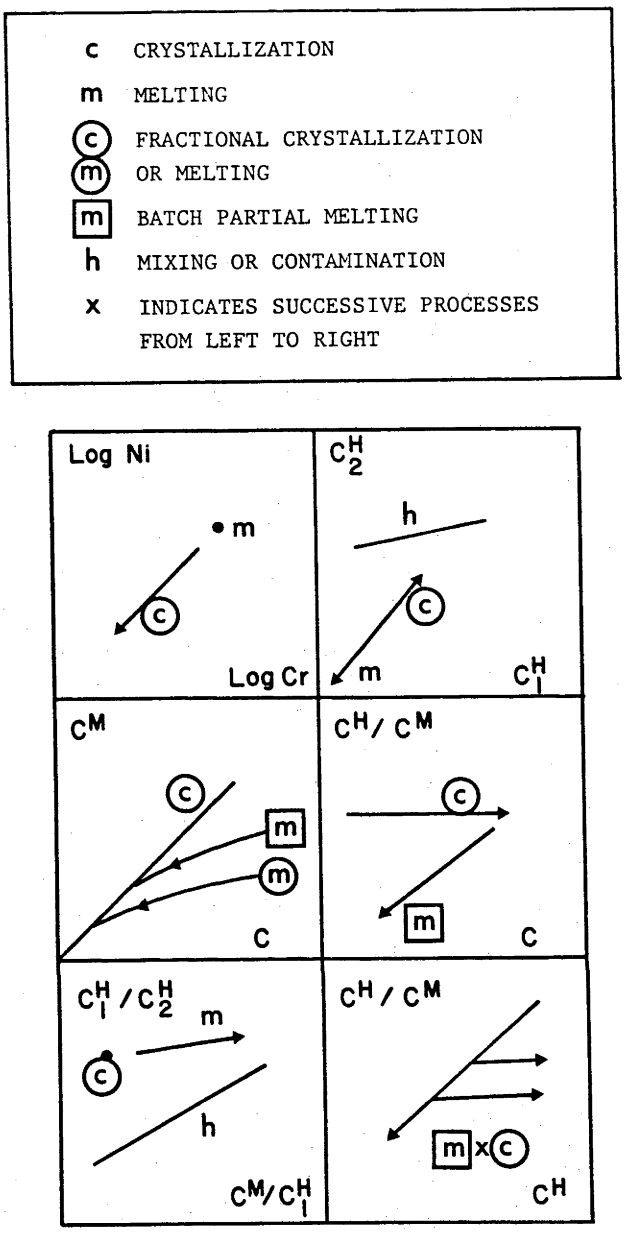

Figure 14. Qualitative interpretation of the behaviour of trace elements in igneous processes (after Minster and Allègre, 1978). Additional explanation in the text.

incompatible (C^H) while those that decrease in abundance with increasing SiO_2 are moderately incompatible (C^M) (P_2O_5,La,Y, Nb, Zr, Sr). Ni, Cr, V, and Sc are elements with high mineral/melt partition coefficients.

The highly incompatible elements (Ba, K, Rb, Pb), when plotted against one another (C^H vs C^H - Fig. 14) result in positive correlations for the rocks from the Mormon Mountain complex (Fig. 15). Such behaviour indicates that either fractional crystallization or partial melting may have occurred. The andesites and rhyodacite from other localities (Round, Table and Hutch Mountains, Mormon Lookout) are distinct from the Mormon Mountain rocks.

Rb/Sr vs. Rb (Fig. 16) (C^H/C^M vs C^H - Fig. 14) suggests that the trace element characteristics of the andesite , dacites, and rhyodacite of Mormon Mountain are due to batch partial melting. This plot also suggests that the andesite and rhyodacite are not related to the dacites. K/Rb vs Sr/Rb (Fig. 17) (C^H2/C^H1 vs C^M/C^H1 - Fig.14) variations are in agreement with these suggestions. In addition to these initial qualitative observations, it is possible to explore in quantitative detail the petrogenesis of the 'MMVF' silicic suite.

Quantitative Petrogenetic Modeling - There are three possible petrogenetic models, each with internal variations which must be considered in the interpretation of the origins of the silicic rocks. The first model (Model A) assumes a co-magmatic relationship between the andesite and basaltic magmas, in which the andesite is produced by fractional crystallization processes. The dacite and rhyodacite compositions are generated by fractional crystallization of the andesite. The second and third models emphasize the absence of any direct chemical relationship between the basalts and andesites,

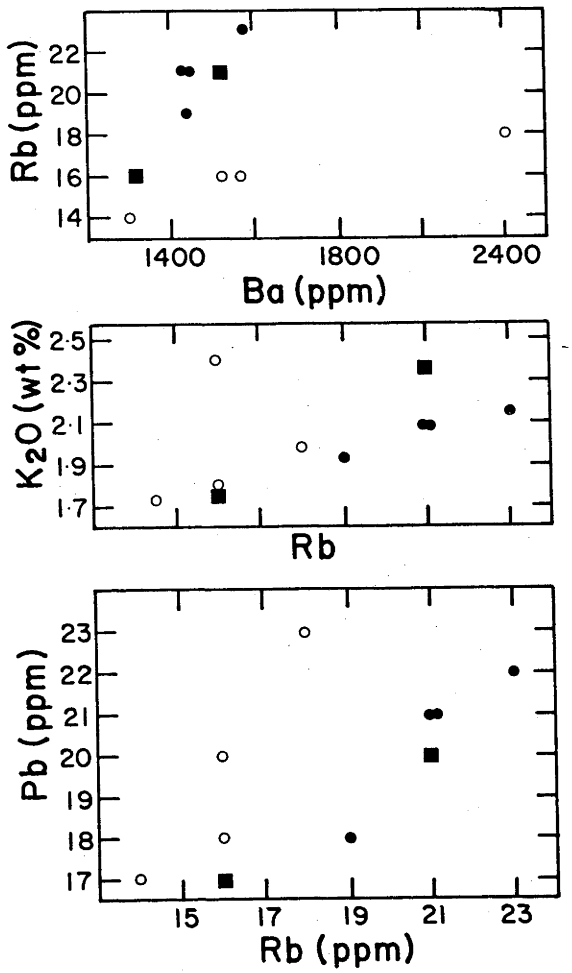

Figure 15. Variation between abundances of several highly incompatible elements (C^H) for the 'MMVF' silicic rocks. Filled circles (dacites) and filled squares (andesite, rhyodacite) are samples from the Mormon Mt. comples. Open circles are samples from other localities in the volcanic field. The positive correlations exhibited by the Mormon Mt. rocks suggest that these rocks may be related by crystallization or melting processes (refer to Figure 14, C^H vs. C^H). The other silicic rocks are distict from the Mormon Mt. suite.

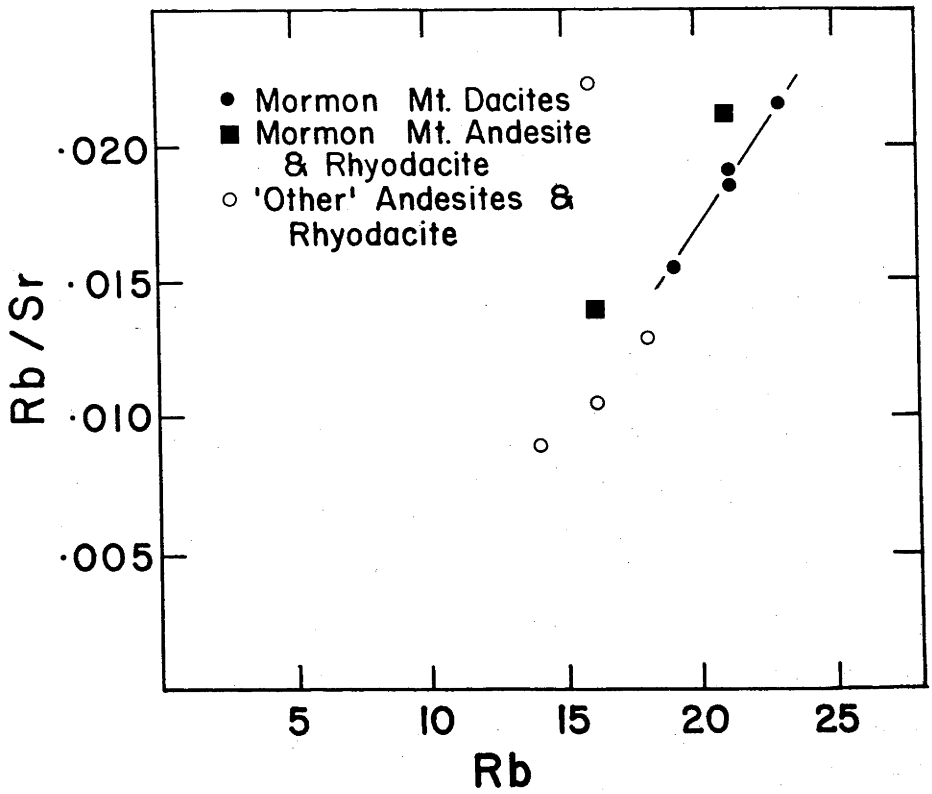

Figure 16. Rb/Sr vs. Rb variation diagram for 'MMVF' silicic rocks. The positive correlation for the dacites indicates either fractional crystallization or partial melting (see Figure 14, C^H/C^M vs. C^H).

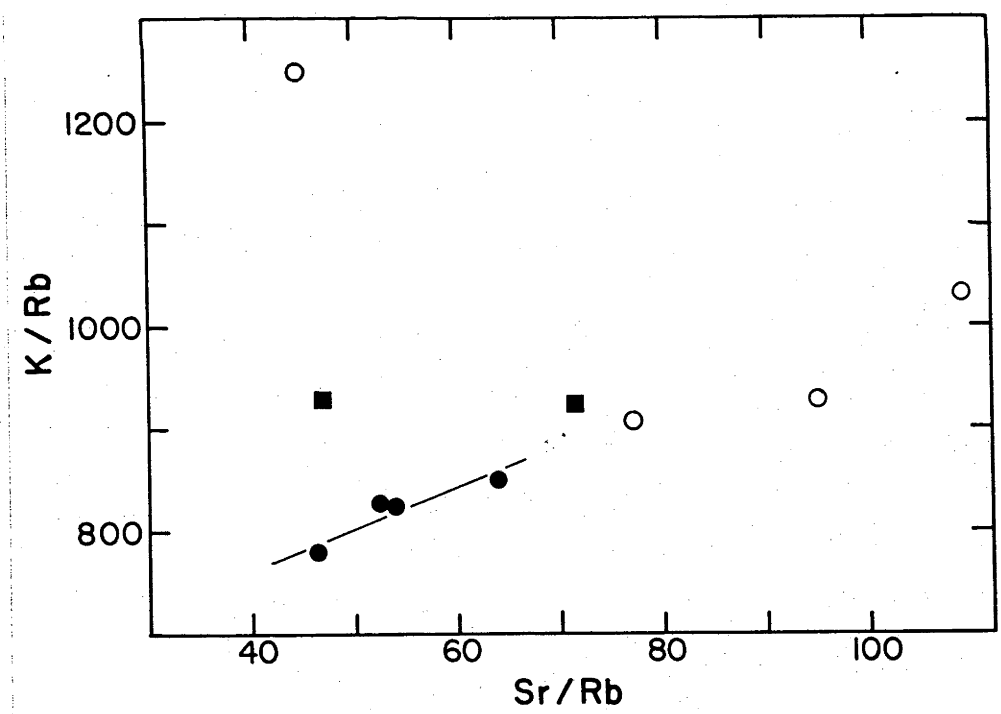

Figure 17. K/Rb vs. Sr/Rb variation diagram for 'MMVF' silicic rocks. Symbols are the same as in Figure 16. The positive correlation of the dacites indicates melting (see Figure 14, C^{H_2}/C^{H_1} vs. C^M/C^{H_1}).

proposing instead that the andesites represent primary melts resulting from crustal anatexis. The difference between the second and third models concerns the generation of the dacites and rhyodacites; in the second model their petrogenesis is explained via fractional crystallization and in the third model, by discrete events of crustal anatexis.

The methods of quantitatively evaluating these different models consist of least-squares mixing equations using major element chemistry and phase chemistry (Wright and Doherty, 1970) and Rayleigh fractional crystallization and partial melting calculations for various trace elements (e.g. Hanson, 1980). There are significant uncertainties in the application of these methods to natural rock associations (e.g. compositional dependance of element partitioning, vapor/melt/crystal interactions) and ensure that a unique solution is not forthcoming.

(a) Model A - Model A, as stated above, assumes that the andesites are derived from basaltic parents by the process of fractional crystallization. The most likely basaltic parents of 'MMVF' andesites are the olivine tholeiites and in particular, the high-Al varieties (Table 7). The fractional crystallization of amphibole from alkali olivine basalt to generate 'calc-alkalic' andesite has been proposed in other regions (Arculus, 1976; Arculus and Wills, 1980; Cawthorn et al., 1973, Cawthorn and O'Hara, 1976). However, the large silica gap which exists between the basalts and the andesites as well as the absence of amphibole in the alkali olivine basalts from 'MMVF', precludes this possibility. The occurrence of possible amphibole psuedomorphs consisting of pyroxene and magnetite in a high-Al olivine tholeiite does not eliminate the inclusion of amphibole from fractional crystallization models involving this type of basalt.

Results of least-squares mixing calculations for numerous basalt-andesite models using either the observed basaltic mineralogy or the andesitic mineralogy (Table 7) suggest that fractional crystallization of a basalt can account for the major element characteristics of the andesites. Upon closer examination, all models reproduce poorly, TiO_2 and to a lesser degree Na_2O and K_2O abundances. Similar situations are observed in other least-squares basalt-andesite models which involve amphibole (Gust and Johnson, 1981; Arculus and Wills, 1980).

Rayleigh fractionation calculations using the proportions of the least squares models developed for the 'MMVF' suite for most incompatible trace elements reveal a multitude of inconsistencies with the fractional crystallization hypothesis (Table 8). Almost all models predict excessive abundances of Rb, Pb, K, Ba, Zr, Nb, La, and Y compared to the observed abundances of the andesites. Calculated Sr contents are either too high or too low. La/Y ratios, which qualitatively model LREE/HREE are also variable and do not compare favorably with observed La/Y ratios. Calculated Ni, Cr, V and Sc contents are extremely low, but these values are highly dependent upon their chosen partition coefficient. Only one model (A8) reproduces, within acceptable limits, a close match to the observed abundances of the trace elements in an andesite. This andesite (MMT-25) has been previously identified by its distinctive geochemical signature, as different from other 'MMVF' andesites. It is proposed that this difference, in conjunction with the results of quantitative petrochemical modeling, can be explained by the generation of the Hutch Mountain andesite by fractional crystallization of a basalt. The field relations of this andesite (i.e. a small plug of limited extent within a basaltic cinder cone) support this suggestion. However, in summary, the derivation of the majority of andesites of

TABLE 7: Summary of Least Squares Solutions for Basalt/Andesite Fractionation

Code	Basaltic Parent	ΣR^2	Daughter %	Mineral %'s						TOTAL	Comments
I. Andesite - MMT-6											
	a) Cores of phenocrysts in andesite			AN69	AN40	AMP	CPX	APT	TMT		
A1	MMT-4	.2796	46.57	8.13	--	36.92	6.11	.55	1.74	100.02	High Ti
A2	MMT-5	.1970	53.16	13.93	11.64	14.02	1.05	.90	5.08	99.78	High Ti, Low K
A3	MMT-8	.2177	44.47	12.58	--	28.32	10.91	.71	4.13	101.12	High Ti, High Na, Low K
A4	MMT-10	.1196	40.04	18.91	--	23.50	12.67	.52	4.35	99.99	High Ti, High K
A5	MMT-15	.1999	36.79	25.82	--	16.44	14.80	.59	6.57	101.01	High Ti, High Na
A6	MMT-16	.2297	53.74	2.69	--	37.77	5.08	.77	1.16	101.21	High Ti, Low K
	b) Rims of phenocrysts in basalts			FO70	CPX	AN69	APT	TMT			
A7	MMT-5	.3861	58.08	4.96	2.91	26.99	.93	4.67		98.54	Low Ti, Low Na, Low K
II. Andesite - MMT-25											
	a) Cores of phenocrysts in andesite										
	ALL SOLUTIONS UNSUCCESSFUL										
	b) Rims of phenocrysts in basalts			FO70	CPX	AN69	APT	TMT			
A8	MMT-5	.1361	65.39	5.68	7.87	16.32	.39	2.89		98.54	Low Ti
A9	MMT-23	.1957	37.92	11.38	25.24	21.94	.30	2.60		99.38	Low Ti, Low Na
III. Andesite - MMT-21											
	a) Cores of phenocrysts in andesite			AN62	AMP	APT	TMT				
A10	MMT-5	.0370	59.84	13.83	22.08	.73	3.62			100.16	Low K
	b) Rims of phenocrysts in basalts			FO70	CPX	AN69	APT	TMT			
A11	MMT-5	.3681	59.54	6.65	4.97	22.40	.75	4.31		98.62	Low Ti, Low Na, Low K
A12	MMT-23	.2483	35.03	11.93	23.69	24.98	.50	3.47		99.61	Low Ti, Low Na, Low K

TABLE 8: Summary of Rayleigh Fractionation Calculations for Trace Elements Using Least Squares Solutions for Basalt/Andesite Fractionation

CODE	MMT-6	A1	A2	A3	A4	A5	A6	A7	MMT-25	A8	A9	MMT-21	A10	A11	A12
Rb	16	29	29	24	14	19	38	27	18	24	25	14	26	26	27
Ba	1310	2285	2438	1753	1471	1448	2032	2261	2200	2057	1210	1300	2208	2227	1298
Sr	1145	1300	1065	1166	754	721	1473	987	1390	1159	734	1530	1264	1083	712
K	14780	16088	25703	17399	12440	13144	17754	24977	16350	16706	16687	14440	22584	24523	17952
Pb	17	25	33	39	14	14	25	30	23	27	18	17	29	29	19
Zr	111	200	279	238	225	253	210	280	175	248	308	145	237	272	333
Nb	25	51	33	61	41	45	66	88	61	79	59	28	69	86	64
La	32	64	69	52	49	58	60	64	76	67	50	47	67	66	50
Y	11	16	22	20	26	32	16	24	17	23	40	13	19	24	39
Ni	34	3	>1	4	>1	2	5	7	4	5	3	8	>1	>	3
Cr	34	>1	>1	>1	>1	>1	>1	>1	1	>1	>1	3	>1	>1	>1
Sc	15	>1	3	>1	>1	>1	>1	25	8	19	19	10	>1	22	20
V	121	>1	>1	>1	>1	>1	>1	44	83	79	95	69	>1	49	66

the Mormon Mountain volcanic field by fractional crystallization of basaltic magma is not consistent with petrochemical modeling.

(b) Model B - An alternative petrogenetic interpretation, Model B emphasizes the role of andesite as a primary melt. The generation of such melts has often been discussed with respect to island arc volcanism and involves the partial melting of amphibolite (Boettcher, 1973; Allen and Boettcher, 1978), hydrous quartz eclogite (Green and Ringwood, 1968; Ringwood 1974), or hydrous peridotite (Kushiro, 1972; Mysen and Boettcher, 1975 a,b). It is not the intention of this discussion to review the controversies which surround these proposals, however it is necessary to comment on some of their features and problems with respect to the anorogenic volcanic suite of the Mormon Mountain volcanic field.

Green (1976) reviewed experimental work on the hydrous melting of peridotite and concluded that melts similar to 'calc-alkalic' andesites could not be in equilibrium with a peridotitic source. Melts which could be derived by partial melting of hydrous peridotite are high-Mg andesites and boninites (Tatsumi, 1981). Stern and Wyllie (1973; 1978) and Gust (Chapter 2) demonstrated that the partial melting of hydrous eclogite at high pressures does not produce andesites, dacites or rhyolites of 'calc-alkalic' affinities. A mantle source, hydrous peridotite or eclogite, for a primary 'calc-alkalic', andesitic magma is ruled out by these experimental studies. A crustal origin for the andesite is therefore, the only alternative.

Potential compositions of crustal sources can be inferred from the variety of nodules which occur in erupted volcanic hosts. The presence of amphibolite, garnet amphibolite, pyroxene and garnet granulite and eclogite nodules from localities close to 'MMVF' (Arculus and Smith, 1979; Stoeser, 1973; Appendix 8) indicates that

the lower crust of the Colorado Plateau contains a variety of basaltic compositions with different parageneses. Pressures and temperatures calculated from the coexisting phases of these nodules establish that 1) they are fragments of the lower crust (P > 5 kb) and 2) the crustal temperatures (800° - 1000°C) at these pressures are significantly higher than a continental geotherm predicts (Clark and Ringwood, 1964). The inferred temperatures within the crust of the Colorado Plateau and crustal fusion are compatible with the partial melting of basaltic compositions only under hydrous conditions (i.e. amphibolite).

The melting relations of basalts under hydrous conditions within the stability field of amphibole have been investigated over an extensive range of $P/T/fH_2O/fO_2$ conditions (Yoder and Tilley, 1962; Green and Ringwood, 1968; Holloway and Burnham, 1970; Boettcher, 1973; Lambert and Wyllie, 1972; Helz, 1973, 1976; Allen, Boettcher and Marland, 1975; Allen and Boettcher, 1978). Experiments which yield information about liquid composition indicate that moderate degrees of melting (30-50%) can produce liquids similar in composition to 'calc-alkaline' andesites. These experimentally produced andesites compare favorably with the andesites and dacites of the Mormon Mountain volcanic field (Table 9), and suggest that partial melting of amphibolite is a reasonable hypothesis for the origin of primary, 'calc-alkalic' andesites of 'MMVF'.

Quantitative treatment of the trace element characteristics of the 'MMVF' andesites with respect to a model of amphibolite fusion yields information on the possible trace element abundances of their source. Comparison of the calculated source compositions with the

TABLE 9:Comparison of Experimental Partial Melts of Amphibolite with Mormon Mountain Volcanic Field Andesites

	A	B	C	D	E	F	G	H	I	J	K	L	M	N
SiO_2	59.7	64.5	63.8	63.0	60.3	60.5	60.3	62.8	59.5	60.4	57.59	59.61	59.82	62.11
TiO_2	0.4	0.1	1.2	1.0	1.14	1.26	.63	.8	1.2	1.3	.86	.68	1.0	.70
Al_2O_3	20.2	19.9	18.6	19.9	19.9	20.0	23.4	23.1	20.2	20.7	19.94	18.97	17.26	17.15
ΣFeO	6.3	4.4	4.3	3.0	4.22	4.15	2.6	2.1	4.49	4.49	6.35	5.00	5.57	5.40
MnO	0.3	0.4	-	-	.13	.12	-	-	.1	.1	-	-	-	.10
MgO	2.1	2.0	0.7	.2	1.03	1.10	.67	.9	5.0	3.6	1.79	2.08	3.68	2.63
CaO	6.7	3.9	6.9	6.4	7.29	8.41	5.34	9.3	7.5	7.5	6.30	6.20	5.86	5.42
Na_2O	3.4	3.6	2.8	4.7	4.3	3.2	4.6	.3	.9	.9	5.04	4.81	4.36	4.33
K_2O	0.9	1.0	1.0	1.0	1.1	.84	1.8	.5	.9	.9	1.97	1.74	1.78	1.94
P_2O_5	-	-	-	-	.54	.44	.69	-	-	-	.56	.38	.27	.29
TOTAL	100.0	99.8	99.3	99.2	99.95	100.02	100.03	99.8	99.79	99.89	100.40	99.47	99.6	100.07

A. Green & Ringwood,1968 - high-Al qtz tholeiite, 10kb, 960°C, 'wet' (undersaturated) conditions, 54% liquid.

B. Green & Ringwood,1968 - high-Al qtz tholeiite, 10kb, 920°C, 'wet' (undersaturated) conditions, 44% liquid.

C. Holloway & Burnham,1972 - ol. tholeiite, 5.2kb, 999°C, H_2O-undersaturated conditions, 30% liquid.

D. Holloway & Burnham,1972 - ol. tholeiite, 7.8kb, 995°C, H_2O-undersaturated conditions, 30% liquid.

E. Helz,1976 - PG tholeiite, 5kb, 1000°C, H_2O-saturated conditions, 63.3% liquid.

F. Helz,1976 - 1921 ol. tholeiite, 5kb, 1015°C, H_2O-saturated conditions, 39.8% liquid.

G. Helz,1976 - 1801 a.o.b., 5kb, 970°C, H_2O-saturated conditions, 31.1% liquid.

H. Allen & Boettcher,1978 - ol. tholeiite, 13kb, 960°C, $X_{H_2O}^{vapor} = 1.0$.

I. Allen & Boettcher,1978 - ol. tholeiite, 13kb, 1010°C, $X_{H_2O}^{vapor} = 0.5$.

J. Allen & Boettcher,1978 - ol. tholeiite, 13kb, 1010°C, $X_{H_2O}^{vapor} = 0.5$.

K. MMT-25 - andesite ; L. MMT-21 - andesite ; M. MMT-6 - andesite ; N. MMT-7 - dacite.

observed trace element contents of crustal rocks of basaltic composition, provide a test of the amphibolite fusion model.

The trace element characteristics of only the hornblende andesite of Mormon Mountain (MMT-6) are quantitatively modeled. The similarities of the other 'MMVF' andesites, except perhaps the Hutch Mountain andesite (MMT-25) to the Mormon Mountain andesite suggest that the conclusions of this examination are also relevant to their petrogenesis.

The quantitative treatment of the trace element geochemistry of the Mormon Mountain andesite by the application of partial melting equations (Hanson, 1980) is dependent upon many different variables. These variables are, for the most part, poorly defined and must be estimated or assumed. Variations in the amphibolite paragenesis, and in partition coefficients for various elements in response to compositional changes in the liquid will affect the calculated result. The approach which has been adopted in this study allows some of these to be assessed.

The mathematical treatment of the data was completed using the computer program 'ANTEK' which is based on the partial melting equations of Hertogen and Gijbels (1976). The program calculates the ratio C_L/C_0 (C_L = concentration of a trace element in the liquid; C_0 = initial concentration of a trace element in the source) for both batch and fractional fusion in specified increments for a particular residual mode. The input parameters on the melting of amphibolite are broadly constrained by the data of Helz (1976) and are summarized in Table 10. Only the results of batch (i.e. equilibrium) partial melting are discussed as the results of fractional fusion may not produce 'calc-alkalic' andesite (Helz, 1976).

TABLE 10: Input Parameters for "ANTEK" Partial Melting Calculation of Amphibolite

Proportions	Amphibole	Plagioclase	Apatite	Magnetite
Initial	50%	47%	1.5%	1.5%
Melting Interval #1	30%	65%	3.5%	1.5%
Melting Interval #2	30%	65%	5%	-

Apatite exhausted at 42.9% partial melting

The interpretation of the 'ANTEK' results is, as previously mentioned, dependent upon the choice of partition coefficients used in the calculation. These coefficients vary substantially with the bulk chemistry of the system (Hanson, 1980; Pearce and Norry, 1979). The Mormon Mountain andesite is intermediate in composition to those for which partition coefficients have been determined (basalt/low-Si andesite and dacite) (Table 11). Consequently, two groups of calculations, using each of these 'end-member' coefficient sets, were performed and provide broad limits on source composition (Fig. 18). The most appropriate result lies somewhere between these two extremes. Thus, while the source chemistry may not be defined with any great accuracy, some generalizations on its basic character are possible.

The amphibolitic source for the Mormon Mountain andesite must be moderately LREE-enriched (Ce = 40-60 x chondrites) and HREE-depleted (Yb = 2 to 6 x chondrites) with Rb(7-8 ppm), Sr(~ 1000 ppm), Ba(600-700 ppm), Y(24 ppm), Zr(90-115 ppm) and Nb(20-25 ppm). This source is not recognizably upper or lower crust if compared to the models of Taylor and McLennan (1981). REE abundances, except for the depleted HREE, Zr, and Y are similar to their values for the total crust; Nb and Ba resemble the upper crust and Rb the lower crust. Sr contents are a factor of 2 higher than any of these model compositions. However, trace element analysis of various crustal nodules from the Colorado Plateau (Appendix 8) indicates that the crust of the Colorado Plateau is more complicated than suggested by average crustal models, so that the variability of trace element abundances in derivative melts may be anticipated. Finally, the abundances of the calculated source are similar to those observed in recently erupted basalts of 'MMVF' (Appendix 7) and the nearby San Francisco volcanic field (Wolfe, pers. comm.). Nodules of amphibole -

TABLE 11: Mineral/Melt Partition Coefficients Used in Petrochemical Modeling[1]

	OL	CPX	AMP			PLAG			APATITE		MT		
	A	A	A	B	C	A	B	C	AB	C	ABC		
Rb[2]	.01	.02	.05	.05	.014	.07	.048	.041	.01	.01	.01		
Ba[2]	.01	.02	.09	.09	.044	.16	.36	.308	.01	.01	.01		
K	.01	.02	.33	-	-	.11	-	-	.01	-	.01		
Pb[2]	.01	.02	.05	.05	.014	.07	.048	.041	.01	.01	.01		
Sr	.01	.08	.23	.04	.022	1.8	2.84	4.4	1.0	1.0	.01		
U[2]	-	-	.01	.1	.1	.01	.01	.01	.46	.46	.01		
Th[2]	-	-	.01	.1	.1	.01	.01	.01	2.13	2.13	.01		
Ce(La)	(.007)	(.15)	.094	.899	1.52	.12	.24	.27	18	34.7	1.0		
Nd	-	-	.189	2.8	4.26	.081	.17	.21	27.4	57.1	1.0		
Sm	-	-	.336	3.99	7.77	.067	.13	.13	29.3	62.8	1.0		
Eu	-	-	.358	3.44	5.14	.34	2.11	2.15	20.5	30.4	1.0		
Gd	-	-	.509	5.48	10.0	.063	.090	.097	25.0	56.3	1.0		
Er	-	-	.484	5.94	12.0	.063	.084	.055	20.0	37.2	1.0		
Yb	-	-	.462	4.89	8.38	.067	.077	.049	13.1	23.9	1.0		
											A	B	C
Y	.01	.5	1.0	2.5	6.0	.03	.06	.1	20	40	.2	.5	2.5
Zr	.01	.1	.5	1.4	4.0	.01	.03	.1	.1	.1	.1	.2	.8
Nb	.01	.1	.8	1.3	4.0	.01	.025	.06	.1	.1	.4	1.0	2.0
Ni[2]	10	6	8	-	-	.01	-	-	.01	-	10	-	-
Cr[2]	.63	30	30	-	-	.01	-	-	.01	-	32	-	-
Sc[2]	.37	3	12.5	-	-	.01	-	-	.01	-	2	-	-
V[2]	.04	1.1	32	-	-	.01	-	-	.01	-	30	-	-

[1] Partition coefficients compiled from Gill, 1978; Hanson, 1980; Pearce and Norry, 1979; Schnetzler and Philpotts, 1970; Philpotts and Schnetzler, 1970; Schock, 1979; Arth and Hanson, 1975; Irving, 1978; Nagasawa, 1970.

[2] Estimated where unavailable.

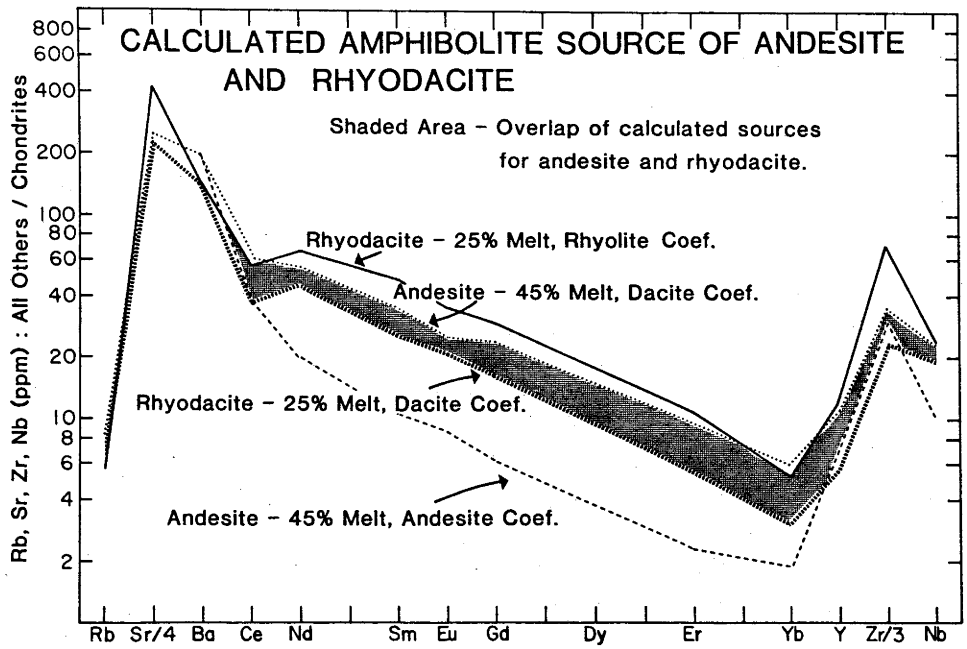

Figure 18. Calculated amphibolite source(s) of the andesite and rhyodacite of Mormon Mt. if each represents a discrete melting episode. Method of calculation described in the text. Three sets of partition coefficients are used in the calculation and are indicated in the figure. The shaded area is the amount of overlap between the most likely coefficient sets, and represents the best approximation of the source composition.

plagioclase - clinopyroxene cumulates of recent derivation (Appendix 8), suggest that some of the basalts may crystallize in the crust under hydrous conditions. These cumulate 'amphibolites' may be remelted to produce andesitic magmas.

Variations introduced by allowing different source mineralogies (pyroxene or garnet amphibolite) show that 1) the addition of clinopyroxene at the expense of amphibole and plagioclase requires the source to be slightly more depleted in all elements and 2) the addition of garnet, replacing plagioclase, to a clinopyroxene amphibolite, lessens the HREE-depletion of the source. The first situation occurs as a product of melting (Helz, 1973) while the second results from higher pressures (Allen and Boettcher, 1978).

In summary, the results of modeling the trace element characteristics of the Mormon Mountain andesite semi-quantitatively define the chemistry of its source. This chemistry is similar to that of lower crustal nodules, and recently erupted basalts from the surrounding area and suggests that a petrogenetic model of amphibolite anatexis to account for the chemical characteristics of 'MMVF' silicic suite is compatible with the observed geologic constraints.

The derivation of the dacites and rhyodacites of the Mormom Mountain volcanic field by fractional crystallization of andesite, is possible only if the proposed parent/daughter pair exhibit geographical, temporal, mineralogical and geochemical continuity. The field relations of the dacites and rhyodacite of the Mormon Mountain complex are consistent with the first two of these criteria as is the mineralogy and geochemistry of the andesite/rhyodacite pair. However the different phenocryst assemblage (orthopyroxene and clinopyroxene) and different trace element characteristics (e.g. HREE-depletion) of the dacite suggest that its derivation by fractional crystallization of andesite is inappropriate.

Least-squares model calculations for the andesite/rhyodacite pair suggest that approximately 50% fractional crystallization of amphibole, plagioclase, apatite and magnetite from andesite (Table 12) could generate the rhyodacite. The coarse-grained inclusions of dominantly amphibole and plagioclase found in the dacites, may be the products of this fractionation. Rayleigh fractionation calculations using the incompatible trace element data do not conclusively confirm or deny the fractional crystallization hypothesis (Fig. 19, Table 13). Variations in the partition coefficients of these elements for amphibole with respect to melt composition are the main cause of this ambiguity. Three sets of partition coefficients have been used in the modeling (Fig. 19) corresponding to (a) low-Si andesitic (b) dacitic and (c) rhyolitic compositions (Table 11). The partition coefficients for the high-Si andesite and the rhyodacite of the Mormon Mountain complex must lie in-between a and b and b and c respectively. The REE's (except Ce and Yb) are best modeled using the dacite coefficients, however Zr, Nb, Y and Sr are in error. Andesitic coefficients (a) are totally inappropriate predicting that the rhyodacite should be enriched in all compatible elements. All sets of partition coefficients predict enrichments in Rb, Ba, U, Th and Ce, in contrast to the observed depletion. These anomalies weaken the hypothesis of fractional crystallization by demanding an ad-hoc explanation of selective partitioning of these elements into a late-stage vapor phase. Finally, an upward turn in the chondrite-normalized REE pattern for the HREE (Er-Yb) associated with amphibole fractionation is not observed in the REE pattern of the rhyodacite.

(c) Model C - The failure of the fractional crystallization hypothesis to explain the origin of the pyroxene dacite requires the evaluation of another petrogenetic model. This hypothesis (Model C)

TABLE 12: Least Squares Solution for Andesite (MMT-6) - Rhyodacite (MMT-3) Fractionation

				CALCULATED DATA					
OXIDE	WEIGHT	CALC	DIFF	MMT-6	MMT-3	AMPH	MT	AN40	APT
SiO_2	4.0	59.82	.0%	59.82	69.92	41.95	1.98	57.95	.00
TiO_2	.5	1.07	7.3%	1.00	.26	2.77	17.95	.00	.00
Al_2O_3	2.0	17.13	-.8%	17.26	14.65	13.50	1.28	26.34	.00
FeO	2.0	5.57	.1%	5.57	3.30	10.80	72.95	.48	.00
MgO	2.0	3.53	-4.1%	3.68	1.33	14.51	1.67	.00	.10
CaO	2.0	6.15	4.9%	5.86	3.16	11.00	.17	8.17	55.84
Na_2O	.5	4.72	8.2%	4.36	4.81	2.82	.00	6.38	.00
K_2O	.5	1.51	-15.2%	1.78	2.35	.70	.00	.54	.00
P_2O_5	20.0	.27	-1.4%	.27	.14	.00	.00	.00	42.05
TOTAL		99.77		99.60	99.92	98.05	96.00	99.86	97.99
SOLUTIONS ARE		100.32%			52.54%	19.24%	2.24%	25.83%	.46%

$\Sigma R^2 = .33$

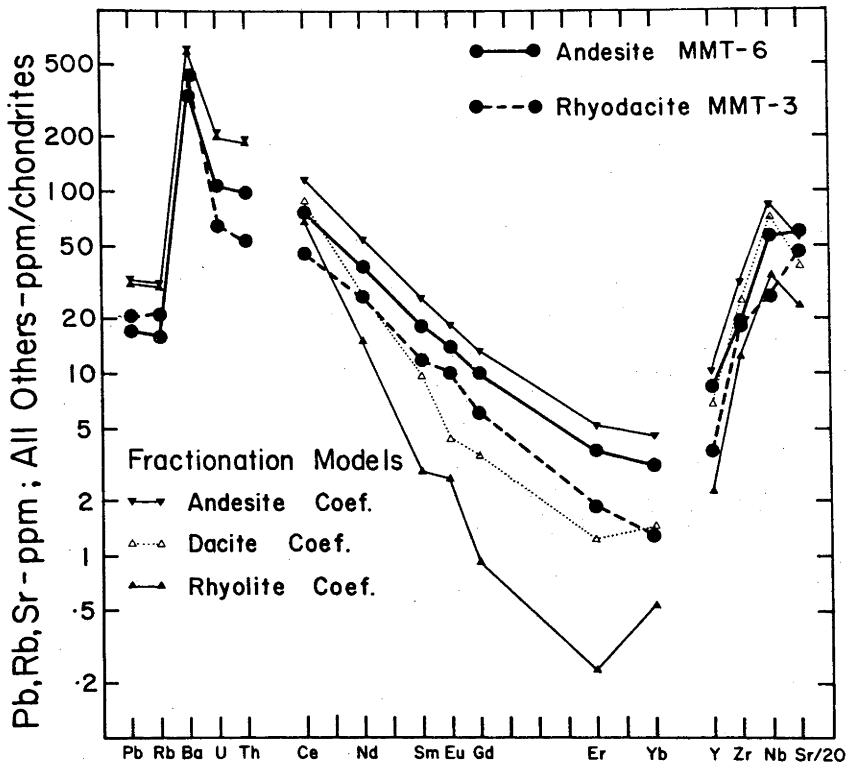

Figure 19. Graphical representation of the results of Rayleigh Fractionation on trace element abundance for the fractionation sequence of andesite (MMT-6) to rhyodacite (MMT-3). The large compositional change between this parent/daughter pair is reflected in the use of three different sets of partition coefficients in the calculation. The closest approximation to observed abundances in the rhyodacite is achieved using the dacite coefficients.

TABLE 13: Rayleigh Fractionation Calculations for Trace Elements Using the Least Squares Solution for Andesite/Rhyodacite Fractionation

	OBSERVED		CALCULATED RHYODACITE		
	ANDESITE-MMT-6	RHYODACITE MMT-3	A	B	C
Ce[1]	76.2	45.9	118	91.7	69.7
Nd[1]	37.9	26.3	54.7	26.9	15.1
Sm[1]	18.6	11.7	25.6	9.7	2.9
Eu[1]	13.9	10.2	18.3	4.4	2.65
Gd[1]	9.8	5.9	13.2	3.6	.92
Er[1]	3.7	1.9	5.2	1.25	.24
Yb[1]	3.1	1.3	4.6	1.44	.55
Ba[2]	1310	1525	2247	--	2213
Rb[2]	16	21	29.3	--	30
Pb[2]	17	20	31	--	31.7
Sr[2]	1145	985	1080	790	465
U[1]	105	67.8	198	--	198
Th[1]	98.7	53.6	184	--	184
Zr[2]	111	107	184	144	70.5
Nb[2]	25	12	38	32	15.5
Y[2]	17.2	7.9	22	14.6	4.8

A- Basalt/Andesite partition coef.

B- 'Dacite' partition coef.

C- Rhyolite partition coef.

1. Chondrite-normalized value

2. ppm

considers each silicic rock type to be the product of crustal anatexis. In this regard, the reasoning and approach are similar to the first part of Model B which examined crustal anatexis as the mechanism for the generation of primary andesitic liquids. Using the same data base as this model, it is possible to produce liquids of approximately dacitic and rhyodacitic compositions by smaller degrees of melting than for andesite (e.g. Helz, 1976). The similarities between Helz's experimental liquids and the silicic rocks of the Mormon Mountain volcanic field are shown in the ternary Ab-Or-Qtz (Fig. 20). The intersection of the Mormon Mountain trend with the Ab-Or join at about Ab_{80} Or_{20} is significant because it signifies the involvement of a K-bearing phase (amphibole, biotite or K-feldspar) in the origin of the suite (Helz, 1976). As neither biotite nor K-feldspar is observed in the andesites, dacites or rhyodacites, the K-bearing phase must be amphibole.

It is apparent from both the petrologic and geochemical data, that although the entire silicic suite of the Mormon Mountain volcanic field may be the product of partial melting of amphibolite, the andesites and rhyodacites are distinct from the dacites. This distinction must reflect differences in the melting and crystallization histories of each group. It is proposed that these differences are due primarily to initial variations in the composition of the vapor phase (i.e. CO_2 - H_2O - F).

Experimental work on the water-saturated and water-undersaturated melting relations of basalt (1921 Kiluea olivine tholeiite) demonstrates that a reduction in fH_2O in the fluid phase systematically shifts all phase boundaries except the solidus to higher temperatures (Fig. 21) (Holloway and Burnham, 1972; Helz 1973; 1976; Allen and Boettcher, 1978). As a consequence, the amount

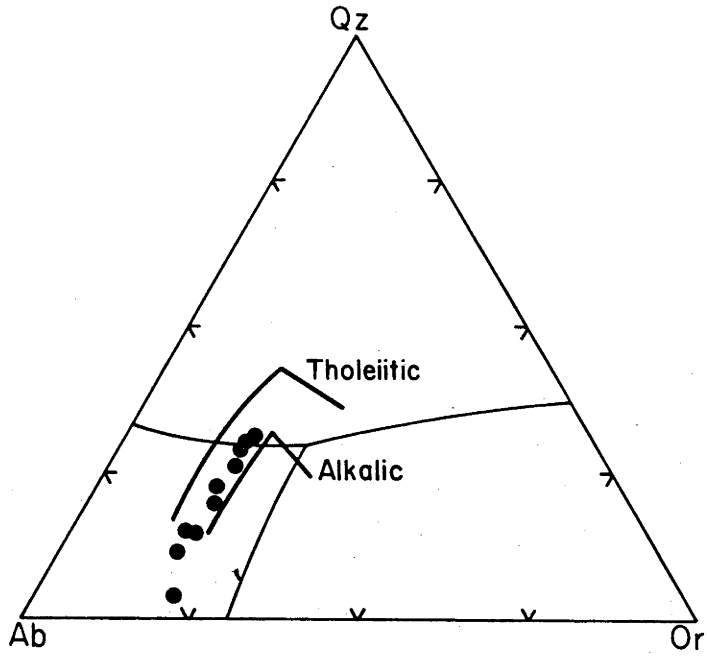

Figure 20. Ab - Or - Qz ternary projection of the 'MMVF' silicic volcanic rocks. Similarities between the trend of this suite and the liquid trends derived by partial melting of amphibolite (tholeiitic and alkalic compositions - Helz (1976)) suggests that the 'MMVF' suite may be the result of different degrees of amphibolite fusion.

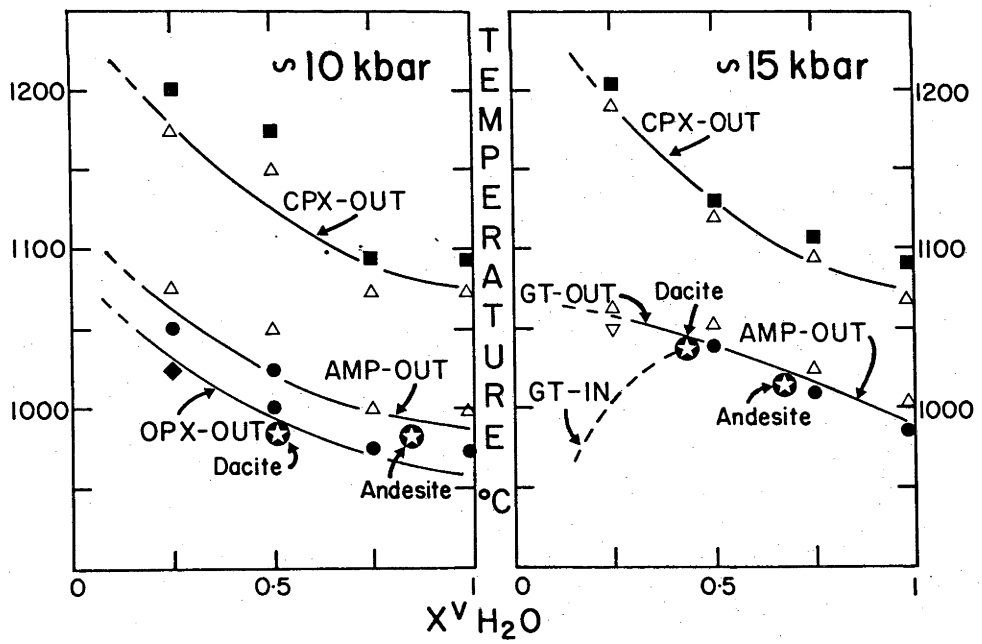

Figure 21. Isobaric T/H_2O phase diagrams for partially melted amphibolite. Constructed from experimental data of Allen and Boettcher (1978). See text for explanation.

of liquid produced decreases with decreasing $f_{H_2O}^{vapor}$ along an isotherm, however, the composition of that liquid will show only small differences compared with liquids generated at higher $f_{H_2O}^{vapor}$ and similar degrees of melting (Helz, 1976). It is possible therefore, to generate the andesite and dacite from a similar source without a significant increase in temperature.

Lower $f_{H_2O}^{vapor}$ also reduces the stability of amphibole with respect to pressure. Under low $f_{H_2O}^{vapor}$ conditions, the decomposition of amphibole to garnet may occur at pressures as low as 15 kbar with both garnet and amphibole coexisting with a liquid (Allen and Boettcher, 1978). These pressures, equivalent to ~45 km, approximate the conditions of the base of the crust of the Colorado Plateau and suggest that the petrogenesis of the dacitic magmas of Mormon Mountain could involve garnet.

The petrologic similarities of the rhyodacite and the andesite suggest that if the rhyodacite is to be considered a primary magma, its petrogenesis should parallel that of the andesite. Liquids which are approximately equivalent to the rhyodacite compositions of the Mormon Mountain volcanic field, can result from 20 to 30% partial melting of an amphibolite (Helz, 1976).

Partial melting calculations similar to those completed for the andesite melt, suggest that the andesite and rhyodacite could be derived from an approximately homogeneous source (Fig. 18). Anomalies in Zr and HREE abundances between the calculated andesite and rhyodacite sources could represent trace amounts of residual zircon in the rhyodacite source (Watson, 1979b). The HREE depletion of the dacite compared to the andesite and the rhyodacite, may reflect either a HREE depletion or alternatively, residual zircon or garnet in the

dacite source. The presence of garnet is consistent with a model involving the fusion of amphibolite vapor at moderate pressures (~15 kbar) under low $f_{H_2O}^{vapor}$ conditions.

Isotopic Constraints - The similar $^{87}Sr/^{86}Sr$ isotopic ratios of the andesites, dacite, rhyodacite and basalts of 'MMVF' and the granulite suggest that Sr isotopic ratios are not diagnostic with regard to a particular petrogenetic hypothesis (i.e. basaltic fractionation vs. lower crustal anatexis). The low isotopic values of the andesites, dacite and rhyodacite indicate that if the genesis of these rocks is a result of crustal anatexis, their source(s) must have a long-term depletion in Rb. The peculiarly low abundances of Rb in the 'MMVF' silicic suite is also indicative of a Rb-poor source.

Summary - Qualitative and quantitative interpretation of the major element and trace element geochemical data of the 'MMVF' silicic suite suggests that (a) the derivation of the andesites by fractional crystallization of basalt is unlikely (b) the andesites represent primary magmas resulting from partial melting of an amphibolitic source (c) fractional crystallization could produce rhyodacitic, but not dacitic magmas from an andesitic parent and (d) the dacite and rhyodacite may also be primary magmas derived by the fusion of amphibolite under different conditions. Quantitative modeling of the amphibolitic source(s) of the andesites, dacites and rhyodacites indicate that the composition of the source is approximately homogeneous. This composition is similar to basalts of 'MMVF' and the San Francisco volcanic field and some samples of the lower crust of the Colorado Plateau (i.e. crustal nodules in basaltic hosts).

ANOROGENIC AND OROGENIC 'CALC-ALKALINE' SERIES

Ewart (1976, 1979) compiled a fairly comprehensive survey which summarized the major mineralogic and geochemical characteristics of

orogenic and anorogenic salic suites. More recently, Bailey (1981) reviewed the geochemistry, in particular the trace element geochemistry, of orogenic andesites to identify features which could discriminate between their various tectonic environments (i.e. oceanic island arcs, continental island arcs and thin continental margins, and thick continental crust). In both of these studies, anorogenic andesites (dacites and rhyodites) were identified as those occurring in areas which were not subject to subduction. These anorogenic andesites are not 'calc-alkalic', but are either more alkalic (hawaiites, mugearites, trachyandesites) or sub-alkalic (icelandites) varieties. 'Calc-alkalic' anorogenic andesites are, in these reviews, either incorrectly identified as orogenic (e.g. Western U.S.A. 'eastern belt' (Ewart, 1976, 1979) or ignored (for instance, 'calc-alkalic' suites are reported from Mt. Ararat, Turkey (Lambert, et al., 1974), Kastamonu, Turkey (Peccerillo and Taylor, 1976) Massif Central, France (Girod and Lefèvre, 1972), Mt Taylor, New Mexico, USA (Baker and Ridley, 1970)), because geochemical information is incomplete.

The high Al_2O_3 (~17%), low ΣFe (FeO 5.0 - 6.4%) and low TiO_2 (.7-1.0%) contents of the 'calc-alkalic' andesites of the Mormon Mountain volcanic field are supposedly, distinguishing major elements characteristics of orogenic andesites (Bailey, 1981). Comparison with average andesite, dacite and rhyodacite major element analyses from different orogenic environments (Ewart, 1976, 1979; Bailey, 1981), shows that the Mormon Mountain salic suite is virtually identical to 'calc-alkalic' suites associated with thick continental crust (e.g. Andes). Another feature of these suites which also characterize anorogenic 'calc-alkalic' suites is their high total content of alkalis. Mildly alkalic trachyandesites and latites are

occasionally associated with some of these suites and may be a reflection of their marginally 'calc-alkalic' affinities.

The trace element geochemistry of the hornblende andesite from the Mormon Mountain complex is compared to that of other 'calc-alkalic'andesites in Figure 22. The abundances are normalized to an average oceanic island arc low-K andesite (Bailey, 1981) to aid in this comparison. The Mormon Mountain andesite is most similar to the average andesite from environments of thick continental crust. This resemblance is even greater if the maximum and minimum values of the various elements for this particular 'tectonic type' are plotted (Fig. 23). There are however, significant deviations which are peculiar to the Mormon Mountain andesite such as the unusual characteristics of low Rb and Cs and high Ba and Sr. The highly fractionated REE's of this andesite are also distinctive; this being due to a depletion in the HREE's. It is more enriched in Nb and TiO_2 than the average 'thick crust' andesite, but depleted with respect to Zr and Hf. Except for the highly incompatible elements, the geochemical coherency of various other elements (Zr-Hf, U-Th, Cr-Ni-Sc,) as observed in their ratios, is preserved.

The unusual phenocryst assemblages of the Mormon Mountain andesite and dacite has been noted before in the explanation of their respective crystallization sequences. The near total absence of plagioclase phenocrysts in 'MMVF' andesites is extremely atypical of orogenic andesite and dacite (Ewart, 1976, 1979). The few samples of plagioclase phenocrysts are less calcic (<AN 70) than those of the majority of orogenic lavas. Clinopyroxene, chiefly augite, orthopyroxene and hornblende are, in addition to plagioclase, the main phenocryst phases of orogenic andesites. The compositions of the pyroxenes of this orogenic salic volcanics and the 'MMVF' suite are

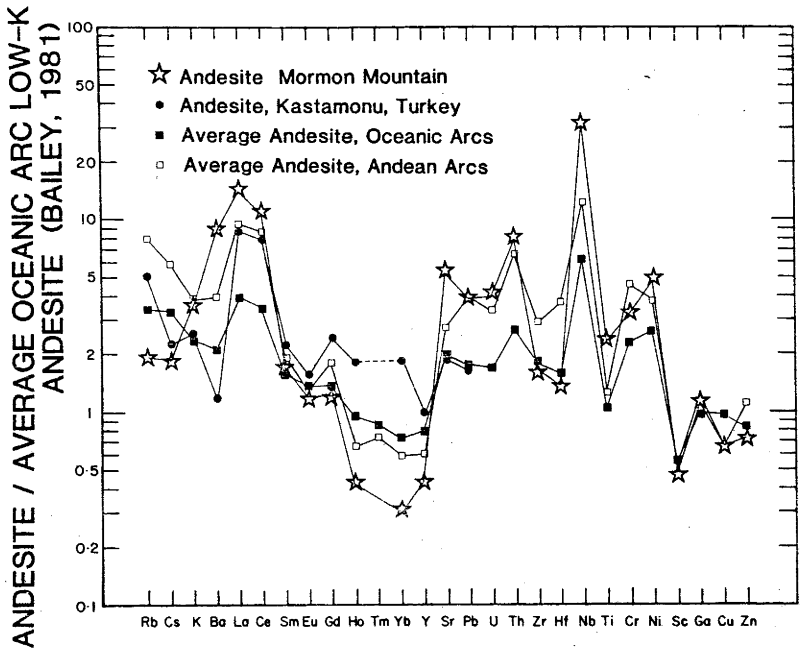

Figure 22. Trace element abundances of andesite (MMT-6) from Mormon Mt. compared with average orogenic andesites from different tectonic environments (Bailey, 1981). All data are normalized to an average oceanic arc low K andesite, also from Bailey (1981).

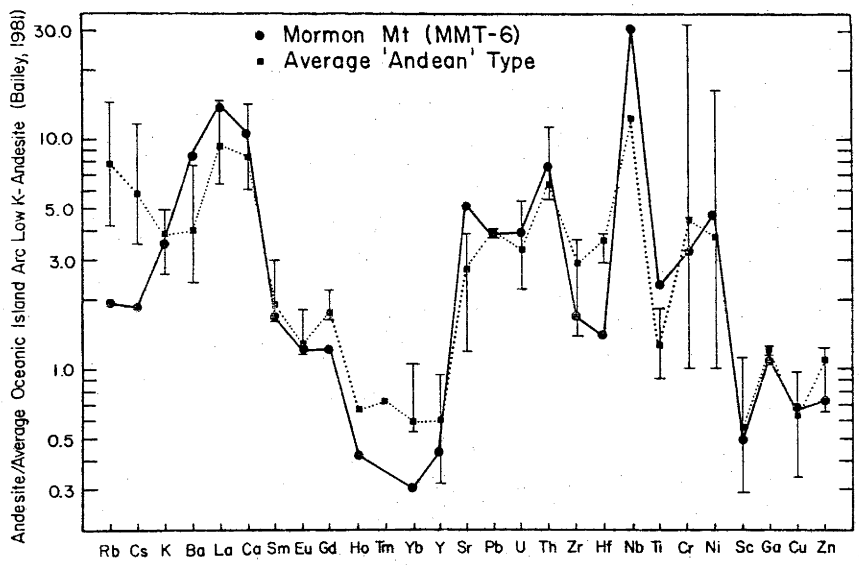

Figure 23. Trace element abundances of andesite (MMT-6) from Mormon Mt. compared to the average value and range of values in 'Andean-type' orogenic andesites (Bailey,1981). All data are normalized to an average oceanic island arc low K andesite, also from Bailey (1981).

indistinguishable. Jakeš and White (1972) suggested, from a study of amphibole compositions in orogenic 'calc-alkaline' rocks, that amphiboles from rocks of similar composition arc distinguishable with regard to their tectonic environment (island arc versus continental arc). In Jakeš and White's division, amphiboles from island arc environments have higher total alkalis, differences in Al content and lower Fe/Mg ratio than do those from continental settings. This suggestion is not substantiated when more recent data are considered, as amphiboles from various continental settings (including Mormon Mountain) are identified as island arcs and vice versa (Fig. 24).

It is apparent that in many respects, the salic suite of the Mormon Mountain volcanic field resembles orogenic series which occur in areas characterized by thick continental crust. These similarities, in conjunction with a proposed crustal origin for the 'MMVF' volcanics, suggest that the crust must also play a fundamental part in the petrogenesis of some orogenic 'calc-alkalic' series. Such an idea is not new (e.g. Pichler and Zeil, 1972; Klerkx et al., 1977) and has been more recently proposed to account for various characteristics of island arc basalts (Arculus and Johnson, 1981). This discussion extends the petrogenetic models proposed for the anorogenic Mormon Mountain suite to continental arc environments to examine the origins of some orogenic andesites.

CONCLUSIONS

The favored hypothesis for the petrogenesis of the andesites, dacites and rhyodacites of the Mormon Mountain volcanic field suggests that these magmas are derived by anatexis of lower crustal amphibolites. These amphibolites may be old crust or recent additions resulting from the high pressure, hydrous crystallization of basaltic

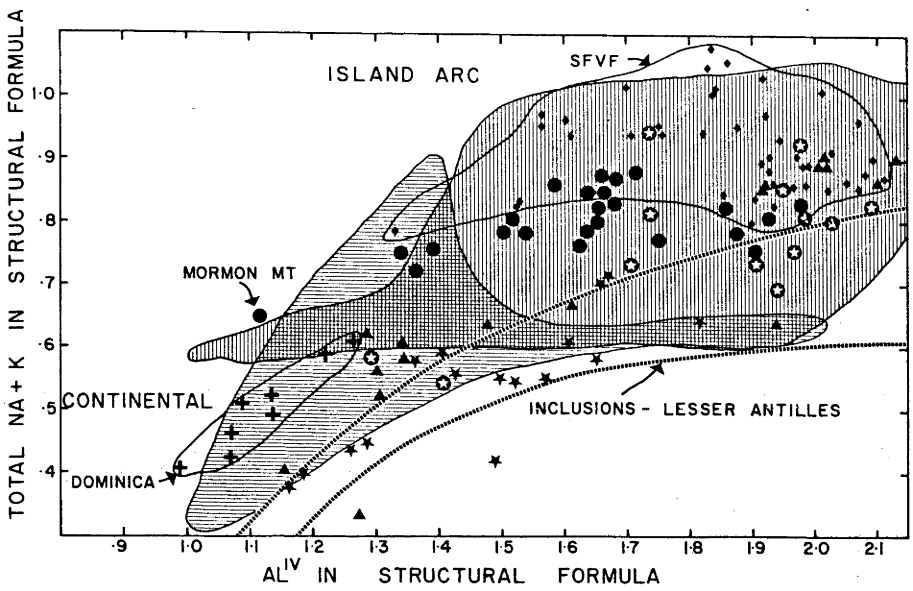

Figure 24. Relationship of total alkali content (Na + K) and tetrahedral aluminum in hornblende structural formula for amphiboles from continental areas - - 'MMVF' (●), San Francisco Volcanic Field (SFVF) (◆), and island arcs - - Dominica (+) (Wills, 1974), Boisa (★) (Gust et al., 1980), Sunda (✪) (Whitford, 1975), Grenada (▲) (Arculus, 1973). Field of amphiboles for coarse-grained inclusions in rocks of the Lesser Antilles (Arculus and Wills, 1980) is indicated by the closely dashed lines. The horizontally ruled area is the field of amphiboles from continental areas and the vertically ruled area signifies amphiboles from island arcs (Jakeš and White, 1972). Note that amphiboles from the areas cited above do not concur with the tectonic distinction suggested by Jakeš and White.

magmas. The geochemical similarities of samples of the lower crust (i.e. nodules) and recently erupted basalts associated with the silicic suite, with a calculated amphibolitic source for the andesite, dacite and rhyodacite of Mormon Mountain supports this interpretation. $^{87}Sr/^{86}Sr$ isotopic ratios do not discriminate between old and new crustal sources as the values of silicic and basaltic rocks, and the lower crust (pyroxene granulite) are similar.

Geochemical similarities between the anorogenic 'MMVF' andesites and some orogenic 'Andean' andesites, suggest that the process of crustal anatexis is possibly important in orogenic arcs characterized by thick continental crust. Basaltic magmas, generated by partial melting of 'wet' peridotite may stagnate at the base of the crust and crystallize to form amphibolite. Partial melting of those amphibolites with island arc basalt geochemistry (Perfit et al., 1980), could produce orogenic, 'calc-alkaline' andesites and explain the occasional lack of basalt near andesitic volcanoes.

REFERENCES

Akimoto, S.; Yamamoto, K., and Aoki, K. (1977) Hydroxyl-clinohumite and hydroxyl-chondrodite: Possible H_2O-bearing minerals in the upper mantle IN High Pressure Research, Applications in Geophysics, Manghnani, M.H. and Akimoto, S. (editors) Academic Press, New York, 163-174.

Albarede, F. and Bottinga, Y. (1972) Kinetic disequilibrium in trace element partitioning between phenocrysts and host lava. Geochim. Cosmochim. Acta, 36, 141-156.

Allen, J.C. and Boettcher, A.L. (1971) The stability of amphiboles in basalts and andesites at high pressures (abstr.). Program. Ann. Meet. Geol. Soc. Am., 3, 490.

Allen, J.C.; Boettcher, A.L., and Marland, G. (1975) Amphiboles in andesite and basalt: I. Stability as a function of P-T-fO_2. Am. Mineral., 60, 1069-1085.

Allen, J.C. and Boettcher, A.L. (1978) Amphiboles in andesite and basalt: II. Stability as a function of P-T-fH_2O-fO_2. Am. Mineral., 63, 1074-1087.

Allen, J.C.; Modreski, P.J.; Haygood, C., and Boettcher, A.L. (1972) The role of water in the mantle of the earth: the stability of amphiboles and micas. International Geol. Cong., 24th Proc. Sec. 2, 231-240.

Anderson, A.T. (1976) Magma mixing: Petrological process and volcanological tool. J. Volcanol. Geotherm. Res., 1, 3-33.

Anderson, R.N.; DeLong, S.E., and Schwartz, W.M. (1978) Thermal model for subduction with dehydration in the downgoing slab. J. Geol., 86, 731-739.

Aoki, K-I. (1975) Origin of phlogopite and potassic richterite-bearing peridotite xenoliths from South Africa. Contrib. Mineral. Petrol., 53, 145-156.

Apted, M.J. (1981) Rare earth element systematics of hydrous liquids from partial melting of basaltic eclogite: A re-evaluation. Earth Planet. Sci. Lett., 52, 172-182.

Arculus, R.J. (1973) The alkali basalt-andesite association of Grenada, Lesser Antilles. Ph.D. Thesis, Durham Univ., 331pp.

Arculus, R.J. (1976) Geology and geochemistry of the alkali basalt-andesite association of Grenada, Lesser Antilles island arc. Geol. Soc. Am. Bull., 87, 612-624.

Arculus, R.J. (1978) Mineralogy and petrology of Grenada, Lesser Antilles island arc. Contrib. Mineral. Petrol., 65, 413-424.

Arculus, R.J. (1981) Island arc magmatism in relation to the evolution of the crust and mantle. Tectonophys., 75, 113-133.

Arculus, R.J. and Curran E.B. (1972) The genesis of the calc-alkaline rock suite. Earth Planet. Sci. Lett., 15, 255-262.

Arculus, R.J. and Johnson, R.W. (1978) Criticism of generalized models for the magmatic evolution of arc trench systems. Earth Planet. Sci. Lett., 39, 118-126.

Arculus, R.J. and Johnson, R.W. (1981) Island-arc magma sources: a geochemical assessment of the roles of slab-derived components and crustal contamination. Geochem. J., 15, 109-133.

Arculus, R.J. and Smith, D. (1979) Eclogite, pyroxenite and amphibolitic inclusions in the Sullivan Buttes Latite, Chino Valley, Yavapai County, Arizona IN The Mantle Sample: Inclusions in Kimberlites and Other Volcanics, A.G.U., Wash., 309-317.

Arculus, R.J. and Wills, K.J.A. (1980) The petrology of plutonic blocks and inclusions from the Lesser Antilles island arc. J. Petrol., 21, 743-799.

Arima, M. and Edgar, A.D. (1980) Stability of wadeite ($Zr_2K_4Si_6O_{18}$) under upper mantle conditions: Petrological implications. Contrib. Mineral. Petrol., 72, 191-195.

Armstrong, R.L. (1971) Isotopic and chemical constraints on models of magma genesis in volcanic arcs. Earth Planet. Sci. Lett., 12,137-142.

Arth, J.G. (1976) Behaviour of trace elements during magmatic processes - a summary of theoretical models and their applications. J.Res. U.S. Geol. Surv., 4,41-47.

Arth, J.G. and Hanson, G.N. (1975) Geochemistry and origin of the early Precambrian crust of northeastern Minnesota. Geochim. Cosmochim. Acta., 39,325-362.

Atwater, T. (1970) Implications of plate tectonics for the Cenozoic tectonics of western North America. Geol. Soc. Am. Bull., 81, 3513-3536.

Bailey, J.C. (1981) Geochemical criteria for a refined tectonic discrimination of orogenic andesites. Chem. Geol., 32,139-154.

Baker, I. and Ridley, W.I. (1970) Field evidence and K, Rb, Sr data bearing on the origin of the Mt. Taylor volcanic field, New Mexico, U.S.A. Earth Planet. Sci. Lett., 10,106-114.

Baker, P.E. (1968) Comparative volcanology and petrology of the Atlantic island arcs. Bull. Volcanol., 32,189-206.

Banks, R. (1979) The use of linear programming in the analysis of petrological mixing problems: Contrib. Mineral. Petrol., 70,237-244.

Banno, S. and Matsui, Y. (1965) Eclogite types and partition of Mg, Fe, and Mn between clinopyroxene and garnet. Proceed. Jap. Acad., 41,716-721.

Bence, A.E.; Baylis, D.M.; Bender, J.F., and Grove, T.L. (1979) Controls on the major and minor element chemistry of mid-ocean ridge basalts and glasses IN Deep Drilling in the Atlantic Ocean: Ocean crust, Maurice Ewing Series, Talwani, M., Harrison, C.G., and Hayes D.E. (editors), A.G.U. 2,331-341.

Best, M.G. (1975) Migration of hydrous fluids in upper mantle and potassium variation in calc-alkalic rocks. Geology, 3,429-432.

Best, M.G. and Mercy, E.L.P. (1967) Composition and crystallization of mafic minerals in the Guadalupe igneous complex, California. Am. Mineral., 52,436-474.

Beswick, A.E. (1973) An experimental study of alkali metal distribution in feldspars and micas. Geochim. Cosmochim. Acta, 37,183-208.

Beswick, A.E. (1976a) K and Rb relations in basalts and other mantle derived materials. Is phlogopite the key? Geochim. Cosmochim. Acta, 40, 1167-1183.

Beswick, A.E. (1976b) Author's reply to Comment on 'Is phlogopite the key?' by M. Menzies. Geochim. Cosmochim. Acta, 42,149-150.

Boettcher, A.L. (1970) The system $CaO-Al_2O_3-SiO_2-H_2O$ at high pressures and temperatures. J. Petrol., 11,337-379.

Boettcher, A.L. (1973) Volcanism and orogenic belts - the origin of andesites. Tectonophys., 17,223-240.

Boettcher, A.L. (1977) The role of amphiboles and water in Circum-Pacific volcanism IN High Pressure Research, Applications in Geophysics, Manghnani, M.H. and Akimoto, S. (editors), Academic Press, New York, 107-126.

Boettcher, A.L. and Modreski, P.J. (1975) Phase relationships in natural and synthetic peridotite - H_2O and peridotite-H_2O-CO_2 systems at high pressures. Phys. Chem. Earth, 9, 855-867.

Boettcher, A.L.; O'Neil, J.R.; Windom, K.E.; Stewart, D.C. and Wilshire, H.G. (1979) Metasomatism of the upper mantle and the genesis of kimberlites and alkali basalts IN The Mantle Sample: Inclusions in Kimberlites and Other Volcanics, A.G.U., Wash., 173-182.

Bonatti, E.; Honnorez, J.; Kirst, P., and Radicati, F. (1975) Metagabbros from the mid-Atlantic ridge at 06°N; Contact-hydrothermal-dynamic metamorphism beneath the axial valley. J. Geol., 83,61-78.

Bowen, N.L. (1928) The Evolution of Igneous Rocks, Princeton Univ. Press, Princeton, New Jersey, 332p.

Boyd, F.R. and England, J.L. (1960) Apparatus for phase equilibria measurements at pressures up to 50 kilobars and temperatures up to 1750°C. J. Geophys. Res., 65,741-748.

Bruhn, R.L.; Stern, C.R., and deWitt, M.J. (1978) New field and geochemical data bearing on the development of a Mesozoic volcano-tectonic rift zone and back-arc basin in southernmost South America. Earth Planet. Sci. Lett., 41,32-46.

Bryan, W.B., and Moore, J.G. (1977) Compositional variations of young basalts in the Mid-Atlantic Ridge rift valley near lat 36° 49'N. Geol. Soc. Am. Bull., 88, 556-570.

Bryan, W.B.; Thompson, G.; Frey, F.A., and Dickey, J.G. (1976) Inferred geologic settings and differentiation in basalts from the deep sea drilling project. J. Geophys. Res., 81,4285-4304.

Buddington, A.F. and Lindsley, D.H. (1964) Iron-titanium oxide minerals and synthetic equivalents. J. Petrol., 5,310-357.

Bultitude, R.J.; Johnson, R.W., and Chappell, B.W. (1978) Andesites of Bagana volcano, Papua New Guinea: chemical stratigraphy and a reference andesite composition. BMR J. Aust. Geol. Geophys., 3,281-295.

Burnham, C.W. (1979) The importance of volatile constituents IN The evolution of the Igneous Rocks, Fiftieth Anniversary Perspectives, H.S. Yoder, Jr. (editor), Princeton Univ. Press, Princeton, 439-482.

Cann, J.R. (1970) New model for the structure of the oceanic crust. Nature, 226,928-930.

Cann, J.R. (1971) Major element variations in ocean-floor basalts. Phil. Trans. Roy. Soc. Lond., 268,495-505.

Cann, J.R. (1979) Metamorphism in the ocean crust IN Deep Drilling Results in the Atlantic Ocean: Ocean Crust, Maurice Ewing Series, Talwani, M., Harrison, C.G., and Hayes, D.E. (editors),A.G.U. 2,230-238.

Carmichael, I.S. (1967) The iron-titanium oxides of salic volcanic rocks and their associated ferro-magnesium silicates. Contrib. Mineral. Petrol., 14,36-64.

Carmichael, I.S.; Turner, F.,and Verhoogen, J. (1974) Igneous Petrology, McGraw Hill Book Co., New York, 739p.

Carswell, D.A. and Gibb, F.G.F. (1980) Geothermometry of garnet/lherzolite nodules with special reference to those from the kimberlites of northern Lesotho. Contrib. Mineral. Petrol., 74,403-416.

Cawthorn, R.G. (1976) Melting relations in part of the system CaO-MgO-Al_2O_3-SiO_2-Na_2O-H_2O under 5 kb pressure. J. Petrol., 17,44-72.

Cawthorn, R.G. and Collerson, K.D. (1974) The recalculation of pyroxene end-member parameters and the estimation of ferrous and ferric iron content from electron microprobe analyses. Am. Mineral., 59, 1203-1208.

Cawthorn, R.G., Curran, E.B., and Arculus, R.J. (1973) A petrogenetic model for the origin of the calc-alkaline suite of Grenada, Lesser Antilles. J. Petrol., 14,327-337.

Cawthorn, R.G. and O'Hara, M.J. (1976) Amphibole fractionation in calc-alkaline magma genesis. Am. J. Sci., 276,309-329.

Christiansen, R.L. and Lipman, P.W. (1972) Cenozoic volcanism and the plate tectonic evolution of the western United States, II. Late Cenozoic. Phil. Trans. Roy. Soc. London, 271,249-284.

Clark, S.P. and Ringwood, A.E. (1964) Density distribution and constitution of the mantle. Rev. Geophys., 2,35-88.

Clark, D.B. and O'Hara, M.J. (1979) Nickel, and the existence of high-MgO liquids in nature. Earth Planet. Sci. Lett., 44,153-158.

Cohen, L.H.; Ito, K., and Kennedy, G.C. (1967) Melting and phase relations in an anhydrous basalt to 40 kilobars. Am. J. Sci, 265,475-518.

Coleman, R.G.; Lee, D.E.; Beatty, L.B., and Brannock, W.W. (1965) Eclogites and Eclogites: Their differences and similarities. Geol. Soc. Am. Bull., 76,483-508.

Daly, R.A. (1933) Igneous Rocks and the Depths of the Earth. McGraw-Hill Book Co., New York.

Damon, P.E.; Shafiqullah, M., and Leventhal, J. (1974) K-Ar chronology for the San Francisco volcanic field and rate of erosion of the Little Colorado River, IN Geology of Northern Arizona Part I. Regional Studies. Geol. Soc. Am. Guidebook, Rocky Mt. Section Mtg., p.221-235.

Dawson, J.B. and Smith, J.V. (1977) The MARID (mica-amphibole-rutile-ilmenite-diopside) suite of xenoliths in kimberlites. Geochim. Cosmochim. Acta, 41:309-323.

Delany, J.M. and Helgeson, H.C. (1978) Calculation of the thermodynamic consequences of dehydration in subducting oceanic crust to 100 kb and 800°C. Am. J. Sci., 278,638-686.

DeLong, S.E.; Schwarz, W.M., and Anderson, R.N. (1979) Thermal effects of ridge subduction. Earth Planet. Sci. Lett., 44,239-246.

DePaolo, D.J. and Johnson, R.W. (1979) Magma genesis in the New Britain island arc: Constraints from Nd and Sr isotopes and trace element patterns. Contrib. Mineral. Petrol., 70,367-379.

Dewey, J.F. and Bird, J.M. (1970) Mountain belts and the new global tectonics. J. Geophys. Res., 75,2625-2647.

Dickinson, W.R. and Hatherton, T. (1967) Andesitic volcanism and seismicity around the Pacific. Science, 157,801-803.

Dostal, J.; Dupuy, C., and Leyreloup, A. (1980) Geochemistry and petrology of meta-igneous granulitic xenoliths in Neogene volcanic rocks of the Massif Central, France - implications for the lower crust. Earth Planet. Sci. Lett., 50,31-40.

Dungan, M.A. and Rhodes, J.M. (1978) Residual glasses and melt inclusions in basalts from DSDP Legs 45 and 46: evidence for magma mixing. Contrib. Mineral. Petrol., 67,417-431.

Edgar, A.D., Green, D.H., and Hibberson, W.O. (1976) Experimental petrology of a highly potassic magma. J. Petrol., 17,339-356.

Eggler, D.H. (1972) Water-saturated and undersaturated melting relations in a Paricutin andesite and an estimate of water content in the natural andesite. Contrib. Mineral. Petrol., 34,261-271.

Eggler, D.H. and Burham, C.W. (1973) Crystallization and fractionation trends in the system andesite-H_2O-CO_2-O_2 at pressures to 10 kilobar. Geol. Soc. Am. Bull., 84,2517-2532.

Ehrenberg, S.N., and Griffin, W.L. (1979) Garnet granulite and associated xenoliths in minette and serpentinite diatremes of the Colorado Plateau. Geology, 7,483-487.

Eichelberger, J.C. (1974) Magma contamination within the volcanic pile: origin of andesite and dacite. Geology, 2,29-33.

Eichelberger, J.C. (1975) Origin of andesite and dacite: Evidence of mixing at Glass Mountain in California and at other Circum-Pacific volcanoes. Geol. Soc. Am. Bull., 86,1381-1391.

Eichelberger, J.C. (1978) Andesites in island arcs and continental margins, Relationship to crustal evolution. Bull. Volcanol., 41,480-500.

Ellis, D.J. and Green, D.H. (1979) An experimental study of the effect of Ca upon garnet-clinopyroxene Fe-Mg exchange equilibria. Contrib. Mineral. Petrol., 71,13-22.

Elston, W.E. (1976) Tectonic significance of mid-Tertiary volcanism in the Basin and Range province: A critical review with special reference to New Mexico IN Cenozoic Volcanism in Southwestern New Mexico, New Mexico Geol. Soc. Spec. Publ. 5,93-102.

Engel, C.G. Engel, A.F. and Havens, R.G. (1965) Chemical characteristics of oceanic basalts and the upper mantle. Geol. Soc. Am. Bull., 76,719-725.

Ernst, W.G. (1973) Blue schist metamorphism and P-T regimes in active subduction zones. Tectonophys., 17,255-272.

Ernst, W.G. and Dal Piaz, G.V. (1978) Mineral parageneses of eclogitic rocks and related mafic schists of the Piemonte ophiolitic nappe, Breuil-St. Jacques area, Italian Western Alps. Am. Mineral., 63,621-640.

Essene, E.J.; Hensen, B.J., and Green, D.H. (1970) Experimental study of amphibolite and eclogite stability. Phys. Earth Planet. Interiors, 3,378-384.

Ewart, A. (1976) Mineralogy and chemistry of modern orogenic lavas - Some statistics and implications. Earth Planet. Sci. Lett., 31,417-432.

Ewart, A. (1979) A review of the mineralogy and chemistry of Tertiary-Recent dacitic, latitic, rhyolitic, and related salic volcanic rocks IN Trondhjemites, Dacites, and Related Rocks, Barker, F. (editor), Elsevier Scientific Publishing Co., Amsterdam, 13-121.

Ewart, A.; Mateen, A., and Ross, J.A. (1976) Review of mineralogy and chemistry of Tertiary central volcanic complexes in southeast Queensland and northeast New South Wales IN Volcanism in Australasia, Johnson, R.W. (editor), Elsevier Scientific Publishing Co. Amsterdam 31-39.

Ferguson, J.; Arculus, R.J., and Joyce, J. (1979) Kimberlite and kimberlitic intrusives of southeastern Australia: a review. BMR J. Aust. Geol. and Geophys., 4,227-241.

Forbes, W.C. and Flower, M.F.J. (1974) Phase relations of a titan-phlogopite, $K_2Mg_4TiAl_2Si_6O_{20}(OH)_4$: A refractory phase in the upper mantle. Earth Planet. Sci. Lett., 22,60-66.

Frey, F.A.; Bryan, W.B. and Thompson, G. (1974) Atlantic ocean floor: Geochemistry and petrology of basalts from Legs 2 and 3 of the Deep Sea Drilling Project. J. Geophys. Res., 79,5507-5527.

Fudali, R.F. (1965) Oxygen fugacities of basaltic and andesitic magma. Geochim. Cosmochim. Acta, 29,1063-1075.

Fyfe, W.S. (1960) Stability of epidote minerals. Nature, 187,497.

Game, P.M. (1954) Zoisite-amphibolite with corundum from Tanganyika. Am. Mineral., 39,842.

Garcia, M.O. and Jacobson, S.S. (1979) Crystal clots, amphibole fractionation and the evolution of calc-alkaline magmas. Contrib. Mineral. Petrol., 69,319-327.

Gilbert, M.C. and Briggs, D.F. (1974) Comparison of the stabilities of OH- and F-potassic richterites - a preliminary report (abs.). Trans. Am. Geophys. Union, 55,480.

Gill, J.B. (1974) Role of underthrust oceanic crust in the genesis of a Fijian calc-alkaline suite. Contrib. Mineral. Petrol., 43,29-45.

Gill J.B. (1978) Role of trace element partition coefficients in models of andesite genesis. Geochim. Cosmochim. Acta, 42,709-724.

Gill, J.B. (1981) Orogenic Andesites and Plate Tectonics, Springer-Verlag, Berlin-New York, 390 pp.

Gilluly, J. (1971) Plate tectonics and magmatic evolution. Geol. Soc. Am. Bull., 82,2383-2396.

Girod, M. and Lefèvre, C. (1972) Nature et origine des 'andesites' et 'trachy-andesites' cenozoiques du Massif Central Francais. Contrib. Mineral. Petrol., 36,315-328.

Green, D.H. (1973a) Experimental melting studies on a model upper mantle composition at high pressure under water-saturated and water-undersaturated conditions. Earth Planet. Sci. Lett., 19, 37-53.

Green, D.H. (1973b) Contrasted melting relations in pyrolite upper mantle under mid-ocean ridges, stable crust and island arc environments. Tectonophys., 17,285-297.

Green, D.H. (1976) Experimental testing of 'Equilibrium' partial melting of peridotite under water-saturated, high-pressure conditions. Canadian Mineral., 14,255-268.

Green, D.H.; Hibberson, W.O. and Jaques, A.L. (1979) Petrogenesis of mid-ocean ridge basalls. IN The Earth: Its Origin, Structure and evolution, McElhinny, M.W. (editor), Academic Press, London, 265-299.

Green, D.H. and Ringwood, A.E. (1967) The genesis of basaltic magmas. Contrib. Mineral. Petrol., 15,103-190.

Green, T.H. (1967) High pressure experimental investigations on the origin of high-alumina basalt, andesite, and anorthosite, Ph.D. Thesis, Aust. Nat. Univ.

Green, T.H. (1972) Crystallization of calc-alkaline andesite under controlled high pressure hydrous conditions. Contrib. Mineral. Petrol., 34,150-166.

Green, T.H. (1981a) Experimental evidence for the role of accessory phases in magma genesis. J. Volcanol. and Geotherm. Res. 10,405-422.

Green, T.H. (1981b) Experimental studies relevant to petrogenesis of andesite (b) Anatexis of mafic crust and high pressure crystallization of andesite IN Andesites, Thorpe, R.S. (editor) John Wiley and Sons, New York, (in press).

Green, T.H., and Ringwood, A.E. (1967) Crystallization of basalt and andesite under high pressure hydrous conditions. Earth Planet. Sci. Lett., 3,481-489.

Green, T.H. and Ringwood, A.E. (1968) Genesis of the calc-alkaline igneous rock suite. Contrib. Mineral. Petrol., 18,105-162.

Green, T.H. and Ringwood, A.E. (1972) Crystallization of garnet-bearing rhyodacite under high pressure hydrous conditions. J. Geol. Soc. Australia, 19,203-212.

Gust, D.A.; Johnson, R.W., and Chappell, B.W. (1980) Petrological data catalogue for Boisa Island, an andesitic volcano in Papua New Guinea: whole-rock, mineral, and modal analyses and modelling data. Bur. Miner. Resour. Aust., Rpt 227, BMR Microform MF147.

Gust, D.A. and Johnson, R.W. (1981) Amphibole-bearing inclusions from Boisa Island, Papua New Guinea: Evaluation of the role of fractional crystallization in an andesitic volcano. J. Geol., 89,219-232.

Hall, J.M. and Robinson, P.T. (1979) Deep crustal drilling in the north Atlantic Ocean. Science, 204,573-586.

Hamilton, W. (1969) The volcanic central Andes - a modern model for the Cretaceous batholiths and tectonics of western North America IN Proceedings of the Andesite Conference, Bull. 65, Dept. of Geology and Mineral Resources, State of Oregon, 175-184.

Hanson, G.N. (1978) The application of trace elements to the petrogenesis of igneous rocks of granitic composition. Earth Planet. Sci. Lett., 38,26-43.

Hanson, G.N. (1980) Rare earth elements in petrogenetic studies of igneous systems. Ann. Rev. Earth Planet. Sci., 8,371-406.

Harpum, J.R. (1954) Formation of epidote in Tanganyika. Geol. Soc. Am. Bull., 65, 1075-1092.

Hasbe, K.; Fujii, N., and Uyeda, S. (1970) Thermal processes under island arcs. Tectonophys., 10,335-355.

Hawkesworth, C.J.; O'Nions, R.K. and Arculus, R.J. (1979) Nd- and Sr-isotope geochemistry of island arc volcanics. Grenada, Lesser Antilles. Earth Planet. Sci. Lett., 45,237-248.

Hellman, P.L. and Green, T.H. (1979) The role of sphene as an accessory phase in the high-pressure partial melting of hydrous mafic compositions. Earth Planet. Sci. Lett., 42,191-201.

Helz, R.T. (1973) Phase relations of basalts in their melting range at PH_2O = 5kb as a function of oxygen fugacity. Part 1. Mafic phases. J. Petrol., 14,249-302.

Helz, R.T. (1976) Phase relations of basalts in their melting ranges at PH_2O = 5 kb. Part II- Melt Compositions. J. Petrol., 17,139-193.

Heltz, R.T. (1979) Alkali exchange between hornblende and melt: a temperature-sensitive reaction. Am. Mineral., 64,953-965.

Hertogen, J. and Gijbels, R. (1976) Calculation of trace element fractionation during partial melting. Geochim. Cosmochim. Acta, 40,313-322.

Hess, H.H. (1960) The Stillwater Igneous Complex, Montana. Geol. Soc. Am. Memoir, 80.

Hill, R.E.T. and Boettcher, A.L. (1970) Melting relationships in basalt-H_2O-CO_2 to 30 kilobars (abstr.). Am. Geophys. Union Trans., 51, 438.

Hodges, F.N. and Papike, J.J. (1976) DSDP Site 334: Magmatic cumulates from oceanic layer 3. J. Geophys. Res., 81,4135-4151.

Holdaway, M.J. (1972) Thermal stability of Al-Fe epidote as a function of fO_2 and Fe content. Contrib. Mineral. Petrol., 37,307-340.

Holloway, J.R. and Burnham, C.W. (1972) Melting relations of basalt with equilibrium water pressure less than total pressure. J. Petrol., 13,1-29.

Holloway, J.R. and Ford, C.E. (1975) Fluid-absent melting of the flouro-hydroxy amphibole pargasite to 35 kilobars. Earth Planet. Sci. Lett., 25,44-48.

Holmes, A. (1932) The origin of igneous rocks. Geol. Mag., 69,543-558.

Humphris, S.E. and Thompson, B. (1978) Hydrothermal alteration of oceanic basalts by seawater. Geochim. Cosmochim. Acta., 42,107-125.

Irvine, T.N. and Baragar, W.R. (1971) A guide to the chemical classification of the common volcanic rocks. Canadian J. Earth Sci., 8,523-548.

Irving, A.J. (1974) Geochemical and high-pressure experimental studies of garnet pyroxenite and pyroxene granulite xenoliths from the Delegate basaltic pipes, Australia. J. Petrol., 15,1-40.

Irving, A.J. (1978) A review of experimental studies of crystal/liquid trace element partitioning. Geochim. Cosmochim. Acta., 42,743-770.

Ito, K. (1973) Analytical approach to estimating the source rock of basaltic magmas: Major elements. J. Geophys. Res., 78,412-431.

Ito, K. and Kennedy, G.C. (1974) The composition of liquids formed by partial melting of eclogites at high temperatues and pressures. J. Geol. 82,383-392.

Jackson, E.D., and Wright., T.L. (1970) Xenoliths in the Honolulu Volcanic Series, Hawaii. J. Petrol., 11,405-430.

Jakeš, P. and White, A.J.R. (1971) Composition of island arcs and continental growth. Earth Planet. Sci. Lett., 12, 224-230.

Jakeš, P. and White, A.J.R. (1972) Hornblendes from calc-alkaline volcanic rocks of island arcs and continental margins. Am. Mineral., 57,887-902.

Johnson, R.W. (1977) Distribution and major-element chemistry of late Cainozoic volcanoes at the southern margin of the Bismarck Sea, Papua New Guinea. Bur. Miner. Resour. Aust. Rpt 188, 170 pp.

Johnson, R.W. (1981) Papua New Guinea IN Andesites, Thorpe, R.S. (editor) John Wiley and Sons, New York (in press).

Johnson R.W. and Arculus, R.J. (1978) Volcanic rocks of the Witu Islands, Papua New Guinea: the origin of magmas above the deepest part of the New Britain Benioff zone. Bull. Volcanol., 41,609-655.

Johnson, R.W.; Smith, I.E.M., and Taylor, S.R. (1978) Hot-spot volcanism in St Andrew Strait, Papua New Guinea: geochemistry of a Quaternary bimodal rock suite. BMR J. Aust. Geol. Geophys., 3,55-69.

Karig, D.E. and Sharman, G.F. (1975) Subduction and accretion in trenches. Geol. Soc. Am. Bull., 86,377-389.

Katsui, Y.; Yamamoto, M.; Nemoto, S., and Niida, K. (1979) Genesis of calc-alkalic andesites from Oshima-Oshima and Ichinomegata volcanoes, North Japan. J. Fac. Sci., Hokkaido Univ., 19,157-168.

Kay, R.W. (1977) Geochemical constraints on the origin of Aleutian magmas IN: Island Arcs, Deep Sea Trenches and Back-Arc Basins, Maurice Ewing Series, Talwani, M. and Pitman, W.C. (editors), A.G.U., 1, 229-242.

Kay, R.W. (1978) Aleutian magnesian andesites: melts from subducted Pacific Ocean crust. J. Volcanol. and Geotherm. Res., 4,117-132.

Kay, R.W. (1980) Volcanic arc magmas: Implications of a melting-mixing model for element recycling in the crust-upper mantle system.

Kay, R.; Hubbard, N.J., and Gast, P.W. (1970) Chemical characteristics and origin of oceanic ridge vollanic rocks. J. Geophys. Res., 75,1585-1610.

Kay, R.W. and Kay, S.M. (1981) The nature of the lower continental crust: Inferences from geophysics, surface geology and crustal xenoliths. Rev. Geophys. and Space Phys., 19,271-297.

Kinomura, N.; Kume, S., and Koizumi, M. (1975) Synthesis of $K_2SiSi_3O_8$ with silicon in 4- and 6- coordination. Mineral. Mag., 40,401-404.

Klerkx, J.; Deutsch, S.; Pichler, H., and Zeil, W. (1977) Strontium isotopic composition and trace element data bearing on the origin of Cenozoic volcanic rocks of the central and southern Andes. J. Volcanol. and Geotherm. Res., 2,49-71.

Kuno, H. (1950) Petrology of Hakone volcano and the adjacent areas. Geol. Soc. Am. Bull., 61,957-1020.

Kushev, V.G. (1977) Zoisite as an indicator of coexistence of eclogite and rocks originally containing lawsonite. Dokl. Acad. Sci. USSR, Earth Sci. Sect., 237,228-230.

Kushiro, I. (1972) Effect of water on the composition of magmas formed at high pressure. J. Petrol., 13,311-334.

Kushiro, I.; Shimizu, N.; Nakamura, Y., and Akimoto, S. (1972) Compositions of coexisting liquid and solid phases formed upon partial melting of natural garnet lherzolites at high pressures: a preliminary report. Earth Planet. Sci. Lett., 14,19-25.

Kushiro, I.; Syono, Y., and Akimoto, S. (1967) Stability of phlogopite at high pressures and possible presence of phlogopite in the Earth's upper mantle. Earth Planet. Sci. Lett., 3,197-203.

Kushiro, I.; Syono, Y., and Akimoto, S. (1968) Melting of peridotite at high pressures and high water pressures. J. Geophys. Res., 73, 6023-6029.

Kushiro, I. and Yoder, H.S. (1969) Melting of forsterite and enstatite at high pressures under hydrous conditions. Carn. Inst. Wash. Yearbook, 67,153-158.

Lambert, I.B. and Wyllie, P.J. (1968) Stability of hornblende and a model for the low velocity zone. Nature, 219,1240-1241.

Lambert, I.B. and Wyllie, P.J. (1972) Melting of gabbro (quartz eclogite) with excess water to 35 kilobars with geologic applications. J. Geol., 80,693-708.

Lambert, R. St.J.; Holland, J.G., and Owen, P.F. (1974) Chemical petrology of a suite of calc-alkaline lavas from Mt. Ararat, Turkey. J. Geol., 82,419-438.

Larsen, E.S.; Irving, J., and Gonyer, F.A. (1936) Petrologic results of a study of the minerals from the Tertiary volcanic rocks of the San Juan region, Colorado. Am. Mineral., 21,679-701.

Leake, B.E. (1978) Nomenclature of amphiboles. Can. Mineral., 16,501-520.

Leeman, W.P.; Ma M.-S.; Murali, A.V., and Schmitt, R. A. (1978) Empirical estimation of magnetite/liquid distribution coefficients for some transition elements. Contrib. Mineral. Petrol., 65, 269-272.

Lewis, J.F., (1973) Petrology of the ejected plutonic blocks of the Soufriere volcano, St. Vincent, West Indies. J. Petrol., 14,81-112.

Liou, J.G. (1971) Synthesis and stability relations of prehnite, $Ca_3Al_2\ Si_3\ O_{10}\ (OH)_2$. Am. Mineral., 56,507-531.

Liou, J.G. and Ernst, W.G. (1979) Oceanic ridge metamorphism of the east Taiwan ophiolite. Contrib. Mineral. Petrol., 68,335-348.

Lipman, P.W., Prostka, H.J. and Christiansen, R.L. (1972) Cenozoic volcanism and plate tectonic evolution of western United States I. Early and Middle Cenozoic. Phil. Trans. Roy. Soc. Lond., 271,217-248.

Lovering, J.F. and White, A.J.R. (1969) Granulitic and eclogitic inclusions from basic pipes at Delegate, Australia. Contrib. Mineral. Petrol., 21,9-52.

MacDonald, G.A. and Katsura, T. (1965) Eruption of Lassen Peak, Cascade Range, California in 1915: Example of mixed magmas. Geol. Soc. Am. Bull., 76,475-482.

MacGregor, I.D. (1964) The reaction 4 enstatite + spinel $\rightleftarrows$ forsterite + pyrope. Carn. Inst. Wash. Yearbook, 63,157.

Markov, V.K.; Petrov., V.P.; Delitsin, I.S., and Ryabinin, Y. (1966) Phlogopite transformations at high pressures and temperatures, Geochem. Intl., 2,1112-1120.

Mathez, E.A. (1973) Refinement of the Kudo-Weill plagioclase thermometer and its application to basaltic rocks. Contrib. Mineral. Petrol., 41,61-72.

McBirney, A.R. (1979) Effects of assimilation IN The Evolution of the Igneous Rocks, Fiftieth Anniversary Perspectives, Yoder H.S. Jr. (editor), Princeton Univ. Press, Princeton, 307-388.

McGetchin, T.R.; Silver, L.T. and Chodos, A.A. (1970) Titanoclinohumite: A possible mineralogical site for water in the upper mantle. J. Geophys. Res., 75,255-259.

McLennan, S.M. (1981) Trace element geochemistry of sedimentary rocks: Implications for the composition and evolution of the continental crust. Ph.D. Thesis, Aust. Nat. Univ., 609 pp.

McLennan, S.M. and Taylor, S.R. (1981) Role of subducted sediments in island-arc magmatism: Constraints from REE patterns. Earth Planet. Sci. Lett., 54,423-430.

Menzies, M. (1976) Comment on "Is phlogopite the key?" by A.E. Beswick, Geochim. Cosmochim. Acta., 42,146-149.

Middlemost, E.A.K. (1973) A simple classification of volcanic rocks: Bull. Volcanol., 30,382-397.

Millholen, G.L. and Wyllie, P J. (1974) Melting relations of brown-hornblende mylonite from St. Paul's rocks under water-saturated and water-undersaturated conditions to 30 kilobars. J. Geol., 82, 589-606.

Minster, J.F. and Allègre, C.J. (1978) Systematic use of trace elements in igneous processes, Part III. Inverse problem of batch partial melting in volcanic suites. Contrib. Mineral. Petrol., 68,37-52.

Misch, P. (1964) Stable association wollastonite-anorthite and other calc-silicate assemblages in amphibolite facies crystalline schists of Nanga Parbat, northwest Himalayas. Contrib. Mineral. Petrol., 10,315-356.

Modreski, P.J. and Boettcher, A.L. (1972) The stability of phlogopite + enstatite at high pressures: A model for micas in the interior of the Earth. Am. J. Sci., 272,852-869.

Modreski, P.J. and Boettcher, A.L. (1973) Phase relationships of phlogopite in the system K_2O-MgO-CaO-Al_2O_3-SiO_2-H_2O to 35 kilobars: A better model for micas in the interior of the Earth. Am. J. Sci., 273,385-414.

Myer, G.H. (1966) New data on zoisite and epidote. Am. J. Sci., 264, 364-385.

Mysen, B.O. (1979) Trace-element partitioning between garnet peridotite minerals and water-rich vapor: Experimental data from 5 to 30 kbar, Am. Mineral., 64,274-287.

Mysen, B.O. and Boettcher, A.L. (1975a) Melting of a hydrous mantle: I. Phase relations of natural peridotite at high pressures and temperatures with controlled activities of water, carbon-dioxide, and hydrogen. J. Petrol., 16,520-548.

Mysen, B.O. and Boettcher, A.L. (1975b) Melting of a hydrous mantle: II. Geochemistry of crystals and liquids formed by anatexis of mantle peridotite at high pressures and high temperatures as a function of controlled activities of water, hydrogen and carbon-dioxide, J. Petrol. 16,549-593.

Mysen, B.O. and Boettcher, A.L. (1976) Melting of a hydrous mantle: III. Phase relations of garnet websterite + H_2O at high T and P. J. Petrol., 17,1-14.

Nagasawa, H. (1970) Rare earth concentrations in zircons and apatites and their host dacites and granites. Earth Planet. Sci. Lett., 9,359-364.

Newton, R.C. (1965) The thermal stability of zoisite. J. Geol., 73,431-441.

Newton, R.C. (1966) Some calc-silicate equilibrium relations. Am. J. Sci., 264,204-222.

Newton, R.C. and Kennedy, G.C. (1963) Some equilibrium reactions in the join $CaAl_2Si_2O_8$-H_2O. J. Geophys. Res., 68,2967-2983.

Nicholls, I.A. (1974) Liquids in equilibrium with peridotitic mineral assemblages at high water pressures. Contrib. Mineral. Petrol., 45,289-316.

Nicholls, I.A. and Harris, K.L. (1980) Experimental rare earth element partition coefficients for garnet, clinopyroxene, and amphibole coexisting with andesitic and basaltic liquids. Geochim. Cosmochim. Acta., 44,287-308.

Nicholls, I.A. and Ringwood, A.E. (1972) Production of silica-saturated tholeiitic magmas in island arcs. Earth Planet. Sci. Lett., 17,243-246.

Nicholls, I.A. and Ringwood, A.E. (1973) Effect of water on olivine stability in tholeiites and production of SiO_2-saturated magmas in the island arc environment. J. Geol., 81,285-300.

Nicholls, I.A. and Whitford, D.J. (1976) Primary magmas associated with Quaternary volcanism in the western Sunda arc, Indonesia IN Volcanism in Australasia, Johnson, R.W. (editor), Elsevier, Amsterdam, 77-90.

Nielsen, R.L. and Drake, M.J. (1979) Pyroxene-melt equilibra. Geochim. Cosmochim. Acta., 43,1259-1272.

Nitsch, K.H. and Winkler, H.G.F. (1965) Bildungsbedingungen von epidot und orthozoisit. Beitr. Mineral. Petrog., 11,470-486.

Nockolds, S.R. (1934) The production of normal rock types of contamination and their bearing on petrogenesis. Geol. Mag., 71, 31-39.

Norrish, K. and Chappell, B.W. (1977) X-ray Fluorescene Spectrometry. IN Physical Methods of Determinative Mineralogy, Zussman, J. (editor), Academic Press, London, 201-272.

O'Hara, M.J. (1963) The join diopside-pyrope at 30 kb. Carn. Inst. Wash. Yearbook, 62,116-118.

O'Hara, M.J. (1977) Geochemical evolution during fractional crystallization of a periodically refilled magma chamber. Nature, 266,503-507.

O'Hara, M.J.; Saunders, M.J., and Mercy, E.L.P. (1975) Garnet-peridotite, primary ultrabasic magma and eclogite; Interpretation of upper mantle processes in kimberlite. Phys. Chem. Earth, 9, 681-713.

O'Hara, M.J. and Yoder, H.S. Jr. (1967) Formation and fractionation of basic magma at high pressures. Scott. J. Geol., 3,67-117.

Osborn, E.F. (1959) Role of oxygen pressure in the crystallization and differentiation of basaltic magma. Am. J. Sci., 257,609-647.

Osborn, E.F. (1962) Reaction series for subalkaline igneous rocks based on different oxygen pressure conditions. Am. Mineral., 47,211-226.

Osborn, E.F. (1969) The complementariness of orogenic andesite and alpine peridotite. Geochim. Cosmochim. Acta., 33,307-325.

Osborn, E.F. and Watson, E.B. (1977) Studies of phase relations in subalkaline volcanic rock series. Carn. Inst. Wash. Yearbook, 76, 472-477.

Oxburgh, E.R. and Turcotte, D.L. (1970) Thermal structure of island arcs. Geol. Soc. Am. Bull., 81,1665-1688.

Palfreyman, W.D., and Cooke, R.J.S. (1976) Eruptive history of Manam volcano, Papua New Guinea, IN Johnson, R.W., (editor), Volcanism in Australasia. Elsevier, Amsterdam, 117-131.

Pearce, J.A. and Norry, M.J. (1979) Petrogenetic implications of Ti, Zr, and Nb variations in volcanic rocks. Contrib. Mineral. Petrol., 69,33-47.

Peccerillo, A. and Taylor, S.R. (1976) Geochemistry of Eocene calc-alkaline volcanic rocks from the Kastamonu area, northern Turkey. Contrib. Mineral. Petrol., 58,63-81.

Peck, D.L.; Wright, T.L., and Moore, J.G. (1966) Crystallization of tholeiitic basalt in Alae lava lake, Hawaii. Bull. Volcanol. 29,629-656.

Peirce, H.W.; Damon, P.E., and Shafiqullah, M. (1979) An Oligocene (?) Colorado Plateau edge in Arizona. Tectonophys., 61,1-24.

Perfit, M.R.; Gust, D.A.; Bence, A.E.; Arculus, R.J., and Taylor, S.R. (1980) Chemical characteristics of island-arc basalts: Implications for mantle sources. Chem. Geol., 30,227-256.

Perfit, M.R.; McCulloch, M.T., and Froude, D. (1981) Sr- and Nd-isotopic variations in volcanic and plutonic rocks from the Aleutian Islands and Taupo volcanic zone, New Zealand: Implications for island arc magma genesis IN 1981 IAVCEI Symposium - Arc Volcanism, Abstracts (Japan), 292-293.

Perfit, M.R.; Nagle, F., and Bowin, C. (1981) Petrochemistry of eclogites and amphibolites from Hispaniola, Greater Antilles. In prep.

Philpotts, J.A. and Schnetzler, C.C. (1970) Phenocryst-matrix partition coefficients for K, Rb, Sr, and Ba, with applications to anorthosite and basalt genesis. Geochim. Cosmochim. Acta., 34, 307-322.

Pichler, H. and Zeil, W. (1972) The Cenozoic rhyolite-andesite association of the Chilean Andes. Bull. Volcanol., 35,424-452.

Pistorius, C.W.F.T. (1961) Synthesis and lattice constants of pure zoisite and clinozoisite. J. Geol., 69,604-609.

Pistorius, C.W.F.T.; Kennedy, G.C., and Sourirajan, S. (1962) Some relations between the phases anorthite, zoisite and lawsonite at high temperatures and pressures. Am. J. Sci., 260,44-56.

Poldervaart, A. (1955) Chemistry of the earth's crust IN Crust of the Earth, Poldervaart, A. (editor), Geol., Soc. Am. Spec. Paper 62,119-144.

Poldervaart, A. and Elston, W. (1954) The calc-alkaline series and the trend of fractional crystallization of basaltic magma. A new approach at graphical representation. J. Geol., 62,150-162.

Powell, M. (1978) Crystallization conditions of low-pressure cumulate nodules from the Lesser Antilles island arc. Earth Planet. Sci. Lett., 39,162-172.

Powell, M. and Powell, R. (1977) Plagioclase-alkali-feldspar geothermometry revisited. Mineral. Mag., 41,253-256.

Powell, R. and Powell, M. (1977) Geothermometry and oxygen barometry using coexisting iron-titanium oxides: a reappraisal. Mineral. Mag., 41,257-263.

Presnall, D.C. (1969) The geometrical analysis of partial fusion. Am. J. Sci., 267,1178-1194.

Presnall, D.C.; Dixon, J.R.; O'Donnell, T.H., and Dixon, S.A. (1979) Generation of mid-ocean ridge tholeiites. J. Petrol., 20,3-35.

Prinz, M.; Keil, K.; Green. J.A.; Reid, A.M.; Bonatti, E., and Honnorez, J. (1976) Ultramafic and mafic dredge samples from the equatorial mid-Atlantic ridge and fracture zones. J. Geophys. Res., 81,4087-4103.

Prodehl, C. (1970) Seismic refraction study of crustal structure in the western United States. Geol. Soc. Am. Bull., 81,2629-228.

Råheim, A. (1974) Pressure, temperature and time relationship in eclogite metamorphic terranes. Ph.D. thesis. Aust. Nat. Univ., 263 pp.

Råheim, A. and Green, D.H. (1974) Experimental determination of the temperature and pressure dependence of the Fe-Mg partition coefficient for coexisting garnet and clinopyroxene. Contrib. Mineral. Petrol., 48,179-203.

Råheim, A. and Green, D.H. (1975) P, T paths of natural eclogites during metamorphism - a record of subduction. Lithos, 8,317-328.

Rea, W.J. (1974) The volcanic geology and petrology of Montserrat, West Indies. J. Geol. Soc. London, 130,341-366.

Reed, S.J.B. and Ware, N.G. (1973) Quantitative electron microprobe analysis using a lithium drifted silicon detector. X-ray Spectrometry, 2,69-74.

Reed, S.J.B. and Ware, N.G. (1975) Quantitative electron microprobe analysis of silicates using energy-dispersive X-ray spectrometry. J. Petrol., 16,499-519.

Rhodes, J.M.; Dungan, M.A.; Blanchard, D.P., and Long, P.E. (1979) Magma mixing at mid-ocean ridges: evidence from basalts drilled near 22°N on the mid-Atlantic ridge. Tectonophys., 55,35-61.

Ringwood, A.E. (1966) The chemical composition and origin of the Earth. IN Advances in Earth Science, Hurley, P.M. (editor) MIT Press, Cambridge Mass., 287-356.

Ringwood, A.E. (1974) The petrological evolution of island arc systems. J. Geol. Soc. London., 130,183-204.

Ringwood, A.E. (1975) Composition and Petrology of the Earth's Mantle, McGraw-Hill Book Co., New York, 618 pp.

Ringwood, A.E. (1977) Petrogenesis in island arc systems IN Island Arcs, Deep Sea Trenches and Back Arc Basins, Maurice Ewing Series, Talwani, M. and Pitman, W.C. (editors) A.G.U., 1,311-324.

Robertson, J.K. and Wyllie, P.J. (1971) Rock-water systems, with special reference to the water-deficient region. Am. J. Sci., 271,252-277.

Robinson, H.H. (1913) The San Francisco volcanic field, Arizona. U.S. Geol. Survey Prof. Paper 76, 213 pp.

Roeder, P.L. and Emslie, R.F. (1970) Olivine-liquid equilibrium. Contrib. Mineral. Petrol., 29,275-289.

Ryburn, R.J.; Råheim, A., and Green, D.H. (1976) Determination of the P, T paths of natural eclogites during metamorphism - record of subduction. A correction to a paper by Råheim and Green (1975). Lithos, 9,161-164.

Schnetzler, C.C. and Philpotts, J.A. (1970) Partition coefficients of rare-earth elements between igneous matric material and rock-forming mineral phenocrysts - II. Geochim. Cosmochim. Acta., 34, 331-340.

Schock, H.H. (1979) Distribution of rare-earth and other trace elements in magnetites. Chem. Geol., 26,119-133.

Schubert, G.; Yuen, D.A. and Turcotte, D.L. (1975) Role of phase transitions in a dynamic mantle. Royal. Astron. Soc. Geophys. J., 42,705-735.

Seeley, D.R.; Vail, P.R., and Walton, G.C. (1974) Trench slope model IN Geology of Continental Margins, Burk, C.A. and Drake, C.L. (editors), Springer-Verlag, New York, 249-260.

Sekine, T. (1981) Experimental studies on magmas derived from subduction zones. IN 1981 IAVCEI Symposium - Arc Volcanism, Abstracts (Japan), 329-330.

Siefert, F. and Schreyer, W. (1971) Synthesis and stability of micas in the system K_2O-MgO-SiO_2-H_2O and their relations to phlogopite. Contrib. Mineral. Petrol., 30,196-215.

Sigurdsson, H., and Shepherd, J.B. (1974) Amphibole-bearing basalt from the submarine volcano Kick'em-Jenny in the Lesser Antilles island arc. Bull. Volcanol., 38,891-910.

Smyth, J.R. (1980) Cation vacancies and the crystal chemistry of breakdown reactions in kimberlitic omphacites. Am. Mineral., 65, 1185-1191.

Snyder, W.S.; Dickinson, W.R. and Silberman, M.L. (1976) Tectonic implications of space-time patterns of Cenozoic magmatism in the western United States. Earth Planet. Sci. Lett., 32,91-106.

Sobolev, N.V. (1977) Deep-Seated Inclusions in Kimberlites and the Problem of the Composition of the Upper Mantle, A.G.U., Washington D.C., 279 pp.

Stern, C.R. (1974) Melting products of olivine tholeiite basalt in subduction zones. Geology, 1,227-230.

Stern, C.R. and Wyllie, P.J. (1973) Melting relations of basalt-andesite-rhyolite-H_2O and a pelagic red clay at 30 kb. Contrib. Mineral. Petrol., 42,313-323.

Stern, C.R. and Wyllie, P.J. (1975) Effect of iron absorption by noble-metal capsules on phase boundaries in rock-melting experiments at 30 kilobars. Am. Mineral., 60,681-689.

Stern, C.R. and Wyllie, P.J. (1978) Phase compositions through crystallization intervals in basalt-andesite-H_2O at 30 kbar with implications for subduction zone magmas. Am. Mineral., 63,641-663.

Stern, R.J. (1979) On the origin of andesite in the northern Mariana island arc: implications from Agrigan. Contrib. Mineral. Petrol., 68,207-219.

Stoeser, D.B. (1973) Mafic and ultramafic xenoliths of cumulus origin San Francisco volcanic field, Arizona. Ph.D. Thesis, Univ. Oregon, 260 pp.

Stromberg, H.D. and Stephens, D.R. (1964) Effects of pressure on the electrical resistance of certain metals. J. Phys. Chem. Solids, 25,1015-1023.

Sun, S.S., and Hanson, G.N. (1976) Rare earth element evidence for differentiation of McMurdo volcanics, Ross Island, Antarctica. Contrib. Mineral. Petrol., 54,139-155.

Sun, S.S.; Nesbitt, R.W., and Sharaskin, A.Y. (1979) Geochemical characteristics of mid-ocean ridge basalts. Earth Planet. Sci. Lett., 44,119-138.

Sydora, L.J.; Jones, F.W., and Lambert, R. St. J. (1978) The thermal regime of the descending lithosphere: the effect of varying angle and rate of subduction. Can. J. Earth Sci., 15,626-641.

Takahashi, E. (1980) Melting relations on an alkali-olivine basalt to 30 kbar, and their bearing on the origin of alkali basalt magmas. Carn. Inst. Wash. Yearbook., 79,271-276.

Takahashi, E.; Kushiro, I., and Tatsumi, Y. (1981) Melting of peridotite at high pressures and its bearing on island arc magmas. IN 1981 IAVCEI Symposium - Arc Volcanism, Abstracts (Japan), 365-366.

Tarney, J. and Windley, B.F. (1979) Continental growth, island arc accretion and the nature of the lower crust - a reply to S.R. Taylor and S.M. McLennan. J. Geol. Soc. Lond., 136,501-504.

Tatsumi, Y. (1981) Melting experiments on a high-magnesium andesite. Earth Planet. Sci. Lett., 54,357-365.

Taylor, S.R. (1967) The origin and growth of continents. Tectonophys. 4,17-34.

Taylor, S.R. (1977) Island arc models and the composition of the continental crust IN Island Arcs, Deep Sea Trenches and Back Arc Basins, Maurice Ewing series, Talwani, M. and Pitman, W.C. (editors), 1,325-336.

Taylor, S.R. (1979) Chemical composition and evolution of the continental crust: the rare earth element evidence. IN The Earth: Its Origin, Structure and Evolution, McElhinny, M.W. (editor), Academic Press, London, 353-376.

Taylor, S.R. and Gorton, M.P. (1977) Geochemical application of spark source mass spectrography-III. Element sensitivity, precision and accuracy. Geochim. Cosmochim. Acta, 41,1375-1380.

Taylor, S.R. and McLennan, S.M. (1981) The composition and evolution of the continental crust: rare earth element evidence from sedimentary rocks. Phil. Trans. Roy. Soc. Lond. 301,381-399.

Thompson, R.N. (1972) Evidence for a chemical discontinuity near the basalt-andesite transition in many anorogenic volcanic suites. Nature, 236,106-110.

Thompson, R.N. (1974) Some high-pressure pyroxenes. Mineral. Mag., 39, 768-87.

Thorpe, R.S.; Potts, P.J., and Francis, P.W. (1976) Rare earth data and petrogenesis of andesite from the north Chilean Andes. Contrib. Mineral. Petrol., 54,65-78.

Tilley, C.E. (1936) The paragenesis of kyanite-eclogites. Mineral. Mag., 24,422-431.

Tilley, C.E. (1937) The paragenesis of kyanite-amphibolites. Mineral. Mag., 24,555-569.

Tilley, C.E. (1950) Some aspects of magmatic evolution. Quart. J. Geol. Soc. Lond., 106,37-61.

Toksöz, M.N.; Minear, J.W., and Julian, B.R. (1971) Temperature field and geophysical effects of a downgoing slab. J. Geophys. Res., 76,1113-1138.

Turner, F.J. and Verhoogen, J. (1960) Igneous and Metamorphic Petrology. McGraw-Hill Book Co., New York.

Walker, D.; Shibata, T., and DeLong, S.E. (1979) Abyssal tholeiites from the Oceanographer Fracture zone. Contrib. Mineral. Petrol., 70,111-125.

Ware, N.G. (1981) Computer programs and caaibration with the PIBS technique for quantitative electron probe analysis using a lithium-drifted silicon detector. Computers Geosci., 7,167-184.

Waters, A.C. (1955) Volcanic rocks and the tectonic cycle IN Crust of the Earth, Poldervaart, A. (editor) Geol. Soc. Am. Spec. Paper 62, 703-722.

Watson, E.B. (1979a) Apatite saturation in basic to intermediate magmas. Geophys. Res. Letters., 6,937-940.

Watson, E.B. (1979b) Zircon saturation in felsic liquids: Experimental results and applications to trace element geochemistry. Contrib. Mineral. Petrol., 70,407-419.

Watson, K.D. (1942) Zoisite-prehnite alteration of gabbro. Am. Mineral., 27,638-645.

Wells, P.R.A. (1977) Pyroxene thermometry in simple and complex systems. Contrib. Mineral. Petrol., 62,129-139.

Wendlandt, R.F. and Eggler, D.H. (1980a) The origins of potassic magmas: 2. Stability of phlogopite in natural spinel lherzolite and in the system $KAlSiO_4$-MgO-SiO_2-H_2O-CO_2 at high pressures and high temperatures. Am. J. Sci., 280,421-458.

Wendlandt, R.F. and Eggler, D.H. (1980b) Stability of sanidine + forsterite and its bearing on the genesis of potassic magmas and the distribution of potassium in the upper mantle. Earth Planet. Sci. Lett., 51,215-220.

White, A.J.R. (1964) Clinopyroxenes from eclogites and basic granulites. Am. Mineral., 49,883-888.

White, W.M., and Bryan, W.B. (1977) Sr-isotope, K, Rb, Cs, Sr, Ba and rare-earth geochemistry of basalts from the FAMOUS area. Geol. Soc. Am. Bull., 88,571-576.

Whitford, D.J. (1975) Geochemistry and petrology of volcanic rocks from the Sunda Arc, Indonesia. Ph.D. Thesis, Aust. Nat. Univ., 449 pp.

Wilcox, R.E. (1954) Petrology of Paricutin Volcano, Mexico, U.S. Geol. Survey Bull., 965-C.

Wilkinson, J.F.G. (1966) Some aspects of calc-alkali rock genesis. Proc. Roy. Soc. New South Wales, 99,69-77.

Wills, K.J.A. (1974) The geological history of southern Dominica and plutonic nodules from the Lesser Antilles. Ph.D. Thesis, Durham Univ., 414 pp.

Wilson, J.T. (1959) Geophysics and continental growth. Am. J. Sci., 47,1-24.

Winkler, H.G.F. and Nitsch, K.H. (1962) Zoisitebildung bei der experimentellen metamorphose. Naturw., 49,605.

Winkler, H.G.F. (1976) Petrogenesis of Metamorphic Rocks, Fourth Edition, Springer-Verlag, New York, 334 pp.

Wood, B.J., and Banno, S. (1973) Garnet-orthopyroxene and orthopyroxene-clinopyroxene relationships in simple and complex systems. Contrib. Mineral. Petrol., 42,109-124.

Wright, T.L., and Doherty, P.C. (1970) A linear programming and least-squares computer method for solving petrologic mixing problems. Geol. Soc. Am. Bull., 81,1995-2008.

Wyllie, P.J. (1971a) The Dynamic Earth, John Wiley and Sons, Inc., New York, 416 pp.

Wyllie, P.J. (1971b) Role of water in magma generation and initiation of diapiric uprise in the mantle. J. Geophys. Res., 76,1328-1338.

Yamazaki, T.; Onuki, H., and Tiba, T. (1966) Significance of hornblende gabbroic inclusions in calc-alkali rocks. J. Japan Assoc. Mineral. Petrol. Econ. Geol., 55,87-103.

Yoder, H.S., Jr. (1969) Calc-alkaline andesites, experimental data bearing on the origin of their assumed characteristics IN Proceedings of the Andesite Conference, McBirney, A.R. (editor), Bull. 65, Dept. Geol. Mineral Industries, State of Oregon, 77-89.

Yoder, H.S., Jr. and Chinner, G.A. (1960) Grossular-pyrope-water system at 10,000 bars. Carn. Inst. Wash. Yearbook, 59,78-81.

Yoder, H.S., Jr. and Kushiro, I. (1969) Melting of a hydrous phase: Phlogopite, Am. J. Sci., 267-A,558-582.

Yoder, H.S. and Tilley, C.E. (1962) Origin of basalts: An experimental study of natural and synthetic rock systems. J. Petrol., 3,342-532.

APPENDIX 1

EXPERIMENTAL AND ANALYTICAL METHODS

PREPARATION OF STARTING MATERIALS

The preparation of the starting materials used in the eclogite fusion, zoisite stability, and phlogopite stability studies is described in detail in each of the relevant chapters. A list of the analytical-grade chemical reagents used in the different starting mixes is given in Table A1, along with their respective conversion factors to equivalent oxides.

At least two grams of each starting mix was prepared to minimize errors due to weighing inaccuracies. The starting mixtures were kept in a 110°C oven to prevent hydration by atmospheric H_2O.

Table A1: Analytical-grade Chemical Reagents and their Conversion Factors to Equivalent Oxides.

Oxide	Reagent	Conversion Factor
SiO_2	$SiO_2.xH_2O$	1.1631
Al_2O_3	$Al(OH)_3$	1.5307
TiO_2	TiO_2	--
MgO	MgO	--
CaO	$CaCO_3$	1.785
Na_2O	Na_2CO_3	1.76
K_2O	K_2CO_3	1.675
Fe	Metal	--
Fe_2O_3	Fe_2O_3	--

Preparation of the Experimental Charge- Anhydrous experiments were done only on DG-1 at 35 kbar (Chapter 2). Approximately 15 mg of sample was loaded into a graphite capsule, compressed by tamping and sealed with a close-fitting graphite lid. The capsule was then placed in a 110°C oven to evaporate any atmospheric H_2O which may have been absorbed during preparation.

Hydrous runs consisted of two types, those in which H_2O was physically added (DG-1+ 5 wt.% H_2O, Chapter 2) and those in which H_2O was structurally bound in a hydrous phase (amphibole/ DG-1+1.5 wt.% H_2O, Chapter 2; zoisite, Chapter 3; phlogopite, Chapter 4). Except for the steps involving the addition of H_2O, the preparation of all hydrous runs is the same.

Approximately 15 mg of sample was loaded into a preweighed, annealed, $Ag_{75}Pd_{25}$ ($T<1200^{\circ}C$) or Pt ($T>1200^{\circ}C$) capsule and compressed by tamping. The open end of the capsule was cleaned with Kleenix to remove loose powder, and then the capsule was dried in a 110°C oven for ~15 minutes. It was weighed to determine the amount of sample which had been added. The amount of H_2O necessary to achieve a desired weight percentage of H_2O in the final charge was calculated from this weight. H_2O (distilled-deionized) was added by a teflon-tipped microsyringe ($\pm$ 0.01 µl). The 'wet' capsule and sample were weighed to check the amount of H_2O which had been added, and if correct, the capsule was then crimped, cold-sealed with snips, weighed and arc-welded. During welding, the capsule was kept cool by either wet paper tissue or a bath of H_2O and dry ice. Ag-Pd capsules were welded inside a glove bag filled with Ar to prevent the alloy from sputtering. The welded capsules were weighed and the seal checked by examination with a binocular microscope. Those capsules which experienced no or negligible weight loss, were checked a final time by placing them in a 110°C oven for 30 minutes and reweighing. If they remained the same weight, the capsules were used

in the experiments. The water contents are considered to be accurate to $\pm$ 0.2 wt. percent.

Furnace Assemblies -

a) Piston Cylinder - the 1/8" 'dry' and 5/32" 'wet' (internal dimensions) graphite furnace assemblies used in the experiments employing the 1/2" piston cylinder solid media apparatus are shown in Figures 1a and 1b. Although basically similar to the assemblies described by Green et al. (1966), internal talc components have been replaced by fired pyrophyllite ('dry') and boron nitride ('wet') components. Another modification to the 'wet' assembly consists of drilling a hole into, instead of cutting a slit through, the bottom internal spacer to accomodate longer capsules. This modification prevents the capsule from accidently touching the graphite and melting. The 'dry' assembly substitutes 'Pyrex' glass for boron nitride around the graphite furnace.

b) H.P.G. - the 0.180" diameter graphite furnace assembly used in the experiments with the high pressure girdle apparatus (H.P.G.) is shown in Figure 2. All pyrophyllite and boron nitride components are unfired. In constructing the H.P.G. assembly, it is important to carefully adjust each component to within $\pm$ 0.002" of its ideal dimension. The various components are held together with clear nail polish.

Temperature: Measurement and Calibration - Temperatures were measured with Pt/PtRh (10%) thermocouples, and are uncorrected for the effect of pressure on e.m.f. A single, vertical thermocouple, separated from the capsule by a thin wafer of alumina, is used in the piston cylinder experiments. Two horizontal thermocouples measure the temperature within a H.P.G. cell and usually differ by 15-20^{o}C. The higher temperature of the two was always taken to be the run temperature.

The thermal gradient of the 1/8" 'dry' assembly has been determined by Green (1967). The 5/32" 'wet' assembly was only recently cal-

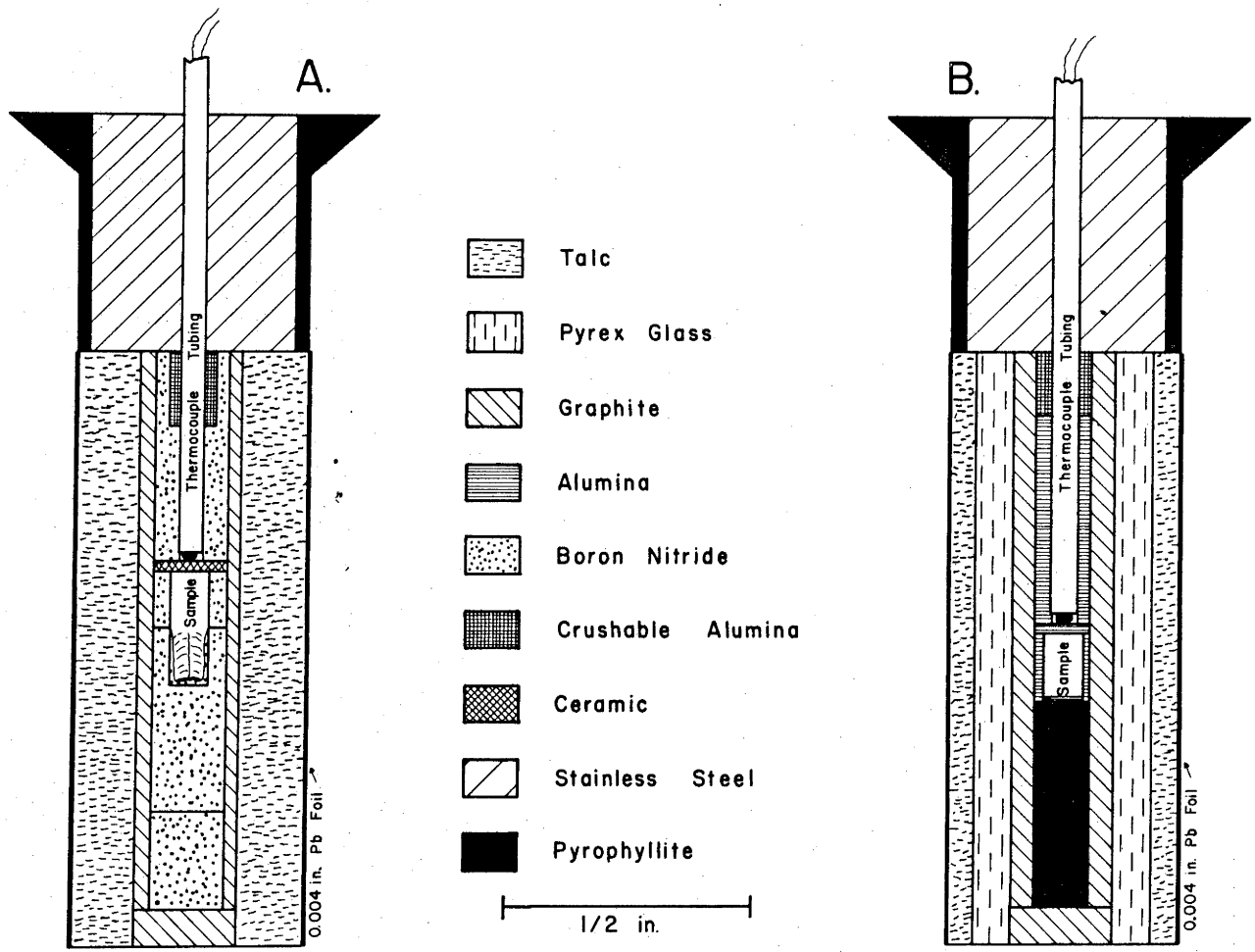

Figure 1A. Components of the 5/32" 'wet' graphite furnace assembly used in ½" pistion cylinder apparatus.

B. Components of the 1/8" 'dry' graphite furnace assembly used in ½" piston cylinder apparatus.

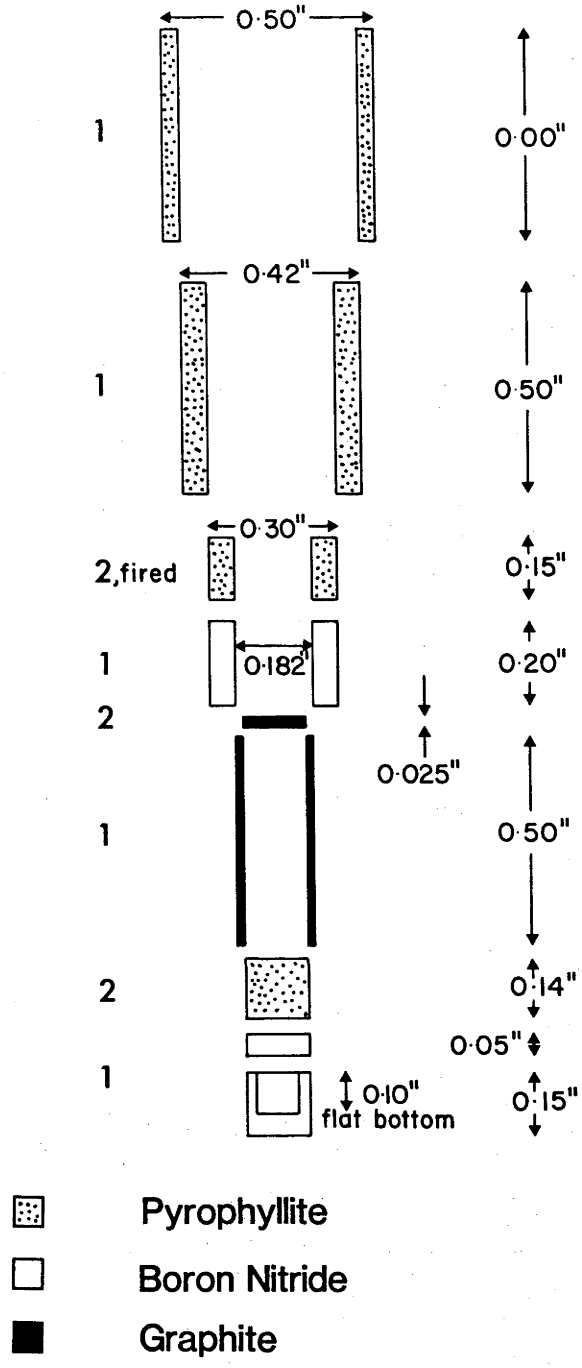

Figure 2. 'Exploded' view of the components used in the construction of the 0.180" diameter graphite furnace assembly for runs in the HPG apparatus. Numbers on the left side indicate the number of components used in the cell.

ibrated with respect to temperature (Gust and Hibberson, 1979) (Fig. 3). The H.P.G. assembly is uncalibrated with respect to temperature.

Pressure Apparatuses: Calibration and Run Procedure - Two pressure apparatuses were used in the experimental studies.

a) Piston Cylinder - The single-stage, piston cylinder, solid media apparatus and its calibration are described by Green et al.(1966). Piston-in techniques were used exclusively in the various studies. All reported pressures include a 10% friction correction with accuracy of the pressure determinations being ∿0.5 kbar. Temperature is considered to be accurate to within 10°C. Normal run procedure consisted of applying the desired pressure before increasing temperature, with frequent adjustments made during the course of the run. Total power (VxA) was monitered as a check on thermocouple contamination.

b) H.P.G.- The H.P.G. apparatus (Stromberg and Stephens, 1964), was modified by Ringwood and Major (unpublished data) and used for experiments within the 50-70 kbar range. The 0.180" graphite furnace assembly with 0.20" high gaskets, was calibrated using the fayalite olivine -β spinel transition (Ringwood and Major, 1970) (Fig. 4). Additional calibration attempts were made by using DTA to record the change in the melting points of Au and Ag with pressure (Mirwald and Kennedy, 1979). These attempts were unsuccessful.

Normal run procedure consisted of a gradual application of pressure until the required run pressure was reached. Temperature was applied gradually until the desired temperature was attained. Only minor corrections were made to the pressure over the duration of a run. Pressures are thought to be accurate to within 1 kbar and temperatures to within 15°C.

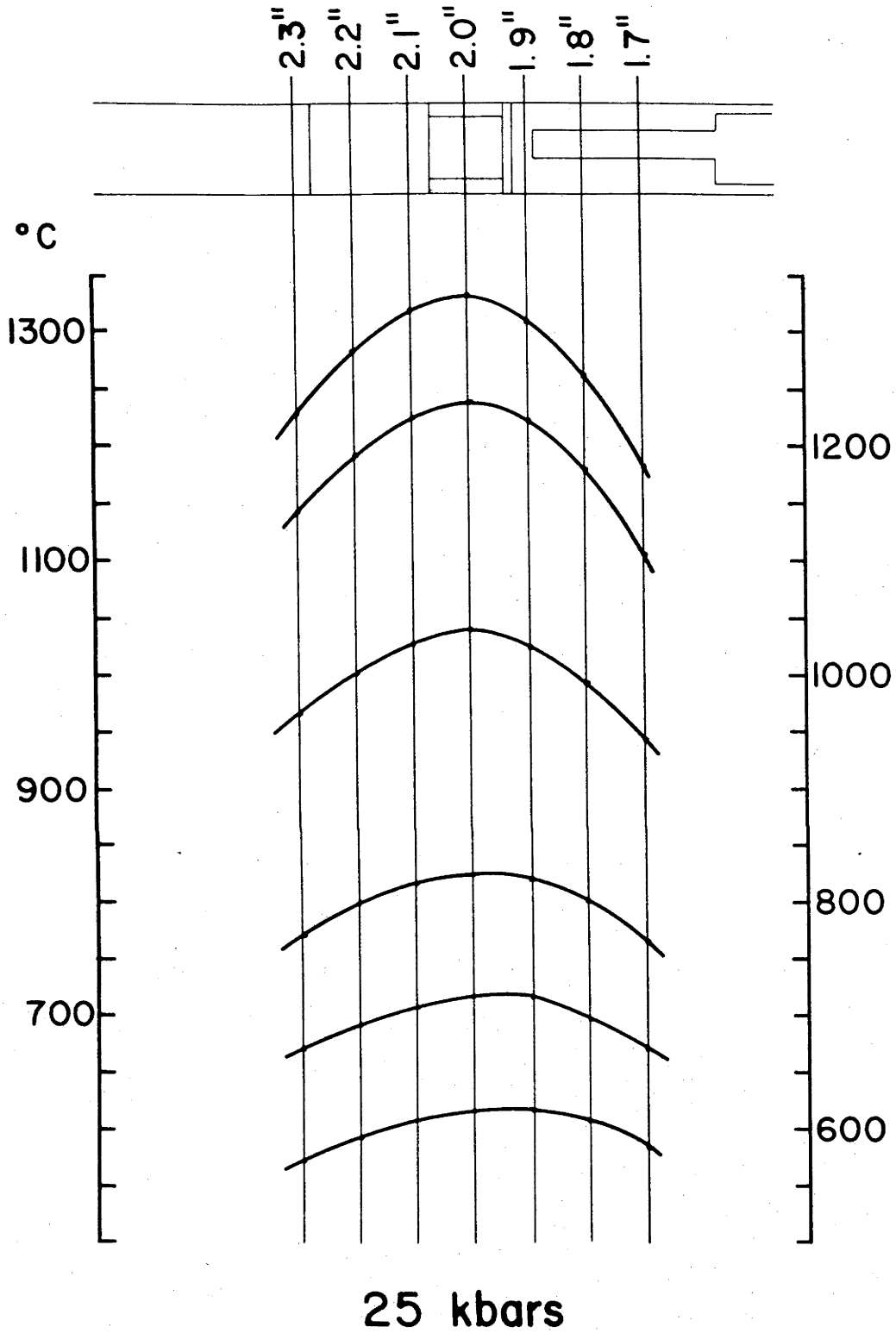

Figure 3. Temperature distribution in the 5/32" 'wet' graphite furnace assembly with boron nitride inserts at 25 kbar.

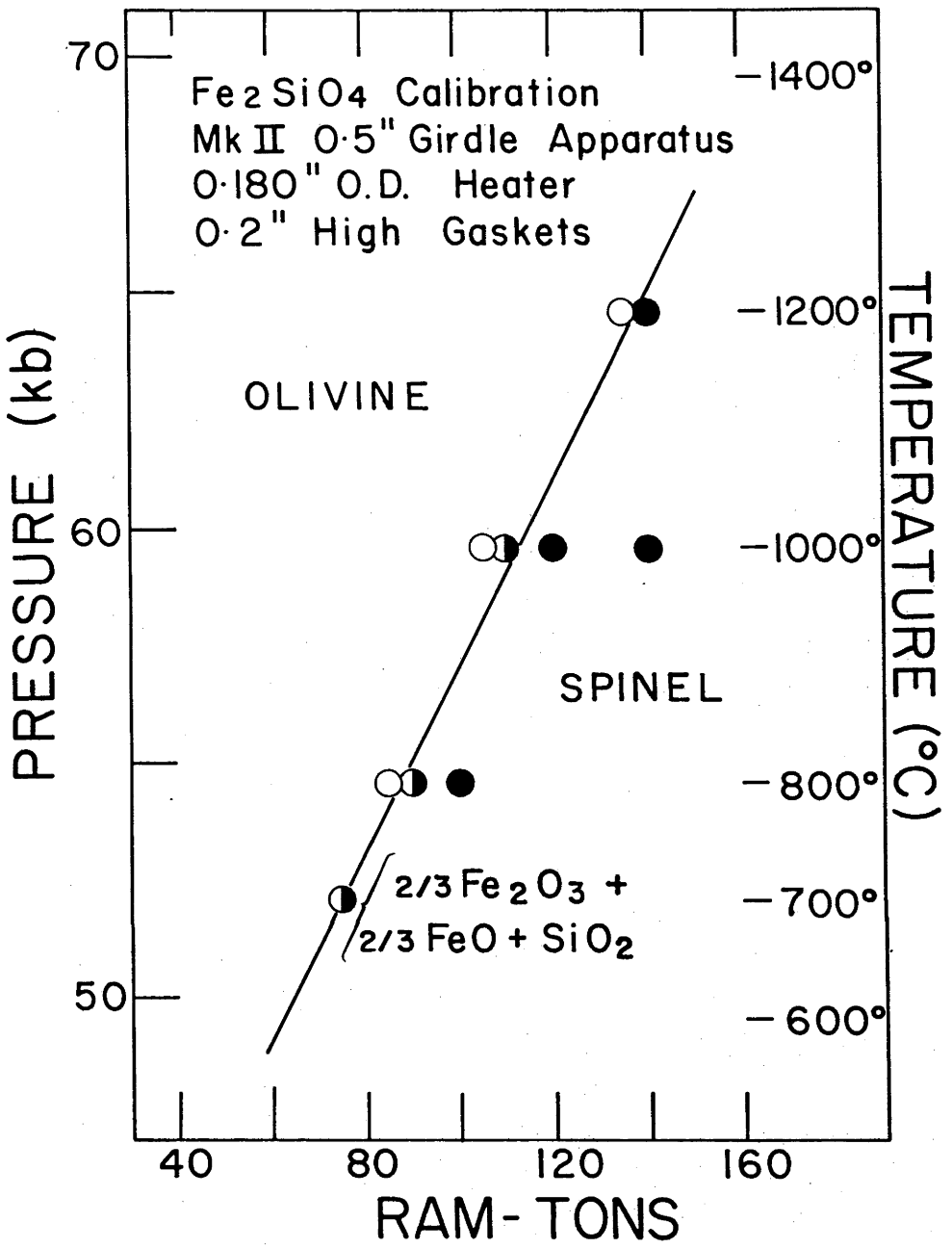

Figure 4. Pressure calibration of the 0.180" graphite furnace assembly with 0.20" high gaskets in a modified high pressue girdle (HPG) apparatus. The calibration is based on the fayalite olivine - spinel transition (Ringwood and Major, 1970).

ANALYTICAL TECHNIQUES

Optical and X-Ray Diffraction - Experimental charges were opened and divided into two splits- one for microprobe analysis, the other for optical and X-ray diffraction (XRD) analysis. The optical and XRD split was crushed to a fine powder. Optical analysis consisted of mounting the powder in oils with different refractive indices (RI) and examining the mounts by high-power petrographic microscopy. Approximate RI, birefringence and extinction angle were recorded.

About 1 mg of powder was mixed with clear nail polish, formed into a slender needle and mounted in a 114 mm diameter Debye-Scherrer powder camera for XRD analysis. Cu, Fe, or Co radiation with standard or fine (slit beam) collimators were used depending on the sample being analyzed. X-ray film was developed for 1½-2 minutes. Relative intensities were estimated and mineral phases were identified by matching observed d spacings with published standards (Berry, 1974). XRD-analysis was not suitable for assemblages which contained more than three phases.

Electron Microprobe - Major element oxide analyses of the mineral and liquid phases in the experimental samples were studied using the TPD electron microprobe with a lithium drifted silicon detector (Reed and Ware, 1973; 1975). This system uses an energy-dispersive technique, which enables all elements within a particular phase to be simultaneously analyzed without moving the beam. Accelerating voltage was 15 Kv; beam current 3nA; and the counting interval 100 sec. Data was reduced by the PIBS technique using the computer program "OXIDE" (Ware, 1981). The limits of detection of the TPD electron microprobe are ∿0.1 wt. percent (SiO_2, Al_2O_3, FeO, MgO, Na_2O, Cr_2O_3) and ∿0.05 wt. percent (CaO, TiO_2, K_2O). An accuracy of approximately 2 percent is expected with the TPD (Reed and Ware, 1975).

REFERENCES

Berry, L.G. (1974) Selected Powder Diffraction Data for Minerals. Joint Committee on Powder Diffraction Studies, Swarthmore, Pennsylvania, 833 p.

Green, T.H. (1967) High pressure experimental investigations on the origin of high-alumina basalt, andesite and anorthosite. Ph.D. Thesis, Australian National University.

Green, T.H.; Ringwood, A.E. and Major, A. (1966) Friction effects and pressure calibration in a piston cylinder apparatus at high pressure and temperature. J. Geophys. Res., 71, 3589-3594.

Gust, D.A. and Hibberson, W. (1979) Temperature calibration of the 5/32" graphite furnace assembly. Research School Earth Sciences Annual Report. Australian National University, 126-128.

Mirwald, P.W. and Kennedy, G.C. (1979) The melting curve of gold, silver, and copper to 60 kbar pressure: a reinvestigation. J. Geophys. Res., 84, 6750-6756.

Reed, S.J.B. and Ware, N.G. (1973) Quantitative electron microprobe analysis using a lithium drifted silicon detector. X-ray Spectrometry, 2, 69-74.

Reed, S.J.B. and Ware, N.G. (1975) Quantitative electron microprobe analysis of silicates using energy-dispersive x-ray spectrometry. J. Petrol., 16, 499-519.

Ringwood, A.E. and Major, A. (1970) The system Mg_2SiO_4 - Fe_2SiO_4 at high pressures and temperatures. Phys. Earth Planet. Interiors, 3, 89-108.

Stromberg, H.D. and Stephens, D.R. (1964) Effects of pressure on the electrical resistance of certain metals. J. Phys. Chem. Solids, 25, 1015-1023.

Ware, N.G. (1981) Computer programs and calibration with the PIBS technique for quantitative electron probe analysis using a lithium-drifted silicon detector. Computers Geosci., 7, 167-184.

APPENDIX 2

MICROPROBE ANALYSES OF LIQUIDS, CLINOPYROXENES, AND GARNETS FROM HIGH PRESSURE EXPERIMENTS ON DG-1 ECLOGITE, CHAPTER 2

Table A2-1. Microprobe analyses of liquids from high pressure experiments on DG-1 eclogite.

Table A2-2. Microprobe analyses of clinopyroxenes from high pressure experiments on DG-1 eclogite.

Table A2-3. Microprobe analyses of garnets from high pressure experiments on DG-1 eclogite.

Table A2-1. Microprobe analyses of liquids from high pressure experiments on DG-1 eclogite.

DG-1 ANHYDROUS

	1440°C					1472°C			1490°C			1550° C				
Run #	8652	8652	8652	8652	8652	8864	8864	8864	8650	8650	8650	8841	8841	8841	8841	8841
SiO_2	57.28	57.82	57.81	59.06	59.06	53.92	52.13	53.46	54.15	56.25	54.05	51.50	51.93	53.00	52.10	53.06
TiO_2	1.44	1.65	1.65	1.65	1.58	1.77	1.65	1.76	2.23	1.83	1.74	1.85	2.04	2.26	2.08	2.03
Al_2O_3	15.51	15.65	15.70	16.04	15.81	14.94	15.24	14.93	15.41	15.85	16.17	15.79	15.81	16.27	15.46	15.68
FeO	8.33	8.23	9.00	9.00	8.58	10.16	10.63	11.23	11.93	10.81	10.62	14.03	12.63	11.64	12.39	13.45
MgO	3.66	3.27	2.20	2.18	3.32	4.93	6.22	5.31	1.55	1.19	3.94	4.17	2.88	2.47	2.64	2.05
CaO	7.27	7.08	6.85	5.97	7.53	9.42	10.26	9.21	7.56	4.87	8.61	8.21	7.43	6.56	6.61	6.16
K_2O	1.23	1.35	1.30	1.39	1.18	.75	.57	.72	1.21	1.35	.81	.66	.87	1.08	.98	1.13
Na_2O	3.14	3.44	3.90	3.36	3.29	3.31	3.31	3.38	2.95	3.83	3.50	3.79	3.56	3.99	3.42	3.13
Total	97.86	98.49	98.11	98.65	100.36	99.20	100.00	100.00	97.0	95.98	99.43	100.00	97.15	97.26	95.69	96.69

	DG-1 ANHYDROUS											DG-1+1.5% H_2O		DG-1+5% H_2O		
	1535°C			1550°C				1560°C					1260°C		1200°C		
Run #	8659	8659	8659	8880	8880	8880	8880	8656	8656	8656	8656	8656	8865	8865	8868	8868	8868
SiO_2	52.84	54.14	54.19	51.06	51.05	59.81	58.0	48.63	49.01	48.74	48.93	48.76	61.25	61.42	67.79	61.18	62.56
TiO_2	2.22	2.31	2.14	1.47	1.60	1.78	1.75	1.41	1.39	1.34	1.25	1.40	.49	.32	.34	2.69	.91
Al_2O_3	16.79	16.82	16.81	15.26	15.32	16.81	15.32	16.20	16.22	16.27	16.25	16.13	13.16	11.39	11.92	10.07	12.28
FeO	13.42	13.50	14.38	10.49	10.29	8.31	7.35	10.84	10.48	10.68	10.93	10.81	1.70	1.70	.36	2.13	1.49
MgO	2.21	1.76	1.45	6.47	4.25	.52	.42	8.21	8.32	8.30	8.29	8.21	.42	1.70	.16	2.82	.36
CaO	6.05	6.16	5.92	10.22	7.77	3.46	3.27	11.47	11.33	11.48	11.26	11.38	1.25	3.24	.77	5.55	1.42
K_2O	1.29	1.45	1.14	.42	.74	1.83	1.64	.17	.18	.20	.20	.21	1.20	.58	2.85	1.27	1.34
Na_2O	4.12	3.86	3.98	3.11	2.86	2.92	2.44	3.06	3.06	3.00	2.89	3.03	4.62	2.98	5.58	4.28	4.52
Total	98.94	100.00	100.01	98.50	93.87	95.44	90.20	99.99	99.99	100.01	100.00	99.93	84.10	83.32	89.77	90.00	84.86

Table A2-2. Microprobe analyses of clinopyroxenes from high pressure experiments on DG-1 eclogite.

DG-1 ANHYDROUS

	1350°C					1440°C							1450°C					1472°C			
RUN #	8665	8665	8665	8665	8665	8652	8652	8652	8652	8652	8652	8652	8845	8845	8845	8845	8845	8864	8864	8864	8864
SiO_2	50.90	50.67	50.59	52.03	51.25	50.47	48.87	49.32	49.01	49.51	49.36	50.02	49.83	49.43	50.16	50.89	48.89	49.92	49.90	50.13	50.34
TiO_2	1.27	1.29	1.30	1.37	1.44	1.22	1.22	1.14	1.08	1.37	1.16	1.24	1.25	1.27	1.37	1.27	1.18	1.16	.89	1.15	1.17
Al_2O_3	14.04	14.92	15.16	12.96	14.07	14.52	15.15	14.87	15.25	15.21	14.74	14.29	15.70	15.70	15.67	14.10	15.87	14.90	14.82	14.84	14.77
FeO	8.12	9.14	9.02	8.23	8.11	8.69	9.11	8.93	9.26	8.64	8.71	8.68	9.92	10.21	10.03	9.65	10.06	9.69	9.51	9.64	9.79
MgO	8.40	8.42	8.09	8.50	8.40	8.42	9.10	9.17	9.38	8.99	9.00	8.84	7.94	8.03	7.75	8.07	8.47	8.53	9.21	8.58	8.38
CaO	13.40	12.77	12.54	13.97	13.59	13.14	13.10	13.17	12.79	13.34	13.47	13.33	12.04	12.06	11.59	12.37	12.29	12.43	12.53	12.32	12.26
K_2O	-	-	-	.07	.07	-	-	-	-	-	-	-	.17	.11	.21	.21	-	.08	-	-	-
Na_2O	3.83	3.72	3.79	3.68	3.78	3.55	3.49	3.40	3.23	3.56	3.57	3.60	3.15	3.19	3.22	3.44	3.24	3.28	3.14	3.34	3.29
Cations/6 oxygens																					
Si	1.841	1.819	1.821	1.868	1.840	1.827	1.777	1.791	1.780	1.786	1.794	1.815	1.807	1.796	1.816	1.846	1.778	1.812	1.809	1.817	1.824
Ti	.034	.035	.035	.037	.039	.033	.033	.031	.030	.037	.032	.034	.034	.035	.037	.035	.032	.032	.024	.031	.032
Al	.598	.631	.643	.548	.595	.619	.650	.637	.653	.646	.631	.611	.671	.673	.669	.603	.680	.637	.633	.634	.631
Fe	.246	.274	.272	.247	.244	.263	.277	.271	.281	.261	.265	.263	.301	.310	.304	.293	.306	.294	.288	.292	.297
Mg	.453	.451	.434	.455	.450	.454	.493	.496	.508	.484	.487	.478	.429	.435	.418	.436	.459	.462	.498	.464	.453
Ca	.519	.491	.484	.537	.523	.509	.511	.512	.498	.515	.525	.518	.468	.469	.450	.481	.479	.484	.487	.479	.476
K	-	-	-	.003	.003	-	-	-	-	-	-	-	.008	.005	.010	.010	-	.003	-	-	-
Na	.269	.259	.265	.256	.263	.249	.246	.240	.228	.249	.251	.253	.221	.225	.226	.242	.228	.231	.220	.235	.231
Total	3.960	3.960	3.954	3.951	3.957	3.955	3.987	3.979	3.978	3.978	3.985	3.972	3.938	3.948	3.930	3.944	3.963	3.955	3.960	3.952	3.944
Mg#	65.0	62.3	61.7	69	65	63.5	64.2	64.8	64.5	65.1	65.0	64.6	58.9	58.5	58.0	60	60.1	61.2	63.5	61.5	60.5
Ca	42.6	40.4	40.7	43.4	43.0	41.5	39.9	40.0	38.7	40.9	41.1	41.1	39.1	38.7	38.4	39.7	38.5	39.0	38.2	38.8	38.8
Mg	37.2	37.0	36.5	36.7	37.0	37.0	38.5	38.8	39.5	38.4	38.2	38.0	35.8	35.8	35.7	36.1	36.9	37.2	39.1	37.6	36.9
Fe	20.2	22.6	22.8	19.9	20.0	21.5	21.6	21.2	21.8	20.7	20.7	20.9	25.1	25.5	25.9	24.2	24.6	23.7	22.7	23.7	24.2
Pyroxene End-members																					
Jadeite	28.0	27.0	27.8	27.0	27.5	26.1	24.9	24.5	23.3	25.5	25.4	26.0	23.7	23.8	24.5	25.8	23.7	24.3	22.9	24.7	24.5
CaTiTs	3.5	3.6	3.7	3.9	4.0	3.4	3.3	3.2	3.1	3.8	3.2	3.5	3.6	3.7	4.0	3.7	3.3	3.3	3.3	3.2	3.4
CaTs	13.6	15.7	16.1	11.5	13.3	15.9	17.1	17.1	18.7	16.5	16.0	14.9	20.5	20.0	20.0	15.5	20.1	17.9	18.2	17.7	17.8
Wo	18.4	15.9	15.4	20.6	18.7	17.0	15.6	16.0	14.6	16.2	17.0	17.4	13.0	13.0	12.4	16.0	13.1	14.8	14.6	14.7	14.6
En	23.6	23.4	22.7	24.0	23.6	23.8	25.0	25.3	26.0	24.7	24.7	24.5	23.0	23.0	22.6	23.2	23.8	24.2	25.9	24.4	24.0
Fs	12.8	14.3	14.2	13.0	12.8	13.8	14.0	13.8	14.3	13.3	13.5	13.5	16.1	16.4	16.5	15.6	15.9	15.4	15.0	15.3	15.7
Jadeite %	29.0	28.0	28.8	28.0	28.7	27.0	25.8	25.3	24.0	26.5	26.4	27.0	24.6	24.7	25.5	26.8	24.5	25.1	23.7	25.5	25.3
CaTs %	14.1	16.3	16.7	12.0	13.9	16.5	17.7	17.7	19.2	17.1	16.6	15.5	21.2	20.8	20.8	16.1	20.8	18.6	18.8	18.3	18.4
Quad %	56.9	55.7	54.4	60.0	57.4	56.5	56.5	57.0	56.8	56.4	57.0	57.5	54.1	54.4	53.6	57.0	54.7	56.3	57.5	56.2	56.2

DG-1 ANHYDROUS

	1490°C							1500°C						1525°C				
RUN #	8650	8650	8650	8650	8650	8650	8650	8841	8841	8841	8841	8841	8841	8880	8880	8880	8880	8880
SiO_2	48.55	48.33	49.50	49.38	49.88	48.78	49.21	49.60	49.25	49.61	49.10	49.01	48.44	49.82	49.60	49.53	49.98	50.23
TiO_2	.83	1.02	1.08	1.00	1.26	.94	.93	1.25	1.35	.94	.87	.91	.89	.81	.75	.88	.62	.73
Al_2O_3	14.76	15.75	14.79	14.22	14.70	15.10	14.60	14.95	15.34	14.44	14.46	14.69	15.70	13.99	14.62	14.53	13.75	13.64
FeO	8.14	9.72	8.56	8.56	10.24	8.52	8.57	9.21	11.47	8.10	8.40	8.18	8.15	6.85	6.69	7.38	6.49	6.76
MgO	10.70	9.43	9.39	9.76	8.27	9.92	9.91	8.84	7.67	9.80	10.32	10.27	10.18	11.11	10.63	10.22	11.60	11.26
CaO	13.74	11.91	13.53	13.84	12.21	13.83	13.76	12.86	11.66	14.00	13.80	13.82	13.56	14.46	14.61	14.41	14.54	14.38
K_2O	-	-	-	-	.11	-	-	.08	.16	-	-	-	-	-	-	-	-	-
Na_2O	2.99	3.02	3.15	3.22	3.33	2.93	3.02	3.20	3.10	3.12	3.05	3.12	3.08	2.96	3.10	3.05	3.02	3.00
Cations/6 oxygens																		
Si	1.767	1.769	1.795	1.795	1.815	1.771	1.787	1.800	1.799	1.798	1.783	1.779	1.756	1.798	1.790	1.792	1.802	1.811
Ti	.023	.028	.029	.027	.035	.026	.025	.034	.037	.026	.024	.025	.024	.022	.020	.024	.017	.020
Al	.633	.679	.623	.609	.631	.646	.625	.639	.660	.617	.619	.628	.671	.595	.622	.619	.584	.580
Fe	.248	.298	.260	.260	.312	.259	.260	.280	.350	.245	.255	.248	.247	.207	.202	.223	.196	.204
Mg	.581	.514	.507	.529	.448	.537	.536	.478	.418	.529	.558	.556	.550	.598	.572	.551	.623	.605
Ca	.536	.467	.526	.539	.476	.538	.535	.500	.456	.544	.537	.537	.527	.559	.565	.559	.562	.555
K	-	-	-	-	.005	-	-	.004	.008	-	-	-	-	-	-	-	-	-
Na	.211	.214	.221	.227	.235	.206	.212	.225	.219	.219	.215	.220	.216	.207	.217	.214	.211	.210
Total	3.999	3.970	3.970	3.987	3.956	3.983	3.981	3.961	3.947	3.978	3.991	3.992	3.992	3.986	3.987	3.982	3.995	3.984
Mg#	70.2	63.5	66.3	67.2	59.1	67.6	67.5	63.2	54.5	68.4	68.8	69.2	69.1	74.3	73.9	71.2	76.0	74.8
Ca	39.3	36.5	40.7	40.6	38.5	40.3	40.2	39.8	37.3	41.2	39.8	40.1	39.8	41.0	42.2	41.9	40.7	40.7
Mg	42.6	40.2	39.3	39.8	36.3	40.3	40.3	38.0	34.1	40.1	41.3	41.4	41.5	43.8	42.7	44.3	45.2	44.3
Fe	18.2	23.3	20.1	19.6	25.2	19.4	19.5	22.2	28.6	18.6	18.9	18.5	18.7	15.2	15.1	14.9	14.2	14.9
Pyroxene End-members																		
Jadeite	21.1	22.1	22.8	23.0	24.7	21.0	21.6	23.5	23.3	22.4	21.7	22.1	21.7	21.0	21.9	21.8	21.2	21.3
CaTiTs	2.3	2.9	2.9	2.7	3.7	2.6	2.5	3.6	3.9	2.6	2.4	2.5	2.4	2.2	2.0	2.4	1.7	2.0
CaTs	18.8	21.1	18.1	17.6	17.1	19.7	18.5	18.1	19.5	17.7	18.0	18.0	20.5	17.4	18.5	18.1	17.0	16.7
Wo	16.3	12.1	16.5	17.6	14.6	16.2	16.7	15.3	12.5	17.6	16.9	16.8	15.1	18.5	18.3	18.1	18.9	18.8
En	29.1	26.5	26.1	26.8	23.5	27.3	27.3	25.0	22.2	27.0	28.1	28.0	27.7	30.3	28.9	28.0	31.3	30.7
Fs	12.4	15.3	13.3	13.2	16.4	13.2	13.2	14.6	18.6	12.5	12.8	12.4	12.5	10.5	10.2	11.3	9.0	10.4
Jadeite %	21.6	22.7	23.5	23.6	25.6	21.5	22.2	24.4	24.2	23.0	22.2	22.7	22.3	21.5	22.4	22.3	21.6	21.8
CaTs %	19.3	21.7	18.7	17.2	17.8	20.2	19.0	18.7	20.3	18.1	8.4	18.5	21.0	17.8	18.8	18.6	17.3	17.1
Quad %	59.1	55.6	57.7	59.2	56.6	58.2	58.8	56.9	55.5	58.9	59.4	58.7	56.6	60.7	58.7	59.0	61.1	61.1

	DG-1 ANHYDROUS								DG-1 + 1.5% H_2O									
	1535°C						1550°C		700°C					750°C	800°C		850°C	
RUN #	8659	8659	8659	8659	8659	8659	8879	8879	6944	6944	6944	6944	6944	6880	7373	7373	7372	7372
SiO_2	48.77	48.55	47.62	48.91	49.88	49.07	50.88	49.69	50.97	53.99	53.13	53.23	53.31	52.37	53.23	53.70	53.98	53.61
TiO_2	.69	.99	1.21	.69	.53	.69	1.51	1.02	.25	.27	.19	.26	.24	1.07	.34	.23	.39	.25
Al_2O_3	14.57	14.61	16.32	14.46	13.17	14.23	16.20	15.47	15.82	10.88	12.91	13.40	13.20	12.03	10.97	12.43	12.53	15.25
FeO	6.27	9.12	8.87	6.21	6.14	6.38	8.97	8.10	7.54	6.94	6.22	6.01	6.06	7.89	8.22	5.82	7.12	4.35
MgO	12.07	11.21	10.17	12.07	12.65	12.30	6.66	9.38	8.75	10.09	9.86	9.38	9.33	9.37	9.36	9.46	9.46	8.29
CaO	15.18	13.04	13.29	15.12	14.92	14.96	11.23	12.93	12.72	13.72	13.50	13.26	13.34	13.42	13.24	13.33	13.18	12.41
K_2O	-	-	-	-	-	-	.30	-	-	-	-	-	.07	-	-	.15	-	.19
Na_2O	2.40	2.41	2.80	2.54	2.41	2.37	3.46	3.41	3.95	4.11	4.19	4.46	4.45	4.28	4.65	4.87	4.35	5.66
Cations /6 oxygens																		
Si	1.761	1.765	1.727	1.765	1.801	1.770	1.843	1.794	1.830	1.938	1.900	1.900	1.905	1.885	1.925	1.920	1.903	1.898
Ti	.018	.027	.033	.019	.014	.019	.041	.028	.007	.007	.005	.007	.007	.029	.009	.006	.010	.007
Al	.620	.626	.698	.615	.561	.605	.691	.658	.669	.460	.544	.564	.556	.510	.468	.524	.530	.636
Fe	.190	.277	.269	.187	.185	.192	.272	.245	.226	.208	.186	.179	.181	.238	.249	.174	.214	.129
Mg	.649	.607	.550	.649	.681	.661	.360	.505	.468	.540	.525	.499	.497	.503	.505	.504	.507	.438
Ca	.587	.508	.516	.585	.577	.578	.436	.500	.489	.528	.517	.507	.510	.517	.513	.511	.507	.471
K	-	-	-	-	-	-	.014	-	-	-	-	-	.003	-	-	.007	-	.009
Na	.168	.170	.197	.177	.169	.166	.243	.239	.275	.286	.291	.309	.308	.299	.326	.337	.303	.388
Total	3.993	3.980	3.989	3.997	3.989	3.992	3.899	3.969	3.966	3.968	3.968	3.965	3.967	3.981	3.995	3.984	3.973	3.975
Mg#	77.5	68.8	67.3	77.7	78.7	77.6	60.0	67.3	67.5	72.3	74.0	73.7	73.4	68.0	67.1	74.5	70.4	77.3
Ca	41.2	36.5	38.7	41.1	40.0	40.4	40.8	40.0	41.3	41.4	42.1	42.8	43.0	41.1	40.5	43.0	41.3	45.4
Mg	45.6	43.6	41.2	45.7	47.2	46.2	33.7	40.4	39.6	42.3	42.8	42.1	41.8	40.0	39.9	42.4	41.3	42.2
Fe	13.3	19.9	20.2	13.2	12.8	13.4	25.5	19.6	19.1	16.3	15.1	15.1	15.2	18.9	19.6	14.6	17.4	12.4
Pyroxene End-member																		
Jadeite	16.9	17.3	19.9	17.7	17.1	16.7	27.3	24.7	28.5	29.6	30.0	32.0	32.0	30.4	32.7	34.4	31.1	40.0
CaTiTs	1.8	2.7	3.3	1.9	1.4	1.9	4.6	2.9	.7	.7	.5	.7	.7	2.9	.9	.6	1.0	.7
CaTs	20.9	20.5	22.0	20.0	18.4	20.2	20.6	18.7	19.7	8.3	12.5	12.5	12.1	7.8	6.2	8.9	10.6	12.1
Wo	18.1	14.2	13.4	18.3	19.3	18.0	11.9	15.0	15.1	22.8	20.2	19.7	20.0	21.0	22.2	21.3	20.2	17.9
En	32.6	30.9	27.8	32.5	34.4	33.3	20.2	26.0	24.2	27.9	27.1	25.8	25.8	25.6	25.4	25.7	26.0	22.6
Fs	9.5	14.1	13.6	9.4	9.4	9.7	15.3	12.6	11.7	10.7	9.6	9.3	9.4	12.1	12.5	8.9	11.0	6.7
Jadeite %	17.2	17.8	20.6	18.1	17.3	17.1	28.6	25.4	28.7	29.8	30.2	32.2	32.2	31.4	33.0	34.6	31.4	40.3
CaTs %	21.3	21.1	22.7	20.4	18.7	20.6	21.5	19.3	19.8	8.3	12.6	12.6	12.2	8.0	6.3	8.9	10.7	12.2
Quad %	61.5	61.1	56.7	61.5	64.0	62.3	49.8	55.3	51.4	61.9	57.2	55.2	55.6	60.5	60.6	56.4	57.8	47.5

DG-1 + 1.5% H_2O

	1000°C								1100°C						1200°C			
RUN #	7559	7551	7550	7550	7550	8829	8829	8829	8818	8818	8818	8866	8866	8866	8808	8808	8808	8808
SiO_2	54.57	54.90	54.22	52.05	54.03	54.91	55.77	54.41	52.96	54.07	53.12	53.69	53.96	53.34	52.91	53.71	52.71	53.15
TiO_2	.43	.49	.50	.58	.53	.43	.59	.48	.76	.87	.77	.85	.78	.67	1.15	.87	.58	.81
Al_2O_3	12.41	11.94	11.86	13.57	12.55	11.29	11.98	12.22	10.79	11.69	11.66	11.05	10.98	11.20	11.32	11.46	11.92	11.43
FeO	4.91	5.02	4.77	6.94	4.71	4.57	4.68	5.13	5.48	5.26	5.36	5.82	5.46	5.80	5.95	5.86	5.82	5.95
MgO	8.91	9.24	9.49	8.88	8.96	9.14	8.32	8.92	9.48	8.84	9.40	9.27	9.14	9.54	9.36	8.98	9.74	9.42
CaO	13.63	14.14	14.56	13.50	13.91	14.20	13.32	13.54	14.76	13.95	14.55	14.33	14.51	14.56	14.44	14.32	14.55	14.56
K_2O	-	-	-	-	-	-	.09	-	-	-	-	-	-	-	-	-	-	-
Na_2O	5.14	5.05	5.38	4.48	5.32	5.47	5.24	5.30	4.80	5.24	5.14	5.00	5.17	4.90	4.86	4.80	4.68	4.68
Cations/6 oxygens																		
Si	1.941	1.942	1.924	1.872	1.925	1.957	1.976	1.939	1.922	1.935	1.908	1.928	1.936	1.918	1.905	1.927	1.895	1.911
Ti	.012	.013	.013	.016	.014	.011	.016	.013	.021	.023	.021	.023	.021	.018	.031	.023	.016	.022
Al	.520	.498	.496	.575	.527	.474	.500	.513	.462	.493	.493	.468	.464	.475	.480	.485	.505	.484
Fe	.146	.148	.141	.209	.140	.136	.139	.153	.166	.157	.161	.175	.164	.174	.179	.176	.175	.179
Mg	.472	.487	.502	.476	.476	.485	.440	.470	.513	.471	.503	.496	.489	.511	.502	.480	.522	.505
Ca	.519	.536	.554	.520	.531	.542	.506	.513	.574	.539	.560	.551	.558	.561	.557	.550	.560	.561
K	–	–	–	–	–	–	.004	-	-	-	-	-	-	-	-	-	-	-
Na	.354	.346	.370	.313	.368	.378	.360	.379	.337	.363	.358	.348	.360	.341	.339	.334	.326	.326
Total	3.965	3.970	4.000	3.981	3.981	3.984	3.940	3.981	3.995	3.977	4.004	3.909	3.991	3.998	3.994	3.975	4.000	3.988
Mg#	76.5	76.7	78.1	69.6	77.3	78.2	76.1	75.5	75.6	75.1	75.8	70.8	74.9	74.6	73.8	73.3	75.0	73.9
Ca	45.6	45.7	46.3	43.2	46.3	46.6	46.6	45.2	45.8	46.0	45.7	45.1	46.1	45.0	45.0	45.6	44.6	45.1
Mg	41.5	41.6	41.9	39.5	41.5	41.7	40.6	41.4	40.9	40.5	41.1	40.6	40.4	41.0	40.6	39.8	41.5	40.6
Fe	12.8	12.7	11.8	17.3	12.2	11.7	12.8	13.5	13.3	13.5	13.2	14.3	13.5	14.0	14.5	14.6	13.9	14.4
Pyroxene End-members																		
Jadeite	36.7	35.6	37.0	32.5	37.5	38.4	38.4	38.6	33.9	37.1	35.7	35.1	36.3	34.2	34.1	34.2	32.6	33.00
CaTiTs	1.2	1.3	1.3	1.6	1.4	1.1	1.7	1.3	2.1	2.3	2.1	2.3	2.1	1.8	2.1	2.3	1.6	2.2
CaTs	7.4	6.5	5.0	11.7	6.7	3.7	5.7	5.5	4.2	4.3	4.6	3.7	3.1	4.9	4.0	5.4	7.3	5.8
Wo	22.6	23.7	24.6	19.8	23.0	25.1	23.2	22.7	25.7	24.0	24.5	24.8	25.5	24.8	24.5	24.3	23.5	24.4
En	24.5	25.1	25.1	24.2	24.2	24.7	23.4	24.0	25.7	24.1	25.0	25.1	24.7	25.6	25.3	24.6	26.1	25.5
Fs	7.6	7.6	7.0	10.6	7.1	6.9	7.4	7.8	8.3	8.0	8.0	8.8	8.3	8.7	9.0	9.0	8.7	9.0
Jadeite %	37.2	36.2	37.5	32.4	38.0	38.9	39.0	39.2	34.6	38.0	36.4	36.0	37.0	34.8	35.2	35.1	33.1	33.7
CaTs %	7.5	6.6	5.0	11.9	6.8	3.8	5.9	5.6	4.3	4.4	4.7	3.8	3.2	5.0	4.1	5.5	7.5	5.9
Quad %	55.3	57.2	57.4	55.6	55.2	57.3	55.1	55.2	61.1	57.6	58.8	60.2	59.8	60.2	60.7	59.4	59.4	60.4

	DG - 1 + 1.5% H_2O						DG - 1 + 5% H_2O										
	1260° C		1300° C				1000° C				1100° C				1200° C		
Run #	8865	8865	8816	8816	8816	8816	8869	8869	8869	8869	8867	8867	8867	8867	8868	8868	8868
SiO_2	52.76	51.67	52.06	51.78	51.82	51.17	54.16	52.37	52.0	54.11	54.37	53.85	55.52	54.26	53.81	52.82	53.04
TiO_2	.89	.41	.73	.58	.91	.84	.39	.96	1.35	.39	.85	1.06	.97	.83	.46	.51	.56
Al_2O_3	9.55	8.60	12.16	10.85	11.81	12.00	9.62	12.34	11.07	10.23	9.52	10.54	11.05	10.09	10.71	8.41	9.20
FeO	5.95	6.09	4.61	4.81	3.83	4.14	5.21	7.24	5.41	4.97	5.53	6.07	5.66	5.58	5.31	6.19	6.15
MgO	10.90	12.36	10.92	11.85	11.38	11.48	10.35	8.81	8.31	10.10	9.88	9.11	8.46	9.36	9.93	11.55	10.96
CaO	16.40	18.00	15.81	17.01	16.95	17.12	15.43	13.31	13.27	15.21	15.44	14.39	13.42	15.02	15.04	17.05	16.39
K_2O	-	-	-	-	-	-	-	.10	.15	-	-	-	.10	-	-	-	-
Na_2O	3.55	2.87	3.70	3.12	3.29	3.25	4.56	4.43	4.59	4.49	4.40	4.99	4.82	4.85	4.75	3.46	3.69
Cations/6 Oxygens																	
Si	1.907	1.882	1.866	1.865	1.857	1.840	1.950	1.895	1.935	1.941	1.953	1.937	1.977	1.949	1.931	1.917	1.919
Ti	.024	.011	.020	.016	.025	.023	.011	.026	.038	.011	.023	.029	.026	.022	.012	.014	.015
Al	.407	.369	.514	.461	.499	.509	.408	.526	.486	.432	.403	.447	.464	.427	.453	.360	.392
Fe	.180	.186	.138	.145	.115	.124	.157	.219	.168	.149	.166	.182	.168	.168	.159	.188	.186
Mg	.587	.671	.583	.636	.608	.615	.555	.475	.461	.540	.529	.489	.449	.501	.531	.625	.591
Ca	.635	.703	.607	.656	.651	.659	.595	.516	.529	.585	.594	.554	.512	.578	.578	.663	.636
K	-	-	-	-	-	-	-	.005	.007	-	-	-	.005	-	-	-	-
Na	.249	.202	.257	.218	.229	.227	.319	.311	.331	.347	.306	.348	.333	.338	.330	.244	.259
Total	3.989	4.024	3.986	3.997	3.983	3.997	3.995	3.973	3.954	4.005	3.975	3.985	3.934	3.984	3.995	4.011	3.999
Mg#	76.5	78.3	81.0	81.5	84.2	83.2	78.0	68.4	73.2	78.3	76.1	72.8	72.7	74.9	77.0	76.8	76.1
Ca	45.3	45.1	45.7	45.7	47.4	47.1	45.5	42.6	45.7	45.9	45.1	45.2	45.3	46.4	45.6	44.9	45.0
Mg	41.9	43.0	43.9	44.3	44.3	44.0	42.5	39.3	39.8	42.4	41.0	39.9	39.8	40.2	41.9	42.3	41.8
Fe	12.8	11.9	10.4	10.1	8.4	8.9	12.0	18.1	14.5	11.7	12.9	14.9	14.9	13.4	12.6	12.7	13.2
Pyroxene End-members																	
Jadeite	25.1	19.7	26.1	21.9	23.3	22.8	32.0	32.1	34.9	34.5	31.4	35.3	35.8	34.4	33.1	24.1	26.0
CaTiTs	2.4	1.0	2.0	1.6	2.5	2.3	1.0	2.7	4.0	1.1	2.3	2.9	2.8	2.2	1.2	1.4	1.5
CaTs	5.5	7.1	11.0	10.6	11.1	11.8	3.4	8.4	4.1	3.1	2.6	2.1	4.2	2.2	4.9	4.4	5.1
Wo	28.1	30.2	24.2	26.8	26.3	26.0	27.7	21.0	23.8	27.0	28.0	25.6	24.0	27.1	26.0	29.9	28.5
En	29.7	32.8	29.5	31.9	30.9	30.9	27.9	24.5	24.3	26.8	27.1	24.8	24.1	25.5	26.7	30.9	29.6
Fs	9.0	9.1	7.0	7.3	5.8	6.2	7.9	11.3	8.8	7.4	8.5	9.2	9.0	8.5	8.0	9.3	9.3
Jadeite %	25.8	19.9	26.7	22.2	23.9	23.3	32.4	32.9	36.3	34.9	32.1	36.4	36.8	35.1	33.6	24.5	26.3
CaTs %	5.7	7.1	11.2	10.7	11.5	12.1	3.4	8.6	4.3	4.3	2.7	2.1	4.4	2.4	5.0	4.4	5.2
Quad %	68.5	72.9	62.1	67.1	64.6	64.6	64.2	58.4	59.4	61.9	65.2	61.5	58.8	62.5	61.4	71.1	68.4

Table A2-3. Microprobe analyses of garnets from high pressure experiments on DG-1 eclogite.

DG-1 ANHYDROUS

	1350°C					1440°C							
Run #	8665	8665	8665	8665	8665	8652	8652	8652	8652	8652	8652	8652	8652
SiO_2	39.17	40.48	40.35	39.06	39.42	39.54	38.77	38.89	38.73	39.71	39.89	39.83	38.91
TiO_2	1.16	1.32	1.49	1.38	1.35	1.73	1.75	1.67	1.74	1.77	1.73	1.69	1.77
Al_2O_3	22.14	20.59	20.58	21.80	21.32	21.72	22.09	21.85	21.76	21.37	21.20	20.99	21.94
FeO	19.49	18.76	18.36	19.56	19.07	17.78	18.12	18.21	18.27	18.34	17.72	17.92	18.17
MgO	9.49	9.47	9.38	9.47	9.37	10.58	10.69	10.84	11.05	10.55	10.55	10.54	10.81
CaO	8.56	9.32	9.01	8.66	8.90	8.20	8.12	8.31	8.24	8.41	8.48	8.58	8.40
Na_2O	-	.66	.81	.27	.25	.47	.45	.23	.20	.24	.43	.45	-
Cations/12 oxygens													
Si	2.959	3.040	3.043	2.952	2.989	2.967	2.918	2.927	2.917	2.975	2.994	2.994	2.926
Ti	.066	.074	.085	.079	.077	.098	.099	.094	.099	.100	.097	.095	.100
Al	1.971	1.823	1.830	1.942	1.905	1.920	1.959	1.938	1.932	1.887	1.875	1.860	1.944
Fe	1.232	1.178	1.158	1.237	1.209	1.116	1.141	1.146	1.151	1.149	1.112	1.127	1.143
Mg	1.068	1.060	1.055	1.067	1.059	1.181	1.199	1.216	1.241	1.178	1.180	1.181	1.212
Ca	.693	.750	.728	.701	.723	.659	.655	.670	.665	.675	.682	.691	.676
Na	-	.096	.119	.039	.037	.069	.066	.034	.030	.035	.062	.066	-
Total	7.989	8.021	8.017	8.018	8.000	8.010	8.037	8.026	8.034	7.999	8.003	8.013	8.002
Mg #	46.6	47.5	47.8	46.5	46.8	51.6	51.4	51.6	52.0	50.8	51.6	51.3	51.6
Ca	23.2	25.1	24.8	23.3	24.2	22.3	21.9	22.1	21.8	22.5	22.9	23.0	22.3
Mg	35.7	35.5	35.9	35.5	35.4	40.0	40.1	40.1	40.6	39.2	39.7	39.4	40.0
Fe	41.1	39.4	39.4	41.1	40.4	37.7	38.1	37.8	37.7	38.3	37.4	37.6	37.7

DG-1 ANHYDROUS

	1450 °C									1472°C						
Run #	8845	8845	8845	8845	8845	8845	8845	8845	8845	8864	8864	8864	8864	8864	8864	8864
SiO_2	38.70	38.49	38.79	38.54	38.91	39.14	38.47	39.63	38.64	38.89	39.20	39.53	38.74	39.23	39.06	39.09
TiO_2	1.53	1.72	1.77	1.82	1.56	1.29	1.71	1.82	1.86	1.47	1.00	1.55	1.59	1.62	1.35	1.33
Al_2O_3	22.13	21.90	21.79	21.63	21.62	21.94	22.00	21.23	21.86	22.10	22.49	21.81	21.84	22.04	22.35	22.45
FeO	19.65	20.05	19.63	20.40	20.41	20.26	19.93	18.89	19.57	19.09	18.09	17.89	18.67	17.79	17.70	18.65
MgO	9.87	9.84	9.96	9.63	9.42	9.91	9.77	10.00	10.03	10.18	11.18	10.97	10.60	11.18	11.02	10.40
CaO	8.01	7.89	7.97	7.88	7.94	7.71	7.89	8.19	7.90	8.18	7.94	8.16	8.06	8.05	7.85	7.98
Na_2O	.10	.10	.10	.10	.15	.35	.22	.25	.14	.10	.10	.10	.10	.10	.10	.10
Cations/12 oxygens																
Si	2.927	2.918	2.934	2.927	2.952	2.948	2.916	2.986	2.923	2.934	2.934	2.963	2.931	2.940	2.941	2.939
Ti	.087	.098	.101	.104	.089	.073	.098	.103	.106	.083	.057	.087	.090	.092	.077	.075
Al	1.973	1.957	1.942	1.936	1.933	1.948	1.966	1.885	1.949	1.965	1.987	1.927	1.947	1.946	1.983	1.989
Fe	1.243	1.271	1.241	1.296	1.295	1.276	1.263	1.190	1.238	1.205	1.134	1.120	1.181	1.115	1.114	1.173
Mg	1.113	1.112	1.123	1.090	1.065	1.113	1.104	1.123	1.131	1.144	1.249	1.226	1.195	1.248	1.236	1.166
Ca	.649	.641	.646	.641	.646	.622	.641	.662	.640	.662	.638	.655	.653	.646	.633	.643
Na	.015	.015	.015	.015	.022	.051	.032	.037	.021	.014	.014	.015	.015	.015	.015	.015
Total	8.006	8.012	8.001	8.009	8.003	8.031	8.019	7.986	8.008	8.007	8.018	7.993	8.013	8.002	7.998	7.999
Mg #	47.4	46.8	47.6	45.8	45.3	46.7	46.8	48.7	47.9	48.9	52.6	52.4	50.45	53.0	52.7	50.0
Ca	21.6	21.2	21.5	21.2	21.5	20.7	21.3	22.2	21.3	22.0	21.1	21.8	21.6	21.5	21.2	21.6
Mg	37.0	36.8	37.3	36.0	35.4	37.0	36.7	37.7	37.6	38.0	41.3	40.8	39.5	41.5	41.4	39.1
Fe	41.4	42.0	41.2	42.8	43.1	42.4	42.0	40.0	41.1	40.0	37.5	37.3	39.0	37.0	37.3	39.3

DG-1 ANHYDROUS

	1490°C					1500°C								1525°C		
Run #	8650	8650	8650	8650	8650	8841	8841	8841	8841	8841	8841	8841	8841	8880	8880	8880
SiO_2	39.36	40.68	39.60	39.30	39.34	39.13	39.55	39.47	39.43	39.46	39.22	39.19	40.28	40.76	40.18	40.52
TiO_2	1.31	1.37	1.38	1.36	1.27	1.26	1.40	1.23	1.23	1.26	1.25	1.38	1.23	1.20	1.33	1.15
Al_2O_3	22.76	21.26	22.16	22.46	22.44	22.71	22.51	22.77	22.60	22.88	22.59	22.55	21.91	22.15	22.22	22.41
FeO	15.48	14.98	15.62	15.75	15.74	16.09	15.84	15.95	15.67	15.35	15.66	15.76	15.03	13.23	14.63	13.66
MgO	12.38	12.18	12.29	12.42	12.66	12.27	12.52	12.34	12.70	12.60	12.66	12.66	12.35	13.26	12.74	13.32
CaO	8.43	8.95	8.57	8.47	8.35	8.40	8.08	8.14	8.36	8.40	8.52	8.34	9.05	9.10	8.71	8.64
Na_2O	.28	.58	.38	.24	.21	.13	.10	.10	-	.05	.10	.10	.15	.30	.20	.30
Cations/12 oxygens																
Si	2.922	3.016	2.944	2.923	2.924	2.913	2.936	2.931	2.927	2.924	2.915	2.913	2.985	2.994	2.969	2.979
Ti	.073	.077	.077	.076	.071	.070	.078	.068	.069	.070	.070	.077	.068	.066	.074	.064
Al	1.992	1.858	1.942	1.969	1.966	1.993	1.969	1.993	1.977	1.998	1.979	1.976	1.913	1.918	1.935	1.942
Fe	.961	.929	.971	.980	.978	1.002	.983	.991	.972	.952	.973	.980	.931	.812	.904	.840
Mg	1.369	1.346	1.362	1.377	1.402	1.362	1.385	1.366	1.405	1.392	1.403	1.403	1.364	1.452	1.403	1.460
Ca	.671	.711	.683	.675	.665	.670	.643	.648	.665	.667	.678	.665	.718	.716	.690	.680
Na	.041	.084	.055	.035	.031	.019	.014	.014	-	.007	.014	.014	.022	.042	.029	.043
Total	8.029	8.020	8.035	8.034	8.037	8.029	8.009	8.011	8.016	8.010	8.033	8.028	8.001	8.002	8.004	8.008
Mg #	58.9	59.2	58.5	55.0	59.1	57.8	58.6	58.1	59.2	59.7	59.2	59.6	59.6	64.1	60.8	63.5
Ca	22.4	23.8	22.6	22.3	21.8	22.1	21.3	21.6	21.9	22.2	22.2	21.8	23.8	24.0	23.0	22.8
Mg	45.6	45.1	45.2	45.4	46.0	44.9	46.0	45.5	46.2	46.2	45.9	46.0	45.3	48.7	46.8	49.0
Fe	32.0	31.1	32.2	32.3	32.1	33.0	32.6	33.0	32.0	31.6	31.9	32.2	30.9	27.3	30.2	28.2

	DG-1 ANHYDROUS								DG-1 + 1.5% H_2O								
	1535°C						1550°C		700°C					750°C	800°C		
Run #	8659	8659	8659	8659	8659	8659	8879	8879	6944	6944	6944	6944	8010	6880	7373	7373	7373
SiO_2	39.98	39.83	39.94	40.38	40.05	39.89	39.52	40.23	41.89	38.85	39.21	38.90	40.12	36.52	40.41	38.18	37.69
TiO_2	.99	.99	.78	.62	.98	.79	1.43	1.22	1.43	.80	.76	.57	.60	6.63	.88	4.39	5.07
Al_2O_3	23.09	22.99	23.04	23.51	23.13	22.79	22.43	21.97	19.46	21.41	21.55	21.85	20.68	20.43	20.37	20.23	20.75
FeO	13.14	13.21	12.94	12.31	12.67	13.98	17.03	17.70	18.30	21.95	21.77	21.63	21.44	19.92	19.87	20.11	19.73
MgO	14.59	14.26	14.62	15.22	14.58	13.84	10.74	10.35	7.24	6.99	6.76	7.26	6.11	6.67	7.08	7.12	6.69
CaO	8.10	8.49	8.56	7.97	8.39	8.58	8.51	8.02	10.43	9.71	9.95	9.62	10.40	9.45	10.33	9.32	9.27
Na_2O	.12	.23	.12	-	.20	.13	.34	.50	1.26	.28	-	.17	.64	.37	1.06	.64	.81
Cations/12 oxygens																	
Si	2.929	2.925	2.928	2.941	2.931	2.938	2.954	3.009	3.165	2.985	3.004	2.979	3.076	2.805	3.080	2.922	2.883
Ti	.054	.054	.043	.034	.054	.044	.080	.069	.081	.046	.044	.033	.035	.383	.051	.252	.292
Al	1.993	1.990	1.990	2.018	1.995	1.978	1.976	1.936	1.733	1.938	1.946	1.973	1.869	1.850	1.830	1.825	1.870
Fe	.805	.812	.793	.749	.776	.861	1.065	1.107	1.156	1.410	1.395	1.386	1.375	1.280	1.267	1.288	1.262
Mg	1.593	1.561	1.598	1.653	1.590	1.520	1.197	1.154	.815	.800	.772	.829	.699	.764	.805	.812	.763
Ca	.636	.668	.672	.622	.658	.678	.681	.642	.844	.799	.817	.790	.854	.778	.843	.765	.759
Na	.018	.032	.017	-	.029	.019	.049	.072	.184	.042	-	.025	.095	.055	.157	.096	.120
Total	8.029	8.042	8.042	8.016	8.032	8.038	8.002	7.990	7.979	8.021	7.978	8.014	8.002	7.914	8.033	7.960	7.950
Mg #	66.6	65.9	67.0	68.9	67.4	64.0	52.9	51.0	41.3	36.1	35.6	37.4	33.7	37.4	38.9	38.7	37.7
Ca	21.0	22.0	21.9	20.6	21.8	22.2	23.2	22.1	30.0	26.6	27.4	26.3	29.2	27.6	28.9	26.7	27.3
Mg	52.5	51.3	52.2	54.7	52.6	49.7	40.7	39.7	29.0	26.6	25.9	27.6	23.9	27.1	27.6	28.4	27.4
Fe	26.5	26.7	25.9	24.8	25.7	28.2	36.2	38.1	41.0	46.9	46.7	46.1	47.0	45.4	43.5	45.0	45.3

DG-1 + 1.5% H_2O

	850°C		1000°C													
Run #	7372	7372	7550	7550	7550	7550	7550	7551	7551	7551	7551	8829	8829	8829	8229	8229	8229
SiO_2	42.73	39.58	40.46	39.90	38.29	40.13	39.67	39.31	40.11	40.16	39.61	40.69	39.30	41.08	39.79	39.15	42.23
TiO_2	.65	.85	1.03	.99	4.89	1.32	1.01	1.35	.95	1.20	3.17	1.20	2.40	1.33	1.07	3.79	1.06
Al_2O_3	19.90	21.37	21.60	21.83	20.63	21.23	21.76	21.56	21.56	20.81	20.29	20.63	20.56	20.76	21.32	20.60	19.59
FeO	15.43	20.27	17.38	17.81	18.05	18.12	17.70	16.22	17.10	17.06	16.35	18.54	18.20	18.09	18.72	18.30	17.36
MgO	8.98	7.88	8.70	9.10	8.37	8.08	8.74	9.42	9.18	8.99	9.32	8.29	8.32	7.87	8.75	8.07	8.37
CaO	10.89	10.05	10.63	10.51	9.85	10.09	10.92	11.50	10.31	10.78	10.67	10.16	10.67	10.26	10.14	9.52	10.35
Na_2O	1.41	-	.20	.10	.48	.59	.20	.65	.63	.77	.59	.49	.56	.61	.20	.58	1.03
Cations/12 oxygens																	
Si	3.186	3.012	3.039	2.998	2.890	3.041	2.993	2.961	3.020	3.034	2.981	3.073	2.982	3.094	3.010	2.964	3.171
Ti	.037	.049	.058	.056	.278	.075	.057	.076	.054	.068	.179	.068	.137	.075	.061	.216	.060
Al	1.749	1.917	1.913	1.933	1.835	1.896	1.935	1.914	1.913	1.852	1.800	1.836	1.838	1.843	1.901	1.838	1.734
Fe	.962	1.290	1.092	1.119	1.139	1.148	1.117	1.022	1.077	1.078	1.029	1.171	1.155	1.140	1.184	1.159	1.091
Mg	.997	.893	.974	1.019	.941	.913	.982	1.057	1.030	1.012	1.046	.933	.941	.884	.987	.911	.937
Ca	.870	.820	.856	.846	.797	.819	.882	.928	.832	.872	.861	.822	.867	.828	.822	.772	.833
Na	.204	-	.029	.015	.070	.087	.029	.095	.091	.112	.085	.072	.083	.090	.029	.085	.150
Total	8.005	7.981	7.961	7.987	7.949	7.980	8.997	8.053	8.016	8.028	7.982	7.976	8.003	7.954	7.994	7.944	7.977
Mg #	50.9	40.9	47.1	47.6	45.2	44.3	46.8	50.8	48.9	48.4	50.4	44.3	44.9	43.7	45.5	44.0	46.2
Ca	30.7	27.3	29.3	28.3	27.7	28.4	29.6	30.9	28.3	29.4	29.3	28.1	29.3	29.0	27.5	27.2	29.1
Mg	35.2	29.7	33.3	34.2	32.7	31.7	32.9	35.2	35.0	34.2	35.6	31.9	31.8	31.0	33.0	32.0	32.8
Fe	34.0	43.0	37.4	37.5	39.6	39.9	37.5	34.0	36.7	36.4	35.1	40.0	39.0	40.0	39.6	40.8	38.1

DG-1 + 1.5% H_2O

	1100°C						1200°C				1260°C			1300°C					
Run #	8818	8818	8818	8866	8866	8866	8808	8808	8808	8808	8865	8865	8865	8816	8816	8816	8816	8816	8816
SiO	39.88	39.44	40.08	40.89	40.93	39.50	39.88	39.87	40.30	40.62	39.74	39.82	40.37	40.21	40.67	39.92	39.75	40.18	40.47
TiO_2	1.19	1.09	.93	1.80	1.02	1.04	1.47	1.11	1.60	1.17	.88	.64	.59	.97	1.57	1.21	1.40	.81	1.59
Al_2O_3	21.27	21.80	21.32	20.22	20.71	21.39	21.27	21.57	21.17	21.37	22.17	22.42	22.48	22.48	20.24	22.00	21.98	22.74	21.37
FeO	18.13	17.80	18.39	17.19	17.62	18.54	16.87	17.81	17.22	17.07	15.08	14.52	14.22	13.27	17.31	15.03	14.68	13.83	14.94
MgO	8.91	9.30	9.01	8.36	8.76	8.52	9.41	9.06	9.09	9.18	11.01	11.44	11.45	12.52	9.85	11.07	11.13	12.54	10.61
CaO	10.41	10.56	10.16	10.61	10.46	10.55	10.78	10.37	10.41	10.10	11.02	11.06	10.80	10.44	9.89	10.77	11.00	9.91	11.03
Na_2O	.20	-	.10	.94	.51	.46	.31	.20	.21	.49	.09	.10	.10	.10	.47	-	-	-	-
Cations/12 oxygens																			
Si	3.011	2.974	3.024	3.079	3.079	2.994	2.999	3.004	3.027	3.046	2.963	2.961	2.991	2.966	3.056	2.972	2.959	2.964	3.012
Ti	.067	.062	.053	.102	.058	.059	.083	.063	.090	.066	.049	.036	.033	.054	.089	.068	.078	.045	.089
Al	1.892	1.938	1.896	1.795	1.837	1.910	1.885	1.915	1.874	1.888	1.949	1.965	1.963	1.955	1.792	1.931	1.929	1.977	1.875
Fe	1.145	1.123	1.160	1.083	1.109	1.175	1.061	1.122	1.082	1.070	.941	.903	.881	.819	1.088	.936	.914	.854	.930
Mg	1.003	1.046	1.013	.939	.983	.963	1.055	1.018	1.018	1.026	1.224	1.268	1.264	1.377	1.103	1.229	1.235	1.379	1.177
Ca	.842	.853	.821	.856	.843	.857	.869	.837	.838	.812	.880	.881	.857	.825	.796	.859	.882	.783	.879
Na	.029	-	.015	.137	.074	.067	.045	.030	.030	.071	.013	.014	.015	.014	.069	-	-	-	-
Total	7.990	7.995	7.982	7.990	7.982	8.026	7.997	7.990	7.960	7.980	8.020	8.028	8.003	8.010	7.993	7.994	7.998	8.002	7.961
Mg #	46.7	48.2	46.7	46.4	47.0	45.0	50.0	47.6	48.5	48.9	56.5	58.4	58.9	62.7	50.3	56.8	57.4	61.7	55.9
Ca	28.2	28.2	27.4	29.7	28.7	28.6	29.1	28.1	28.5	27.9	28.9	28.9	28.6	27.3	26.7	28.4	29.1	26.0	29.5
Mg	33.5	34.6	33.8	32.6	33.5	32.2	35.3	34.2	34.7	35.3	40.2	41.6	42.1	45.6	36.9	40.6	40.7	45.7	39.4
Fe	38.3	37.2	38.7	37.6	37.8	39.2	35.6	37.7	36.8	36.8	30.9	29.6	29.3	27.1	36.4	30.9	30.1	28.3	31.1

DG-1 + 5% H_2O

	1000°C		1100°C			1200°C		
Run #	8869	8867	8867	8867	8867	8868	8868	8868
SiO_2	39.76	39.24	39.23	39.49	39.42	39.65	39.79	39.35
TiO_2	.95	1.13	1.20	1.29	1.36	1.01	.98	.87
Al_2O_3	21.81	21.65	21.74	21.61	21.63	22.02	21.92	22.09
FeO	17.94	17.60	17.28	17.44	17.62	15.22	14.90	16.07
MgO	8.92	9.01	9.60	9.21	8.88	10.57	11.31	10.49
CaO	10.23	11.17	10.76	10.77	10.89	11.29	10.77	10.79
Na_2O	.40	.20	.20	.20	.20	.23	.33	.34
Cations/12 oxygens								
Si	2.998	2.966	2.958	2.978	2.976	2.963	2.966	2.951
Ti	.054	.064	.068	.073	.077	.057	.055	.049
Al	1.938	1.929	1.931	1.920	1.924	1.940	1.926	1.952
Fe	1.131	1.113	1.090	1.099	1.113	.952	.929	1.008
Mg	1.002	1.016	1.079	1.035	.999	1.178	1.257	1.173
Ca	.827	.904	.869	.870	.881	.904	.860	.867
Na	.058	.029	.029	.029	.029	.033	.048	.049
Total	8.008	8.020	8.023	8.004	7.999	8.027	8.040	8.049
Mg #	47.4	47.7	49.7	48.5	47.3	55.3	57.5	53.8
Ca	27.9	29.8	28.6	28.9	29.4	29.8	28.2	28.5
Mg	33.9	33.5	35.5	34.5	33.4	38.8	41.3	38.5
Fe	38.2	36.7	35.9	36.6	37.2	31.4	30.5	33.1

APPENDIX 3

TRACE ELEMENT ANALYSIS OF ZOISITE

The zoisite separated from the zoisite amphibolite from Tanzania, and used in the study of zoisite stability at high pressures (Chapter 3), was analyzed by spark source mass spectrometry for various trace elements (M.R. Perfit, analyst). This analysis is given in Table A3.1. The chondrite-normalized REE pattern is similar to that obtained for a plagioclase separate from an andesitic basalt (Schnetzler and Philpotts, 1970) (Fig. A3.1).

TABLE A3.1: Trace element analysis of zoisite from a zoisite-amphibolite from Tanzania

ELEMENT	ppm	ELEMENT	ppm
La	2.18	Rb	0.25
Ce	3.32	Ba	15.5
Pr	0.43	U	0.20
Nd	1.76	Th	0.19
Sm	0.42	Zr	4.40
Eu	0.73	Nb	0.57
Gd	0.58	Y	2.55
Tb	0.10	Bi	0.10
Dy	0.55	W	0.17
Ho	0.09	Sn	1.37
Er	0.24	Mo	0.36
Yb	0.27		

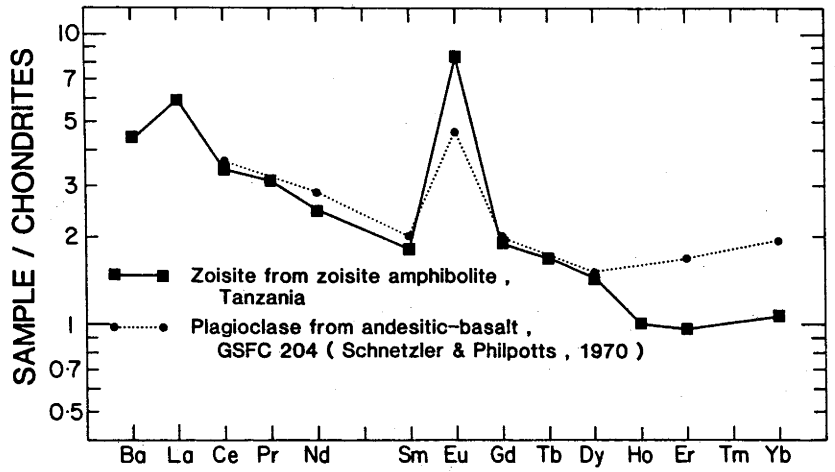

Figure A3-1. Chondrite-normalized abundances of rare earth elements in zoisite separated from a zoisite amphibolite from Tanzania. Abundances of rare earth elements in a plagioclase from an andesitic-basalt (Schnetzler and Philpotts, 1970) are shown for comparison.

REFERENCES

Schnetzler, C.C. and Philpotts, J.A. (1970) Partition coefficients of rare-earth elements between igneous matrix material and rock-forming mineral phenocrysts.II. Geochim.Cosmochim. Acta, 34, 331-340.

APPENDIX 4

PETROLOGICAL DATA CATALOGUE, BOISA ISLAND, PAPUA NEW GUINEA

D.A. GUST, R.W. JOHNSON, AND B.W. CHAPPELL

Published as: BMR Report 227, BMR Microfiche MF147 (1980)

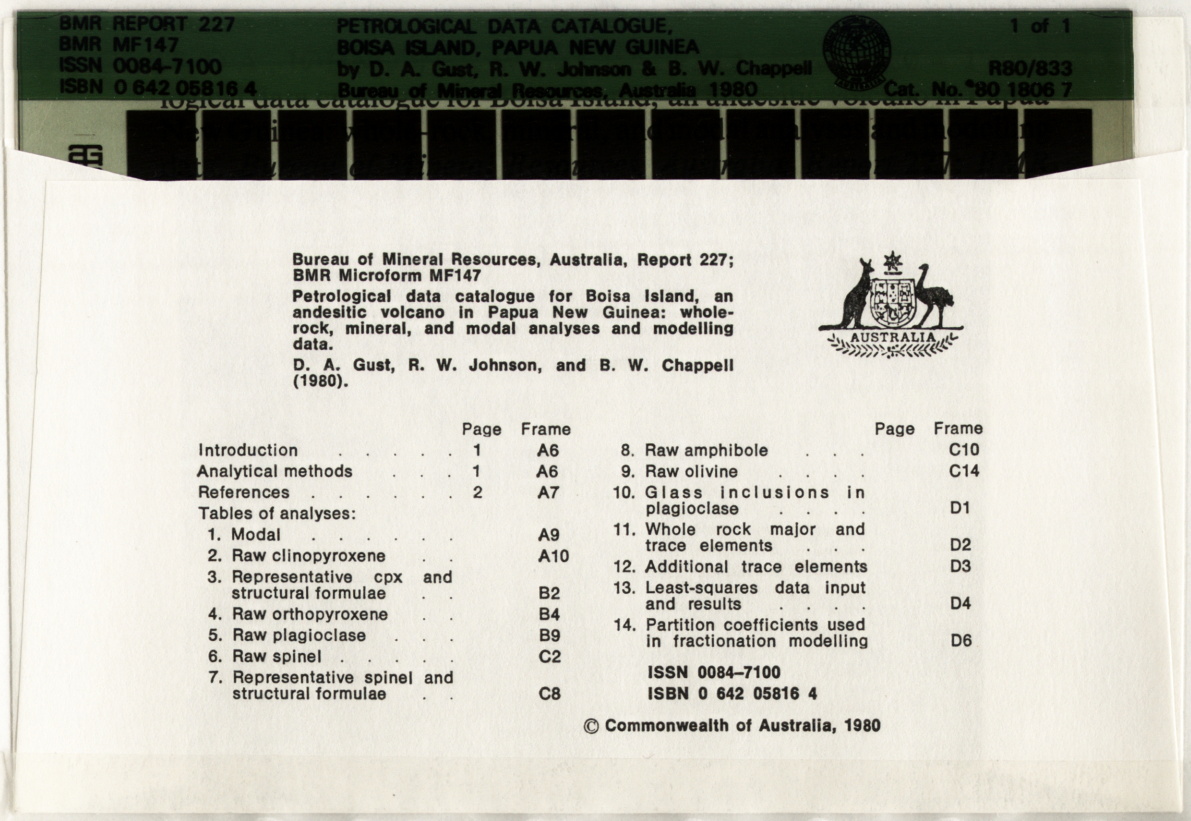

BMR REPORT 227
BMR MF147
ISSN 0084-7100
ISBN 0 642 05816 4

PETROLOGICAL DATA CATALOGUE,
BOISA ISLAND, PAPUA NEW GUINEA
by D. A. Gust, R. W. Johnson & B. W. Chappell
Bureau of Mineral Resources, Australia 1980

1 of 1
R80/833
Cat. No. 80 1806 7

Bureau of Mineral Resources, Australia, Report 227;
BMR Microform MF147

Petrological data catalogue for Boisa Island, an andesitic volcano in Papua New Guinea: whole-rock, mineral, and modal analyses and modelling data.

D. A. Gust, R. W. Johnson, and B. W. Chappell (1980).

AUSTRALIA

ISSN 0084-7100
ISBN 0 642 05816 4

APPENDIX 5

CHEMICAL CHARACTERISTICS OF ISLAND-ARC BASALTS: IMPLICATIONS FOR MANTLE SOURCES

M.R. PERFIT, D.A. GUST, A.E. BENCE, R.J. ARCULUS, AND S.R. TAYLOR

Published in: Chemical Geology, 30 (1980) 227 - 256.

Chemical Geology, 30 (1980) 227—256
Elsevier Scientific Publishing Company, Amsterdam — Printed in The Netherlands

CHEMICAL CHARACTERISTICS OF ISLAND-ARC BASALTS: IMPLICATIONS FOR MANTLE SOURCES

M.R. PERFIT[1], D.A. GUST[1], A.E. BENCE[2], R.J. ARCULUS[1] and S.R. TAYLOR[1]

[1] *Research School of Earth Sciences, Australian National University, Canberra, A.C.T. 2600 (Australia)*
[2] *Department of Earth and Space Sciences, State University of New York, Stony Brook, NY 11794 (U.S.A.)*

(Accepted for publication June 30, 1980)

ABSTRACT

Perfit, M.R., Gust, D.A., Bence, A.E., Arculus, R.J. and Taylor, S.R., 1980. Chemical characteristics of island-arc basalts: implications for mantle sources. In: R.W. Le Maitre and A. Cundari (Guest-Editors), Chemical Characterization of Tectonic Provinces. Chem. Geol., 30: 227—256.

Major-element, trace-element and isotopic compositions of approximately 1200 basalts (<53 wt.% SiO_2) from intra-oceanic island arcs have been compiled to assess the nature and possible sources of primitive island-arc basalts (IAB). The chemical characteristics of IAB are examined with reference to those of mid-ocean ridge basalts (MORB) and intra-plate oceanic basalts (IPB). Major-element compositions of primitive [$Mg/(Mg+Fe^{2+}) > 65$] IAB and MORB are similar, but differ significantly from IPB. In general, IAB do not have higher Al_2O_3, lower TiO_2 or a lack of Fe enrichment compared to primitive MORB but many do have greater K_2O contents. Differences in major- and minor-element contents between more evolved IAB and MORB result from the dominance of plagioclase + olivine crystal fractionation in MORB magmas vs. clinopyroxene + olivine controlled fractionation in IAB suites. This difference in crystallization history may be related to the higher P_{H_2O} or greater depth of crystallization of IAB magmas compared to those inferred for MORB.

IAB are characteristically enriched in large-ion-lithophile (LIL) elements and depleted in high-field-strength ions (e.g., Zr, Nb and Hf) relative to normal MORB (N-type) and IPB. The enrichment of some LIL elements (e.g., Sr, Rb, Ba and Pb) relative to the rare-earth elements in IAB is difficult to explain by simple partial melting alone and suggests a multi-stage petrogenesis involving an LIL-enriched component. Low abundances of high-field-strength ions in evolved IAB are explicable in terms of fractional crystallization, but the cause for consistently low abundances in primitive IAB remains problematic.

Island-arc lavas contain greater concentrations of volatiles and have higher CO_2/H_2O and Cl/F ratios than either MORB or IPB, suggesting involvement of a slab-derived volatile component. However, this is not consistent with $^3He/^4He$ data which indicate that only near-trench volcanics have been significantly affected by dehydration of the oceanic crust.

Sr-, Nd-, Pb- and O-isotopic data, in conjunction with the trace-element data, clearly indicate that IAB are derived from heterogeneous, LIL-depleted mantle sources most similar to those which give rise to enriched MORB (E-type). The marked shift towards higher $^{87}Sr/^{86}Sr$ in IAB compared to oceanic lavas with similar $^{143}Nd/^{144}Nd$ values cannot be explained simply by the addition of radiogenic Sr from the slab. Variable degrees of contamination from a crustally-derived sedimentary component is consistent with the

0009-2541/80/0000—0000/$02.25

isotopic and trace-element data from a number of arcs. However, the lack of correlation between LIL/REE ratios and more radiogenic isotopic ratios suggests that this enrichment/contamination process is complex. A multi-stage petrogenetic model involving subducted oceanic crust (± sediments), dehydration/volatile transfer, and partial melting of metasomatized mantle beneath island arcs is considered the most reasonable, although least constrained, method to generate a variety of primitive IAB.

INTRODUCTION

Basalts represent a major portion of the igneous rocks generated on Earth and apparently, on extra-terrestrial bodies. Their major-element, trace-element and isotopic compositions can provide us with much information about the nature and history of their sources provided we can decipher the physical and chemical processes involved during magmatic evolution (i.e. partial melting, fractionation, mixing, contamination). In order to aid understanding of the processes involved in basalt generation and the characteristics of their sources, it is instructive to examine the chemical variability of a large number of samples from specific tectonic environments. In general, basalts erupted in different tectonic regimes have particular chemical characteristics that serve to distinguish them from one another (e.g., Pearce and Cann, 1973; R.C.O. Gill, 1979; Pearce and Norry, 1979; Wood et al., 1979a; Bence et al., 1980a) as well as minor, but significant, differences between basalts from a single tectonic province such as the North Atlantic (e.g., Schilling, 1975; Flower and Robinson, 1979; Tarney et al., 1979; Wood et al., 1979b).

The basalt—andesite—dacite—rhyolite association of orogenic suites is second in volumetric importance only to mid-ocean ridge basalts (MORB) in the terrestrial volcanic environment. Orogenic lavas may be divided into those occurring in island arcs and those from continental margins. The distinction between the two groups is not entirely clear, given that many of their chemical characteristics overlap and that some arcs are situated in regions that have quasi-continental crustal structure (e.g., Japan, New Zealand). It appears, however, that many lavas erupted through thick (often old) continental crust are affected by upper-crustal contamination (e.g., James et al., 1976; Briqueu and Lancelot, 1979) thus altering their primary chemical characteristics. With this in mind, discussion will be limited to those basalts from intra-oceanic or quasi-continental environments where crustal contamination has been least likely.

This paper examines the major-, minor- and trace-element (where available) variations in island-arc basalts ($<53\%$ SiO_2) and illustrates some of the chemical regularities that exist despite their wide spatial distribution and differences in major-element chemistry. The data ($\sim$1200 analyses) were taken from the literature and our own unpublished work (primarily from Papua New Guinea, Lesser Antilles, Aleutians). Major contributions to the data base are from the Lesser Antilles (36% of total), Japan—Kuriles (15%), Papua New Guinea (13%), New Hebrides (8%), Aleutians (7%) and Indonesia (7%). A list

of the number of analyses and sources of data for each island arc is available from the authors.

Bence et al. (1979, 1980b) have examined the major- and minor-element chemistry of MORB crystalline basalts and basaltic glasses and reviewed similar data for intra-plate basalts. Trace-element variations in MORB have also been discussed in numerous publications (e.g., Kay and Hubbard, 1978; Flower and Robinson, 1979; Sun et al., 1979; Tarney et al., 1979; Wood et al., 1979b, c). This paper relies heavily upon these publications for comparison of the major-, minor- and trace-element chemistry of IAB with MORB.

The obvious spatial relationship between island-arc magmatism and subduction of oceanic plates suggests a genetic link between the two. To date, however, the physical and chemical effects of the subducted slab on the geochemical characteristics of arc magmas is enigmatic. In intra-oceanic arc environments there are at least three different potential sources that can be involved in the generation of island-arc basalts: (1) subducted oceanic crust, with or without the sediment trapped between basalt flows or lying on top of the crust; (2) mantle material in the wedge above the subducted slab; (3) the basement of an arc, which might be pre-existing oceanic crust, earliest formed island-arc material and/or crust derived from the metamorphism and possible melting of subducted sediments. Numerous arguments for and against each of these regions being the sole source for arc magmas have appeared in the literature. More recently, comprehensive investigations of trace-element abundances and isotopic systematics have placed severe constraints on any one source being the sole contributor to arc magma genesis (e.g., J.B. Gill, 1974, 1978; Lopez-Escobar et al., 1977; Kay, 1980).

Our understanding of the processes that occur in and above subducted oceanic crust is in its infancy. A good deal more confidence can be placed on our knowledge about the sub-oceanic mantle, based primarily on studies of MORB and intra-plate basalts (i.e. oceanic islands and seamounts). Intra-oceanic arcs *may* involve mantle sources similar in composition to sub-oceanic mantle from which MORB and intra-plate basalts (IPB) are generated by the process of partial melting. It is important therefore, to compare the chemistry of IAB with MORB and IPB.

PRIMITIVE MAGMAS AND SOURCES

Island-arc magmatism embraces a diversity of rock types ranging in composition from basalt to rhyolite. There is considerable debate regarding the relative proportions of rock types and the composition of parental magmas in island arcs. In many arcs, basaltic andesite and andesite are the most voluminous rocks sampled (Ewart, 1976), however, Arculus and Johnson (1978) pointed out that surface sampling may not be representative of the entire arc since a great portion of the islands are unexposed or submarine. Petrologic and geochemical evidence suggest the development of basalt—andesite—dacite suites by low-pressure fractional crystallization of primary

basaltic magmas in a number of island arcs (Heming, 1974; Gorton, 1977; Tarney et al., 1977; Katsui et al., 1978; Perfit, 1978; Stern, 1979; Arculus and Wills, 1980; Perfit et al., 1980). In such arcs where basalts are associated with more fractionated rock types (which may even be more voluminous), and there is sufficient evidence to involve fractional crystallization, it seems unnecessary to require a primary andesitic melt. Thus, we consider only the chemical characteristics of basalts, suggesting that they provide the best estimate of the distinctive features of island-arc magmatism.

Partial melting (20—30%) of mantle lherzolite (Mg-number = 90) should yield basaltic magmas with high Mg-numbers ($[Mg/Mg+Fe^{2+}] \times 100 = 70—74$), high Ni contents (250—350 ppm) and high Cr concentrations (500—600 ppm) (Green et al., 1974; Green, 1976; Hanson and Langmuir, 1978; Bence et al., 1979; Sun et al., 1979). Most terrestrial basalts have undergone some olivine fractionation as indicated by Mg-numbers <70 and Ni contents <250 ppm (Nicholls and Whitford, 1976; Clarke and O'Hara, 1979; Bence et al., 1980). Only ~19 of the IAB compiled here contain >15 wt.% MgO (see Fig.1A) and many of these appear to have accumulated olivine. Few IAB have Mg-numbers >70 (see Fig.1B) and those which do generally have Ni contents <150 ppm. The average Mg-number (57.4 ± 10.4, n = 1172) of IAB is similar to that of MORB glasses (58.6, Wilkinson, in press) and most crystalline MORB and IPB range between 55 and 65 (Wilkinson, in press). Ni and Cr contents at equivalent Mg-numbers are also lower in IAB than OFB and IPB* (Pearce, 1975; R.C.O. Gill, 1979). Such data suggest that even the most primitive rocks from island arcs represent derivative melts. Hence, although we believe that relatively primitive magmas can be identified in island arcs, the majority of IAB have suffered fractionation. In the following sections we argue that the effects of such fractionation can be accounted for and that the use of a large data base of all basalts yields significant information on the distinctive features of island-arc magmas and their sources.

Compositions of IAB believed to be the most primitive parental basalt from six island arcs are presented in Table I. Also shown for comparative purposes are primitive MORB and IPB. Aside from differences in alkali content, the major-element compositions are surprisingly similar for the most primitive MORB and IAB. The estimated parental magma for IPB from Hawaii is, however, significantly different. The convergence of primitive IAB and MORB major-element compositions suggests that the sources of these magmas may in fact be similar.

MAJOR-ELEMENT CHARACTERISTICS

Comparison of the major-element geochemistry of IAB with basalts from other tectonic regimes is meaningful only if the effects of fractional crystal-

*Note that Mg-numbers have been calculated with Fe_2O_3 set at 0.1 of the total Fe. There is much evidence to suggest that IAB have much higher intrinsic Fe_2O_3 which would increase the Mg-numbers but accentuate the Ni and Cr anomaly.

TABLE I

Parental magma compositions

Reference*[1] No.	*1* *527-1-1*	*2* V30-RD8 P12	*3* *3-14*	*4* Ch43-23	*5* IA-5	*6* *505*	*7* *1741*	*8* TB2/3	*9* *8014*	*10* MK15	*11* GU-1	*12* H-est.	*13* Avg.
SiO_2 (wt.%)	49.1	49.33	49.7	49.5	49.2	49.40	51.0	50.75	48.65	51.2	51.13	48.0	51.56
TiO_2	0.62	1.20	0.72	0.81	0.52	0.70	0.93	0.81	0.82	0.75	0.76	2.2	0.89
Al_2O_3	16.5	16.27	16.4	15.7	15.3	13.29	13.6	18.03	19.17	15.69	19.46	11.0	17.51
FeO^{*}(*[2])	8.78	8.35	7.89	7.45	9.00	10.15	8.11	7.97	8.79	9.21	9.10	11.0	9.25
MnO	0.15	0.15	0.12	0.15	0.18	0.20	0.14	0.15	0.16	0.16	0.16	—	0.17
MgO	10.3	8.04	10.1	10.0	10.1	10.44	12.5	5.19	5.64	9.64	4.69	14.5	6.19
CaO	12.4	12.34	13.2	13.0	13.0	12.22	7.92	10.43	12.81	10.12	11.48	9.0	10.35
Na_2O	1.92	2.44	2.00	1.95	1.51	2.16	2.67	3.23	2.20	2.77	2.38	2.0	2.65
K_2O	0.07	0.36	0.01	0.17	0.17	1.06	2.37	2.28	0.50	0.42	0.40	0.4	0.85
P_2O_5	0.06	0.17	—	0.08	0.06	0.20	0.59	0.27	0.13	0.21	0.13	—	0.19
Mg-number*[3]	70	66	72	73	69	68	75	57	56	68	51	70	57
Ni (ppm)	232	121	320	249	119	150	340	27	34	91	28	—	—
Cr	510	—	480	960	386	490	608	38	25	337	30	—	—
V	140	—	—	—	258	380	210	276	294	271	313	—	—
Sc	34	—	—	36	42	36	25	29	—	—	32	—	—

*[1] *References: 1* = Bender et al. (1978), ocean-floor tholeiite, FAMOUS area, Mid-Atlantic Ridge; *2* = Shibata et al. (1979), ocean-floor tholeiite, Oceanographer Fracture Zone, Mid-Atlantic Ridge; *3* = Frey et al. (1974), ocean-floor tholeiite, Western Atlantic Ocean; *4* = Dungan and Rhodes (1978), ocean-floor tholeiite, 45°N Atlantic Ocean; *5* = Taylor et al. (1980), island-arc tholeiite, Kimbe Island, New Britain; *6* = Gorton (1977), island-arc basalt, Aoba Island, New Hebrides; *7* = Mackenzie (1976), high-K olivine basalt, Mount Hagan, Papua New Guinea; *8* = Wallace et al. (in press), potassic trachybasalt, Tatau Island, Tabar Group, Papua New Guinea; *9* = Heming (1974), high-alumina basalt, Rabaul Caldera, New Britain; *10* = Perfit (1978), olivine basalt, Makushin Volcano, Unalaska Island, Aleutians; *11* = Dixon and Batiza (1979), high-alumina basalt, Guyuan Island, Marianas; *12* = Bence et al. (1980b), estimated parental basalt for Kilauea tholeiites, Hawaii; and *13* = Ewart (1976), average island-arc basalt.

*[2] FeO^{*} = FeO total

*[3] Mg-number calculated with Fe_2O_3= 0.1 FeO^{*}.

232

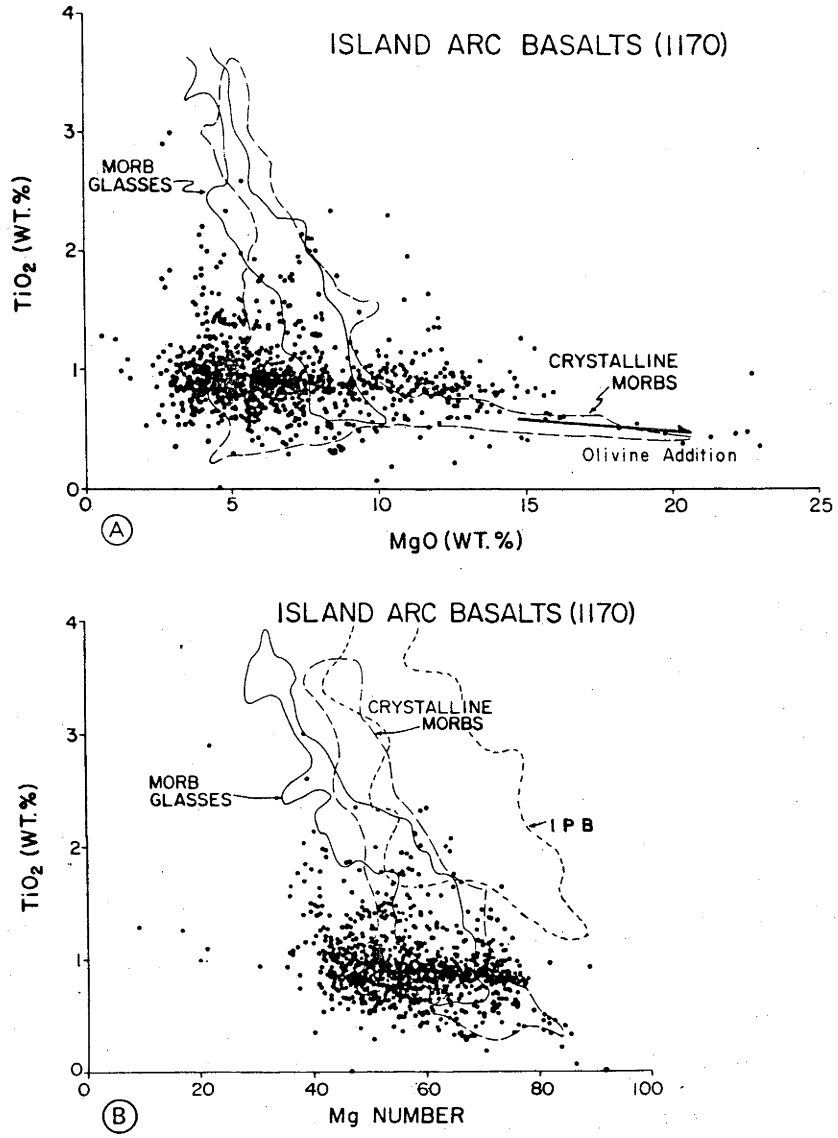

Fig. 1. A. TiO_2 vs. MgO variation diagram for island-arc basalts (IAB). Fields for ~1100 ocean-floor basalt glasses (MORB glasses) and ~ 1300 crystalline ocean-floor basalts (MORB) from Bence et al. (1979). Relative direction of chemical change is indicated for olivine accumulation.
B. TiO_2 vs. Mg-number for IAB. Fields for MORB glasses, crystalline ocean-floor basalts from Bence et al. (1979) and ~600 intraplate basalts (IPB) from Bence et al. (1980a) are outlined for comparison.

lization are adequately assessed. Although these effects are known generally (e.g., Wilcox, 1979), they are complicated by differences in the physical conditions of crystallization and the initial composition of the parental magma.

Variations in basaltic chemistry are often examined with respect to MgO or Mg-number since decreasing values reflect fractionation of liquidus or near-liquidus ferromagnesian phases (Bowen, 1928). The chemical variation found, for example in MORB glasses, corresponds to a liquid-line-of-descent involving olivine (±spinel) and olivine + plagioclase (Bender et al., 1978; Bence et al., 1979) and in some instances, plagioclase + clinopyroxene (Walker et al., 1979). Crystalline MORB, however, exhibit much more variation in chemistry than the glasses due to the effects of crystal accumulation, but in general reflect a similar liquid-line-of-descent. In general, IAB glasses are uncommon and the crystalline basalts have higher phenocryst contents than do crystalline MORB. Thus the effects of accumulation on their chemistry may be more marked and variations with respect to Mg content more erratic. The criteria for recognizing crystal accumulation are not well established (Clarke and O'Hara, 1979) so these effects are difficult to assess. We therefore include in the presentation of variation diagrams of IAB, fields of MORB glasses and crystalline basalts (Bence et al., 1979) and in some cases crystalline IPB (Bence et al., 1980a), to aid in comparing the possible petrogenetic histories of these different basalts.

A majority of IAB have TiO_2 contents of less than 1.2 wt.% which increases slightly with decreasing MgO (Fig. 1A). IAB and MORB with Mg-numbers ~70 have comparable TiO_2 concentrations (0.4—1.2 wt.%) but IPB have distinctly higher contents (1.5—2.5 wt.%) (Fig. 1B). Small differences in TiO_2 in primitive IAB and MORB may reflect differences in the degrees of partial melting (10—30%) of similar sources. However, the 6-fold enrichment of Ti in MORB cannot be explained by fractional crystallization alone, consequently multiple sources with low to moderate TiO_2 are implied for MORB (Hanson and Langmuir, 1978; Bence et al., 1979). The greater enrichment of TiO_2 in IPB compared to IAB and MORB must also reflect inherent differences in the Ti contents of IPB sources (Bence et al., 1980a). Increasing Ti with decreasing MgO in MORB glasses is consistent with olivine ± plagioclase ± clinopyroxene fractionation. The consistently low titanium trend in IAB is compatible with a petrogenesis involving a Ti-bearing phase (e.g., phlogopite, amphibole, Fe—Ti-oxide) as a liquidus or near-liquidus phase.

IAB have a wide range of Al_2O_3 contents (13—18 wt.%) and overlap with the fields defined by MORB glasses and crystalline MORB on an Al_2O_3—MgO diagram (Fig. 2). The majority of MORB with Al_2O_3 contents greater than 18 wt.% show effects of plagioclase accumulation whereas IAB with high MgO contents, show little or no effects of plagioclase accumulation. The field defined by MORB glasses (15—18 wt.%) overlaps with the IAB field at high MgO contents but the fields diverge at lower MgO contents (Fig. 2). This decreasing Al_2O_3 with MgO in MORB again reflects strong plagioclase + olivine (±clinopyroxene) control; whereas the opposite trend in IAB suggests

234

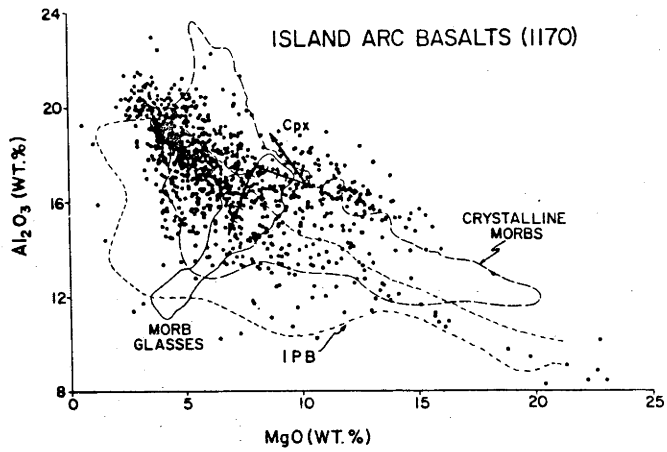

Fig. 2. Al_2O_3 vs. MgO for IAB with fields of MORB glasses, crystalline MORB and IPB. Calculated crystal fractionation paths for a FAMOUS basalt composition (see Table I) from Bence et al. (1979) for 30% crystallization: 6% olivine and 24% olivine + plagioclase in the proportion 1: 2. Direction of fractionation path due to clinopyroxene fractionation is also shown.

a lack of plagioclase controlled fractionation. Compared with IAB, IPB contain less Al_2O_3 at comparable MgO but display a similar Al_2O_3 enrichment with decreasing MgO (Fig. 2). The initially low concentrations in IPB may reflect either source differences or the presence of a residual aluminous phase (i.e. garnet or spinel) after partial melting (Bence et al., 1980a). The similar Al_2O_3 trend of IPB also argues for an absence of plagioclase fractionation. Thus, although the overall Al_2O_3 contents of IAB resemble MORB, their subsequent petrogenetic history is more like IPB. Generalizations which have stressed high primary alumina contents of IAB as a distinctive feature from OFB are not valid and reflect solely the consequences of plagioclase-absent fractionation.

Total iron (as FeO) concentrations in IAB range from ~6 to 15 wt.%, similar to that of crystalline MORB but consistently lower than in IPB (Fig. 3). Parental IAB have FeO contents (~8—10 wt.%) equivalent to those observed in primitive MORB glasses. FeO varies inversely with MgO in MORB glasses but is extremely variable in crystalline MORB and IAB. There is a general increase in FeO/MgO with increasing SiO_2 in IAB; a characteristic which is supposedly uncharacteristic of island-arc lavas in general. In fact, a majority of the IAB samples plot in the tholeiitic field defined by Miyashiro (1974) on a SiO_2—FeO/MgO diagram. Fe enrichment trends, characteristic of tholeiitic MORB and IPB, are also observed in IAB (Fig. 4). It is important to note that there is a slight increase in total alkalis with increasing FeO in IAB and crystalline MORB and that the trend of constant FeO/MgO with alkali enrichment is not developed until more differentiated rocks are formed.

MgO in IAB ranges from ~23 wt.% to less than 2 wt.%, with a majority of

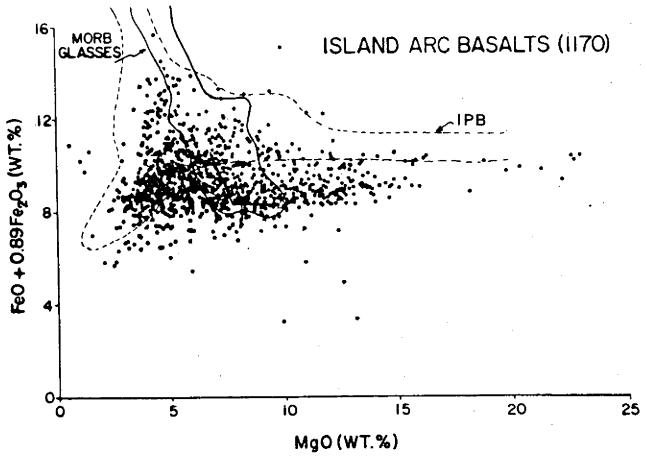

Fig. 3. Total FeO vs. MgO variation diagram. Fractionation path as explained in the caption to Fig. 2.

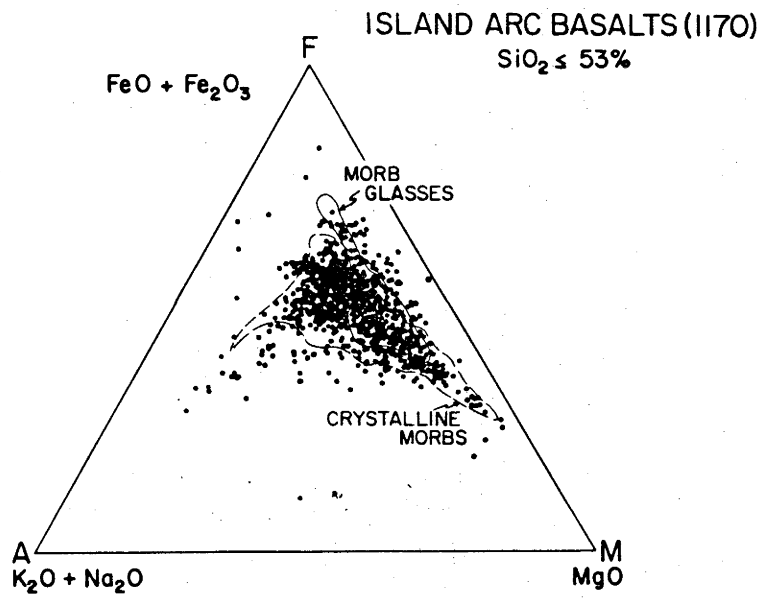

Fig. 4. *AFM* (K_2O+Na_2O — $FeO+Fe_2O_3$ — MgO) variation diagram for IAB.

samples between 3 and 13 wt.%. Few MORB contain <5 wt.% MgO, whereas, many IAB have MgO < 5 wt.%. Since parental MORB and IAB have comparable FeO and MgO contents; the overall shift towards lower Mg-numbers in IAB may be a consequence of the dominance of fractionating ferromagnesium phases in island-arc magmas compared to plagioclase-dominated crystal fractionation in MORB.

The abundance of alkalis in IAB is extremely variable. IAB have been clas-

sified as tholeiitic, calc-alkalic and alkalic as defined by their K_2O- or $(Na_2O + K_2O)$-values. Although the classification of IAB into artificial rock associations is often meaningless (Arculus and Johnson, 1978; Johnson et al., 1978), it illustrates the wide range in alkalinity of IAB. The most significant major-element difference, however, between IAB and MORB is the extremely low K_2O contents in MORB. MORB have K_2O concentrations less than 1 wt.% with many samples having less than 0.25 wt.%, whereas IAB range from ~0.25 wt.% to greater than 8 wt.% with a majority containing less than 2 wt.% (Fig. 5). Na_2O on average, is only slightly higher (<4 wt.%) in IAB than MORB (<3 wt.%). Na and K contents of IPB are similar to IAB. Plagioclase fractionation and magma mixing may effectively keep alkali contents low in MORB suites. Conversely, alkali enrichment in IAB suggests that an alkali-rich phase (i.e. plagioclase, phlogopite, amphibole) was not a dominant phase crystallizing in most IAB suites.

IAB and island-arc lavas, in general, have restricted CaO/Al_2O_3 ratios which show positive correlation with MgO. Increasing CaO/Al_2O_3 with decreasing MgO, observed in MORB can be attributed to fractional crystallization of olivine (~6%) followed by olivine + plagioclase (~24%; molar proportions 1:2) (Bence et al., 1979) (Fig. 6).

The compositions of IAB, recast into normative end members (olivine, plagioclase, high-Ca pyroxene, quartz and spinel) and projected in a pseudo-quaternary system Ol—Plag—Cpx—Qtz [see Bence et al. (1979) for discussion of this procedure], illustrate further these crystal—melt controls. IAB show a great deal of scatter on both the normative Pyx—Plag—Ol (Fig. 7) and ternary subprojections of Ol—Plag—Qtz (Fig. 8), in contrast to MORB glasses which define narrow fields corresponding to the experimentally determined olivine + plagioclase cotectic. The immense scatter of IAB suggest a lack of plagioclase

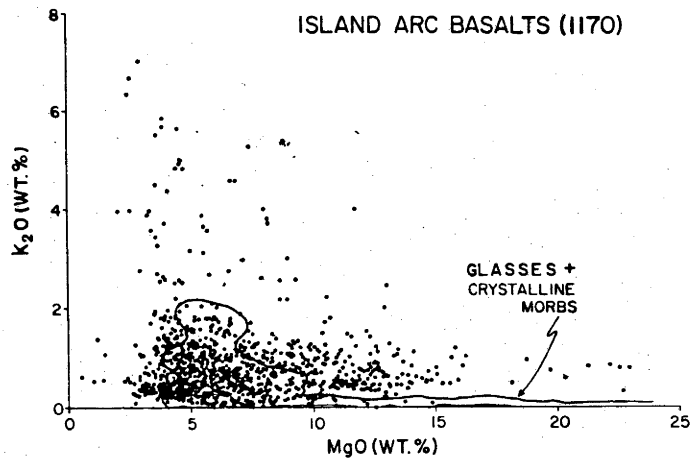

Fig. 5. K_2O vs. MgO variation in IAB. K_2O variation in crystalline MORB plus MORB glasses is outlined.

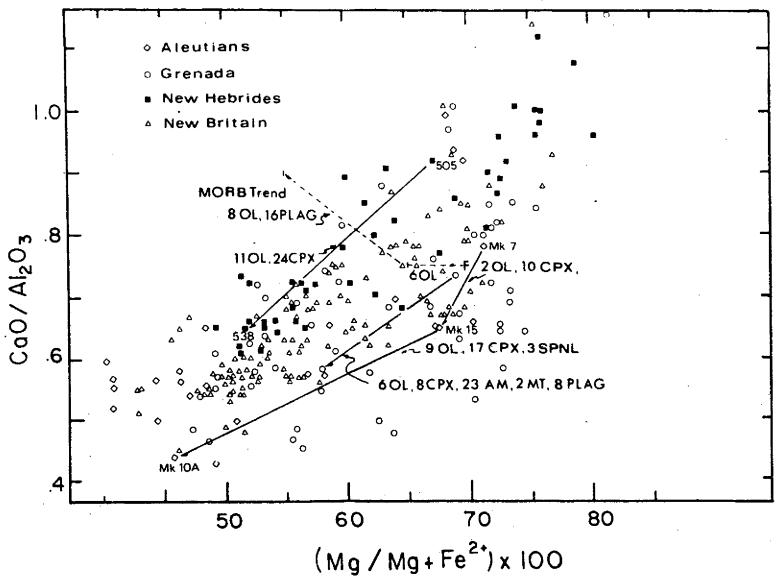

Fig. 6. CaO/Al_2O_3 vs. Mg-number for selected IAB suites. Calculated fractionation paths were determined by least-squares modelling of all the major elements. The values next to each mineral name refer to weight percent of that mineral subtracted from a parental liquid. Data are from Papua New Guinea; the New Hebrides (Gorton, 1977); Witu Islands (Johnson and Arculus, 1978); Aleutians (Perfit, 1978) and Grenada, Lesser Antilles (Arculus, 1976). FAMOUS basalt composition (F) and fractionation trends are from Bence et al. (1979) (see caption to Fig. 2).

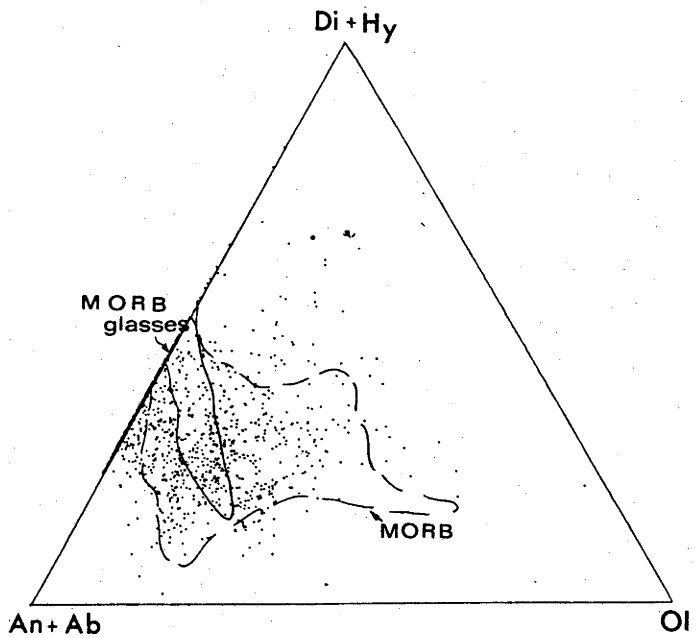

Fig. 7. Normative proportions of pyroxene, plagioclase and olivine for IAB. MORB glasses plot in the vicinity of the inferred plagioclase—olivine cotectic.

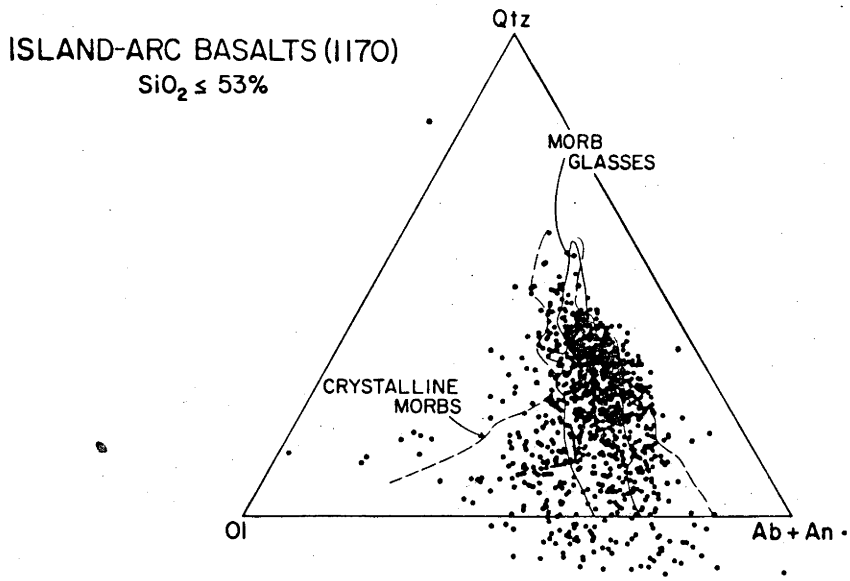

Fig. 8. Subprojection olivine—quartz—plagioclase in the olivine—quartz—clinopyroxene—plagioclase pseudo-quaternary [see Bence et al. (1979) for details of projection]. *Solid line* is the equilibrium liquid line of descent for a FAMOUS basalt from Bender et al. (1978).

control. Individual IAB suites (e.g., New Hebrides, New Britain, Japan), however, reveal systematic trends on the Ol—Cpx—Qtz subprojection (see Walker et al., 1979) which correspond to olivine (± spinel) and olivine + clinopyroxene (± spinel) fractional crystallization. More complex processes (magma-mixing, crystal accumulation) rather than simple fractional crystallization may be responsible for the scatter of IAB data on these projections but need to be investigated in detail.

TRACE-ELEMENT VARIATIONS

The abundances and relative proportions of trace elements, in particular the incompatible*, large-ion-lithophile (LIL) elements, are especially sensitive to crystal fractionation, melting processes and source composition provided they are not a major stoichiometric component in a minor refractory phase. Therefore, they provide information not readily obtainable from the major-element data. In contrast, the ferromagnesian elements are not useful indicators of melting percentages but are sensitive to small degrees of fractionation of Fe—Mg-silicates and -oxides and to source abundances.

The anomalously-low concentrations of Ni and Cr in IAB compared to those of MORB and IPB at similar MgO levels have been discussed previously. We

*Called HYG (hygromagmatophile) by Treuil and Varet (1973) to refer generally to elements with a bulk solid/liquid distribution coefficient less than 0.1 in the generation of basaltic melts.

wish to emphasize that even parental IAB basalts with high MgO contents and low Ni contents (~100 ppm) cannot be explained by an increased D_{Ni}^{Ol} during olivine fractionation in low MgO melts (Hart and Davis, 1978). Other ferromagnesian elements such as Co and Sc are only slightly less abundant, whereas V (100—400 ppm) is often more abundant in IAB than in MORB or IPB. High V/Ni, Co/Ni and V/Cr ratios distinguish IAB from other basalt types (Taylor et al., 1980). Ni and Cr contents drop to very low levels in basalts due to the initial crystallization of olivine, clinopyroxene and Cr-spinel while V and Sc appear to remain at fairly constant levels until the onset of magnetite and/or amphibole fractionation in more differentiated liquids (J.B. Gill, 1978). Note, however, that the K_d for V between magnetite and melt is strongly dependent on the f_{O_2} of the equilibrium (Lindström, 1976). Ratios of ferromagnesian elements thus appear to reflect different crystallization histories in MORB, IPB and IAB and possibly f_{O_2} differences prevailing during crystallization.

The LIL elements and the rare-earth elements (REE) are extremely variable in island-arc basalts. In general, there are: (1) positive correlations between alkalinity, LIL and REE abundances in different rock suites; and (2) negative correlations between MgO content, LIL and REE within individual rock suites. The later trend is readily explained by enrichment of the incompatible elements during fractional crystallization. Sr is a major exception to the above generalizations, in that it varies considerably between suites and may not vary regularly within a suite (J.B. Gill, 1978). Absolute abundances of LIL elements such as Ba, Rb, Sr, Cs and Pb are commonly greater in IAB than in normal (N-type) MORB. In most arcs, an enrichment of these elements mimics that of K_2O.

It is noteworthy, that MORB from "plume" regions (E-type) and marginal basins have K, Ba, Sr, Cs and Rb abundances that overlap with those in certain low-K IAB (J.B. Gill, 1976; Hawkins, 1976; Tarney et al., 1977; Johnson and Arculus, 1978; Lordkipanidze et al., 1979; Saunders and Tarney, 1979; Sun et al., 1979; Weaver et al., 1979; Taylor et al., 1980). The ranges of Rb/Sr (0.01—0.05) and K/Rb (240—1100) in IAB, likewise overlap with those in MORB and IPB at each extreme (Sun et al., 1979; Chow et al., 1980). A majority of MORB (N-type) have K/Rb and K/Ba distinctly higher than in IAB because of the low concentrations of Rb and Ba in MORB (see Fig. 11, p. 242).

Chondrite-normalized REE patterns of IAB vary from relatively flat ($La/Yb_{ch} \simeq 1$, in low-K basalts to light-REE enriched ($La_{Ch} \simeq 20$—100, $Yb_{Ch} \simeq 6$—30) in basalts with moderate to high K. The most alkaline IAB generally exhibit the greatest light- — to heavy — REE fractionation and rarely show mild heavy-REE depletions (e.g., Grenada, Arculus, 1976; Papua New Guinea highlands, Mackenzie, 1976). N-type MORB have distinct light-REE depletions ($La/Sm_{Ch} = 0.4$—0.7) whereas E-type MORB show significant light-REE enrichments ($La/Sm_{Ch} \simeq 1$—4.8) so as to have REE patterns indistinguishable from many IAB and IPB.

Although the large cations and REE in basalts from these three tectonic

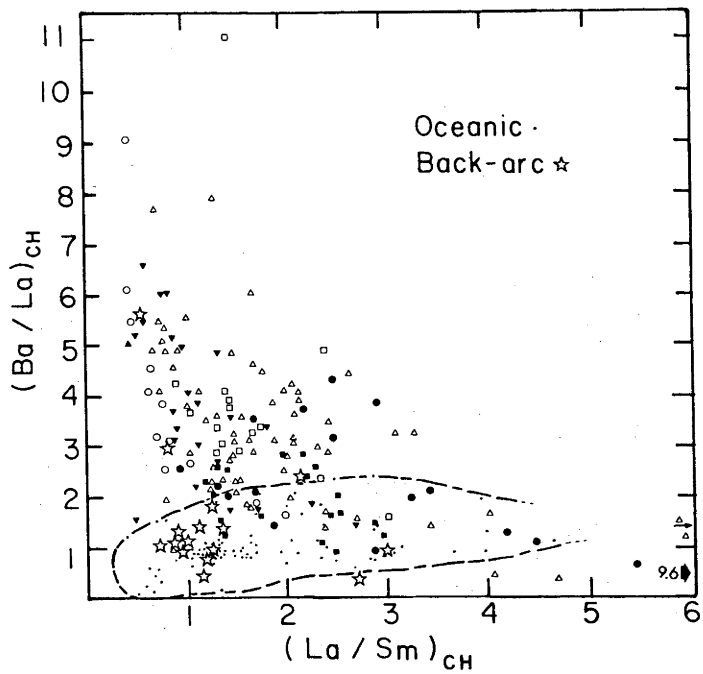

Fig. 9. $(Ba/La)_{Ch}$ vs. $(La/Sm)_{Ch}$ adapted from Kay (1980). Oceanic basalts include MORB and IPB. The data are from Kay (1980) and sources in the caption to Fig. 11. Symbols for IAB are as in Figs. 10 and 11. Low-K basalts from back-arc, marginal-sea environments are indicated by *stars* (Gill, 1976; Hawkins, 1976; Tarney et al., 1977; Taylor et al., 1980). 85 samples comprise the oceanic field.

settings can have comparable values, there is an enrichment of Ba, Rb, Cs, Pb, K and U relative to REE in IAB that distinguishes these lavas from MORB and IPB (Kay, 1977; Sun, 1979). Plots of chondrite normalized Ba/La (= Ba/La_{Ch}) and Pb/La_{Ch} against La/Sm_{Ch} clearly show this feature (Fig. 9). N-type MORB with depleted light-REE patterns have $Ba/La_{Ch} < 1.5$. This ratio increases to a maximum of 2 with increasing light-REE fractionation, characteristic of E-type MORB and alkalic IPB. In contrast Ba/La_{Ch} ratios of IAB with relatively flat REE patterns are generally >2 and may be as great as 10. As REE fractionation increases in more alkaline IAB, there is a gradual decrease in Ba/La_{Ch} to a point where the IAB field overlaps the oceanic field. A few low-K, low La/Sm arc basalts that are tectonically associated with back-arc marginal basins (e.g., Witu Islands, Johnson and Arculus, 1978; Bransfield St., Weaver et al., 1979) plot in the oceanic field. Conversely, a few samples from marginal basins lie within the arc field (see Fig. 9). A plot of TiO_2 vs. Ba/La_{Ch} (Fig. 10) clearly discriminates IAB from MORB and IPB which Fig. 9 does not do.

The trace elements Y, Tb, Zr, Hf, Nb, Ta and Th have high charge/ionic radius ratios and consequently tend to be incompatible with respect to common basalt and peridotite minerals. This group of trace elements is characteristically depleted in IAB relative to IPB and many MORB. The low abundances of these

elements show only slight variation between different types of IAB and do not correlate with other incompatible elements (LIL) as they do in MORB and IPB. Nb vs. Ba (Fig. 11) illustrates this point and suggests that different Nb/Ba ratios reflect heterogenous source compositions. Crystal fractionation or partial melting of a common source cannot generate such large differences in incompatible element ratios. The concentrations of Ti, Zr, Y, Nb, Ta, Hf and Th have been successfully used to discriminate basaltic rocks from differing tectonic settings (Pearce and Norry, 1979; Wood et al., 1979c). These authors have compared the abundances of the above elements in basalts from a variety of regions and concluded that: (1) most IAB have lower absolute abundances of Ti, Zr, Nb and Ta than all types of MORB and IPB (which have the greatest abundances); and (2) IAB have the lowest Nb/Zr, Ti/Y, Zr/Y, Ta/Hf ratios whereas IPB have the highest. An example of the Ti—Y variation in IAB, MORB and IPB is shown in Fig. 12. Jordan and Treuil (1977) and Wood et al. (1979a) have stressed the transitional nature of MORB and IPB with regard to these elements and mention that some back-arc basalts may have sources with island-arc affinities. A similar point was made above with regard to the abundances of LIL elements.

Intra-suite variations in Ti, Zr, Y and Nb contents of IAB can be interpreted in terms of fractional crystallization. Pearce and Norry (1979) have convincingly shown that the observed variability of these elements in basic to basic-intermediate island-arc suites corresponds to fractionation trends

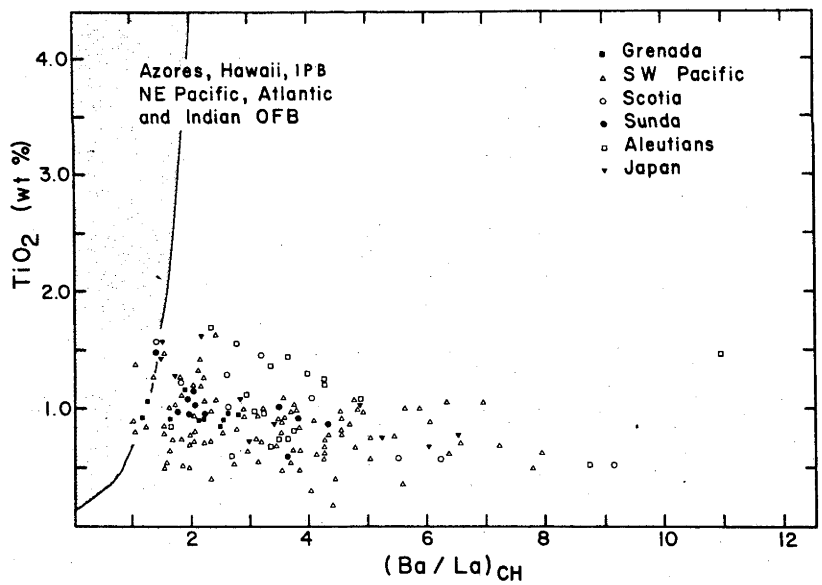

Fig. 10. TiO_2 vs. $(Ba/La)_{Ch}$ variation diagram for IAB. General fields for MORB and IPB are presented [data as in the caption to Fig. 11, extended with White et al., (1979)]. Low-K basalts from back-arc regions (see caption to Fig. 9) plot near the junction of the arc and oceanic trends.

controlled by the removal of plagioclase—olivine—clinopyroxene ± magnetite, approximately in the proportions 5:3:2. It is noteworthy, that similar fractionation paths for parental magmas would be predicted if only olivine—clinopyroxene ± magnetite were the fractionating phases since olivine and plagioclase have sim-

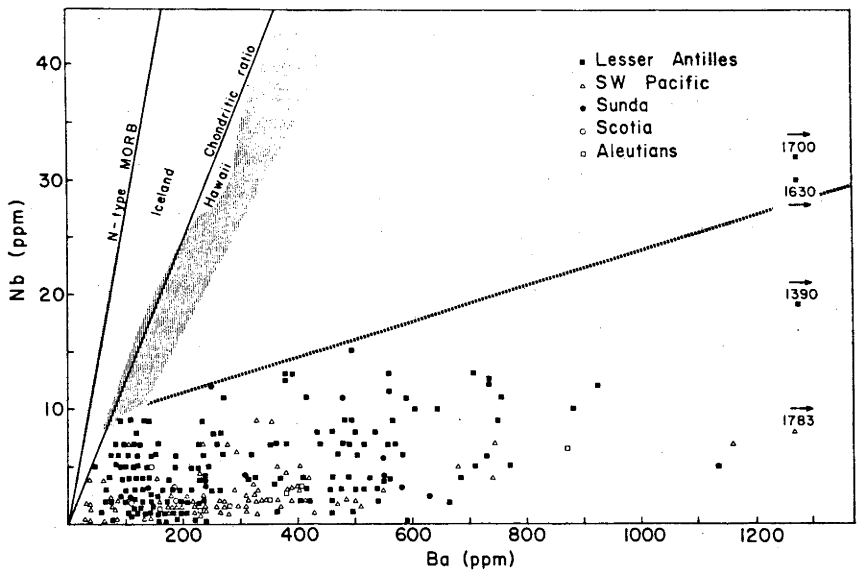

Fig. 11. Nb vs. Ba variation diagram for IAB. Fields and trends are shown for N- and E-type MORB (represented by Iceland and the surrounding sea floor) and IPB represented by Hawaiian basalts. Data from Kay and Hubbard (1978), Flower and Robinson (1979), Sun et al. (1979), Tarney et al. (1979), Wood et al. (1979a) and Bence et al. (1980c).

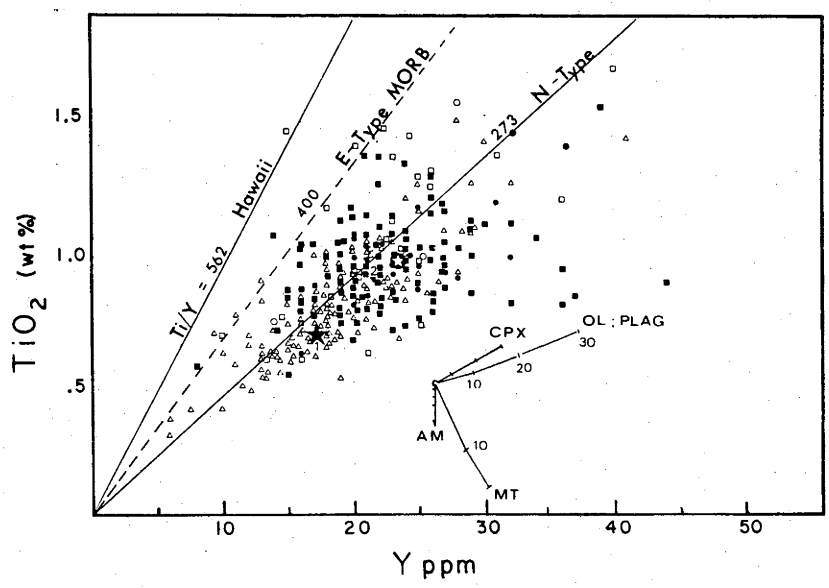

ilar, low distribution coefficients for all the elements in question. This would be more in agreement with our conclusions based on major-element variations. On a Ti—Y variation diagram (Fig. 12) calculated fractionation models exhibit increases in Ti and Y, but Ti will primarily be controlled by the percentage (and composition) of magnetite crystallizing out of a magma. Ti contents should rapidly diminish when as little as 5% titanomagnetite is removed. Amphibole fractionation will also serve to decrease Ti in residual liquids but may also decrease Y. Such a trend is not prominent in basalt suites from most island arcs but does occur in some alkalic IAB suites (e.g., Grenada; Arculus, 1976) where amphibole and magnetite are important fractionating phases.

ISOTOPIC VARIATIONS

Isotopic measurements (Sr, Nd, Pb, O, He) of rocks from island arcs have provided us with a number of constraints regarding the sources of IAB. These isotope ratios are particularly useful in deciphering the genesis of basalts when used in conjunction with trace-element data. Unfortunately, many samples with isotopic analyses lack complete chemical analyses. Likewise the different individual isotopes are not always measured on the same sample. These failings thus restrict our use of a large number of isotopic measurements on IAB.

$^{87}Sr/^{86}Sr$ ratios are generally greater than 0.7029 in IAB (Kay et al., 1978) but range in value from 0.7026 in Japan to around 0.709 in Indonesia. This wide range covers the spectrum observed in fresh MORB to altered MORB (0.7020—0.7070) and IPB (0.7028—0.7065) (Hofmann and Hart, 1978). There is a tendency for $^{87}Sr/^{86}Sr$ to increase from N-type to E-type MORB which corresponds to the enrichment in LIL elements (e.g., Wood et al., 1979a). Similar correlations of $^{87}Sr/^{86}Sr$ with LIL enrichment are observed in several island arcs (Lesser Antilles, Papua New Guinea, Indonesia).

The recognition of a systematic covariation of $^{87}Sr/^{86}Sr$ and $^{143}Nd/^{144}Nd$ in MORB, and IPB has proved extremely useful in interpreting the long-term history of Rb relative to Sr and Nd relative to Sm (e.g., DePaolo and Wasserburg, 1976; O'Nions et al., 1977). The Sr- and Nd-isotope data is consistent with hypotheses, based on trace-element abundances, that suggest the sources

Fig. 12. TiO_2 vs. Y variation diagram for IAB. The symbols are identical to those in Figs. 10 and 11. Ti/Y trends are approximate fits to the data from the sources given in the caption to Fig. 9. Most of the oceanic basalts fall between the Hawaiian and N-type MORB lines. Fractionation trends are shown for clinopyroxene (*CPX*), olivine (*OL*), plagioclase (*PLAG*), magnetite (*MT*) and amphibole (*AM*); calculations were based on mineral—liquid distribution coefficients for basic melts given by Pearce and Norry (1979) and the Rayleigh fractionation equation. Individual *ticks* represent increments of 10 wt. % fractional crystallization. The *solid star* (with numeral *1*) is a presumed parental basalt composition (*505*; see Table I) (Gorton, 1977); the *enclosed star* represents the calculated residual liquid after crystallization of 11% Ol, 24% Cpx. The observed residual liquid composition is indicated by the numeral *2*. See also caption to Fig. 6.

of MORB and IPB have been depleted in incompatible elements and light REE relative to estimated primordial mantle values. A limited number of Nd-isotopic measurements have been made on island-arc rocks (DePaolo and Wasserburg, 1977; Hawkesworth et al., 1977; DePaolo and Johnson, 1979; Hawkesworth et al., 1979c; Whitford et al., 1979). In general, the Nd-isotope results suggest that arc lavas have been derived from mantle sources in which Nd has been depleted relative to Sm resulting in $^{143}Nd/^{144}Nd$-values greater than that of a present-day chondritic reservoir (Chur $^{143}Nd/^{144}Nd = 0.511836$). Consequently, nearly all of the island-arc lavas measured thus far, plot above the estimated bulk-Earth line at $\epsilon Nd^{Chur} = 0$ in Fig. 13. The significant variation previously mentioned in $^{87}Sr/^{86}Sr$ of IAB causes some of the fields to diverge from the "mantle array" which is defined by the nearly linear trend of MORB and IPB through the estimated bulk-Earth composition.

A number of points should be emphasized with regard to the Sr—Nd diagram (Fig. 13).

(1) IAB have $^{143}Nd/^{144}Nd$ ratios similar to those of E-type MORB (i.e. Iceland), IPB (i.e. Hawaii) and some continental basalts but not to N-type MORB.

(2) There is a marked shift towards higher $^{87}Sr/^{86}Sr$ at a given Nd-value in

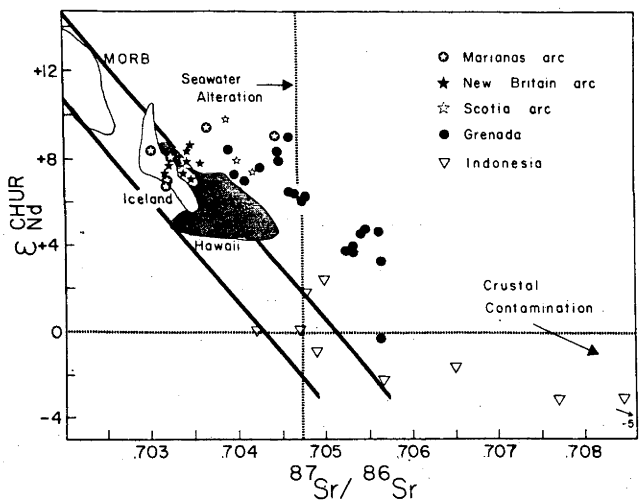

Fig. 13. Nd- and Sr-isotopic compositions of island-arc volcanic rocks. The "mantle array" is from DePaolo and Wasserburg (1976) and passes through the present-day bulk-Earth composition. The effects of seawater addition or alteration would drive ratios horizontally in the direction shown. Approximate direction of isotopic change due to crustal contamination or sediment involvement is based on upper and lower crustal estimates from DePaolo and Wasserburg (1979). Other fields are from the following sources: MORB and Hawaii, O'Nions et al. (1977); DePaolo and Wasserburg (1977); Marianas, DePaolo and Wasserburg (1977); New Britain, DePaolo and Johnson (1979); Scotia arc, Hawkesworth et al. (1977); Grenada, Lesser Antilles, Hawkesworth et al. (1979c); Iceland, Zindler et al. (1979) and O'Nions et al. (1977); Indonesia, Whitford et al. (1979).

some IAB suites in comparison to IPB. This shift has been interpreted as evidence for the involvement of seawater, which contains relatively radiogenic Sr, derived from subducted oceanic crust during petrogenesis. However, there are a few IPB samples from the Galapagos (White and Hofmann, 1978) and Azores Islands (Hawkesworth et al., 1979b) that have high $^{87}Sr/^{86}Sr$ relative to the mantle array, which cast doubts upon the role of the slab *alone* to produce this shift. Furthermore, IAB from Grenada, Lesser Antilles plot to the right of, but parallel to, the "mantle array" so that the higher $^{87}Sr/^{86}Sr$ values cannot be explained simply by the addition of radiogenic Sr from the slab.

(3) The effects of crustal contamination, possibly by subducted sediment involvement would be to increase $^{87}Sr/^{86}Sr$ while decreasing $^{143}Nd/^{144}Nd$. This would shift points originally lying along the "mantle array" towards the fields defined for continental crust and oceanic sediments as indicated in Fig. 13. Lavas from the Banda arc exhibit just such an array, and project back toward samples from the Sunda arc believed to have been derived from uncontaminated mantle (Whitford et al., 1979). Calc-alkaline rocks erupted in continental settings (i.e. Chile, Patagonia) also exhibit a much wider range of Sr- and Nd-isotopic values which also extend towards the fields defined for continental crustal rocks (e.g., Hawkesworth et al., 1979a). Furthermore, a positive correlation between $^{87}Sr/^{86}Sr$ and $^{18}O/^{16}O$ in lavas from the Banda arc are indicative of contamination by a sialic component, probably from subducted sediments (Magaritz et al., 1978). Clearly, the available Nd-isotope data suggests that a small sedimentary component added to a primary source with N- or E-type MORB characteristics is permissable.

In general, the range of Pb-isotopic ratios in arc lavas overlaps those of MORB and some IPB, but all island-arc suites have steeper slopes than those of MORB and IPB in Pb-isotope ratio plots (Sun, 1979; Arculus, 1980). Pb-isotopic ratios in some arcs (Japan, Tonga—Kermadec, Aleutians) define fields that are confined between the Pb-isotopic composition of the oceanic sediment near each arc and the broad MORB array. This feature of arc lavas has been used as evidence for small amounts of sediment involvement (2%) in the genesis of IAB (Kay et al., 1978; Sun, 1979). This further suggests that IAB are constrained as two-component mixes (i.e. oceanic crust, or its source, and sediment). However, the range of Pb-isotopic ratios in individual arcs and the lack of correlation between Pb and Sr isotopes suggests that simple mixing of end-members is not a satisfactory explanation. A point that has been overlooked in Pb arguments, is that E-type MORB from the North Atlantic (Cumming, 1976; Cohen et al., 1980) have a range of Pb-isotopic values that encompass that of many island arcs and in some cases are more radiogenic than oceanic sediments. This fact eliminates the need to envoke a sediment-mixing hypothesis and suggests that IAB could be derived from a variety of E-type MORB sources. Interestingly, volcanic rocks from island arcs that are furthest from continental regions (e.g., Marianas, New Hebrides) exhibit the least deviation in Sr-, Nd- and Pb-isotopic values from N-type MORB and hence argue against sediment involvement in their petrogenesis (Meijer, 1976; Lancelot et al., 1978).

To summarize; the Pb-, Sr- and Nd-isotopic data do *not* rigorously constrain: (1) the type of mantle source for IAB, (2) the existence or amount of sedimentary contamination, or (3) the presence of a melt/vapour component from the subducted slab. The data does, however, indicate that IAB magmas are not simply melts formed from subducted N-type MORB alone nor can they be derived from the mantle sources that give rise to N-type MORB. In fact, it appears that IAB are derived (in part) from depleted mantle sources that have quite heterogeneous isotopic characteristics.

VOLATILE CONCENTRATIONS

Quenched glassy rims of MORB, Hawaiian submarine basalts (IPB) and pillow basalts from the Marianas arc and trough have been studied to determine the distribution of volatiles in parental magmas (Delaney et al., 1978; Garcia et al., 1979; Muenow et al., 1979). Although the number analysed thus far is small, the results suggest that arc lavas have relatively low volatile contents (<2.5% total with $H_2O < 1.5$, $S < 0.01$, $CO_2 < 0.44$, $F < 0.34$ and $Cl < 0.24$ wt.%). However, with the exception of S, these values and the CO_2/H_2O ratios are significantly greater than those measured in MORB or Hawaiian samples. As one might expect from the other data presented here, back-arc basalts have volatile components intermediate between IAB and MORB. Garcia et al. (1979) conclude that the subducted slab makes a significant contribution to the generation of arc magmas in the Marianas. It is important to note, however, that submarine basaltic glasses are liable to volatile contamination from seawater/hydrothermal alteration (Muenow et al., 1979).

The Cl concentrations in basalts appear to increase from N-type MORB (~40 ppm) to E-type MORB (80—234 ppm) and IPB (~150—250 ppm) to orogenic lavas (~460—>2000 ppm) (Garcia et al., 1979; Muramatsu and Wedepohl, 1979). Ito (1979) has noted that the amounts of Cl produced by subduction zone magmatism are about twice the amount being subducted via amphibole and chlorite in altered oceanic crust (+ sediment) while the total water produced in arc environments is only ~20% of that contained in subducted oceanic crust. Cl may also be transported into subduction zones by high-Cl serpentinites or oxyhalide minerals (Edmond et al., 1979).

Island-arc lavas have a relative over-abundance of Cl and F compared to MORB. Perhaps the most significant fact is that island-arc and back-arc lavas have average Cl/F ratios significantly greater than those of MORB and IPB (~1 as compared to 0.26 and 0.42), suggesting that the excess Cl may indeed be ultimately derived from the subducted oceanic crust. The high absolute abundances may simply be related to the relatively more hydrous nature of the island-arc environment. Alternatively, the high Cl/F ratios may also be due to higher vapour/magma distribution coefficients for Cl compared to F (Flynn and Burnham, 1978) if vapour transport is an important mechanism. The data are sparse and more information is needed on the F composition of altered oceanic sea floor before any conclusions are reached.

In contrast to the above studies, Craig et al. (1978) have argued that similar $^3He/^4He$ ratios in rocks from arc and non-arc settings (~7—8 times the atmospheric ratio) indicate they were derived from primordial sources and not by dehydration/melting of the subducted slab. The addition of small amounts of water (0.6 wt.%) from dehydration of subducted hydroxyl-minerals would probably not introduce sufficient He to change the ratio (Muenow et al., 1979). Recently, Bloomer et al. (1979) and Poreda and Craig (1979) have shown that a boninite with 3 wt.% H_2O from the inner wall of the Marianas trench has $^3He/^4He$ ratio only 1.6 times atmospheric, which, suggests that volatiles involved during petrogenesis were derived from the dehydration of subducted oceanic crust; but at shallower levels than those characteristic of most arc magmatism.

DISCUSSION AND CONCLUSIONS

Certainly, one of the most characteristic features of IAB is their association with voluminous andesites and more differentiated volcanic rocks; a feature not typical of MORB or IPB. If basalts in island arcs do represent parental magmas, then either the processes of fractional crystallization are more efficient in arc environments than at spreading centers or the constancy of magma formation at accreting plate margins inhibits extensive differentiation (O'Hara, 1977; Dungan and Rhodes, 1978; Walker et al., 1979).

The geochemical data presented above display the wide variations in IAB chemistry, but also point out the lack of any clustering into different basalt types. The differences in major-element chemistry, with the exception of K, between IAB and MORB with high MgO content are minor yet significant. Greater concentrations of K and LIL elements in IAB compared to MORB cannot simply be a result of smaller degrees of partial melting of identical sources. Such processes would also enrich the high-field-strength ions in IAB relative to MORB, a result which is not observed. We must conclude, therefore, that although IAB and MORB sources are broadly similar, they are not identical. In a similar manner, the high-TiO_2, -FeO, and low-Al_2O_3 of IPB as compared to IAB argue for significantly different source chemistry or residual mineralogy.

The differences in the major-element compositional trends of evolved IAB and MORB are not explicable by appealing to different sources, but appear to reflect variations in crystallization histories. It is suggested from consideration of chemical trends of Al_2O_3, CaO/Al_2O_3 and the alkalis that plagioclase fractionation is initially absent or very minor in IAB. This suggestion is in strong contrast to the liquid-line-of-descent proposed for OFB in which plagioclase is an important liquidus phase.

Experiments on a FAMOUS basalt (0—10.5 kbar pressure, anhydrous conditions) obtain olivine and plagioclase as liquidus phases (Bender et al., 1978) and add support to the argument. Clinopyroxene becomes a significant fractionating phase only in more evolved MORB, or above 10.5 kbar where it replaces olivine as a liquidus phase (Kushiro, 1973; Bender et al., 1978; Walker

et al., 1979), or when magma-mixing occurs in open-system magma chambers (Dungan and Rhodes, 1978; Walker et al., 1979). The effect of clinopyroxene fractionation lowers the CaO/Al_2O_3 ratio and Mg-numbers (Fig. 6). Liquidus phase relations of basalt under hydrous conditions show, however, that plagioclase is not a liquidus phase and that clinopyroxene, olivine and magnetite are the important phases (e.g., Holloway and Burnham, 1972). Least-squares modelling of major-element trends in a number of individual IAB suites (e.g., New Hebrides, New Britain, Aleutians) indicate that clinopyroxene + olivine ± spinel are the principal fractionating phases and that plagioclase is noticeably absent (Gorton, 1977; Johnson and Arculus, 1978; Perfit, 1978). The calculated trends for some of these models (Fig. 6) are different from MORB fractionation paths calculated by Bence et al. (1979). The clinopyroxene ± olivine (±spinel) cotectic control in IAB agrees closely with other major- and trace-element variations discussed previously. We therefore suggest that the decreasing CaO/Al_2O_3 ratio with decreasing Mg-numbers in IAB is a consequence of fractional crystallization dominated by clinopyroxene + olivine with an absence of plagioclase. The fractionation of near-liquidus Fe—Ti-spinel is also stressed in order to minimize TiO_2 enrichment in derivative liquids. This crystallization sequence may be related to the increased water content of IAB relative to MORB.

Primitive IAB have major-element characteristics similar to MORB but isotopic characteristics more similar to IPB than to N-type MORB. However, trace-element characteristics differ significantly from both MORB and IPB and are not adequately explained by processes of fractional crystallization, partial melting to different degrees of homogeneous mantle sources or variations in proportions of major mantle phases. We turn, therefore, to the concept of heterogeneous mantle sources to explain the unique petrogenesis of IAB.

There is a substantial body of geochemical and isotopic data which suggests that the mantle is heterogeneous, vertically and horizontally, on a regional (10—100 km) and small (millimeters to centimeters) scale (Frey and Green, 1974; White et al., 1976 1979; O'Nions et al., 1979; Sun, 1979; Tarney et al., 1979; Wood et al., 1979a,b, 1980; Zindler et al., 1979; Menzies and Murthy, 1980). The exact geochemical and isotopic nature of this heterogeneity and the processes which govern it are poorly understood (e.g., metasomatic events). In consequence, petrogenetic models proposed for the generation of IAB are based on a number of unevaluated parameters and are inconclusive. We briefly review perhaps the strongest of these models in light of the geochemical and isotopic characteristics of IAB.

Wood et al. (1979a) and Saunders et al. (1980) propose a model in which IAB are generated from a mantle veined with an enriched, but variable component from the subducted slab. Wood et al. (1979a) have utilized a variation of this concept to model the progressive enrichment observed in LIL elements from N- to E-type MORB. The veining process they propose (~1—5% veins) would cause an enrichment in the more compatible LIL elements (Y—Ta) relative to the incompatible elements (Ta—Cs). A general increase in more com-

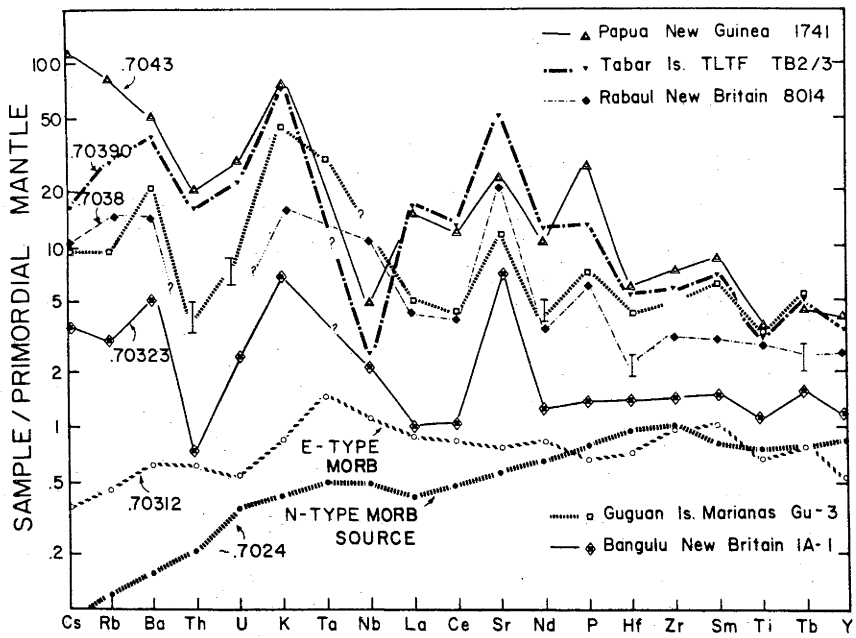

Fig. 14. LIL-element abundances in IAB normalized to primordial mantle abundances estimated by Wood et al. (1979a). The elements are arranged in approximate order of increasing bulk partition coefficients between presumed MORB mantle mineral assemblages and MORB basaltic melts. Estimated LIL contents for N- and E-type MORB mantles are shown. Derivative basalts from these two sources have LIL patterns similar to their sources but ~10—15 times more enriched. The IAB presented range from low-K tholeiites to high-K alkalic basalts (see Table I for sources of data). Measured $^{87}Sr/^{86}Sr$ ratios for these IAB are shown on the left-hand side of the diagram. Note the $^{87}Sr/^{86}Sr$ increase with LIL enrichment and the unsystematic enrichments in LIL elements relative to the MORB mantle compositions.

patible elements is noted in low-K to high-K IAB, however, there are striking anomalies in relative elemental abundances in IAB compared to MORB (Fig. 14). The overabundances of LIL cations (Cs, Rb, Ba, K, Sr) and depletions of high-field-strength ions (Th, Nb, Hf, Ti, Zr, Y) in IAB relative to MORB are perhaps, the most distinctive feature. The overabundances of LIL elements are explicable in principle by multi-stage enrichment models (Nicholls and Ringwood, 1973; Best, 1975; Thorpe et al., 1976; Johnson, 1977; Kay, 1977; Perfit, 1977; Dixon and Batiza, 1979; Sun, 1979; Whitford and Jezek, 1979; Saunders et al., 1980), however, the depletions of high-field-strength ions remains problematical.

The proportions of components (oceanic crust, depleted mantle, sediment) and probably melting percentages, would have to vary in order to produce the variations in IAB erupted in arcs (Kay, 1980). This type of process would shift Sr-, Nd- and Pb-isotope compositions in MORB sources toward those measured in IAB. However, it also predicts that IAB with the highest Ba/La

and Pb/La ratios should have the highest $^{87}Sr/^{86}Sr$ and lowest $^{143}Nd/^{144}Nd$ and this is clearly not the case in many island arcs. Furthermore, if sediments play a significant role in IAB magma genesis, we would expect the chemical composition of IAB from different arcs to exhibit characteristics influenced by the particular sedimentary components subducted. At present, we know little about the behaviour of sediments and phase changes that may occur along the slab—mantle interface.

Wood et al. (1979a) and Saunders et al. (1980) require the presence of a residual Ti phase in the subducted oceanic crust and mantle to control the depletion of those elements. Sphene and/or rutile have been shown to be stable at pressures up to 20 kbar in hydrous tholeiitic basalt (Hellman and Green, 1979), but this cannot be extrapolated to peridotite compositions or higher pressures where melting is presumed to occur. Fractionation of sphene from primitive IAB may account for the depletion of high-field-strength ions but is not considered likely due to the profound effects this would have on REE patterns.

An inherent feature of the multi-stage model is the release of volatiles via dehydration or partial melting of the slab. Volatile-LIL transport may be a significant process in metasomatically enriching the mantle beneath arcs without influencing the concentrations of high-field-strength ions. The stabilization of a Ti—Zr—Nb-bearing phase (or phases) in the mantle wedge due to increased P_{H_2O} or P_{O_2} (Saunders et al., 1980) is intriguing but needs to be verified. Note, however, the evidence from He-isotopic ratios is not in accord with a slab-derived volatile contribution.

There are many questions which remain unanswered about the petrogenesis of IAB. We believe that a general geochemical and isotopic signature distinguishes IAB from basalts generated in other tectonic environments. The meaning of this signature, however, is not unambiguous and requires additional geochemical and experimental information regarding mantle heterogeneities and the multi-stage processes of IAB magma generation.

ACKNOWLEDGEMENTS

The authors wish to thank L. Bindman for archiving and plotting the major-element data and R. Curtin for assisting in preparation of the manuscript. We gratefully acknowledge J.F.G. Wilkinson and R.W. Kay for providing us with their unpublished manuscripts and R.W. Johnson for critically reviewing the paper. We also thank the Bureau of Mineral Resources (Aust.) and the Geological Survey of Papua New Guinea for providing island arc basalt samples. This research was, in part, funded by NSF grants INT-79-19383 and OCE-78-20058.

REFERENCES

Arculus, R.J., 1976. Geology and geochemistry of the alkali basalt—andesite association of Grenada, Lesser Antilles island arc. Geol. Soc. Am. Bull., 87: 612—624.

Arculus, R.J., 1980. Island arc magmatism in relation to the evolution of the crust and mantle. Tectonophysics (in press).

Arculus, R.J. and Johnson, R.W., 1978. Criticism of generalized models for the magmatic evolution of arc-trench systems. Earth Planet. Sci. Lett., 39: 118—126.

Arculus, R.J. and Wills, K.J.A., 1980. The petrology of igneous blocks and inclusions from the Lesser Antilles island arc. J. Petrol. (in press).

Bence, A.E., Baylis, D.M., Bender, J.F. and Grove, T.L., 1979. Controls on the major and minor element chemistry of mid-ocean ridge basalts and glasses. In: M. Talwani, C.G. Harrison, D.E. Hayes (Editors), Deep Drilling Results in the Atlantic Ocean: Ocean Crust. Am. Geophys. Union, Washington, D.C., pp. 331—341.

Bence, A.E., Grove, T.L. and Papike, J.J., 1980a. Basalts as probes of planetary interiors: constraints on the chemistry and mineralogy of their source regions. Precambrian Res., 10: 249—279.

Bence, A.E., Haskins, L. and Rhodes, J.M., 1980b. Oceanic intraplate volcanism. Lunar Planet. Inst., Houston, Texas (in press).

Bender, J.F., Hodges, F.N. and Bence, A.E., 1978. Petrogenesis of basalts from the Project FAMOUS area: Experimental study from 0—15 kb. Earth Planet. Sci. Lett., 41: 277—302.

Best, M.G., 1975. Migration of hydrous fluids in the upper mantle and potassium variation in calc-alkalic rocks. Geology, 3: 429—432.

Bloomer, S., Melchior, J., Poreda, R. and Hawkins, J., 1979. Mariana arc—trench studies: petrology of boninites and evidence for a "boninite series". EOS (Trans. Amer. Geophys. Union), 60: 968 (abstract).

Bowen, N.L., 1928. The Evolution of the Igneous Rocks. Princeton University Press, Princeton, N.J., 332 pp.

Briqueu, L. and Lancelot, J.R., 1979. Rb—Sr systematics and crustal contamination models for calc-alkaline igneous rocks. Earth Planet. Sci. Lett., 43: 385—396.

Chow, T.J., Stern, R.J. and Dixon, T.H., 1980. Absolute and relative abundances of K, Rb, Sr and Ba in circum-Pacific island-arc magmas, with special reference to the Marianas. Chem. Geol., 28: 111—121.

Clarke, D.B. and O'Hara, M.J., 1979. Nickel and the existence of high-MgO liquids in nature. Earth Planet. Sci. Lett., 44: 153—158.

Cohen, R.S., Evenson, N.M., Hamilton, P.J. and O'Nions, R.K., 1980. U—Pb, Sm—Nd, and Rb—Sr systematics of mid-ocean ridge basalt glasses. Nature (London), 283: 149—153.

Craig, H., Lupton, J.E. and Horibe, Y., 1978. A mantle helium component in circum-Pacific volcanic gases: Hakone, the Marianas and Mt. Lassen. In: E.C. Alexander and M. Ozima (Editors), Advances in Earth and Planetary Sciences, 3. Terrestrial Rare Gases, Center for Academic Publications, Japan Scientific Press, Tokyo, pp. 3—16.

Cumming, G.L., 1976. Lead isotope ratios in DSDP Leg 37 basalts. Earth Planet. Sci. Lett., 31: 179—183.

Delaney, J.R., Muenow, D.W. and Graham, D.G., 1978. Abundance and distribution of water, carbon and sulfur in the glassy rims of submarine pillow basalts. Geochim. Cosmochim. Acta, 42: 581—594.

DePaolo, D.J. and Johnson, R.W., 1979. Magma genesis in the New Britain island arc: constraints from Nd and Sr isotopes and trace element patterns. Contrib. Mineral. Petrol., 70: 367—379.

DePaolo, D.J. and Wasserburg, G.J., 1976. Nd isotopic variations and petrogenetic models. Geophys. Res. Lett., 3: 249—252.

DePaolo, D.J. and Wasserburg, G.J., 1977. The sources of island arcs as indicated by Nd and Sr isotopic studies. Geophys. Res. Lett., 4: 465—468.

DePaolo, D.J. and Wasserburg, G.J., 1979. Petrogenetic mixing models and Nd—Sr isotopic patterns. Geochim. Cosmochim Acta, 43: 615—627.

Dixon, T.H. and Batiza, R., 1979. Petrology and chemistry of recent lavas in the northern Marianas: implications for the origin of island arc basalts. Contrib. Mineral. Petrol., 70: 167—181.

Dungan, M.A. and Rhodes, J.M., 1978. Residual glasses and melt inclusions in basalts from DSDP Legs *45* and *46*: evidence for magma mixing. Contrib. Mineral. Petrol., 67: 417—431.

Edmond, J.M., Measures, C., McDuff, R.E., Chan, L.H., Collier, R., Grant, B., Gordon, L.I. and Corliss, J.B., 1979. Ridgecrest hydrothermal activity and the balances of the major and minor elements in the ocean: the Galapagos data. Earth Planet. Sci. Lett., 46: 1—18.

Ewart, A., 1976. Mineralogy and chemistry of modern orogenic lavas — some statistics and implications. Earth Planet. Sci. Lett., 31: 417—432.

Flower, M.F.J. and Robinson, P.T., 1979. Evolution of the FAMOUS ocean ridge segment: evidence from submarine and deep sea drilling investigations. In: M. Talwani, C.G. Harrison, D.E. Hayes (Editors), Deep Drilling Results in the Atlantic Ocean: Ocean crust. Am. Geophys. Union, Washington, D.C., pp. 314—330.

Flynn, R.T. and Burnham, C.W., 1978. An experimental determination of rare earth partition coefficients between a chloride containing vapor phase and silicate melts. Geochim. Cosmochim. Acta, 42: 685—701.

Frey, F.A. and Green, D.H., 1974. The mineralogy, geochemistry and origin of lherzolite inclusions in Victorian basanites. Geochim. Cosmochim. Acta, 38: 1023—1059.

Frey, F.A., Bryan, W.B. and Thompson, G., 1974. Atlantic Ocean floor: geochemistry and petrology of basalts from Legs *2* and *3* of the Deep-Sea Drilling Project. J. Geophys. Res., 79: 5507—5527.

Garcia, M.O., Liu, N.W.K. and Muenow, D.W., 1979. Volatiles in submarine volcanic rocks from the Marianas Island arc and trough. Geochim. Cosmochim. Acta, 43: 305—312.

Gill, J.B., 1974. Role of underthrust oceanic crust in the genesis of a Fijian calc-alkaline suite. Contrib. Mineral. Petrol., 43: 29—45.

Gill, J.B., 1976. Composition and age of Lau Basin and Ridge volcanic rocks: implications for evolution of an interarc basin and remnant arc. Geol. Soc. Am. Bull., 87: 1384—1395.

Gill, J.B., 1978. Role of trace element partition coefficients in models of andesite genesis. Geochim. Cosmochim. Acta, 42: 709—724.

Gill, R.C.O., 1979. Comparative petrogenesis of Archaean and modern low-K tholeiites — A critical review of some geochemical aspects. Phys. Chem. Earth, 14: 431—447.

Gorton, M.P., 1977. The geochemistry and origin of Quaternary volcanism in the New Hebrides. Geochim. Cosmochim. Acta, 41: 1257—1270.

Green, D.H., 1976. Experimental testing of "equilibrium" partial melting of peridotite under water-saturated, high-pressure conditions. Can. Mineral., 14: 255—268.

Green, D.H., Edgar, A.D., Beasley, P., Kiss, E. and Ware, N.G., 1974. Upper mantle source for some hawaiites, mugearites and benmoreites. Contrib. Mineral. Petrol., 48: 33—43.

Hanson, G.N. and Langmuir, C.H., 1978. Modelling of major elements in mantle—melt systems using trace element approaches. Geochim. Cosmochim. Acta, 42: 725—741.

Hart, S.R. and Davis, K.E., 1978. Nickel partitioning between olivine and silicate melt. Earth Planet. Sci. Lett., 40: 203—219.

Hawkesworth, C.J., O'Nions, R.J., Pankhurst, R.J., Hamilton, P.J. and Evensen, N.M., 1977. A geochemical study of island-arc and back-arc tholeiites from the Scotia Sea. Earth Planet. Sci. Lett., 36: 253—262.

Hawkesworth, C.J., Norry, M.J., Roddick, J.C., Baker, P.E., Francis, P.W. and Thorpe, R.S., 1979a. $^{143}Nd/^{144}Nd$, $^{87}Sr/^{86}Sr$ and the incompatible element variations in the calc-alkaline andesites and plateau lavas from South America. Earth Planet. Sci. Lett., 42: 45—57.

Hawkesworth, C.J., Norry, M.J., Roddick, J.C. and Vollmer, R., 1979b. $^{143}Nd/^{144}Nd$ and $^{87}Sr/^{86}Sr$ ratios from the Azores and their significance in LIL-element enriched mantle. Nature (London), 280: 28—31.

Hawkesworth, C.J., O'Nions, R.K. and Arculus, R.J., 1979c. Nd- and Sr-isotope geochemistry of island arc volcanics, Grenada, Lesser Antilles. Earth Planet. Sci. Lett., 45: 237—248.

Hawkins, J.W., 1976. Petrology and geochemistry of basaltic rocks of the Lau Basin. Earth Planet. Sci. Lett., 28: 283—297.

Hellman, P.L. and Green, T.H., 1979. The role of sphene as an accessory phase in the high-pressure partial melting of hydrous mafic compositions. Earth Planet. Sci. Lett., 42: 191—201.

Heming, R.F., 1974. Geology and petrology of Rabaul caldera, Papua New Guinea. Geol. Soc. Am. Bull., 85: 1253—1264.

Hofmann, A.W. and Hart, S.R., 1978. An assessment of local and regional isotopic equilibrium in the mantle. Earth Planet. Sci. Lett., 38: 44—62.

Holloway, J.R. and Burnham, C.W., 1972. Melting relations of basalt with equilibrium water pressure less than total pressure. J. Petrol., 13: 1—29.

Ito, E., 1979. High-temperature metamorphism of plutonic rocks from the mid-Cayman Rise: a petrographic and oxygen isotopic study. Ph.D. Thesis, University of Chicago, Chicago, Ill., 158 pp.

James, D.E., Brooks, C. and Cuyubamba, A., 1976. Andean Cainozoic volcanism: magma genesis in the light of strontium isotopic composition and trace element geochemistry. Geol. Soc. Am. Bull., 87: 592—600.

Johnson, R.W., 1977. Distribution and major-element chemistry of late Cainozoic volcanoes at the southern margin of the Bismarck Sea, Papua New Guinea. Aust., Bur. Miner. Resour., Rep. 188, 170 pp.

Johnson, R.W. and Arculus, R.J., 1978. Volcanic rocks of the Witu Islands, Papua New Guinea: The origin of magmas above the deepest part of the New Britain Benioff zone. Bull. Volcanol., 41(4): 609—655.

Johnson, R.W., Mackenzie, D.E. and Smith, I.E.M., 1978. Volcanic rock associations at convergent plate boundaries: reappraisal of the concept using case histories from Papua New Guinea. Geol. Soc. Am. Bull., 89: 96—106.

Jordon, J.-L. and Treuil, M., 1977. Utilisation des propriétés des éléments fortement hygro-magmatophiles pour l'étude de la composition chimique et l'hétérogénéité du manteau: Soc. Géol. Fr., Bull., 19: 1197—1205.

Katsui, Y., Oba, Y., Ando, S., Nishimura, S., Masuda, Y., Kurasawa, H. and Fujikami, H., 1978. Petrochemistry of the Quaternary volcanic rocks of Hokkaido, North Japan. J. Fac. Sci., Hokkaido Univ., Ser. IV, 18: 449—484.

Kay, R.W., 1977. Geochemical constraints on the origin of Aleutian magmas. In: M. Talwani and W. Pitman III (Editors), Island arcs, Deep Sea Trenches and Back-Arc Basins, Am. Geophys. Union, Washington, D.C., pp. 229—242.

Kay, R.W., 1980. Volcanic arc magmas: implications of a melting—mixing model for element recycling in the crust—upper mantle system. J. Geol. (in press).

Kay, R.W. and Hubbard, N.J., 1978. Trace elements in ocean ridge basalts. Earth Planet. Sci. Lett., 38: 95—116.

Kay, R.W., Sun, S.-S. and Lee-Hu, C.-N., 1978. Pb and Sr isotopes in volcanic rocks from the Aleutian Islands and Pribilof Islands, Alaska. Geochim. Cosmochim. Acta, 42: 263—273.

Kushiro, I., 1973. Origin of some magmas in oceanic and circum-oceanic regions. Tectonophysics, 17: 211—222.

Lancelot, J.R., Brigneu, L., Westphal, B. and Tatsumoto, M., 1978. Sr and Pb isotopic data bearing on the origin of calc-alkaline lavas of Pliocene—Quaternary age from Peru and New Hebrides active margins. 4th Int. Conf. on Geochronology and Cosmochronology of Isotope Geology, Aspen, Colo., pp. 240—241.

Lindström, D.J., 1976. Experimental study of the partitioning of the transition metals between clinopyroxene and coexisting silicate liquids. Ph.D. Thesis, University of Oregon, Eugene, Oreg., 188 pp.

Lopez-Escobar, L., Frey, F.A. and Vergara, M., 1977. Andesites and high-alumina basalts from the central-south Chile high Andes: geochemical evidence bearing on their petrogenesis. Contrib. Mineral. Petrol., 63: 199—228.

Lordkipanidze, M.B., Zakariadze, G.S. and Popolitou, E.I., 1979. Volcanic evolution of the marginal and interarc basins. Tectonophysics, 57: 71—83.

Mackenzie, D.E., 1976. Nature and origin of late Cainozoic volcanoes in western Papua New Guinea. In: R.W. Johnson (Editor), Volcanism in Australasia, Elsevier, Amsterdam, pp. 221—238.

Magaritz, M., Whitford, D.J. and James, D.E., 1978. Oxygen isotopes and the origin of high $^{87}Sr/^{86}Sr$ andesites. Earth Planet. Sci. Lett., 40: 220—230.

Meijer, A., 1976. Pb and Sr isotopic data bearing on the origin of volcanic rocks from the Mariana island-arc system. Geol. Soc. Am. Bull., 87: 1358—1369.

Menzies, J. and Murthy, V.R., 1980. Nd and Sr isotope geochemistry of hydrous mantle nodules and their host alkali basalts: implications for local heterogeneities in metasomatically veined mantle. Earth Planet. Sci. Lett., 46: 323—334.

Miyashiro, A., 1974. Volcanic rocks series in island arcs and active continental margins. Am. J. Sci., 274: 321—355.

Muenow, D.W., Graham, D.G. and Liu, N.W.K., 1979. The abundance of volatiles in Hawaiian tholeiitic submarine basalts. Earth Planet. Sci. Lett., 42: 71—76.

Muramatsu, Y. and Wedepohl, K.H., 1979. Chlorine in Tertiary basalts from the Hessian depression in NW Germany. Contrib. Mineral. Petrol., 70: 357—366.

Nicholls, I.A. and Ringwood, A.E., 1973. Effect of water on olivine stability in tholeiites and production of SiO_2 — saturated magmas in the island arc environment. J. Geol., 81: 285—300.

Nicholls, I.A. and Whitford, D.J., 1976. Primary magmas associated with Quaternary volcanism in the western Sunda arc, Indonesia. In: R.W. Johnson (Editor), Volcanism in Australasia, Elsevier, Amsterdam, pp. 77—90.

O'Hara, M.J., 1977. Geochemical evolution during fractional crystallization of a periodically refilled magma chamber. Nature (London), 266: 503—507.

O'Nions, R.K., Hamilton, P.J. and Evenson, N.N., 1977. Variations in $^{143}Nd/^{144}Nd$ and $^{87}Sr/^{86}Sr$ ratios in oceanic basalts. Earth Planet. Sci. Lett., 34: 13—22.

O'Nions, R.K., Evensen, N.M., Carter, S.R. and Hamilton, P.J., 1979. Isotope geochemical studies of North Atlantic ocean basalts and their implications for mantle evolution. In: M. Talwani, C.G. Harrison and D.E. Hayes (Editors), Deep Drilling Results in the Atlantic Ocean: Ocean Crust. Am. Geophys. Union, Washington, D.C., pp. 342—357.

Pearce, J.A., 1975. Statistical analysis of major element patterns in basalt. J. Petrol., 17: 15—43.

Pearce, J.A. and Cann, J.R., 1973. Tectonic setting of basic volcanic rocks determined using trace element analyses. Earth Planet. Sci. Lett., 19: 290—300.

Pearce, J.A. and Norry, M.J., 1979. Petrogenetic implications of Ti, Zr, Y and Nb variations in volcanic rocks. Contrib. Mineral. Petrol., 69: 33—47.

Perfit, M.R., 1977. The petrochemistry of igneous rocks from the Cayman Trench and the Captains Bay pluton, Unalaska Island: their relation to tectonic processes at plate margins. Ph.D. Thesis, Columbia University, New York, N.Y., 273 pp.

Perfit, M.R., 1978. The petrochemistry and strontium isotopic composition of mafic basalts from the Aleutian Islands. Abstr. Geol. Soc. Am., 10: 470.

Perfit, M.R., Brueckner, H., Lawrence, J.R. and Kay, R.W., 1980. Trace element and isotopic variations in a zoned pluton and associated volcanic rocks, Unalaska Island, Alaska. Contrib. Mineral. Petrol., 73: 69—87.

Poreda, R. and Craig, H., 1979. Helium and neon in oceanic volcanic rocks. EOS (Trans. Am. Geophys. Union), 60: 969 (abstract).

Saunders, A.D. and Tarney, J., 1979. The geochemistry of basalts from a back-arc spreading center in the East Scotia Sea. Geochim. Cosmochim. Acta, 43: 555—572.

Saunders, A.D., Tarney, J. and Weaver, S.D., 1980. Transverse geochemical variations across the Antarctic Peninsula: implications for the genesis of calc-alkaline magmas. Earth Planet. Sci. Lett., 46: 344—360.

Schilling, J.-G., 1975. Rare-earth variations across "normal segments" of the Reykjanes Ridge, 60°-53°N, Mid-Atlantic Ridge, 29°S, and East Pacific Rise, 2°-19°S, and evidence on the composition of the underlying low-velocity layer. J. Geophys. Res., 80: 1459—1473.

Shibata, T., Thompson, G. and Frey, F.A., 1979. Tholeiitic and alkalic basalts from the Mid-Atlantic Ridge at 43° N. Contrib. Mineral. Petrol., 70: 127—141.

Stern, R.J., 1979. On the origin of andesite in the northern Mariana island arc: implications from Agrigan. Contrib. Mineral. Petrol., 68: 207—219.

Sun, S.-S., 1979. Lead isotopic study of young volcanic rocks from mid-ocean ridges, oceanic islands and island arcs. Philos. Trans. R. Soc. London, (in press).

Sun, S.-S., Nesbitt, R.W. and Sharaskin, A.Y., 1979. Geochemical characteristics of mid-ocean ridge basalts. Earth Planet. Sci. Lett., 44: 119—138.

Tarney, J., Saunders, A.D. and Weaver, S.D., 1977. Geochemistry of volcanic rocks from the island arcs and marginal basins of the Scotia arc region. In: M. Talwani and W. Pitman III (Editors), Island Arcs, Deep Sea Trenches and Back-Arc Basins. Am. Geophys. Union, Washington, D.C., pp. 367—377.

Tarney, J., Saunders, A.D., Weaver, S.D., Donnellin, N.C.B. and Hendry, G.L., 1979. Minor-element geochemistry of basalts from Leg *49*, North Atlantic Ocean. In: B.P. Luyendijk and J. Cann (Editors), Reports of the Deep Sea Drilling Project, 49. U.S. Gov. Print. Off., Washington, D.C., pp. 657—691.

Taylor, S.R., Johnson, R.W., Arculus, R.J. and Perfit, M.R., 1980. The island-arc basalt reference suite. NASA Planet. Basaltic Volcanism Proj., Lunar Planet. Inst., Houston, Texas (in press).

Thorpe, R.S., Potts, P.J. and Francis, P.W., 1976. Rare earth data and petrogenesis of andesite from the north Chilean Andes. Contrib. Mineral. Petrol., 54: 65—78.

Treuil, M. and Varet, J., 1973. Critères volcanologiques, pétrologiques et géochimiques de la genèse et de la différentiation des magmas basaltiques — Exemple de l'Afar. Bull. Soc. Géol. Fr., 15: 506—540.

Walker, D., Shibata, T. and Delong, S.E., 1979. Abyssal tholeiites from the Oceanographer Fracture Zone, II. Phase equilibria and mixing. Contrib. Mineral. Petrol., 70: 111—125.

Wallace, D.A., Chappell, B.W., Arculus, R.J., Johnson, R.W., Perfit, M.R., Taylor, S.R. and Taylor, G.A.M., in press. Geologic data catalogue on the Tabar, Lihir, Tanga and Feni Islands: field geology; major, trace and isotope analyses and mineral analyses. Bur. Miner. Resour., Canberra, A.C.T., Rep.

Weaver, S.D., Saunders, A.D., Pankhurst, R.J. and Tarney, J., 1979. A geochemical study of magmatism associated with the initial stages of back-arc spreading. Contrib. Mineral. Petrol., 68: 151—169.

White, W.M. and Hofmann, A.W., 1978. Geochemistry of the Galapagos Islands: implications for mantle dynamics and evolution. Carnegie Inst., Washington, Yearb., 77: 596—606.

White, W.M., Schilling, J.-G. and Hart, S.R., 1976. Evidence for the Azores mantle plume from the strontium isotope geochemistry of the central North Atlantic. Nature (London), 263: 659—663.

White, W.M., Tapia, M.D.M. and Schilling, J.-G., 1979. The petrology and geochemistry of the Azores Islands. Contrib. Mineral. Petrol., 69: 201—213.

Whitford, D.J. and Jezek, P.A., 1979. Origin of Late-Cenozoic lavas from the Banda arc, Indonesia: trace element and Sr isotope evidence. Contrib. Mineral. Petrol., 68: 141—150.

Whitford, D.J., White, W.M., Jezek, P.A. and Nicholls, I.A., 1979. Nd isotope composition of Recent andesites from Indonesia. Dep. Terrest. Mag., Carnegie Inst., Washington, Yearb. 78: 304—308.

Wilcox, R.E., 1979. The liquid line of descent and variation diagrams. In: H.S. Yoder (Editor), The Evolution of the Igneous Rocks: Fiftieth Anniversary Perspectives. Princeton University Press, Princeton, N.J., pp. 205—232.

Wilkinson, J.F.G., in press. The genesis of mid-ocean ridge basalt. Earh Sci. Rev.

Wood, D.A., Joron, J.-L., Treuil, M., Norry, M. and Tarney, J., 1979a. Elemental and Sr isotope variations in basic lavas from Iceland and the surrounding ocean floor. Contrib. Mineral. Petrol., 70: 319—339.

Wood, D.A., Tarney, J., Varet, J., Saunders, A.D., Bougault, H. and Joron, J.-L., 1979b. Geochemistry of basalts drilled in the North Atlantic by IPOD Leg *49*: Implications for mantle heterogeneity. Earth Planet. Sci. Lett., 42: 77—97.

Wood, D.A., Joron, J.-L. and Treuil, M., 1979c. A re-appraisal of the use of trace elements to classify and discriminate between magma series erupted in different tectonic settings. Earth Planet. Sci. Lett., 45: 326—336.

Wood, D.A., Tarney, J. and Weaver, B.L., 1980. Trace element variations in Atlantic Ocean basalts and Proterozoic dykes from northwest Scotland: their bearing upon the nature and geochemical evolution of the upper mantle. Tectonophysics (in press).

Zindler, A., Hart, S.R., Frey, F.A. and Jakobsson, S.P., 1979. Nd and Sr isotope ratios and rare earth element abundances in Reykjanes Peninsula basalts: evidence for mantle heterogeneity beneath Iceland. Earth Planet. Sci. Lett., 45: 249—262.

APPENDIX 6

REPRESENTATIVE MINERAL AND ADDITIONAL GEOCHEMICAL ANALYSES OF THE 'MMVF' SILICIC SUITE

Table A6-1a. Representative microprobe analyses of pyroxenes from 'MMVF' silicic rocks.

Table A6-1b. Representative microprobe analyses of amphiboles from 'MMVF' silicic rocks.

Table A6-1c. Representative microprobe analyses of feldspars from 'MMVF' silicic rocks.

Table A6-1d. Representative microprobe analyses of oxides from 'MMVF' silicic rocks.

Table A6-2. Additional major element analyses and CIPW normative mineralogies of silicic rocks from Mormon Mountain.

TABLE A6-1a. Representative Microprobe Analyses of Pyroxenes from 'MMVF'

Silicic Rocks

CLINOPYROXENES

	ANDESITES						DACITES							XENOLITH	
Sample	MMT-6	MMT-6	19-2	19-2	19-2	MMT-25	MMT-9	MMT-13	MMT-13	MMT-13	MMT-13	26-12	26-12	X-1	X-1
SiO_2	50.19	51.81	51.57	51.72	51.46	51.41	53.07	52.00	52.76	50.30	52.63	51.45	52.72	50.25	52.44
TiO_2	.71	.41	.34	.45	.28	.27	.30	.29	.23	.35	.25	.32	-	1.06	.55
Al_2O_3	4.56	3.29	2.68	3.02	3.13	2.93	2.71	3.20	2.35	3.56	2.30	2.53	1.90	4.15	2.82
FeO	8.30	7.75	10.14	7.28	11.68	10.99	6.72	7.80	6.89	11.24	6.96	10.50	6.28	5.24	5.60
MnO	.17	-	-	-	-	.51	-	-	-	.24	-	.43	-	-	-
MgO	15.00	15.29	14.60	16.09	12.97	13.25	15.76	15.19	15.95	13.15	16.57	13.75	16.46	15.60	18.00
CaO	19.46	21.09	19.62	20.56	19.64	19.87	21.08	20.96	21.16	20.52	20.81	19.71	21.18	21.78	19.58
Na_2O	.61	.37	.67	.53	.84	.77	.44	.55	.48	.65	.48	.41	.35	.53	.64

ORTHOPYROXENES

	DACITE				XENOLITH	
Sample	MMT-9	MMT-13	MMT-13	26-12	X-1	X-1
SiO_2	55.19	54.47	52.76	54.20	53.72	55.01
TiO_2	.15	-	-	-	.19	-
Al_2O_3	1.53	1.87	1.46	1.18	1.87	.58
FeO	13.45	13.99	21.20	16.36	13.90	14.20
MnO	.24	-	.55	.26	.22	.22
MgO	28.24	28.59	22.20	26.98	28.26	28.53
CaO	1.12	1.07	1.66	1.02	1.24	1.39

TABLE A6-1b. Representative Microprobe Analyses of Amphiboles from 'MMVF' Silicic Rocks

	ANDESITES						RHYODACITES						XENOLITH	
Sample	MMT-6	19-2	19-2	MMT-21	MMT-21	MMT-25	MMT-3	MMT-3	MMT-3	MMT-3	MMT-18	MMT-18	X-1	X-1
SiO_2	41.28	41.80	42.10	40.74	41.57	48.74	42.88	42.55	44.15	45.81	45.28	43.89	43.75	43.30
TiO_2	2.84	2.52	2.75	2.69	2.69	.25	2.00	1.08	1.78	1.53	1.59	1.80	2.53	2.48
Al_2O_3	13.12	13.80	13.39	14.07	13.64	24.68	12.80	12.45	11.74	9.89	11.34	12.74	10.85	11.12
FeO	11.36	10.51	12.47	14.15	12.26	9.39	14.48	16.86	12.42	9.96	11.98	13.92	10.08	10.85
MnO	.12	-	-	.11	.13	-	-	.27	-	-	-	-	-	-
MgO	13.71	15.06	13.38	12.00	13.85	1.20	12.48	11.23	14.08	16.12	15.28	13.30	16.16	14.91
CaO	11.00	11.27	10.77	11.34	11.18	2.56	11.03	10.77	11.10	10.79	11.00	10.77	11.16	11.11
Na_2O	3.12	2.67	2.98	2.55	2.51	.99	2.53	2.49	2.50	2.39	2.56	2.60	2.60	3.31
K_2O	.70	.59	.51	.55	.53	.63	.56	.77	.45	.44	.39	.53	.39	.42

TABLE A6-1c. Representative Microprobe Analyses of Feldspars from 'MMVF' Silicic Rocks

	ANDESITES									DACITES			
Sample	MMT-6	19-2	MMT-21	MMT-21	MMT-21	MMT-25	MMT-25	MMT-25	MMT-25	MMT-9	MMT-9	MMT-13	MMT-13
SiO_2	56.07	53.63	52.15	54.47	56.40	51.77	57.61	62.27	61.91	55.67	55.45	56.27	59.04
Al_2O_3	27.43	29.41	30.25	28.26	26.92	30.70	26.77	22.71	23.86	26.63	27.99	27.85	24.99
FeO	.76	.48	.40	.60	.84	.54	.29	.78	-	.81	.59	.53	.62
CaO	9.47	11.26	12.82	10.61	9.33	13.17	8.75	4.40	3.51	9.11	10.34	9.47	7.74
Na_2O	5.72	5.08	4.08	5.11	5.88	3.75	6.12	7.83	8.22	5.77	5.28	5.90	6.98
K_2O	.37	.13	.15	.24	.35	.20	.47	1.70	2.50	.37	.32	.42	.64
AN	47	55	63	53	46	65	43	21	16	52	47	46	37
AB	51	44	36	46	52	34	54	69	70	46	51	52	60
OR	2	1	1	2	2	1	3	10	14	2	2	2	3

	DACITES				RHYODACITES							XENOLITH	
Sample	MMT-13	MMT-13	26-12	26-12	MMT-3	MMT-3	MMT-3	MMT-3	MMT-18	MMT-18	MMT-18	X-1	X-1
SiO_2	64.93	65.53	57.13	55.91	57.85	60.36	58.80	62.49	56.84	59.17	60.83	54.58	56.98
Al_2O_3	20.57	19.78	26.54	27.81	27.45	25.88	25.87	24.42	27.44	25.81	24.92	28.84	27.32
FeO	.39	.41	.83	.64	.20	.23	.17	.20	.21	.22	.22	.50	.61
CaO	1.85	.87	8.60	9.59	8.10	6.32	7.42	5.45	8.76	6.77	5.70	11.02	8.97
Na_2O	7.40	6.67	5.97	5.42	6.58	7.13	6.68	7.61	6.46	7.76	7.92	5.11	6.52
K_2O	4.65	6.54	.57	.51	.27	.34	.30	59	.17	.26	.40	.36	.50
AN	9	4	54	49	40	32	37	27	42	32	28	53	42
AB	64	58	43	48	58	66	61	70	57	67	70	45	55
OR	27	38	3	3	2	2	2	3	1	1	2	2	3

TABLE A6-1d. Representative Microprobe Analyses of Oxides from 'MMVF"

Silicic Rocks

	ANDESITES												DACITES			
Sample	MMT-6	MMT-6	MMT-6	MMT-6	MMT-21	MMT-21	MMT-21	MMT-25	MMT-25	MMT-25	MMT-25	MMT-25	MMT-9	MMT-9	MMT-13	MMT-13
Oxide	MT	MT	ILM	ILM	MT	MT	ILM	MT	MT	MT	IL	ILM	MT	MT	MT	MT
SiO_2	1.08	1.95	1.06	1.02	.34	.30	.26	.91	.31	.72	.23	.32	-	-	1.61	2.09
TiO_2	15.40	23.54	43.19	48.13	12.17	10.66	48.29	6.98	9.12	5.42	51.47	47.89	12.88	14.38	4.49	5.50
Al_2O_3	1.32	1.12	.96	.78	1.13	1.28	.39	1.32	2.05	4.51	3.20	.74	2.42	1.52	1.66	1.36
V_2O_3	.78	.71	.63	.36	.36	.45	.30	.49	.44	.40	-	-	.73	.86	.78	.74
Fe_2O_3	29.81	18.08	15.91	7.15	43.82	46.77	7.28	52.00	48.97	52.50	.44	8.04	41.79	39.35	53.20	51.40
FeO	48.56	51.98	35.27	37.66	40.07	38.16	42.42	36.34	35.90	33.28	39.99	37.71	39.33	42.00	36.30	37.68
MnO	.40	.29	.62	1.05	.59	.45	.66	.58	.82	.61	1.44	1.26	.28	.35	.16	.32
MgO	1.02	2.04	2.35	3.56	1.52	1.93	.26	1.24	2.07	2.57	2.74	2.41	2.24	1.44	.53	.48
CaO	-	.29	-	-	-	-	.13	.13	.33	-	.37	1.06	.33	.10	.74	.20

	DACITES					RHYODACITES								XENOLITH
Sample	MMT-13	MMT-13	26-12	26-12	26-12	MMT-3	MMT-3	MMT-3	MMT-18	MMT-18	MMT-18	MMT-18	MMT-18	X-1
Oxide	ILM	ILM	MT	MT	MT	MT	MT	MT	MT	MT	MT	MT-I	ILM-I	MT
SiO_2	1.69	2.23	-	-	-	2.05	2.45	2.80	1.82	1.71	1.88	1.54	1.34	1.45
TiO_2	46.67	45.84	12.88	16.02	21.95	4.35	7.55	14.44	4.80	4.42	30.11	31.72	50.54	11.19
Al_2O_3	.64	.70	2.42	.54	1.91	2.93	3.09	2.20	3.34	2.98	.84	1.03	.82	2.20
V_2O_3	-	-	.73	.62	.52	.31	.30	.52	.23	.25	.31	.36	-	1.43
Fe_2O_3	7.15	8.14	41.79	37.24	25.15	52.69	45.48	31.99	51.75	52.71	5.73	3.10	2.43	43.16
FeO	40.87	40.94	39.33	44.45	47.75	35.88	39.21	46.24	36.87	36.47	59.96	61.18	39.61	32.62
MnO	1.55	.97	.28	-	-	.47	51	.43	.29	.25	-	-	.45	.42
MgO	.63	.91	2.24	.76	2.34	1.22	1.41	1.00	.83	1.06	1.08	.93	3.38	6.64
CaO	.61	.27	.33	.36	.37	.10	-	.15	.08	-	.08	.15	.85	-

MT - Magnetite ; - I - inclusion

ILM - Ilmenite ; - I - inclusion

TABLE A6-2. Additional Major Element Analyses and CIPW Normative Mineralogies of Silicic Rocks from Mormon Mountain

	ANDESITE				DACITE							
	MMT-23-1	MMT-25-3	MMT-2-1	MMT-3-4	MMT-13-3	MMT-5-1	MMT-14-10	MMT-2-3	MMT-4-4	MMT-3-7	MMT-3-6	MMT-18-1
SiO_2	60.98	60.68	62.05	63.34	63.60	63.61	64.68	65.01	65.38	66.00	66.30	66.34
TiO_2	.92	.81	.80	.73	.75	.56	.67	.78	.62	.57	.60	.33
Al_2O_3	17.62	17.84	17.29	17.77	17.89	16.99	17.78	17.46	17.30	17.08	16.92	16.89
Fe_2O_3 *	.89	.90	.84	.76	.94	.81	.58	.70	.66	.62	.61	.68
FeO	4.52	4.58	4.29	3.86	4.78	4.13	2.95	3.59	3.36	3.18	3.10	3.45
MnO	.05	.08	.11	.17	.08	.06	.07	.11	.10	.10	.09	.06
MgO	3.53	3.46	3.35	2.80	2.44	1.82	2.19	2.08	2.29	2.40	2.25	1.69
CaO	5.56	5.39	5.32	4.64	5.38	5.18	4.59	4.55	4.22	4.26	4.11	3.88
Na_2O	4.30	4.48	4.10	3.97	2.25	4.99	4.44	3.86	3.98	3.70	3.99	4.51
K_2O	1.71	1.86	1.92	2.04	1.99	1.92	2.09	1.92	2.15	2.16	2.08	2.24
Mg #	58.2	57.37	58.2	56.4	47.6	44.1	56.9	50.9	54.9	57.4	56.5	46.7
CIPW - Normative Mineralogy												
QZ	10.28	8.64	12.41	15.82	24.6	12.24	16.01	20.11	19.36	21.44	20.99	18.27
CO	-	-	-	.61	2.25	-	-	.76	.75	.91	.64	-
OR	10.12	11.00	11.36	12.04	11.77	11.36	12.35	11.36	12.72	12.78	12.31	13.25
AB	36.34	37.86	34.64	33.52	18.97	42.17	37.56	32.61	33.63	31.25	33.71	38.11
AN	23.70	23.05	23.08	22.99	26.67	18.28	22.40	22.55	20.91	21.11	20.36	19.22
DI	3.16	3.01	2.70	-	-	6.18	.31	-	-	-	-	-
HY	13.37	13.60	13.07	12.53	12.96	7.54	9.27	10.10	10.50	10.52	9.97	9.55
MT	1.29	1.30	1.22	1.10	1.36	1.17	.84	1.02	.96	.90	.88	.98
IL	1.75	1.54	1.52	1.39	1.43	1.06	1.27	1.48	1.18	1.08	1.14	.63

APPENDIX 7

THE PETROLOGY, GEOCHEMISTRY AND PETROGENESIS OF THE BASALTS OF THE MORMON MOUNTAIN VOLCANIC FIELD, ARIZONA

INTRODUCTION

The Mormon Mountain volcanic field ('MMVF') of central Arizona is characterized by extensive basalt flows, cinder cones and localized centers of high-silica andesite, dacite and rhyodacite. The field takes its name from the largest of these centers, Mormon Mountain. The basalts and silicic rocks comprise a bimodal suite which is spatially and temporally related. The basalts range from olivine nephelinite to high-Al olivine tholeiite and were generated by the partial melting of a garnet peridotite/ spinel peridotite source. The silicic rocks represent melts derived by crustal fusion processes. The petrology, geochemistry and petrogenesis of the silicic suite are described and discussed in Chapter 6. This appendix examines the petrology, geochemistry and petrogenesis of the basaltic rocks of 'MMVF'.

Geology - The general geology of 'MMVF' is described in Chapter 6. The basalts occur as thin flows which overlap to form a relatively flat plateau of basalt, broken by numerous cinder cones and occasional silicic domes. The basalts are erupted from NW-trending fissures that are recognizable in a few localities (see Fig. 2, Chapter 6). The inherent nature of fissure-type eruptions precludes the distinction of individual flows. Cinder cones are aligned in a NW-orientation and can only occasionally be associated with an individual basalt flow. The NW-trends approximately parallel the trend of the edge of the Colorado Plateau and suggests that the eruption of 'MMVF' basalts was structurally controlled.

Sampling - The details and locations of sampling are given in Chapter 6. Approximately 40 basaltic samples were analyzed for major element abundances with 24 basalts being selected for additional trace element analysis.

Past Research - The past research of the 'MMVF' is also discussed in Chapter 6. In addition, to the information presented there, Moore et al. (1976) and Stoeser (1973) have described the petrology and geochemistry of basalts from the San Francisco volcanic field, located

just north of 'MMVF'. The basalts from the San Francisco volcanic field are similar in many ways to the basalts of 'MMVF', except in age. The 'MMVF' basalts are older than the bulk of the basalts of the San Francisco volcanic field (Damon et al., 1974; Peirce et al., 1979)(see Chapter 6).

PETROLOGY AND PHASE CHEMISTRY

General - The majority of basalts from the Mormon Mountain volcanic field can be classified petrographically on the presence of groundmass olivine and absence of orthopyroxene as alkali olivine basalts. Rare basanites (groundmass nepheline ± leucite) are also present. On a geochemical basis, however, the basalts may be divided into alkali olivine basalt transitional to olivine tholeiite, basanitoids and olivine nephelinite (Green, 1969). Throughout this discussion of the petrography and phase chemistry of the basalts, these geochemical distinctions will be used, with the exception of the term basanite instead of basanitoid.

The olivine tholeiite - alkali olivine basalt - basanite association is petrographically monotonous with the only difference being the relative abundance of the three phenocryst phases, olivine, clinopyroxene and plagioclase. Plagioclase is a rare phenocryst phase except in a few cases where it predominates relative to olivine and clinopyroxene. These unusual cases are represented by high-Al olivine tholeiites, which occur only near Mormon Mountain. The olivine nephelinite resembles the alkali olivine basalts and basanites, but contains groundmass and phenocrystal nepheline and leucite.

Megacrysts of olivine and clinopyroxene occur in the olivine nephelinite. Ultramafic inclusions of olivine, clinopyroxene, orthopyroxene and spinel are present in the olivine nephelinite. Ultramafic inclusions also occur in several other alkali basalt and basanite hosts.

All basalts are aphanitic to fine-grained with intersertal to intergranular textures. Most samples are vesiculated with some containing amygudoles of zeolites or calcite. In general, weathering is minimal and rocks are unaltered.

Groundmass Phases - The groundmasses of the olivine tholeiites, alkali olivine basalts and basanites are similar and constitute between 50 to 90 percent of the mode. The various phases, olivine, clinopyroxene

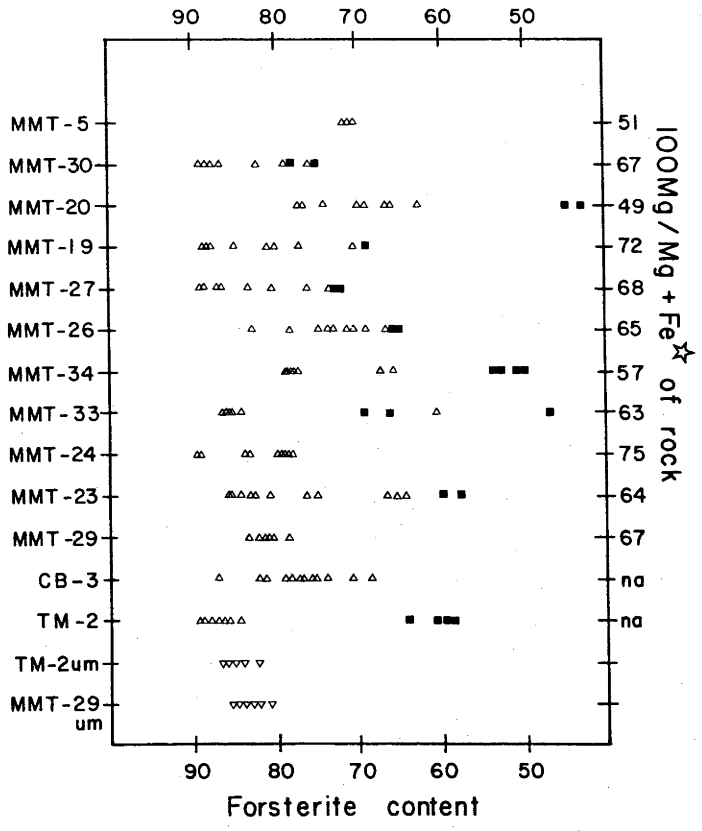

Figure 1. Compositions of olivine phenocrysts (△) and groundmass (■) of 'MMVF' basalts and olivine in ultramafic inclusions (▽).

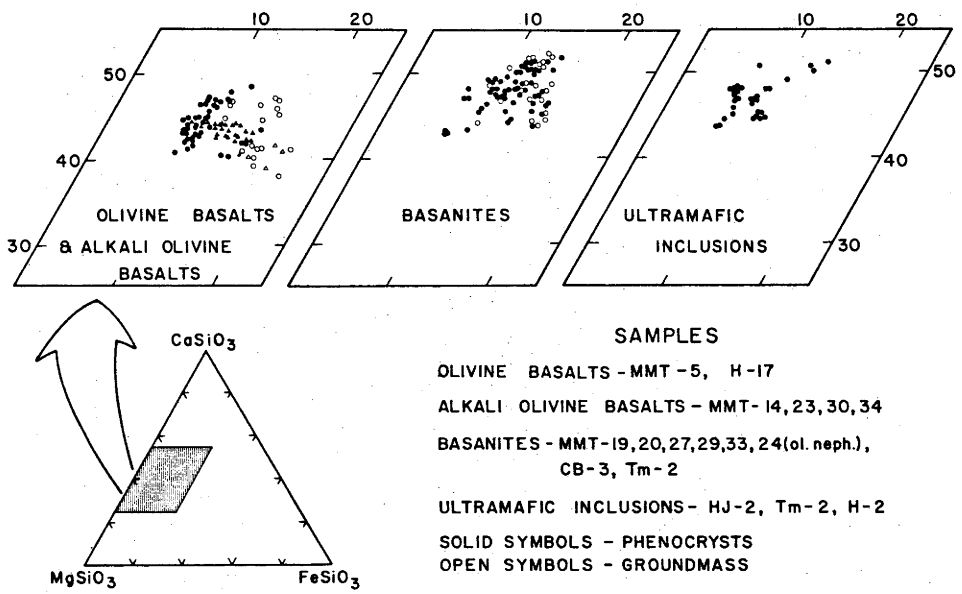

Figure 2. Compositions of clinopyroxene in 'MMVF' basalts and ultramafic inclusions. Olivine basalts are the olivine tholeiites described in the text.

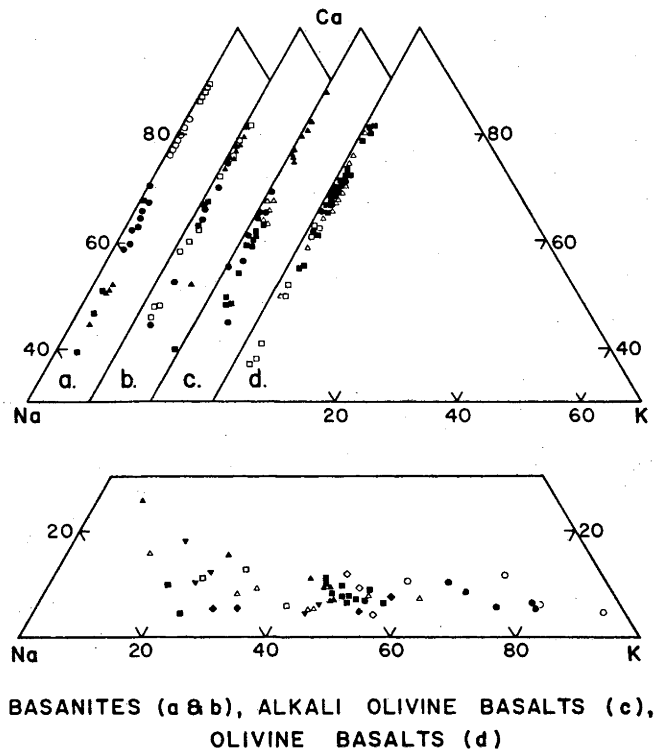

BASANITES (a & b), ALKALI OLIVINE BASALTS (c),
OLIVINE BASALTS (d)

Figure 3. Compositions of plagioclase and groundmass residuum in 'MMVF' basalts. Symbols in the Na - K sub-projection refer to basanites (all closed symbols), a.o.b. (□, ○), and olivine tholeiites (△, ◇).

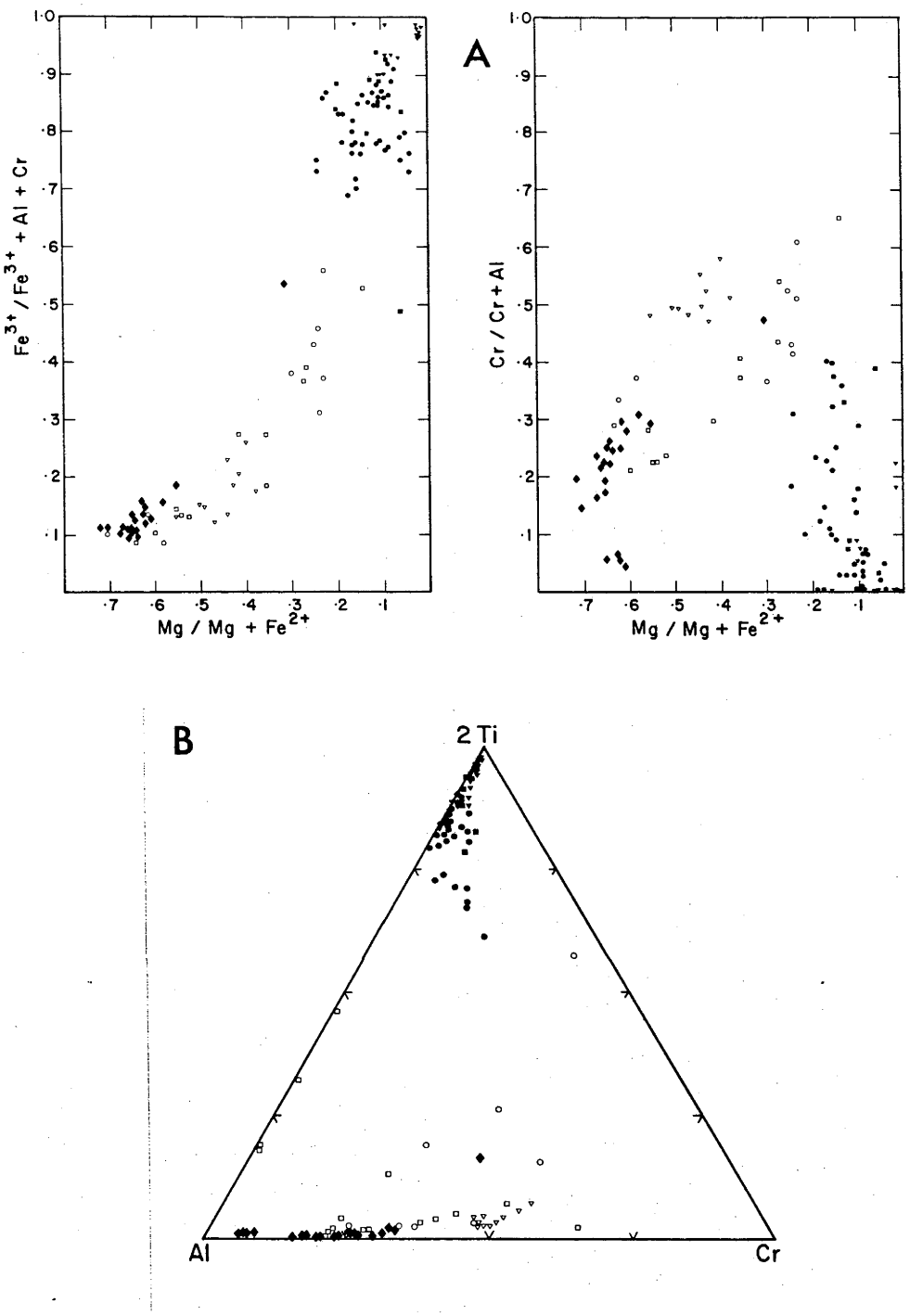

Figure 4.a) Compositions of spinels from 'MMVF' basalts (circles- basanites and olivine nephelinite; squares- a.o.b.; triangles- olivines tholeiites) and ultramafic inclusions (◆). Groundmass spinels of basalts are closed symbols and spinels which occur as inclusions in olivine and clinopyroxene are open symbols. Compositions are projected into $Fe^{3+}/Fe^{3+}+Al+Cr$ vs. Mg# and Cr / Cr + Al vs. Mg#.
b) Spinel compositions projected in the ternary, Al- 2Ti- Cr. Symbols are the same as above.

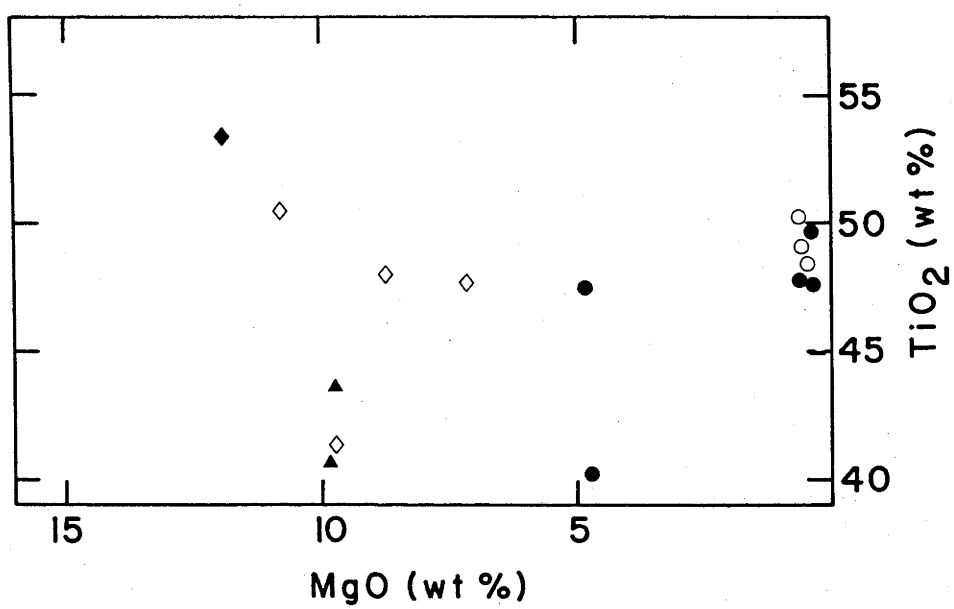

Figure 5. Abundances of MgO and TiO_2 (wt. %) in ilmenites from basalts of 'MMVF'. Symbols are: ◆ - MMT-24, ◇ - MMT-29, ▲ - MMT-30, ○ - MMT-10, ● - MMT-5.

and plagioclase, generally occur in equal proportions, except in some olivine tholeiites in which plagioclase dominates.

a) Olivine - Olivine, Fo_{80}-Fo_{43} (Fig. 1) is present as small (∿50μm), subhedral to euhedral grains and has suffered from varying degrees of iddingsitization. The very low forsterite contents of some of the olivines are compatible with the evolved nature of the basalt (for example, Fo_{43} is found in alkali olivine basalt with Mg#-49).

b) Clinopyroxene - Clinopyroxene, salite to augite in composition (Fig. 2) is subhedral to euhedral and is frequently found in clumps rather than distinct grains. Salites are highly aluminous and titaniferous (up to 11.0 wt.% Al_2O_3 and 2.5 wt.% TiO_2 respectively) and are restricted to the basanites and olivine nephelinite. Augite, with only moderate amounts of aluminum (3.0 wt.% Al_2O_3) and titanium (.9 wt.% TiO_2) are characteristic of the olivine tholeiites. Intermediate compositions are typical of the alkali olivine basalts.

c) Plagioclase - Groundmass plagioclase, occurring as distinct laths and anhedral patches, exhibits a wide variation in An content (An_{89}-An_{37}) (Fig. 3). The range in anorthite content for each rock is reflected accurately in the normative anorthite and normative nepheline of the bulk chemistry. Thus, like the clinopyroxene, plagioclase accurately reflects the alkalinity of the rock olivine tholeiite, alkali olivine basalt or basanite. Sanidine is occasionally observed as the groundmass K-phase in the alkali olivine basalts and basanites with sanidine ± anorthoclase occurring in the olivine basalts. Frequently, the groundmass plagioclase of these basalts coexists with an alkalic residuum of a variable nature (Fig. 3).

d) Spinel - The groundmass spinel phase in all basalts is dominantly dust-like titanomagnetite with a limited compositional range (Fig. 4). In most instances, the titanomagnetite is unexsolved. Ilmenite is a rare phase in the basalts, but has an unusual occurrence in several of the more highly undersaturated basalts (Haggerty, 1976). These ilmenites are present as discrete, unreacted grains and contain up to 13 wt.percent MgO and 1.3 wt.percent MnO. Ilmenites from olivine tholeiites contain less MgO and MnO than do ilmenites from the undersaturated basalts (Fig. 5).

e) Miscellaneous phases - A near ubiquitous groundmass phase in all basalts is apatite. It is present as small (<20μm) grains associated with anhedral patches of plagioclase and alkalic residuum.

Nepheline occurs in the olivine nephelinite and some basanites, usually as an interstitial groundmass phase. The nepheline is fairly

homogeneous ($\sim Ca_4Na_{83}K_{13}$) in the basanites. Unaltered plagioclase coexisting with the nepheline is comparatively anorthite-poor (An_{30}-An_{60}) Nepheline in the olivine nephelinite ($Ca_{10}Na_{77}K_{13}$) coexists with leucite ($Ca_2Na_2K_{96}$).

Sanidine is also present in some of the basanites as a groundmass phase. It is generally associated with patches of alkalic residuum.

Phenocryst Phases - a) Olivine - Olivine occurs as larger (up to 5mm), subhedral to euhedral prismatic phenocrysts with distinctive iddingsite rims. The grains often contain inclusions of Cr-spinel. Olivine composition correlates well with bulk rock Mg# and is not influenced by rock type. As a group, olivine phenocrysts range from cores of Fo_{89} to Fo_{72} and rims of Fo_{84} to Fo_{62} (Fig. 1). The rims are similar to the groundmass olivine compositions.

b) Clinopyroxene - Clinopyroxene phenocrysts, subhedral to euhedral, exhibit sector twinning and concentric zoning. As with groundmass clinopyroxene, the phenocrysts are often clumped into glomercrysts. Their compositional trends are similar to those observed for the groundmass clinopyroxene correlating with the degree of undersaturation of the basalt. Again, olivine tholeiites are characterized by endiopside-augite and basanites by diopside-salite with the clinopyroxene phenocrysts in alkali olivine basalts being intermediate to these groups (Fig. 2). All phenocrysts contain substantial amounts of Al_2O_3 and TiO_2 which increases from core to rim. The phenocrysts are not, however, as enriched in these elements as the groundmass phases. Minor elements, such as Cr and Mn decrease towards the rims, although an exception is observed in the basanites, where Na increases towards the rims. Similar pyroxenes (titanaugite-titansalite) have been reported from other occurrences of alkaline basalts (e.g. Kesson, 1973; Wass, 1979). Spinel inclusions, similar to those observed in olivine phenocrysts occur in cpx phenocrysts, although not in such abundance.

d) Plagioclase - Plagioclase phenocrysts are small subhedral laths which are two to four times the size of groundmass plagioclase. They occur abundantly only in the high-Al olivine tholeiites, and are occasionally associated with clinopyroxene in glomerocrysts. The plagioclase phenocrysts are compositionally slightly more anorthitic than coexisting groundmass plagioclase (An_{82-70} vs An_{67-55}) (Fig. 3).

e) Spinel - The spinel inclusions observed in olivine and rarely in

cpx phenocrysts are small (<20μm) euhedral grains. They range in composition (in all basalt types), from Mg-Al chromites to chromian titanomagnetites (Figs. 4 and 6). This compositional variation is often observed in zoned olivine grains with multiple inclusions. Spinels near the core of the olivine have high Mg/Mg + Fe and low Cr/Cr + Al, while those nearer the rim have lower Mg/Mg + Fe and higher Cr/Cr + Al. Almost all spinels are Ti-poor, with the exceptions being some moderately Ti-rich spinels in several basanites (these, however, may result from analysis of Mg-Al chromite core/ titanomagnetite rim combinations). An unusual group of Mg-Al-magnetites are observed in one alkali olivine basalt (MMT-30).
f) Miscellaneous phases - Large psuedomorphs of possible amphibole phenocrysts (suggested by their crystal morphology) occur in a high Al olivine tholeiite from Mormon Mountain (sample MMT-5). These pseudomorphs now consist of clinopyroxene, magnetite and plagioclase ('black type' - Garcia and Jacobson, 1979).

Occasional xenocrysts of quartz and alkali feldspar (with in one case a zircon inclusion) occur in the basalts. These xenocrysts are generally deeply embayed and surrounded with micro-crystalline reaction rims of clinopyroxene.

Megacrysts and Ultramafic Inclusions - Megacrysts and ultramafic inclusions are occasionally entrained in the more undersaturated lavas. Olivine and clinopyroxene megacrysts (up to 10 cm in length) are similar in composition to the most mafic phenocryst compositions and exhibit similar compositional zoning. This is observed especially in one clinopyroxene, having a core of Cr-diopside and rim of titansalite (Fig. 2). Three types of ultramafic inclusions have been identified consisting of three assemblages:

A) Olivine, clinopyroxene, spinel

B) Olivine, clinopyroxene, orthopyroxene, spinel

C) Clinopyroxene, orthopyroxene, spinel.

Olivine, clinopyroxene and spinel of assemblages A and B are similar in composition. Olivine ranges from Fo_{85} to Fo_{81} (Fig. 1). Clinopyroxene is diopside (Fig. 2) with low TiO_2 (.4 wt.%), moderate Al_2O_3 and Na_2O (6 wt.% and .7 wt.% respectively) and high Cr_2O_3 (1.2 wt.%). Spinels are Mg-Al-rich chromites (Fig. 4, 6). Orthopyroxenes of assemblages B and C are different with those of B being more enstatite and Al_2O_3-rich (En_{85} - 2.5 wt.% Al_2O_3 vs. En_{80} - <2.3 wt.% Al_2O_3, group B and C respectively).

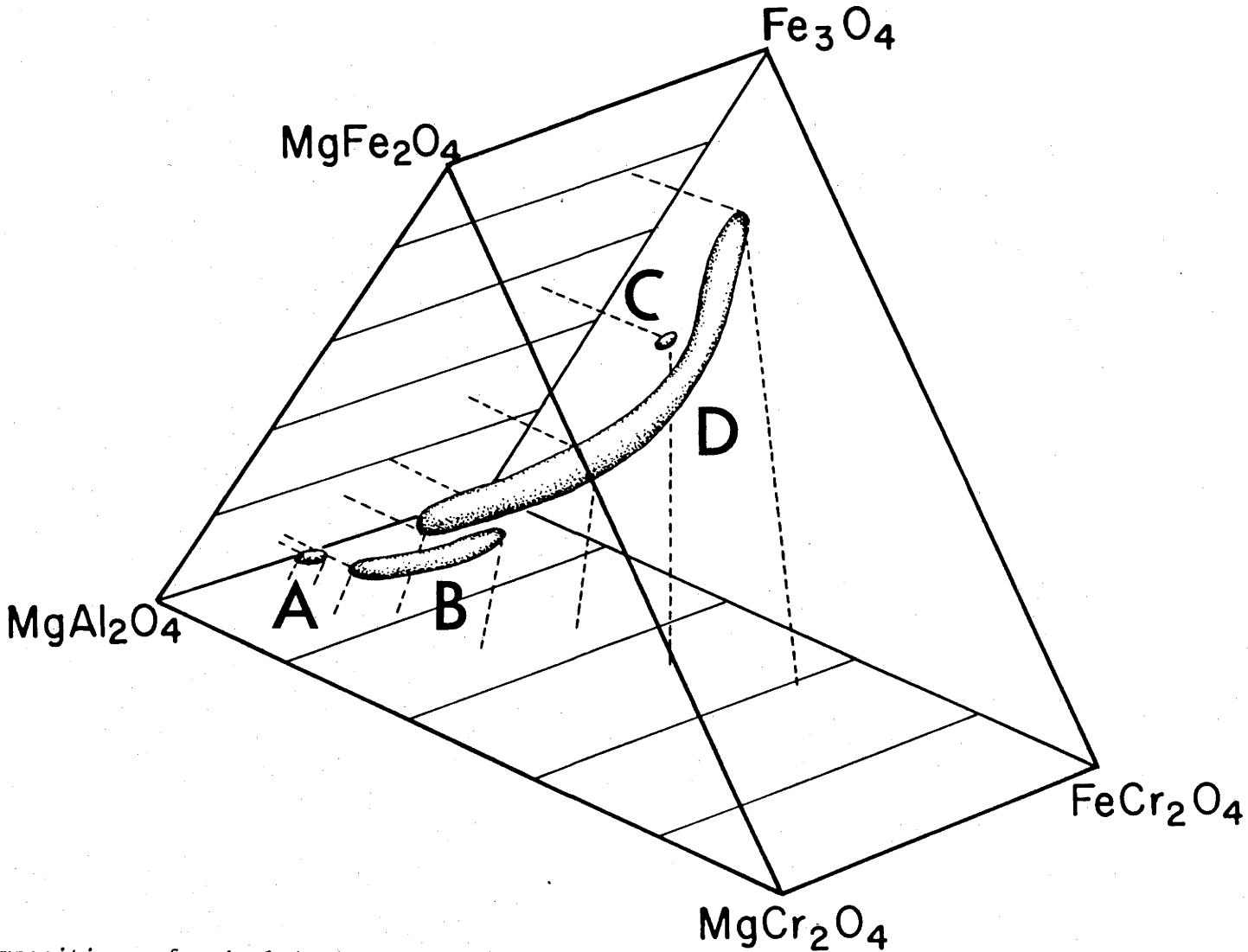

Figure 6: Compositions of spinel inclusions in 'MMVF' basalts and spinels in ultramafic inclusions schematically projected into the spinel prism (Haggerty, 1976). Fields A, B, and C are spinels of different ultramafic inclusions and field D is basaltic spinels.

Assemblage C clinopyroxene is diopsidic to augitic, with lower TiO_2 (.3 wt. %), Al_2O_3 (3.5 wt. %) and Cr_2O_3 (.6 wt. %) contents than clinopyroxene from assemblages A and B. Spinel compositions are also different, being chromian titanomagnetites (Figs. 4 and 6). As in other assemblages, spinel occurs as inclusions in the other major phases.

GEOCHEMISTRY

The basalts of 'MMVF' have been classified using the system of Green (1969) which is based on normative mineralogies. In this classification olivine nephelinite = basalt-like compositions with major normative olivine and nepheline, <2% normative albite and normative leucite, basanite = basalt with normative olivine and nepheline (>5%) and albite (>5%), alkali olivine basalt (aob) = normative olivine and nepheline (<5%), olivine basalt = normative olivine and hypersthene (<3%) and olivine tholeiite = normative hypersthene (>3%) and olivine. As Fe^{2+}/Fe^{3+} ratios are adjusted to an arbitrarily set value of FeO = .85ΣFe, the classification of basalts on normative mineralogy may lead to some misclassification (e.g. Schwarzer and Rogers, 1974) This problem is prevalent among the olivine basalts of 'MMVF'. Consequently, these basalts are grouped with basalts which exhibit similar mineralogical characteristics. In all cases the olivine basalts are identical to the olivine tholeiites in observed mineralogy. On this basis, the basalt classification given above is modified slightly, so that olivine tholeiites consist of all basalts with normative hypersthene and olivine.

Major Elements - Major element abundances were determined for 47 samples by electron microprobe analysis using fused glass beads. Twenty-four representative analyses are given in Table 1. The variations in major element contents versus MgO content for all analyzed basalts is shown in Figure 7. Normative mineralogies are projected onto Nepheline-Diopside-Olivine, Olivine-Diopside-Quartz and Nepheline-Diopside-Plagioclase, Diopside-Plagioclase-Quartz (Fig. 8). The olivine nephelinite (MMT-24) contains both normative and modal nepheline and leucite. It has low contents of SiO_2 (43.5 wt.%) and Al_2O_3 (12.7 wt.%) and high MgO, CaO, TiO_2 and P_2O_5 abundances. It

Table 1. Major element geochemistry and CIPW norms of Mormon Mountain volcanic suite.

	OLIVINE NEPHELINITE	BASANITES										
Sample	MMT-24	MMT-1	MMT-2	MMT-11	MMT-17	MMT-19	MMT-20	MMT-27	MMT-28	MMT-29	MMT-31	MMT-32	MMT-33
SiO_2	43.55	44.66	47.85	49.00	46.66	46.59	48.52	45.81	47.32	45.26	46.66	47.63	44.98
TiO_2	1.80	2.03	1.74	1.63	1.67	1.48	1.52	1.59	1.48	2.33	1.42	1.36	1.85
Al_2O_3	12.66	15.32	15.39	17.56	16.37	13.87	18.60	16.75	16.46	14.83	14.97	15.52	16.93
FeO	9.89	11.35	9.60	9.27	9.22	10.58	10.16	9.52	10.53	10.72	10.63	10.09	10.73
MnO	-	.20	.15	.15	.20	-	-	-	-	-	-	-	-
MgO	14.59	9.66	10.01	5.76	7.89	12.96	4.70	9.66	8.24	10.56	10.71	9.05	8.84
CaO	12.14	12.08	10.50	10.92	12.69	10.51	10.69	12.40	11.25	10.68	11.30	11.98	12.22
K_2O	1.23	.58	.77	1.45	1.20	.87	1.16	.83	.90	.65	.93	.83	.98
Na_2O	3.35	3.76	3.51	3.94	2.84	2.85	3.90	2.97	3.35	3.92	3.15	3.29	3.11
P_2O_5	.89	.70	.63	.48	.59	.38	.53	.48	.45	.73	.43	.38	.60
Total	100.1	100.34	100.15	100.16	99.33	100.09	99.78	100.01	99.98	99.68	100.2	100.13	100.24
Mg#	75.6	64.1	68.6	56.6	64.2	72.0	49.3	68.0	62.2	67.4	67.9	65.3	63.4
CaO/Al_2O_3	.959	.789	.682	.622	.775	.758	.574	.740	.683	.720	.755	.772	.722
K_2O/Na_2O	.37	.15	.22	.37	.42	.31	.30	.28	.27	.17	.30	.25	.32
CIPW NORM													
Diop	33.11	29.84	22.76	23.16	28.37	23.87	19.32	25.58	23.34	26.05	25.96	27.84	25.43
Hyp	-	-	-	-	-	-	-	-	-	-	-	-	-
Oliv	22.89	16.55	18.16	10.09	12.30	24.11	10.47	16.44	15.85	18.40	19.48	15.36	15.93
Or	-	3.43	4.56	8.58	7.17	5.15	6.89	4.92	5.33	3.87	5.50	4.91	5.80
Ab	-	6.67	18.99	19.08	10.58	12.90	21.76	8.86	16.16	11.66	11.73	14.46	6.65
An	13.38	21.26	22.25	24.59	27.00	21.41	28.50	29.62	26.00	19.44	22.98	24.26	28.00
Ne	15.45	13.65	5.85	7.75	7.43	6.09	6.19	8.85	6.64	11.80	8.09	7.25	10.68
Leu	5.73	-	-	-	-	-	-	-	-	-	-	-	-
Mt	2.41	2.75	2.33	2.24	2.25	2.56	2.47	2.31	2.55	2.61	2.57	2.44	2.60
Ilm	3.44	3.86	3.32	3.10	3.21	2.81	2.90	3.03	2.82	4.46	2.70	2.58	3.52
Ap	.78	.61	.55	.42	.52	.33	.46	.42	.39	.51	.30	.26	.42
Qtz	-	-	-	-	-	-	-	-	-	-	-	-	-
Cor	-	-	-	-	-	-	-	-	-	-	-	-	-

	ALKALI OLIVINE BASALTS				OLIVINE BASALTS						
Sample	MMT-14	MMT-26	MMT-30	MMT-34	MMT-4	MMT-5	MMT-8	MMT-10	MMT-15	MMT-16	MMT-23
SiO_2	49.82	47.53	50.60	47.65	50.72	52.30	50.70	50.26	50.11	51.96	49.97
TiO_2	1.36	1.22	1.53	1.40	1.21	1.30	1.49	1.44	1.46	1.30	1.35
Al_2O_3	16.25	15.90	15.30	16.97	15.79	18.50	15.75	16.29	16.94	15.46	15.22
FeO	8.78	11.01	8.73	11.44	8.51	8.65	9.86	9.50	10.57	8.40	10.12
MnO	.17	-	-	-	.17	.13	.15	-	.15	.14	-
MgO	7.62	9.64	8.48	7.32	8.41	4.36	7.71	7.05	6.16	8.65	8.64
CaO	11.08	10.79	9.83	10.46	9.51	8.27	10.06	10.37	10.79	9.20	10.63
K_2O	1.27	.74	1.35	.98	1.09	1.35	1.09	.70	.74	1.36	.80
Na_2O	3.46	2.97	3.76	3.28	3.09	3.96	2.89	2.96	2.78	3.25	3.06
P_2O_5	.36	.36	.60	.32	.36	.52	.42	.33	.35	.47	.33
Total	100.17	100.16	100.18	99.82	98.86	99.34	100.12	98.9	100.05	100.19	100.12
Mg#	64.5	64.8	67.1	57.3	67.5	51.4	62.1	60.9	55.0	68.4	64.2
CaO/Al_2O_3	.682	.679	.642	.616	.602	.447	.639	.636	.637	.595	.698
K_2O/Na_2O	.37	.25	.36	.30	.35	.34	.38	.24	.27	.42	.26
CIPW NORM											
Diop	24.29	28.84	22.58	19.08	17.37	10.26	18.85	18.44	18.08	17.84	22.18
Hyp	-	-	-	-	6.86	8.08	8.24	10.40	10.71	6.54	.34
Oliv	12.89	20.0	14.60	16.78	11.97	6.12	9.95	7.04	6.36	11.93	16.40
Or	7.51	4.37	8.00	5.81	6.53	8.06	6.45	4.19	4.38	8.05	4.73
Ab	21.11	18.14	25.24	19.73	26.49	33.84	24.48	25.36	23.54	27.53	25.89
An	24.23	27.04	19.55	28.03	25.52	28.00	25.82	28.70	30.40	22.52	24.68
Ne	4.42	3.78	3.60	4.39	-	-	-	-	-	-	-
Leu	-	-	-	-	-	-	-	-	-	-	-
Mt	2.12	2.66	2.12	2.77	2.09	2.11	2.39	2.33	2.56	2.03	2.45
Ilm	2.58	2.32	2.91	2.67	2.33	2.49	2.83	2.77	2.78	2.47	2.56
Ap	.25	.25	.42	.22	.25	.36	.29	.23	.24	.33	.23
Qtz	-	-	-	-	-	-	-	-	-	-	-
Cor	-	-	-	-	-	-	-	-	-	-	-

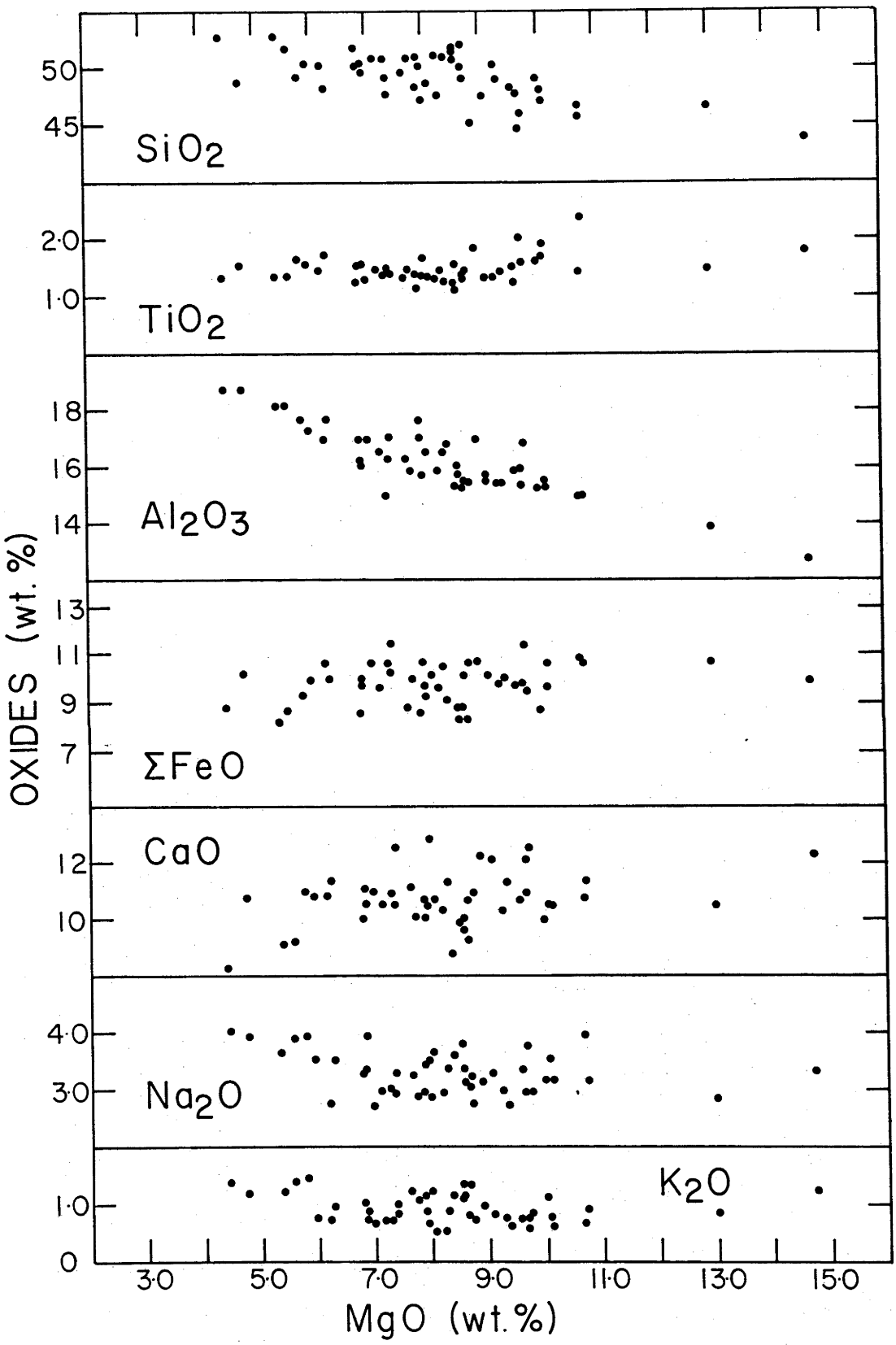

Figure 7: Harker-type variation diagram of the major element oxides of 'MMVF' basalts using MgO as the abscissa.

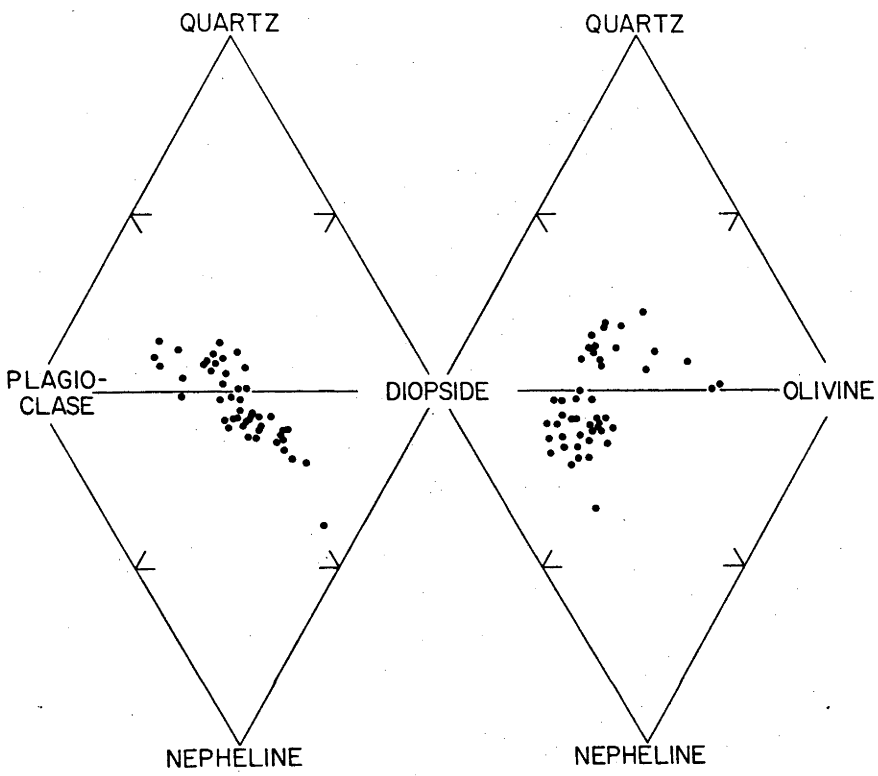

Figure 8. Normative mineralogies of 'MMVF' basalts projected in Nepheline- Plagioclase- Diopside ; Plagioclase- Diopside- Quartz and Nepheline- Diopside- Olivine ; Diopside- Olivine- Quartz (molecular proportions).

also has a high 100Mg/Mg + Fe^{2+} (Mg#) (76) and CaO/Al_2O_3 (.959) relative to the other basalts.

The basanites contain up to 13.5 percent normative nepheline. As a group, they exhibit a moderate degree of variability. Contents of Al_2O_3 and MgO range from ∿14 to 18.6 wt.percent and 5-12 wt.percent respectively. K_2O contents are different by a factor of 2 but CaO, FeO and Na_2O vary little. TiO_2 contents are moderately high (1.3-2.3 wt.%) Mg# shows a significant spread, from Mg#72 to Mg#49. CaO/Al_2O_3 ratios are lower than that of the olivine nephelinite and do not correlate with Mg# (Fig. 9).

Alkali olivine basalts are similar to the basanites with respect to their geochemistry. Mg# range from 67 to 54 and CaO/Al_2O_3 from .68 to .61.

The olivine tholeiites have the highest SiO_2 contents (50 - 52.3 wt.%) of all the analyzed basalts. Al_2O_3 varies from 15 to 18.5 wt. percent, and indicates that some of the olivine tholeiites have high-Al affinities (e.g. MMT-5). TiO_2 contents do not exceed 1.5 wt. percent. Mg# range from 68 to 51 with CaO/Al_2O_3 ratios varying from .70 to .44. No systematic correlation is observed between Mg# and CaO/Al_2O_3 ratios (Fig. 9).

As a suite, the basalts show little systematic behaviour on a Harker-type variation diagram (Fig. 7) with a possible exception being Al_2O_3. Differences between the silica-undersaturated basalts and the silica-saturated basalts are also not readily apparent from this figure. A slight distinction of alkalic and tholeiitic groups can be seen using the AFM (Σalkalis-FeO-MgO) diagram. Figure 10 suggests that the olivine tholeiites can be distinguished by their modest degree of Fe-enrichment without accompanying alkalis-enrichment in contrast to the slight Fe-enrichment and alkalis-enrichment of the basanites.

Trace Elements - Twentyfour samples of basalt were analyzed by XRF (Norrish and Chappell, 1977) for the trace elements Rb, Ba, Sr, Pb, La, Y, Zr, Nb, Ga, Cr, Ni, V, Sc, Cu, Zn. These analyses are given in Table 2.

a) Incompatible Trace Elements - The abundances of the incompatible trace elements (Ba, Rb, Sr, Pb, Zr, La, Y, Nb) are considered with P_2O_5 and K_2O. No correlation is observed between Mg# and the abundances of these elements (Fig. 11). In addition, the distinction of different basalt types on the basis of major element geochemistry (i.e. normative mineralogy) is not evident with regards to the trace

Table 2. Trace element abundances of basalts of the Mormon Mountain volcanic field

	MMT 24	MMT 1	MMT 2	MMT 11	MMT 17	MMT 19	MMT 20	MMT 27	MMT 28	MMT 29	MMT 31	MMT 32
Rb	24	4	11	15	14	11	16	10	10	22	10	11
Ba	1135	610	1120	1475	1065	480	845	1120	785	905	590	600
Sr	1065	1040	1040	1015	870	570	1020	910	750	1040	800	820
Pb	5	6	9	12	9	5	9	12	8	8	8	8
La	92	53	41	45	57	23	39	52	38	51	34	25
Y	24	22	19	20	21	19	24	20	21	21	20	19
Zr	240	206	171	144	156	120	163	116	134	218	139	121
Nb	83	60	48	49	60	28	42	50	36	57	38	26
Ga	14	17	17	17	18	15	20	17	18	17	16	17
Cr	714	488	404	77	195	600	9	310	193	410	461	340
Ni	366	285	190	46	84	372	27	160	108	216	158	138
V	225	268	212	220	247	206	213	268	213	229	194	211
Sc	29	27	22	23	28	27	20	34	27	24	26	29
C	70	54	58	57	73	76	92	81	95	52	85	89
Zn	83	85	83	73	74	86	90	83	85	93	83	83

	MMT 33	MMT 14	MMT 26	MMT 30	MMT 34	MMT 4	MMT 5	MMT 8	MMT 10	MMT 15	MMT 16	MMT 23
Rb	11	11	10	12	7	14	16	11	6	8	21	10
Ba	1315	1120	573	1370	470	1140	1395	835	640	630	1150	490
Sr	1200	850	570	1300	540	855	1120	805	565	540	960	540
Pb	12	11	8	13	5	12	18	8	6	6	14	7
La	68	40	34	62	19	38	52	32	26	31	42	24
Y	23	17	22	20	20	16	19	18	20	21	18	21
Zr	152	127	109	191	120	123	165	133	111	110	146	123
Nb	68	40	32	72	22	37	53	39	23	22	53	24
Ga	18	17	17	18	19	18	21	16	18	18	16	18
Cr	184	371	332	297	167	389	6	337	238	261	495	366
Ni	131	123	170	174	108	155	17	227	87	93	249	130
V	257	221	203	197	206	194	177	194	205	212	180	194
Sc	28	29	30	21	27	28	19	27	28	29	23	27
Cu	65	56	68	67	93	48	39	67	98	85	65	60
Zn	88	80	84	87	88	78	95	80	90	90	72	93

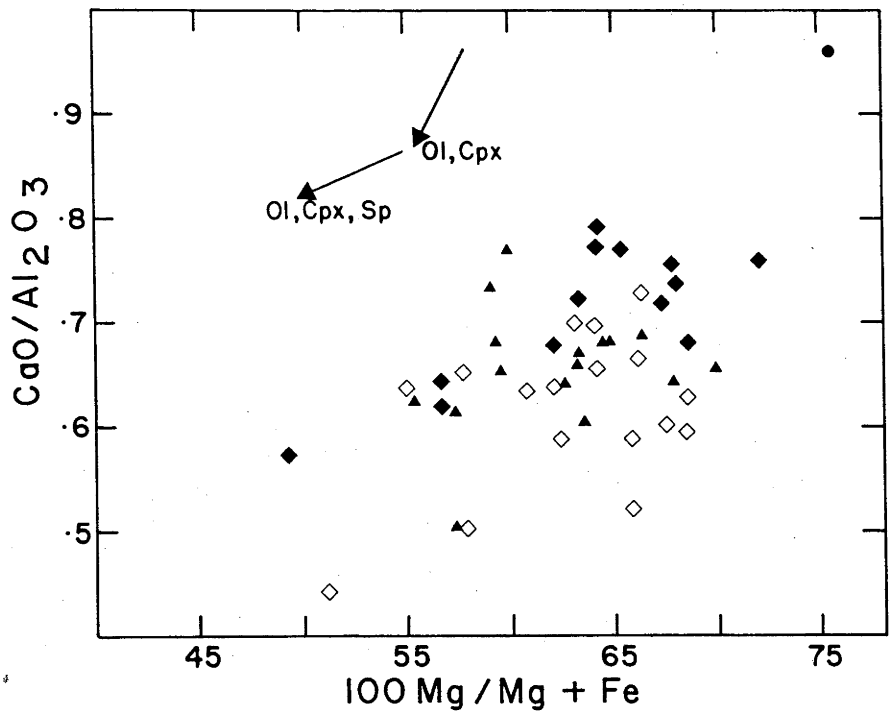

Figure 9. CaO/Al_2O_3 vs. MgO of 'MMVF' basalts. Arrows indicate fractionation trends (qualitatively). Symbols are: ● - olivine nephelinite, ◆ - basanites, ▲ - a.o.b., ◇ -olivine tholeiites.

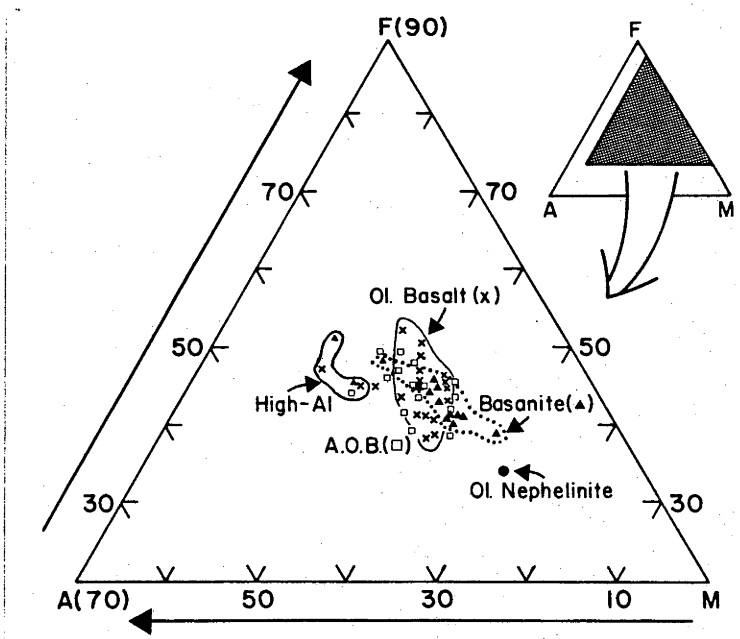

Figure 10. A ($Na_2O + K_2O$) - F (FeO) - M (MgO) projection of 'MMVF' compositions.

Figure 11: Abundances of Zr, Nb, Y, La, Sr, Rb, Ba, Pb, and P_2O_5 vs. Mg # in 'MMVF' basalts. Symbols are: ◇ - olivine nephelinite, ● - basanites, ■ - a.o.b., △ - olivine tholeiites.

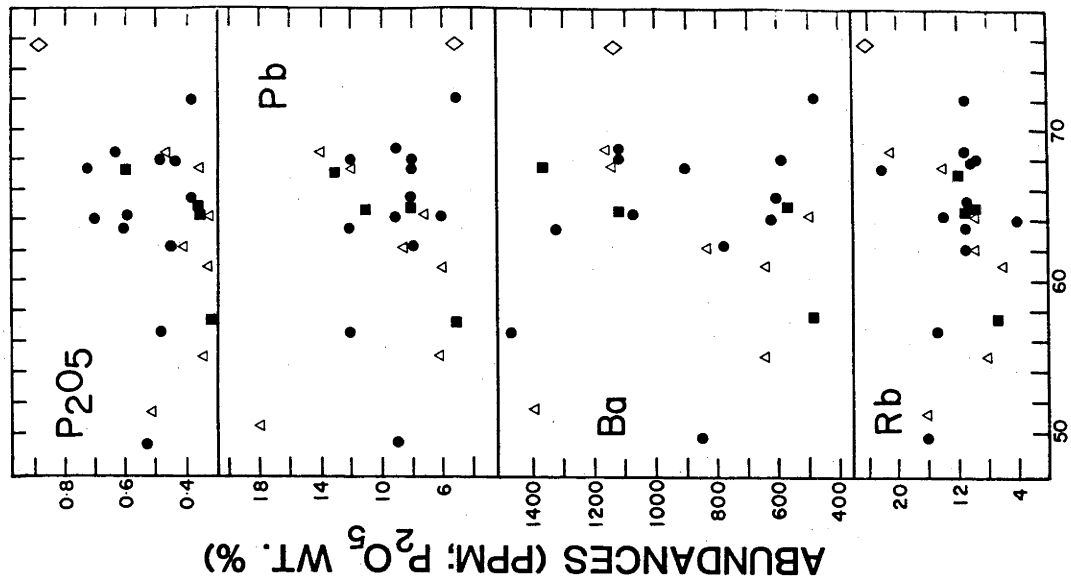
ABUNDANCES (PPM; P_2O_5 WT. %)
P_2O_5
Pb
Ba
Rb
100 MG/MG + FE^{2+}

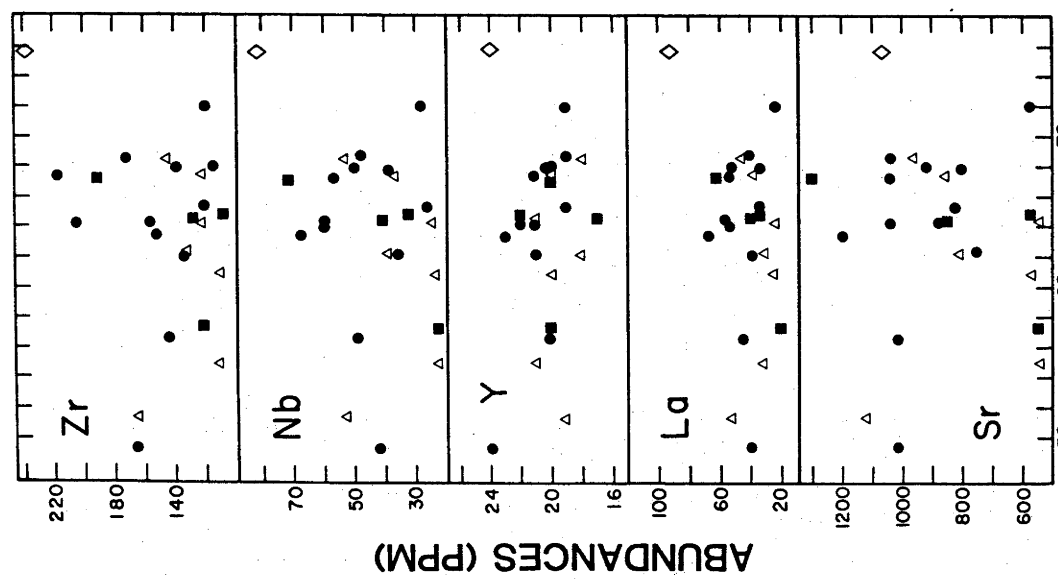
ABUNDANCES (PPM)
Zr
Nb
Y
La
Sr
100 MG/MG +FE^{2+}

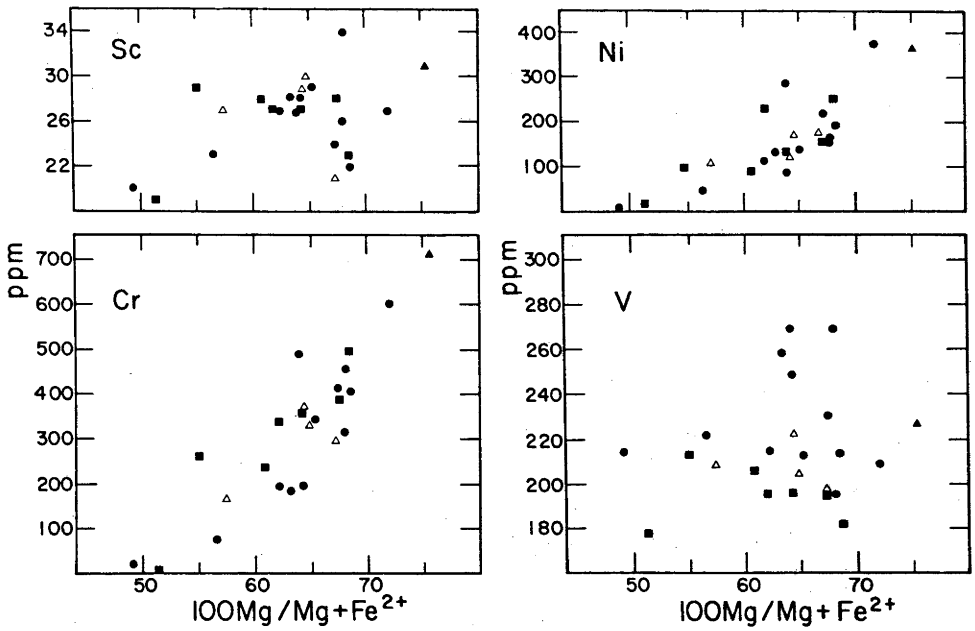

Figure 12: Abundances of Sc, Cr, Ni, and V (ppm) plotted against Mg # for 'MMVF' basalts. Linear correlations are observed only for Ni and Cr. Symbols are: ▲ - olivine nephelinite, ● - basanites, △ - a.o.b., ■ - olivine tholeiites.

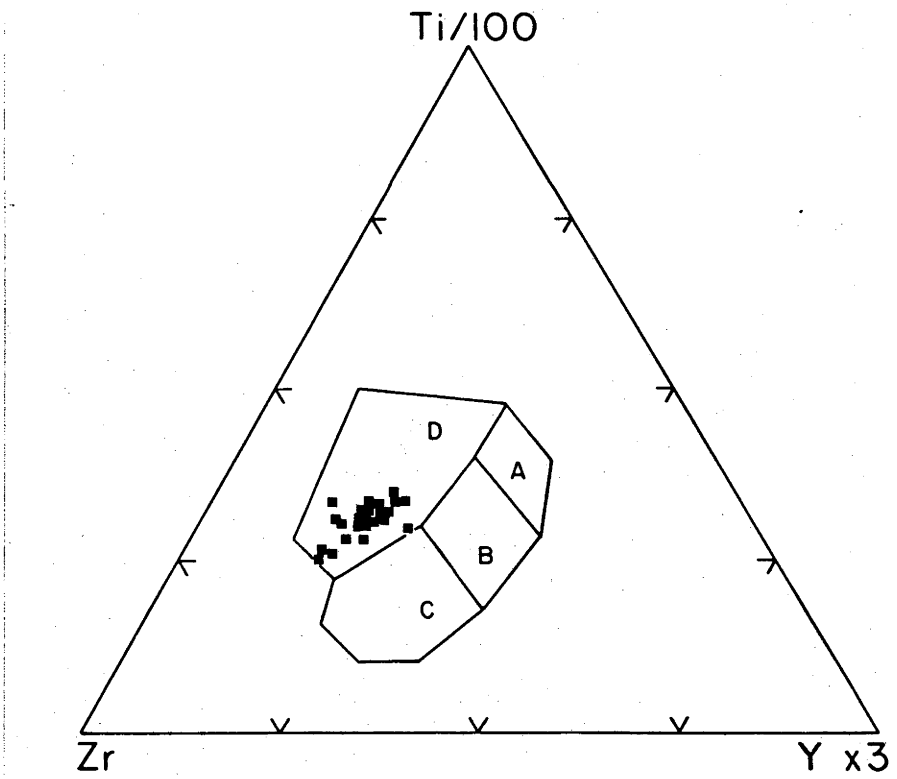

Figure 13: 'MMVF' basalts projected in Zr - Ti/100 - Yx3 ternary, suggested as a useful tectonic discriminant for basalts (Pearce and Cann, 1973). Fields A and B are ocean floor basalts and low K tholeiites; fields B and C are calc-alkalic basalts and field D is ocean island and continental (within) plate basalts.

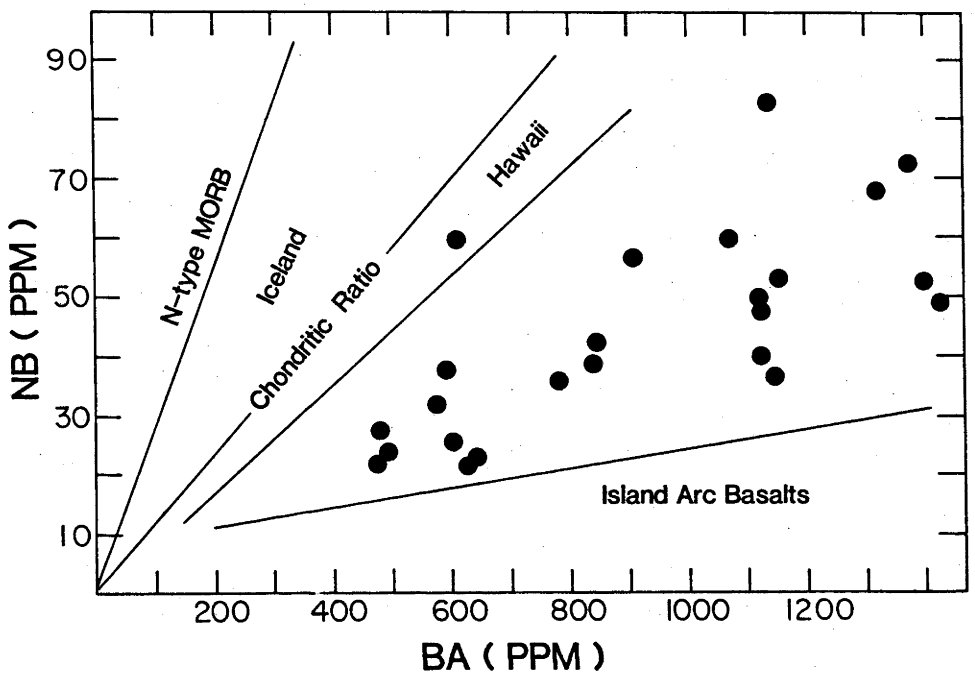

Figure 14. Nb vs. Ba abundances in 'MMVF' basalts. The various fields of basalts from other tectonic environments are taken from Perfit et al. (1980).

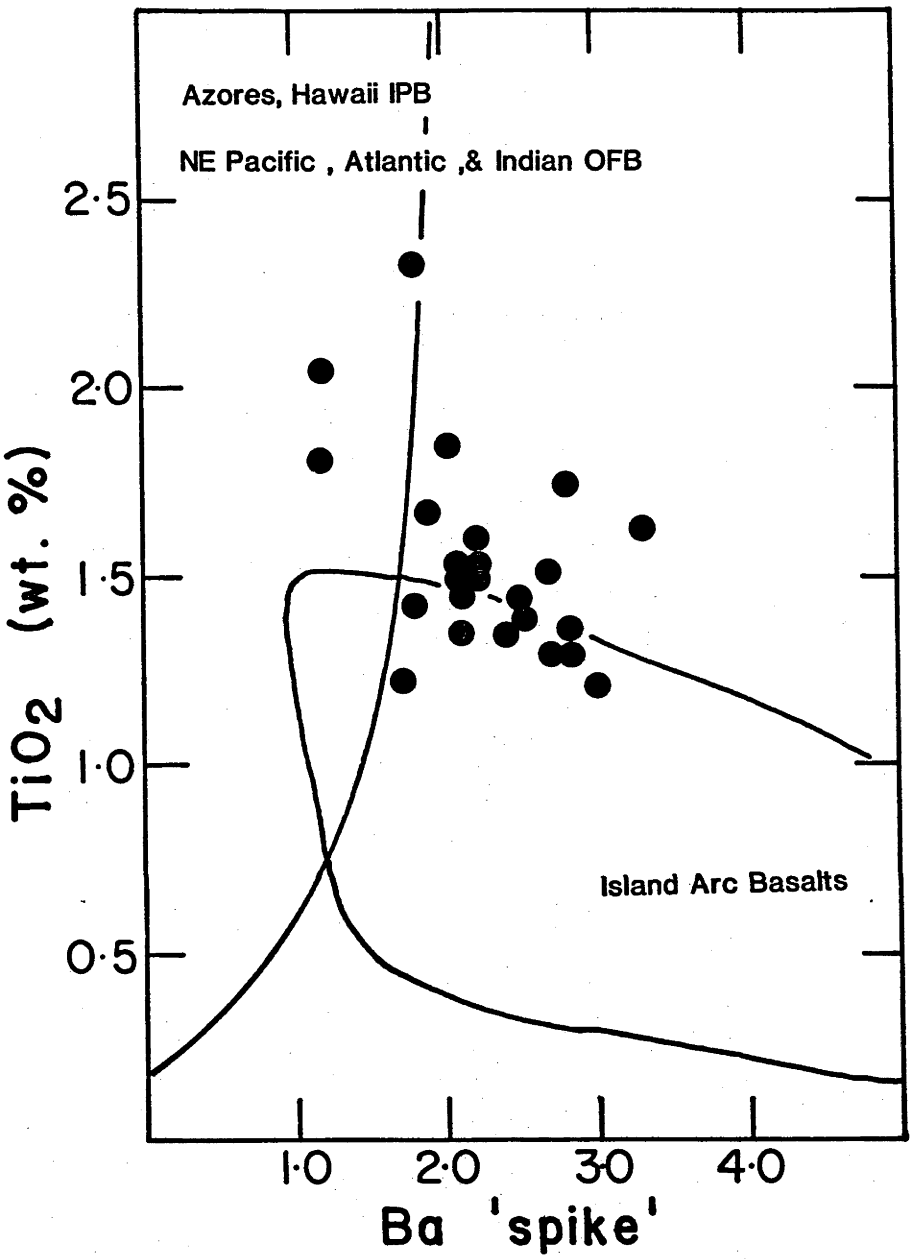

Figure 15. TiO_2 (wt. %) vs. Ba 'spike' (Ba^{CH}/La^{CH}) for 'MMVF' basalts. The fields of island arc basalts and basalts from oceanic environments are from Perfit et al.(1980).

element abundances. Basanites, alkali olivine basalts and olivine tholeiites exhibit considerable overlap with respect to these elements. Only the olivine nephelinite can be recognized by its characteristic trace element signature.

The contents of the incompatible elements vary within the basaltic suite (excluding the olivine nephelinite) by up to a factor of ∿3. There is a suggestion that two groups, with low and high abundances of these elements exist within the suite. However, there are numerous exceptions to this suggestion, for example, MMT-1 has extremely low Rb and Ba, but relatively high Sr, La, Zr and Nb. The least variation is observed in the abundances of Y, which range from 16 to 24 ppm.

b) Compatible Elements - The range in abundances of the compatible elements, Ni, Cr, Sc and V, is similar for the various basaltic groups. Ni and Cr contents exhibit a modest correlation with Mg# (Fig. 12). The olivine nephelinite (Mg# = 75) contains the most Ni and Cr (366 and 714 ppm). Less than 25 ppm Ni and Cr is contained in the basalts with the lowest Mg#. These basalts, a basanite and an olivine tholeiite, are distinctive in their high (>18 wt.%) Al_2O_3 contents. Sc and V do not exhibit any systematic variation with respect to Mg# (Fig. 12). V abundances possibly correlate with the various basaltic types with silica-undersaturated basalts containing $\geq$200 ppm and silica-saturated basalts $\leq$200 ppm.

Comparative Geochemistry - An exhaustive comparison of the 'MMVF' basaltic suite with basaltic suites from other areas and other tectonic environments is beyond the scope of the present investigation. In general, the 'MMVF' basalts are similar to basalts erupted in other continental intra-plate environments, such as the Basin and Range, Western U.S.A. (Leeman and Rogers, 1970; Best and Brimhall, 1974) and SE-Australia (Frey et al., 1978; Irving and Green, 1976; Wass, 1980). This intra-plate characterization is illustrated by the position of the 'MMVF' basalts in the Ti/100 - Zr - 3Y diagram (Fig. 13) advocated by Pearce and Cann (1973) as a useful discriminant for basalts erupted in different tectonic settings. Nb vs. Ba and TiO_2 vs. Ba^{CH}/La^{CH} (Ba 'spike') (Perfit et al., 1980) (Figs. 14, 15) also indicate that 'MMVF' basalts are not similar to island arc basalts or N-type MORB.

DISCUSSION

The petrology and geochemistry of the MMVF basalts are examined

to 1) identify possible primary magmas which may provide information on the chemistry of, and processes operating within, the sub-continental upper mantle beneath the Colorado Plateau; 2) define processes of partial melting, fractional crystallization, magma mixing and contamination which explain the diversity of the basaltic compositions; and 3) provide the necessary data with which to assess the possible relationship with the various occurrences of andesite-rhyodacite of the 'MMVF' (Chapter 6). These aspects are initially treated qualitatively and then quantitatively through application of various types of petrochemical modelling.

Primary Magmas - Criteria for the identification of primary basalts generated by partial melting of a peridotitic source and uncompromised by extensive fractionation processes, have been discussed by many authors (e.g. Frey et al., 1978), and this discussion draws heavily upon these studies. Primary basalts of the Mormon Mountain volcanic field are distinguished by their relatively high Mg# (68-75), and high contents of the compatible trace elements, Ni (>160 ppm), Cr (>295 ppm) and Sc (>21 ppm). Ten basalts have been identified as possible primary basalts and include the olivine nephelinite, six basanites, two alkali olivine basalts and one olivine tholeiite (Table 3). As each of these basalts contain abundant olivine phenocrysts, suggesting that they have 'perhaps' suffered some degree of olivine fractionation. they are 'corrected' to an arbitrary, but uniform Mg # of 71, appropriate for equilibrium with a mantle of Mg# 89. The olivine nephelinite (Mg# = 76) and a basanite (Mg# = 72) were not adjusted.

The addition of olivine to these basalts necessitates an adjustment in the trace element abundances. Olivine contains virtually no incompatible trace elements, hence the correction to these elements is simply a dilution by the amount of olivine added. However, because olivine (and spinel) exhibit a marked affinity for the compatible elements, Ni, Sc, V and Cr, the abundances of these elements cannot be adjusted unequivocally (Frey et al., 1978). The compatible elements are therefore not corrected for olivine addition and abundances not used for arguments relating to source characteristics and degree of partial melting. The adjustments to the abundances of incompatible elements are given in Table 3.

The interpretation of the geochemical characteristics of the primary melts depends upon identifying features which are the result of different pressures, temperatures, and degrees of partial melting in contrast to source heterogeneities. It is simplest to assume,

Table 3 Primary magmas (corrected for olivine addition).

	MMT 24	MMT 29	MMT 1	MMT 2	MMT 30	MMT 27	MMT 16	MMT 31	MMT 19	MMT 26
SiO_2	43.55	44.70	43.93	47.29	49.57	45.32	51.01	46.00	46.59	46.44
TiO_2	1.80	2.06	1.70	1.60	1.38	1.45	1.19	1.27	1.48	1.04
Al_2O_3	12.66	13.15	12.85	14.20	13.77	15.23	14.20	13.40	13.87	13.54
FeO	9.89	10.86	11.59	9.75	9.07	9.74	8.68	10.76	10.58	11.26
MnO	-	-	.17	.14	-	-	.13	-	-	-
MgO	14.59	14.73	15.64	12.90	12.36	13.08	11.82	14.54	12.96	15.15
CaO	12.14	9.48	10.14	9.70	8.86	11.28	8.46	10.13	10.51	9.20
Na_2O	3.35	3.47	3.15	3.24	3.38	2.70	2.98	2.82	2.85	2.52
K_2O	1.23	.58	.49	.71	1.21	.75	1.25	.83	.87	.63
P_2O_5	.89	.65	.58	.58	.54	.44	.43	.39	.38	.31
Mg#	76.0	70.8	70.7	70.3	71.0	70.6	70.9	70.8	72.0	70.7
Ba	1135	797	503	1025	1226	1014	1052	525	480	481
Rb	24	19	3.3	10	11	9	19	9	11	8.4
Sr	1065	915	858	951	1163	823	878	712	570	479
Pb	5	7	5	8	12	10.8	13	7	5	6.7
Zr	240	192	170	156	171	105	133	124	120	91.5
Y	24	18	18	17	18	18	17	18	19	18
Ga	14	15	14	15	16	15	15	14	15	14
Nb	83	50	49	44	64	45	48	34	28	27
Cu	70	46	44	53	60	73	59	76	76	57
Zn	83	82	70	76	78	75	66	74	86	127
La	92	45	44	37	55	47	38	30	23	28
% partial melt	6.7	9.2	10.3	10.3	11.1	13.6	13.9	15.3	15.7	19.3
CaO/Na_2O	3.62	2.73	3.22	2.99	2.62	4.18	2.83	3.59	3.68	3.65
CaO/Al_2O_3	.958	.721	.789	.683	.643	.741	.596	.756	.758	.679
K/Rb	425	253	1232	598	913	693	546	765	656	614
Ba/La	1.25	1.80	1.16	2.82	2.27	2.20	2.82	1.78	2.12	1.75
Zr/Nb^{CH}	2.89	3.84	3.47	3.54	2.67	2.33	2.77	3.64	4.28	3.40
+olivine%	-	12.0	17.5	8.5	10.5	9.5	8.5	11.0	-	16.0

initially, a uniform source composition to evaluate the effects of partial melting before further complications of the model with different sources are considered. This has been done and following the reasoning of Frey et al. (1978), pyrolite (Ringwood, 1966) is chosen as a working mantle composition.

Several key elements and their ratios are useful in understanding the chemistry of the basalts in relation to their genesis. Phosphorus, a highly incompatible element in a mantle assemblage (cf. Beswick and Carmichael, 1978, 1980; Frey et al., 1980; Watson, 1980) defines the degree of partial melting. TiO_2 and CaO contents provide rough estimates on the degree of melting with both decreasing as melting increases. Melts produced by small degrees of melting are enriched in a jadeite component, contributed by the melting of clinopyroxene. This component is diluted in melts produced by greater degrees of melting by the diopside component. Consequently the ratio of CaO/Na_2O increases as the degree of melting increases; this increase provides a qualitative monitor of degree of melting.

Qualitative Assessment - a) Major Element - The olivine nephelinite (Mg# 76) with its low contents of SiO_2 and Al_2O_3 and high contents of MgO, CaO, TiO_2 and P_2O_5 resulted from only a small degree of partial melting. The CaO/Na_2O ratio is high relative to the estimated degree of melting (Table 3) but may be explained by bonding of Ca with $CO_3^=$ in the melt (Frey et al., 1978). Melts formed by small degrees of partial melting would be more sensitive to variation in fluid composition than those formed by higher degrees of melting.

The olivine basanites, adjusted for 0 to 17.5% olivine fractionation, exhibit a moderate degree of variation in composition. The higher SiO_2 and Al_2O_3 contents and lower MgO, CaO, TiO_2 and P_2O_5 contents of the olivine basanites compared with the olivine nephelinite suggests that their genesis involves a higher degree of partial melting. TiO_2 contents and CaO/Na_2O ratios are variable, but correlations with P_2O_5 (Fig. 16), indicate that this variability may be a function of degree of melting, rather than source composition.

Two alkali olivine basalts (+10.5% and 16% olivine) are richer in SiO_2 and Al_2O_3 and poorer in CaO and MgO than the more undersaturated basalts. TiO_2 content is generally lower than in the basanites and increases with P_2O_5 content, consistent with a model involving different degrees of partial melting to account for variations of these oxide abundances. CaO/Na_2O ratios vs P_2O_5

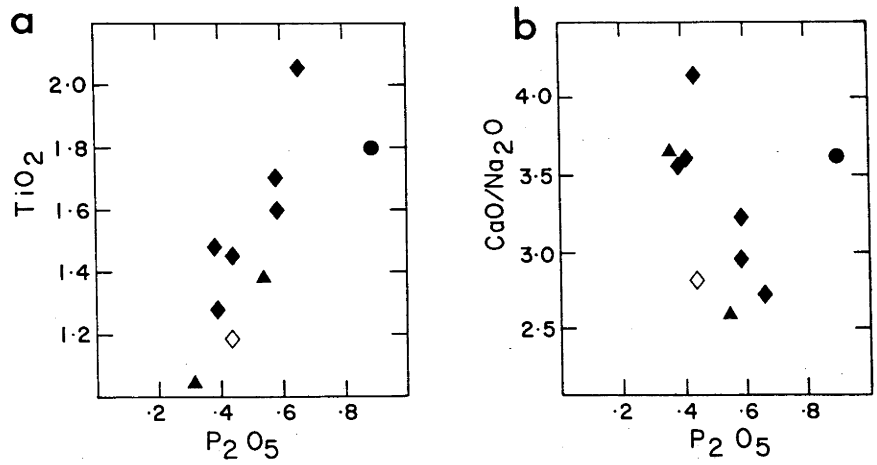

Figure 16.a) TiO_2 vs. P_2O_5 for primary 'MMVF' basalts. Symbols are: ●-olivine nephelinite, ◆-basanites, ▲-a.o.b., ◇-olivine tholeiite. b) CaO/Na_2O vs. P_2O_5 for primary 'MMVF' basalts Symbols as above.

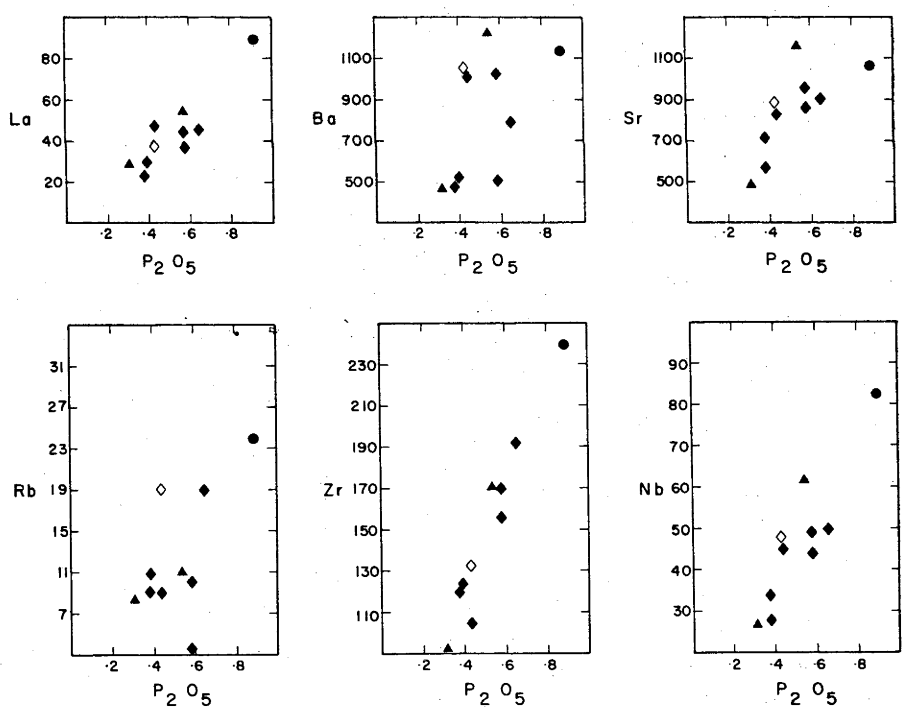

Figure 17.a) La vs. P_2O_5 , b) Ba vs. P_2O_5 , c) Sr vs. P_2O_5 , d) Rb vs. P_2O_5 , e) Zr vs. P_2O_5 , f) Nb vs. P_2O_5 for primary 'MMVF' basalts. Symbols as above.

exhibit a similar behaviour, although these values both overlap with the basanites.

The olivine tholeiite, although it fulfills the basic requirements for consideration as a primary magma, has suffered clinopyroxene fractionation as indicated by its extremely low CaO/Al_2O_3 ratio (.595). The effect of this fractionation on the primary characteristics of the tholeiite is difficult to predict, however, the low TiO_2 contents and CaO/Na_2O ratios, as well as moderate P_2O_5 content, suggest that this basalt was generated by a moderate degree of partial melting.

b) Trace Elements - Qualitative treatment of the adjusted abundances of the incompatible trace elements, Rb, Ba, Sr, Pb, La, Y, Zr and Nb, of the primary MMVF basalts (Table 3) indicates that:

A) abundances of the incompatible elements correlate with degree of melting, decreasing as the amount of melting increases.

B) the status of several basalts classified as primary has probably been compromised by clinopyroxene fractionation.

C) abundances and ratios of several highly incompatible elements (Rb, Pb, Ba) imply crustal contamination

and D) mantle source chemistries are different for the alkalic and subalkalic basalts.

It has already been suggested that the abundance of P_2O_5 provides a good estimate of the degree of partial melting. This suggestion is based on the observation that the most undersaturated magmas (those most likely to form from small degrees of partial melting (Green, 1969)) have the highest P_2O_5 contents. Plots of other incompatible trace elements against P_2O_5 therefore provide information on their variation with respect to degree of partial melting. Variations of La vs. P_2O_5, Ba vs. P_2O_5, Sr vs. P_2O_5, Rb vs. P_2O_5, Sr vs. P_2O_5 and Nb vs. P_2O_5 (Figs. 17a-f), although irregular, define patterns of incompatible element enrichment with decreasing amount of partial melting. The olivine nephelinite, representing the least amount of melting, has the highest abundances of all incompatible trace elements.

The irregularities in the incompatible element abundance trends provide additional information and deeper insight into the geochemical evolution of 'MMVF' primary basalts. One cause for irregular behaviour has been alluded to earlier, that is, that some of the primary basalts appear to have suffered clinopyroxene as well as

Figure 18.a) Zr/Nb vs. P_2O_5 for all 'MMVF' basalts. Primary basalts are indicated by small ,circled symbols. The arrows qualitatively indicate the effects of partial melting a source containing residual garnet and clinopyroxene and fractionation of clinopyroxene. Symbols are: ● -olivine nephelinite, ◆ -basanites, ▲ -a.o.b., ○ -olivine tholeiites.

b) Zr/Nb vs. CaO/Al_2O_3 for all 'MMVF' basalts. Description is the same as given above.

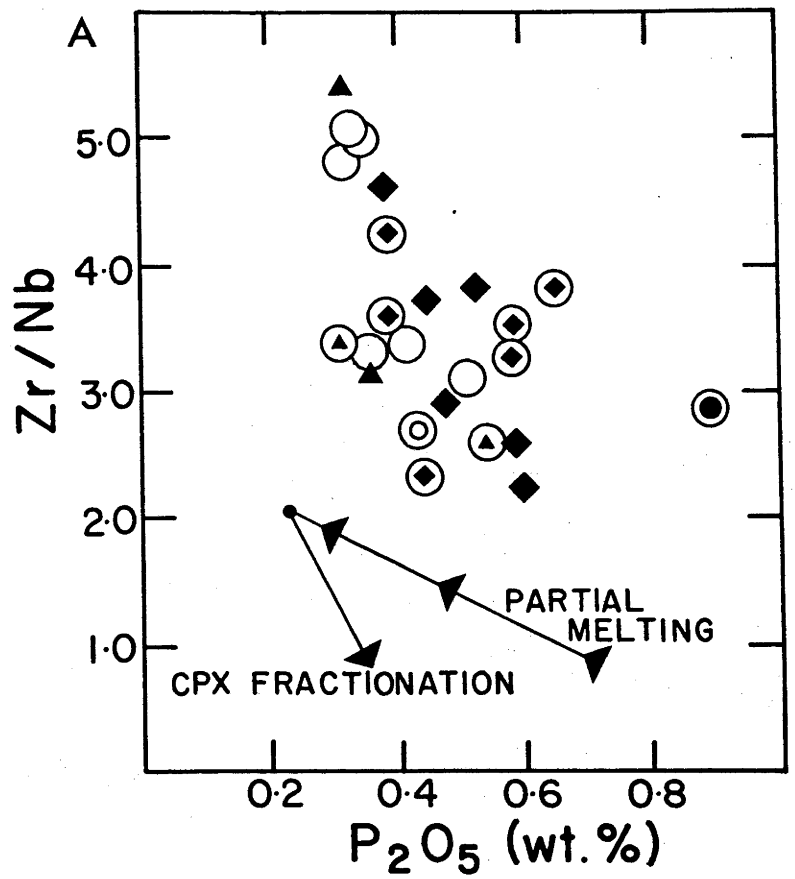
A
5·0
4·0
3·0
2·0
1·0
Zr/Nb
PARTIAL
MELTING
CPX FRACTIONATION
0·2
0·4
0·6
0·8
P2O5 (wt.%)

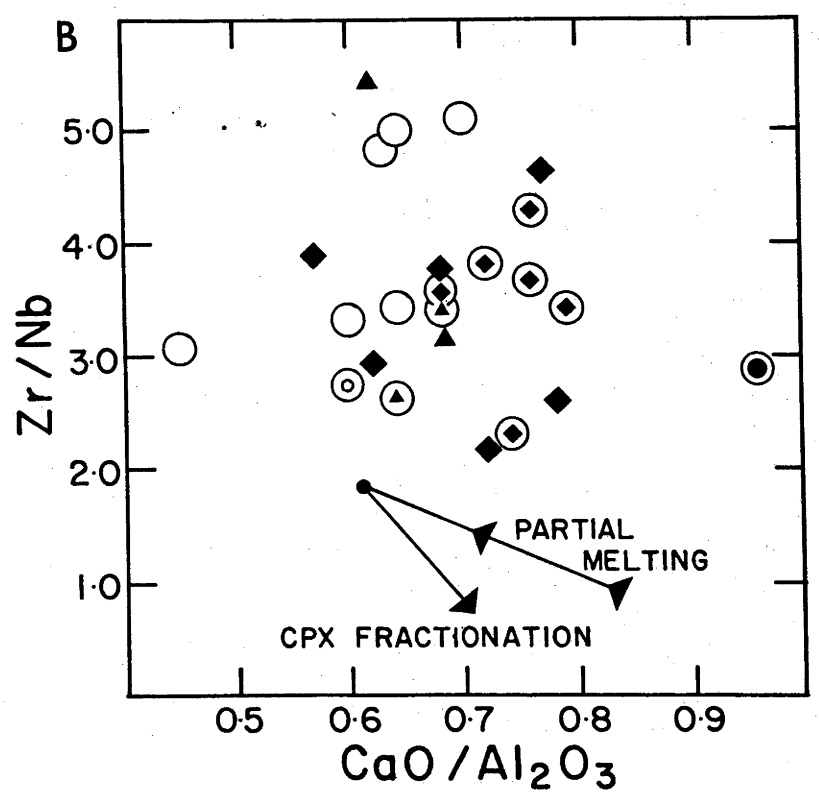
B
5·0
4·0
3·0
2·0
1·0
Zr/Nb
PARTIAL
MELTING
CPX FRACTIONATION
0·5
0·6
0·7
0·8
0·9
CaO/Al2O3

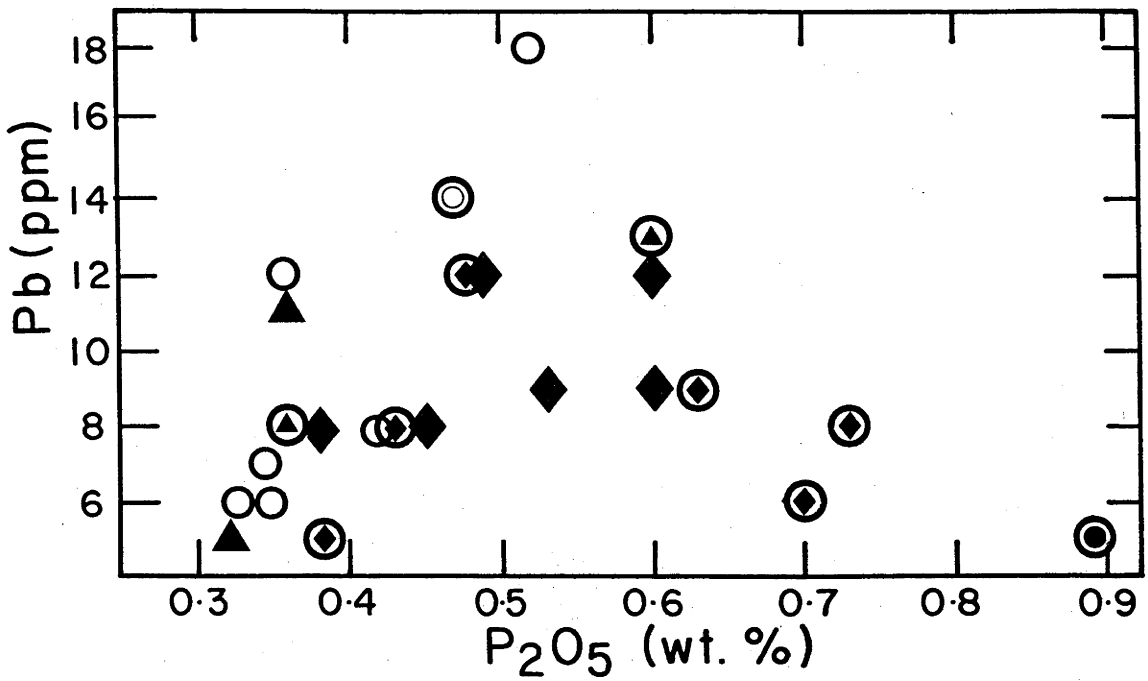

Figure 19. Abundances of Pb vs. P_2O_5 in 'MMVF' basalts. Symbols are described in the caption for Figure 18. The irregularities observed in Pb abundances probably result from contamination of the basalts with a crustal Pb component.

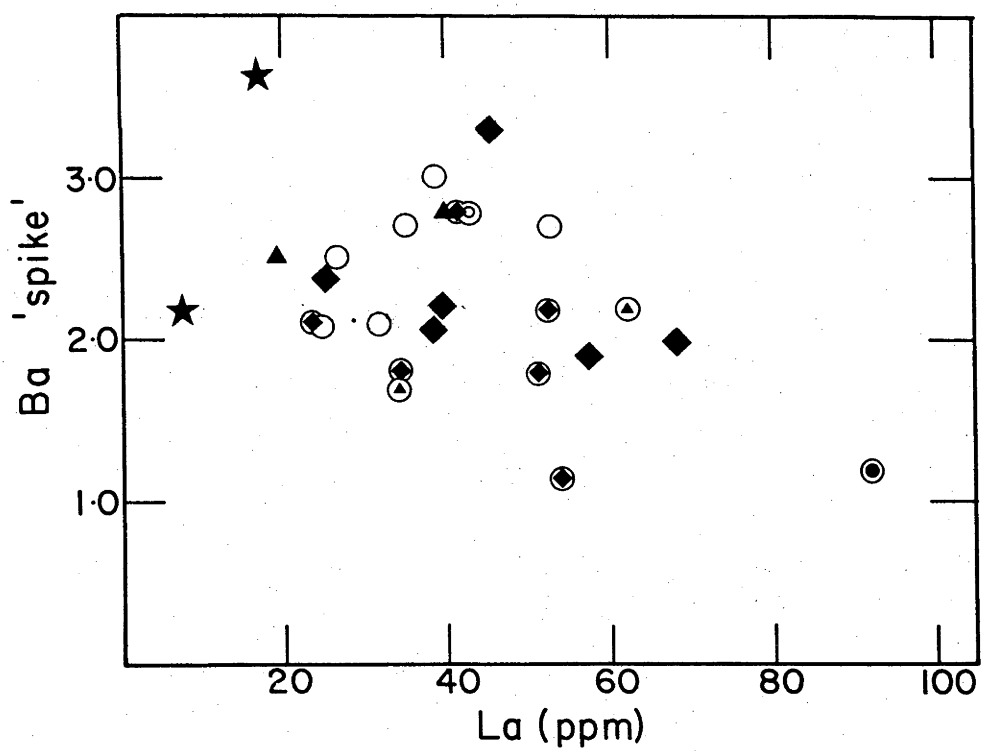

Figure 20. Ba 'spike' vs. La abundance in 'MMVF' basalts. Symbols are described in the caption of Figure 18. The stars are analyses of granulites from the lower crust of the Colorado Plateau. The high Ba 'spike' relative to La is a reflection of crustal contamination. See text for discussion.

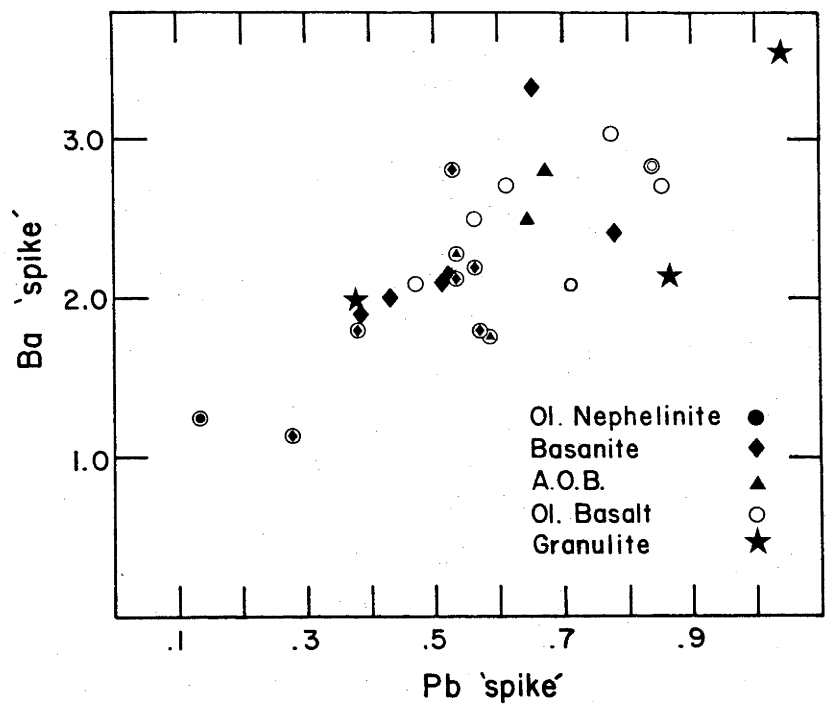

Figure 21. Ba 'spike' vs Pb 'spike' (Pb^{N}/La^{CH} - Pb normalization value of Sun,1980). As in Figure 20, the increase in Ba 'spike' and Pb 'spike' indicates crustal contamination of the basalts with respect to Ba and Pb.

olivine fractionation. The Zr/Nb ratio is a sensitive indicator of clinopyroxene involvement in magma evolution (McCallum and Charette, 1978) with Zr being enriched in clinopyroxene relative to Nb. The variations of Zr/Nb against P_2O_5 or CaO/Al_2O_3 (Figs. 18a,b) for the primary 'MMVF' basalts suggest that some basanites, all alkali olivine basalts and the olivine tholeiite have experienced clinopyroxene fractionation.

Irregularities in the abundances of several highly incompatible elements, Ba, Rb, K, Pb, may be due in part to clinopyroxene fractionation, but also may be explained by contamination with crustal materials. 'MMVF' basalts are erupted through approximately 45 km of crust. It is consequently simplistic to suppose that, except in exceptional circumstances, any basalt, passing through such a thick crust could remain chemically unaffected by the wall rocks. While not perhaps immediately visible in the major element geochemistry of the basalts, the interaction of magma with the crust or crustal fluids may noticeably affect the abundances of highly incompatible elements.

The irregularities observed in the variation of Ba, and Pb versus P_2O_5 (Fig. 17b and Fig. 19) reflect crustal contamination. P_2O_5, due to the likely presence of apatite in crust and consequent immobility of phosphorus, is not subject to contamination. It is interesting to note that La, itself a highly imcompatible element, does not exhibit any apparent effects of contamination (Fig. 17a).

Examination of chondrite-normalised Ba/La ratios (Ba 'spike') and Pb/La (Pb 'spike') against La abundances (Fig. 20) or against each other (Fig. 21) also suggests that crustal contamination may have enriched the primary 'MMVF' basalts in Ba and Pb. The Ba 'spike' and Pb 'spike' should decrease slightly as the degree of melting increases if the magmas are derived from a homogeneous source. The lack of such a trend in either of the Figures, indicates that additional processes beyond partial melting must have occurred. Fractional crystallization of clinopyroxene can slightly increase Ba 'spike' and Pb 'spike', however these increases are much less than those needed to explain the observed characteristics of the 'MMVF' basalts. Contamination of these magmas with crustal-derived Ba and Pb, in addition to clinopyroxene fractionation, is a possible mechanism by which both Ba 'spike' and Pb 'spike' are changed.

With regards to a contamination process, it is important to note the abundances of Ba and Pb in a basalt which exhibits the least contaminated character. The olivine nephelinite, which possiblly

represents the most primary magma of the 'MMVF' basaltic suite, contains high Ba (1135 ppm) but low Pb (5 ppm). Basalts resulting from larger degrees of melting from a similar source as that of the olivine nephelinite, should have lower Ba contents, but even more significantly, lower Pb contents. These observations indicate that the crustal contaminant must be highly enriched in Ba, but only slightly enriched in Pb, to create the variations observed in Ba 'spike' and Pb 'spike'. Abundances of Ba, Pb and La in granulites of lower crustal derivation (Appendix 8) plotted as stars in Figures 20 and 21, such that bulk assimilation of such material within reasonable limits, is inadequate to explain the observed features of the basalts. A more likely contaminant is a fluid or melt phase derived from these granulites by the passage of hot basaltic material, and enriched in highly incompatible elements.

Finally, if the effects of these processes (partial melting, fractionation and crustal contamination) can be identified, then, differences due to variations in source chemistry and conditions of magma generation (P, T, fH_2O) can be recognized. To this purpose, only P, La, Y, Zr and Nb provide information on the mantle source. Referring to the figures utilizing these elements, it becomes apparent that one alkali olivine basalt (MMT-31) and the olivine tholeiite cannot be derived (if they reflect greater degrees of partial melting) from the same source as the basanites and olivine nephelinite. The degree of melting indicated by the P_2O_5 content of this alkali olivine basalt, suggests that the basalt was generated by a degree of melting only slightly greater than the most enriched basanite. This inconsistency with a petrogenetic model in which alkali olivine basalts represent larger degrees of melting than do basanites (e.g. Frey et al., 1978), implies that the source of this anomalous alkali olivine basalt must be enriched in P_2O_5, as well as other incompatible elements. In general however, the abundances of P, La, Y, Zr and Nb of the primary 'MMVF' basalts are compatible with the afore-mentioned model.

Quantitative Models - The application of several petrochemical calculation schemes, even with their numerous assumptions and limitations (see Chapter 6), allows discrimination between likely and unlikely petrogenetic processes. The origins of the primary basalts of 'MMVF' are examined using the theory and equations develped to model the behaviour of trace elements during partial melting (Hertogen and Gijbels, 1976). The results of these calculations are used to

Table 4 Residual mantle compositions and mineralogy.

	(Pyrolite) - (Primary Melt)										
	MMT-24	MMT-29	MMT-1	MMT-2	MMT-30	MMT-27	MMT-16	MMT-31	MMT-19	MMT-26	PYROLITE[1]
% melt	6.7	9.2	10.3	10.3	11.1	13.6	13.9	15.3	15.7	19.3	-
SiO_2	45.27	45.21	45.30	44.91	44.61	45.13	44.21	45.0	44.89	44.59	45.16
TiO_2	.63	.57	.60	.61	.63	.59	.63	.61	.57	.63	.71
Al_2O_3	2.89	2.57	2.47	2.32	2.26	1.70	1.82	1.76	1.62	1.15	3.54
FeO	8.35	8.21	8.09	8.30	8.37	8.24	8.41	8.03	8.05	7.77	8.45
MgO	39.11	39.77	39.98	40.30	40.60	41.30	41.61	41.61	42.03	42.81	37.47
CaO	2.43	2.43	2.27	2.32	2.36	1.79	2.21	1.81	1.70	1.62	3.08
Na_2O	.37	.28	.27	.26	.22	.23	.14	.16	.14	.10	.57
K_2O	.05	.08	.09	.06	.01	.03	-	.005	-	-	.13
P_2O_5	-	-	-	-	-	-	-	-	-	-	.06
	High-Pressure Normative Mineralogy[2]										
Olivine	58.40	61.15	61.16	63.66	65.71		70.21	66.76	68.31		54.44
Orthopyroxene	22.95	21.22	22.79	19.70	17.10		14.37	22.12	21.62		20.10
Clinopyroxene	10.22	11.05	10.09	10.79	11.31		11.26	8.30	7.81		13.66
Garnet	7.62	5.97	5.31	5.13	5.18		3.47	2.21	1.70		10.69
	Residue Calculated from Normative Mineralogy										
SiO_2	45.27	45.21	45.30	44.91	44.61		44.21	45.00	44.89		
TiO_2	.31	.29	.28	.27	.26		.22	.22	.20		
Al_2O_3	2.87	2.51	2.37	2.27	2.21		1.76	1.62	1.47		
FeO	8.45	8.48	8.49	8.53	8.57		8.66	8.63	8.67		
MgO	39.09	39.72	39.90	40.26	40.56		41.56	41.49	41.91		
CaO	2.43	2.44	2.28	2.33	2.36		2.22	1.82	1.71		
Na_2O	.24	.25	.24	.24	.25		.24	.20	.19		

Table 5 Mineral compositions used in mantle norm.

	Olivine	Orthopyroxene	Clinopyroxene	Garnet
SiO_2	41.0	55.5	53.6	40.8
TiO_2	-	.5	.9	1.4
Al_2O_3	-	3.4	4.9	20.8
FeO	9.70	7.1	4.6	9.0
MgO	49.0	31.0	17.8	20.2
CaO	.1	1.7	15.1	5.8
Na_2O	-	.2	1.9	-

characterize the geochemistry of the upper mantle source of the MMVF basalts.

Frey et al. (1978) present one of the most detailed, recent assessments of basaltic petrogenesis, based upon geochemical, petrologic and experimental petrologic considerations. Their approach, which is modified for use here, embodies several assumptions. These are:

A) that in terms of major element compositions, the mantle is homogeneous and equal to pyrolite.

B) that high-pressure experimental data collected by D.H. Green and others on specific basaltic compositions can be extended to encompass similar basaltic compositions which can be ultimately related by partial melting of pyrolite.

and C) P_2O_5 contents of primary basalts accurately reflect the degree of partial melting.

The Frey et al. (1978) approach essentially consists of using the major element chemistry of a primary basalt and its assumed degree of melting (P_2O_5 content) to calculate a residual mantle composition. The normative mineralogy (based on experimental data) is calculated for this residual mantle. Trace element abundances are then calculated using this residual normative mineralogy and matched with the abundances in the basalt to indicate what the trace element characteristics of the original mantle source were prior to melting.

The degrees of partial melting which the primary basalts (olivine fractionation corrected) of 'MMVF' represent are given in Table 3. These values range from ∿7 percent for the olivine nephelinite to ∿20 percent for an alkali olivine basalt. The degree of partial melting exhibits a fairly systematic increase with regards to the increasing silica-saturation of the basalts. Magmas which have suffered modest amounts of clinopyroxene fractionation deviate from this general trend.

Residual mantle compositions and their respective high-pressure normative mineralogies are calculated for each primary basalt (Table 4). The compositions of the phases, olivine, orthopyroxene, clinopyroxene and garnet, used in this normative calculation are from the experimental work of Green (1973) and given in Table 5. The compositions derived from basanitic magma may not be strictly applicable to the extremes of basaltic compositions (i.e. olivine nephelinite, olivine tholeiite) however, considering the breadth of the assumptions of the model, this simplification probably does not sub-

Table 6 Primitive Mantles (ppm)

	Wood et al., 1979	Taylor and McLennan, 1981
Rb	.86	.48
Ba	7.56	4.9
K	252	180
La	.71	.50
Y	4.87	2.9
Sr	23	15.5
Nb	.62	.60
Zr	11	7.8
Pb(1)	.12	.12

(1) Pb values from Sun (1980)

Table 7 Mantle enrichment factors (observed abundance/calculated abundance).

A. Primitive Mantle - Wood et al. (1979).

	MMT-24	MMT-29	MMT-1	MMT-2	MMT-30	MMT-27	MMT-16	MMT-31	MMT-19	MMT-26
Rb	1.92	2.07	.40	1.21	1.45	1.43	3.11	1.61	2.02	1.90
Ba	10.10	9.71	6.70	14.00	18.03	18.27	19.50	10.7	10.00	12.23
Sr	4.17	4.51	3.05	5.08	6.60	5.49	5.97	5.23	4.28	4.24
Zr	2.22	2.13	2.02	1.86	2.14	1.50	1.93	1.94	1.90	1.96
Nb	13.10	9.80	10.40	9.36	14.20	11.6	12.60	9.71	8.00	9.12
La	9.20	6.08	10.60	5.60	8.87	9.23	7.60	6.67	5.20	7.70
Y	1.49	1.07	1.06	1.00	1.05	1.01	.95	.98	1.03	1.00
K	2.73	1.76	1.67	2.42	4.44	3.37	5.74	4.19	4.51	3.93
Pb	2.80	5.38	4.30	6.89	11.10	12.25	15.07	8.93	6.54	10.73

B. Primitive Mantle - Taylor and McLennan (1981).

Rb	3.44	3.70	.72	2.16	2.59	2.56	5.56	2.88	3.61	3.40
Ba	15.55	14.95	10.32	21.60	27.26	28.10	30.03	16.50	15.40	18.83
Sr	5.84	6.32	4.27	7.11	9.24	7.68	8.36	7.32	6.00	5.94
Zr	3.13	3.00	2.85	2.63	3.02	2.11	2.72	2.73	2.68	2.76
Nb	13.50	10.10	10.70	9.64	14.60	11.90	13.00	10.00	8.24	9.40
La	13.00	8.60	15.00	7.95	12.60	13.10	10.80	9.47	7.40	10.90
Y	2.50	1.79	1.78	1.68	1.76	1.69	1.60	1.64	1.73	1.68
K	8.82	2.46	2.34	3.39	6.22	4.72	8.03	5.87	6.31	5.50
Pb	2.80	5.40	4.30	6.89	11.10	12.25	15.07	8.93	6.54	10.73

stantially modify the final result.

The normative mineralogies of the residual mantles are used to calculate the trace element partitioning characteristics for a mantle/melt pair. In the first, the partial melting equations are applied to each normative mineralogy as calculated above while in the second, the various normative mineralogies are used to construct a melting mode for pyrolite. This mode is then used in a sequential calculation in which the partitioning of trace elements between mantle and melt is determined at regular intervals of partial melting. This technique effectively smooths the variations caused by slight differences in the major element chemistry of the primary basalts, but also introduces another simplifying assumption into the petrogenetic model. It is satisfying to note that the results from the two different approaches are comparable.

The results of batch partial melting, using the second technique of calculation, are given in terms of the ratio: abundance in melt/abundance in original source. Two sets of abundances in the melt were calculated by employing two different primitive mantle source compositions. These mantle compositions are those compiled by A) Wood et al. (1979) and B) Taylor and McLennan (1981) (Table 6) which are different by approximately a factor of 1.5 except for similar Nb values. Pb values are taken from Sun (1980).

The calculated abundances of trace elements have then been used to calculate an 'enrichment factor' (observed abundance/ calculated abundance) for the sub-continental upper mantle. The results of this treatment (Table 7) indicate that the mantle source of the'MMVF'primary basalts is approximately homogeneously enriched in the incompatible elements, Rb, Ba, Sr, Zr, Nb, La, Y, K and Pb. The degree of enrichment for a particular element is dependent upon the choice of primitive mantle source composition. A general order of enrichment is, from most to least, Ba, Nb, La, Pb, Sr, K, Rb, Zr and Y.

A major complication in the interpretation of these results concerning mantle enrichments is the possible effects of crustal contamination on the basalts. With regards to this problem, perhaps the best candidate as a mantle probe is the olivine nephelinite, as it was apparently rapidly erupted (presence of ultramafic xenoliths, megacrysts, negligible olivine fractionation). This basalt suggests enrichments in incompatible elements of its mantle source of >9x for Ba, La and Nb and <4x for Sr, K, Rb, Pb, Y and Zr (type A mantle) or

>12x and <6x respectively for type-B mantle (Fig. 22). It is however, somewhat disconcerting that Rb and Pb, both highly incompatible elements, require less enrichment than Ba or La, elements of similar degree of incompatibility. No explanation is readily apparent for this phenomenon. Finally the large degree of enrichment of Nb in the source, when compared to Zr enrichment requires an efficient process to separate these elements. Recent work by Arima and Edgar (1980) on the high pressure stability of wadeite ($Zr_2K_4Si_6O_{18}$) suggests one possible process and there may be others.

The causes of these enrichments in the mantle are highly speculative. Metasomatism of the mantle has been suggested by numerous investigators to explain geochemical anomalies in basalts from many different environments (Wood, 1979; Mysen, 1979; Best, 1975; Menzies and Murphy, 1980; Wass, 1980; Frey et al., 1978; Boettcher et al., 1979). $H_2O + CO_2$ fluids or highly-alkaline melts are proposed as likely metasomatizing agents as both may be enriched in incompatible elements. The origins of these agents are not yet fully understood. The analysis of the 'MMVF' primary basalt data does not clarify the process of mantle metasomatism, but provides only one more example of mantle heterogeneity.

DERIVATIVE BASALTS

Those basalts which have not been identified as primary are derivative, i.e. they have suffered a history of fractional crystallization which has disturbed their mantle-derived chemical signature. This fractionation in addition to other possible processes, has produced the diversity of basaltic compositions observed in the Mormon Mountain volcanic field. As in the case of the primary basalts, the petrogenesis of these derivative magmas is initially considered qualitatively to identify possible processes, which are then treated quantitatively.

Qualitative Assessment - As noted previously, the variation of the major elements with MgO is non-systematic except for the possible example of Al_2O_3. Examination of the variation of Al_2O_3 vs. MgO (Fig. 23) provides information on the likely mineral phases involved in the evolution of the different basaltic groups. All groups exhibit a systematic increase in Al_2O_3 with decreasing MgO. This behaviour, as indicated by the different fractionation pathways of various minerals, identifies olivine and clinopyroxene as the mineral

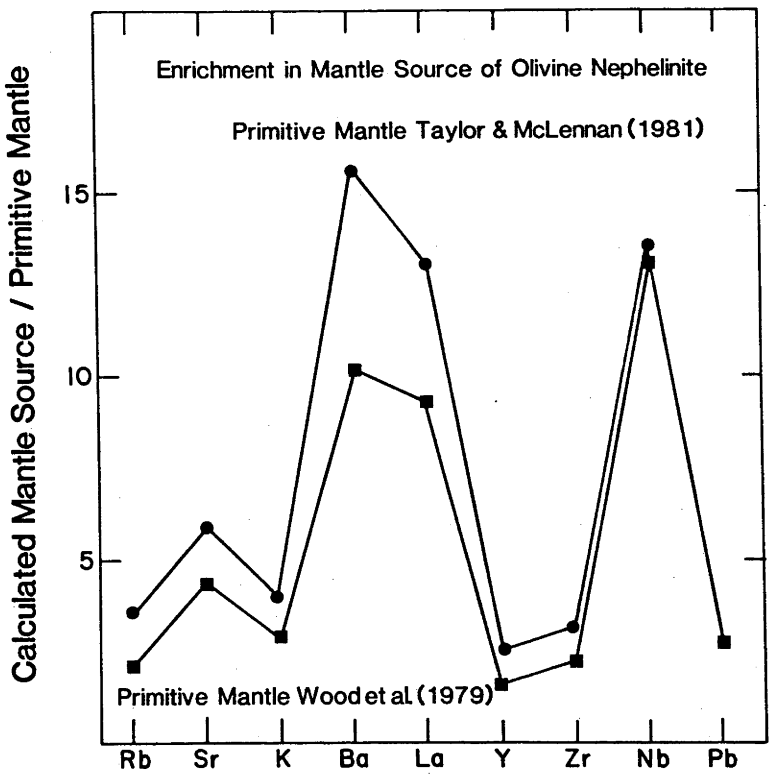

Figure 22. Calculated enrichments in incompatible elements of an upper mantle source for the olivine nephelinite from 'MMVF'. These enrichments are relative to various'primitive' mantles.

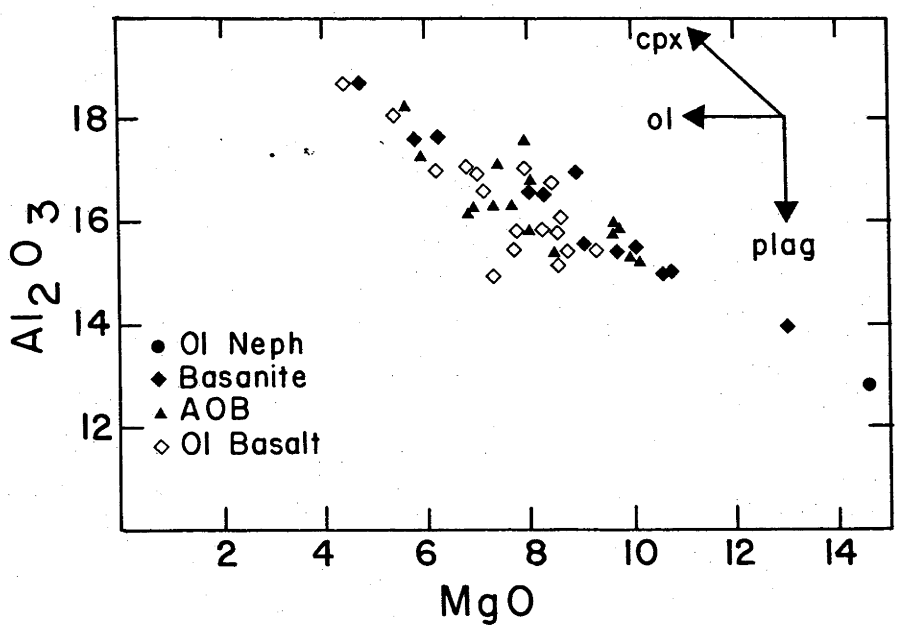

Figure 23. Al_2O_3 vs, MgO abundances of all 'MMVF' basalts. Arrows indicate fractionation trends of clinopyroxene, olivine, and plagioclase. It is evident that plagioclase fractionation is unimportant in the evolution of the 'MMVF' basalts.

phases which control the fractionation processes. Plagioclase fractionation is essentially non-existent.

The abundances and ratios of these elements in the derivative basalts provide information on the nature and extent of fractional crystallization and crustal contamination in the evolution of the Mormon Mountain basalts. As discussed previously in the section on primary basalts, certain groups of incompatible elements are useful indicators of these competing processes. In brief, the incompatible trace element signatures of the derivative basalts are extensions of those observed in the primary basalts.

The ratios, CaO/Al_2O_3 and Zr/Nb, provide means of evaluating the importance of clinopyroxene fractionation. When plotted against one another (Fig. 18b), their negative correlation suggests that clinopyroxene (+ olivine) fracionation occurred in the derivative basalts. Most basalts have low (<.70) CaO/Al_2O_3 ratios, a feature which in itself indicates clinopyroxene fractionation. The three high-Al basalts (Al_2O_3 >17.5 wt.%) are probably the result of extensive olivine, spinel and clinopyroxene fractionation, as evidenced by their low CaO/Al_2O_3. Additionally, Zr/Nb vs. P_2O_5 (Fig. 18a) illustrates further the existence of clinopyroxene (+ olivine) fractionation. There are several basalts which have seemingly anomalous Zr/Nb ratios (4.5) lying above the range of suggested primary basalts. The ratios for these basalts (alkali olivine basalts and olivine tholeiites) can, however, be explained by extensive clinopyroxene fractionation from a primary basalt with even higher Zr/Nb ratios as a result of greater degrees of partial melting of the original source rock (McCallum and Charette, 1978). Primary magmas of this character are apparently not observed due to the high probability that they would suffer fractional crystallization enroute to the surface.

The abundances and ratios of the highly incompatible elements (Ba, K, Rb, Pb and Sr), of the derivative basalts, as with those of the primary basalts, cannot be accounted for by simple crystal fractionation of clinopyroxene and olivine. While this process, no doubt, leaves its impact upon the geochemical signature of those elements, another process, crustal contamination, possibly obscures the recognition of such effects. As indicated in the section on primary magmas, P_2O_5, La and Y do not appear to have been affected by the contamination process, and thus they can be utilized as indicators of crystallization.

If the processes of partial melting and fractional crystallization (involving olivine, clinopyroxene and spinel) were the only explanations for the diversity of the Mormon Mountain basalts, variation diagrams such as K_2O vs. P_2O_5 (Fig. 24) should exhibit good positive correlations. The fact that they do not, and are virtually 'scatter' diagrams instead, suggests additional processes are operative. Selective contamination by crustal materials may account for the abundance variations of the most incompatible elements.

The importance of Ba 'spike' and Pb 'spike' as indicators of contamination have been previously discussed with respect to the primary 'MMVF' basalts. The derivative basalts exhibit the same characteristics, but which are developed to a more extensive degree. These basalts have the highest Ba 'spikes' and Pb 'spikes' of the entire 'MMVF' basaltic suite (Fig. 21), suggesting that their abundances of highly incompatible elements reflect crustal contamination.

The recognition of Pb as an incompatible element precludes the existence of a fractionating sulphide phase. This conclusion is supported by the lack of correlation between Pb and the chalcophile elements, Cu and Zn (Figs. 25a,b), as well as the lack of correlation between Cu and Zn. The Cu contents of the 'MMVF' basalts are relatively high (up to 95 ppm) compared with other basalts (Frey et al., 1978). No distinction of Cu content with alkalinity (i.e. olivine tholeiite versus basanite) is evident. Lower Cu contents (<70 ppm) may be the result of clinopyroxene fractionation (K_D = 1.5 to 2.4; Seward, 1971). The interpretation of the Zn data is limited by lack of understanding of its geochemical behaviour in silicate systems.

Thus, the abundances of the incompatible elements of these derivative magmas can be explained by the processes of partial melting, fractional crystallization and crustal contamination. It appears that only those elements which are the least compatible (i.e. Ba, K, Pb, Sr and Rb) are affected by the contamination process. The absence or at least undetectable influence of such contamination on either the more compatible elements or the major elements, suggests that large scale assimilation of the crust is not operative. Instead, the contamination is accomplished through interaction with crustal fluids or small proportions of crustal melts.

The abundances of the compatible trace elements (Ni, Cr, V, Sc) in the derivative basalts suggest that a fractional crystallization

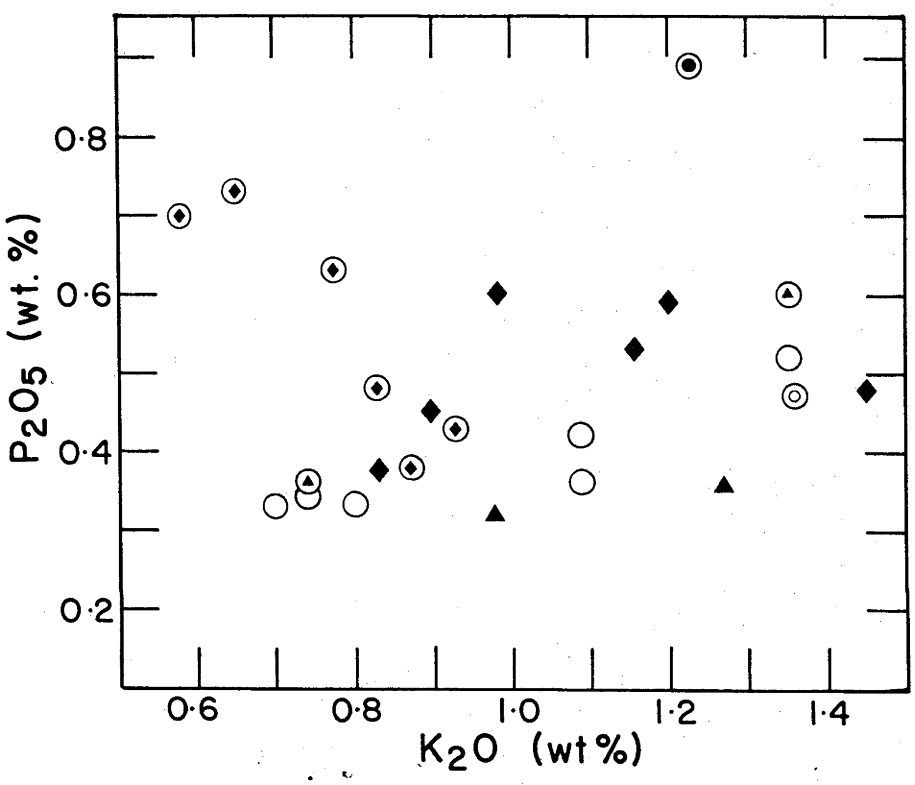

Figure 24. Variation in the abundances of K_2O and P_2O_5 in the 'MMVF' basalts. Lack of any significant correlation of these highly incompatible elements suggests that the abundances of K_2O in the basalts may reflect crustal contamination. Symbols are explained in the caption to Figure 18.

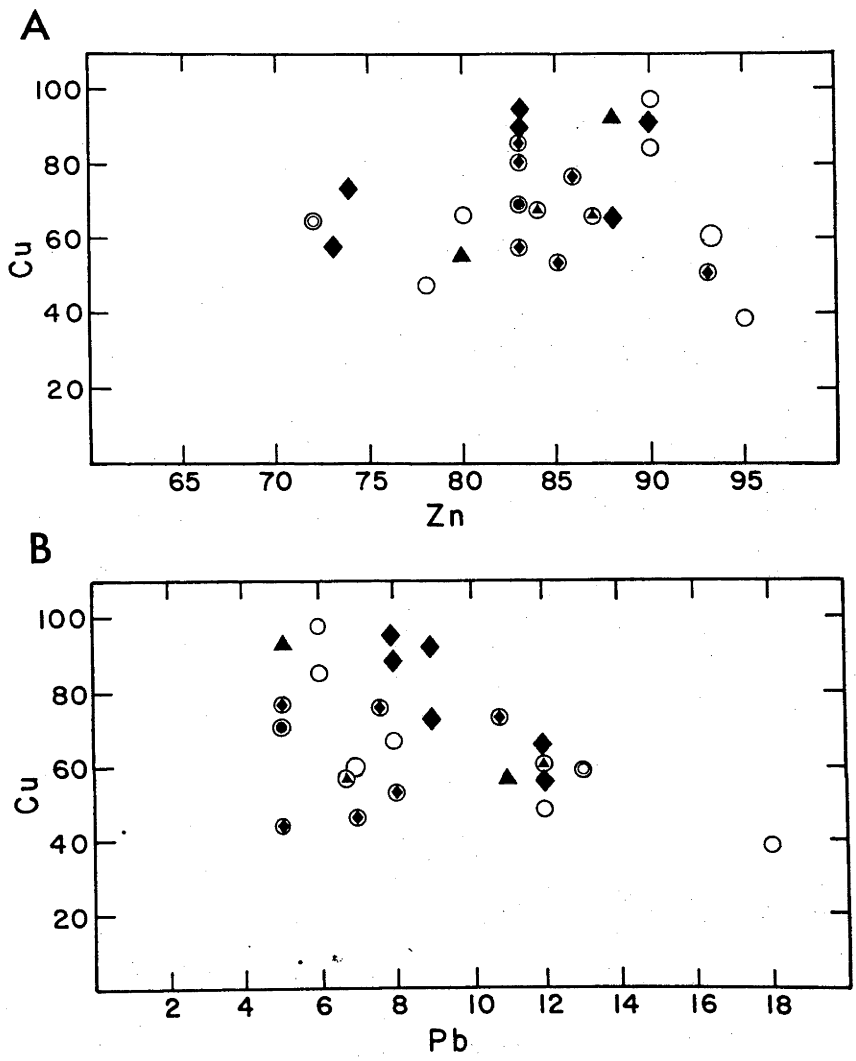

Figure 25. a) Cu vs. Zn and b) Cu vs. Pb abundances in 'MMVF' basalts. The 'scatter' in these diagrams precludes the existence of a fractionating sulphide phase.

sequence of Cr-spinel, olivine and clinopyroxene controlled the petrogenetic evolution of this suite. These deductions are supported by the relative appearances and abundances of these phases as phenocrysts in the basalts themselves. The variability in compatible element abundances amongst the basalts reflect possibly slight differences either in source chemistry, melting mode or crystallization histories. Three basalts, all of high-Al affinities, possess extremely low abundances of all of the compatible trace elements. These basalts must represent the final products of quite extensive fractionation.

In detail, the combined effects of spinel, olivine and clinopyroxene are observed best with respect to Cr and Ni (Fig. 26a). The distinctive break in slope of the fractionation trend, is due to the initiation of clinopyroxene crystallization. The extremely high K_D's of Ni and Cr for olivine and spinel respectively, combined with even slight degrees of fractionation, can account for the observed three- to fourfold drop in the concentrations of these elements (e.g. Sato, 1977), prior to clinopyroxene appearance.

The appearance of clinopyroxene, and its control on the geochemical evolution of the magma, is even more apparent when the behaviour of Sc is considered. As suggested by experimental partitioning data (Irving, 1978), Sc is compatible only in clinopyroxene, a fact borne out by a plot of Sc vs. V (Fig. 26b) (arrows indicate relative directions of magma evolution due to subtraction of olivine, spinel and clinopyroxene). It is more difficult, however, to separate the results of clinopyroxene and spinel fractionation in the histories of Cr and V. Sc vs. Cr and V vs. Ni (Fig. 26c,d) suggest that although spinel was extremely important in the initial stages of fractionation, it is replaced by clinopyroxene. Again, this is apparent when the petrography and phase chemistry of the basalts are examined (i.e. the hiatus in spinel compositions).

Quantitative Assessment - A cursory examination of the petrography and geochemistry of the Mormon Mountain basalts suggest that, in addition to partial melting processes, the diversity of magma compositions is created by fractional crystallization. As noted previously, only olivine, clinopyroxene and spinel occur as phenocryst phases in the majority of the basalts, with plagioclase being restricted to high-Al varieties. Discrimination of alkaline and sub-alkaline basalts can be made not only on a geochemical basis, but also by their respective clinopyroxene compostional trends. Clinopyroxenes of

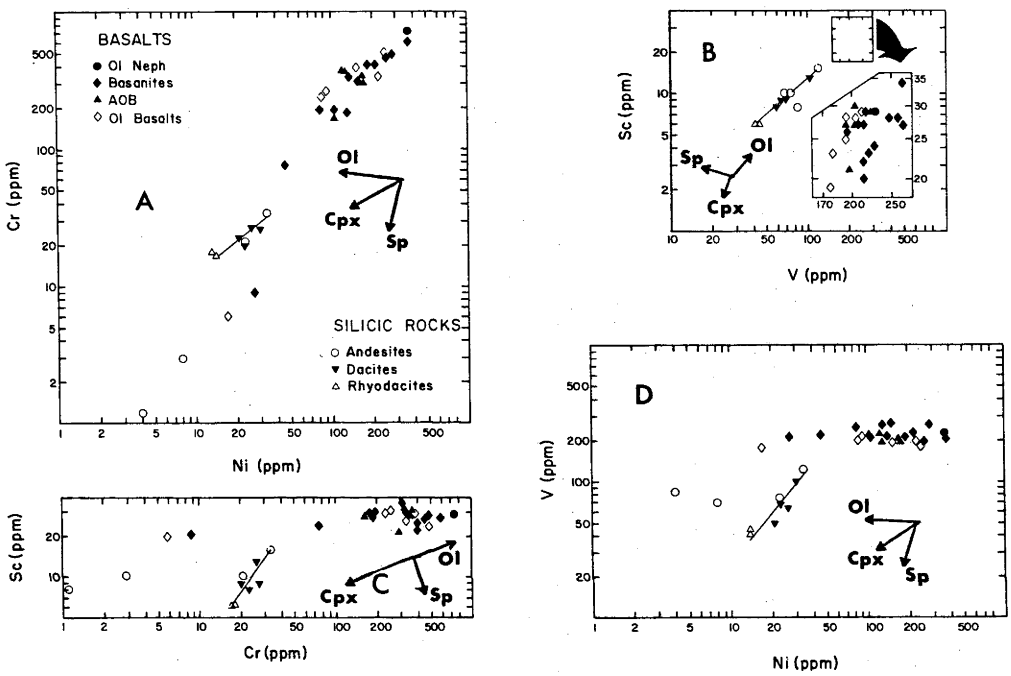

Figure 26. a) Cr vs. Ni, b) Sc vs. V, c) Sc vs. Cr, and d) V vs. Ni abundances in 'MMVF' basalts. Arrows indicate qualitatively, fractionation trends of olivine, clinopyroxene, and spinel. The abundances of these highly compatible elements in the 'MMVF' basalts are controlled by a combination of these fractionating phases.

highly alkaline magmas (basanites) evolve toward high Ti and Al contents while sub-alkaline magmas (olivine tholeiites) exhibit Ti- and Al-poor augitic trends. Mildly alkaline magmas produce crystallization trends intermediate between the two. Fractional crystallization models must take these characteristics into consideration.

Experimental studies on the liquidus and sub-liquidus phase relations of a variey of basalts (Yoder and Tilley, 1962) have established the existance of a low-pressure thermal divide between alkaline and sub-alkaline compositions. Fractional crystallization of alkaline to sub-alkaline compositions (or vice versa), because of this divide, is not generally possible. This barrier may be circumvented however, by the fractional crystallization of amphibole from alkaline lavas (Arculus, 1976; Cawthorn et al., 1973). No evidence of amphibole fractionation is present in any of the Mormon Mountain basalts, hence this possibility is eliminated.

Quantitative fractional crystallization models for the major elements are derived for several parent/daughter pairs from least squares petrologic mixing calculations (computer program 'PETMIX') (Wright and Doherty, 1970). The criteria of geographic proximity, mineralogic and geochemical continuity and low $\Sigma(\text{residuals})^2$ are fulfilled by each successful model. The results of these calculations (Table 8) suggest that it is possible to derive, by small degrees of fractional crystallization of olivine, clinopyroxene and spinel from 'parental' alkaline and sub-alkaline basalts, the range of basanite, alkali olivine basalt and olivine tholeiite compositions observed in the Mormon Mountain field. Plagioclase (+ magnetite) fractionation is important only in the derivation of high-Al olivine basalt.

The absence of plagioclase as a phenocryst phase in the majority of these basalts provides some insight on their eruptive process. Experimental studies on alkali olivine basalts under anhydrous conditions, establish that plagioclase ± olivine are on the liquidus at pressures less than 7 kbar (Green and Ringwood, 1967; Takahashi, 1980), being replaced at higher pressures by clinopyroxene ± olivine. These results, applied to the petrogenesis of the Mormon Mountain basalts, suggest that fractional crystallization occurred only at pressures >7 kbar and that eruption from that depth must have been extremely rapid to prevent plagioclase crystallization.

Rayleigh fractionation calculations (Minster et al., 1977) for a number of trace elements (Table 9) using the 'PETMIX' models, do not

TABLE 8. Summary of Successful Least-squares Models for Basaltic Fractionation, 'MMVF'

Code #	Parent	Daughter	R	Daughter	Solution (%) 01	Cpx	Sp	Mt	Plag	Total	Comments
	SUBALKALINE		BASALTS								
B1	MMT-23	MMT-10	.1704	92.05	3.76	4.53	-	-	-	100.34	Low Alkalis
B2	MMT-23	MMT-10	.1647	88.30	4.16	5.88	-	-	2.06	100.40	Low Alkalis
B3	MMT-23	MMT-10	.2491	91.57	2.72	5.60	1.53	-	-	101.41	Low Alkalis
B4	MMT-10	MMT-5	.1428	69.71	3.69	17.19	-	1.61	7.43	99.63	Low Ti
B5	MMT-10	MMT-5	.2455	78.95	0.20	17.22	5.32	-	-	101.69	High Alkalis, Low Ti
	ALKALINE		BASALTS								
B6	MMT-19	MMT-14	.3779	73.33	11.06	11.20	5.46	-	-	101.05	Low Ti, High Al
B7	MMT-19	MMT-11	.0985	70.00	14.24	13.18	3.65	-	-	101.09	Low Ti
B8	MMT-19	MMT-20	.1476	67.81	15.91	14.71	1.88	-	-	100.32	Low Ti

TABLE 9. Results of Rayleigh Fractionation Using Successful Least-squares Models (Table A7-8) for Basaltic Fractionation, 'MMVF'.

	Rayleigh Fractionation Results								Partition Coefficients [1]				
Code #	B1	B2	B3	B4	B5	B6	B7	B8	Ol	Cpx	Sp	Plg	Mt
Rb	10.8	11.3	10.9	14.3	7.6	15.0	15.6	16.2	.0098	.015	.001	.02	.001
Pb	7.6	7.9	7.6	10.0	7.6	6.8	7.1	7.4	.0098	.015	.001	.02	.001
Ba	532	551	534	685	809	653	683	705	.005	.013	.001	.25	.001
Sr	586	584	586	643	700	765	800	822	.003	.12	.001	1.83	.001
K	7213	7485	7249	9350	7357	9835	10300	10630	.0068	.0014	.001	.2	.001
Zr	133	138	133	171	137	160	167	172	.01	.12	.1	.01	.1
Nb	26	27.1	26	34	28.1	37	39	40.7	.01	.02	.4	.01	.4
La(Ce)	26	26.9	26	33	32	30.7	32	33	.013	.13	.03	.06	.2
Y	22.3	23.0	22.3	25.7	23.0	24.1	25.0	25.6	.01	.5	.1	.03	.2
Ni	124	71.6	84	45	53	48	31	23.5	14	2.0	6	.04	20
Cr	388	362	92	52	>1	1.3	9.0	60	.9	1.6	100	.01	100
V	196	139	86.5	36	8	10.7	19.1	34.3	.04	7.5	38	.01	25
Sc	28.8	27.4	28.4	26.8	27	29	28.8	28.5	.37	1.5	.048	.017	2

[1] Partition coefficients from Arth and Hanson (1975) and Irving (1978)

sucessfully reproduce the trace element characteristics of the derived basalts. In general, these calculations suggest that these derivative magmas are enriched in the highly incompatible elements (Rb, Pb, Ba, Sr, K, Nb, La) beyond that predicted by fractional crystallization. These effects vary only slightly using the range of partition coefficients available, suggesting that they are the result of some other igneous process, perhaps crustal contamination. Similar calculations using the compatible elements Ni, Cr, Sc and V, produce erratic results due to the variability of partition coefficients and are not considered here.

PETROGENETIC SUMMARY

In summary, the basalts of 'MMVF' are the result of a number of processes. Small to moderate degrees of partial melting of a garnet peridotite source enriched in incompatible elements produced a broad range of alkaline to sub-alkaline basaltic magmas. Some of these magmas were erupted sufficiently rapidly without extensive fractionation of olivine. These magmas are represented by the primary basalts of 'MMVF'. Other basaltic magmas were compromised to a greater extent by olivine, clinopyroxene and spinel fractionation. Plagioclase is important only in the petrogenesis of minor high-Al basalts. The geochemical effects of fractionation are partly obscured by contamination of the basalts with crustal material. This contamination is most evident in the abundances of the highly incompatible elements.

REFERENCES - APPENDIX 7

Arculus, R.J. (1976) Geology and geochemistry of the alkali basalt-andesite association of Grenada, Lesser Antilles island arc. Geol. Soc. Am. Bull., 87, 612-624.

Arima, M. and Edgar, A.D. (1980) Stability of wadeite ($Zr_2K_4Si_6O_{18}$) under upper mantle conditions: petrological implications. Contrib. Mineral. Petrol., 72, 191-195.

Best, M.G. (1975) Migration of hydrous fluids in upper mantle and potassium variation in calc-alkalic rocks. Geology, 3, 429-432.

Best, M.G. and Brimhall, W.H. (1974) Late Cenozoic alkalic basaltic magmas in the Western Colorado Plateau and the Basin and Range transition zone, U.S.A. and their bearing on mantle dynamics. Geol. Soc. Am. Bull., 85, 1677-1690.

Beswick, A.E. and Carmichael, I.S.E. (1978) Constraints on mantle source compositions imposed by phosphorus and the rare-earth elements. Contrib. Mineral. Petrol., 67, 317-330.

Beswick, A.E. and Carmichael, I.S.E. (1980) Critical comment of F.A. Frey, M.F. Roden and A. Zindler--a reply. Contrib. Mineral. Petrol., 75, 175-178.

Boettcher, A.L.; O'Neil, J.R.; Windom, K.E.; Stewart, D.C. and Wilshire, H.G. (1979) Metasomatism of the upper mantle and the genesis of kimberlites and alkali basalts IN The Mantle Sample: Inclusions in Kimberlites and Other Volcanics, A.G.U., Wash., 173-182.

Cawthorn, R.G.; Ford, C.E.; Biggar, G.M.; Bravo, M.S. and Clarke, D.B. (1973) Determination of the liquid composition in experimental samples: discrepancies between microprobe analysis and other methods. Earth and Planet. Sci. Letters, 21, 1-5.

Damon, P.E.; Shafiqullah, M. and Leventhal, J. (1974) K-Ar chronology for the San Francisco volcanic field and rate of erosion of the Little Colorado River, IN Geology of Northern Arizona Part I. Regional Studies. Geol. Soc. Am. Guidebook, Rocky Mt. Section Mtg., 221-235.

Frey, F.H.; Green, D.H. and Roy, S.D. (1978) Integrated models of basalt petrogenesis: a study of quartz tholeiites to olivine melilitites from southeastern Australia utilizing geochemical and experimental petrological data. J. Petrol., 19, 463-513.

Frey, F.A.; Roden, M.F. and Zindler, A. (1980) Constraints on mantle source compositions imposed by phosphorus and the rare-earth elements --Critical comments on the paper by A.E. Beswick and I.S.E. Carmichael. Contrib. Mineral. Petrol., 75, 165-174.

Garcia, M.O. and Jacobson, S.S. (1979) Crystal clots, amphibole fractionation and the evolution of calc-alkaline magmas. Contrib. Mineral. Petrol., 69, 319-327.

Green, D.H. (1969) The origin of basaltic and nephelinitic magmas in the Earth's mantle. Tectonophys., 7, 409-422.

Green, D.H. (1973) Contrasted melting relations in pyrolite upper mantle under mid-ocean ridges, stable crust and island arc environments. Tectonophys., 17, 285-297.

Green, D.H. and Ringwood, A.E. (1967) The genesis of basaltic magmas. Contrib. Mineral. Petrol., 15, 103-190.

Haggerty, S.E. (1976) Opaque mineral oxides in terrestrial igneous rocks IN Oxide Minerals, D. Rumble III (editor), Mineral. Soc. Am., Short Course Notes, 3, Hg-101 - Hg-300.

Hertogen, J. and Gijbels, R. (1976) Calculation of trace element fractionation during partial melting. Geochim. Cosmochim. Acta, 40, 313-322.

Irving, A.J. (1978) A review of experimental studies of crystal/liquid trace element partitioning. Geochim. Cosmochim. Acta, 42, 743-770.

Irving, A.J. and Green, D.H. (1976) Geochemistry and petrogenesis of the Newer basalts of Victoria and South Australia. J. Geol. Soc. Aust., 23, 45-66.

Kesson, S.E. (1973) The primary geochemistry of the Monaro alkaline volcanics, southeastern Australia--evidence for upper mantle heterogeneity. Contrib. Mineral. Petrol., 42, 93-108.

Leeman, W.P. and Rogers, J.J.W. (1970) Late Cenozoic alkali olivine basalts of the Basin and Range province, U.S.A.. Contrib. Mineral. Petrol., 25, 1-24.

McCallum, I.S. and Charette, M.P. (1978) Zr and Nb partition coefficients: implications for the genesis of Mare basalts, KREEP, and sea floor basalts. Geochim. et Cosmochim. Acta, 42, 859-869.

Menzies, M. and Murthy, V.R. (1980) Mantle metasomatism as a precursor to the genesis of alkaline magmas-isotopic evidence. Am. J. Sci., 280-A, 622-638.

Minster, J.F.; Minster, J.B.; Treuil, M. and Allègre, C.J. (1977) Systematic use of trace elements in igneous processes, Part II. Inverse problem of the fractional crystallization process in volcanic suites. Contrib. Mineral. Petrol. 61, 49-77.

Moore, R.B.; Wolfe, E.W. and Ulrich, G.E. (1976) Volcanic rocks of the eastern and northern parts of the San Francisco volcanic field, Arizona. U.S. Geol. Survey Jour. Research, 4, 549-560.

Mysen, B.O. (1979) Trace-element partitioning between garnet peridotite minerals and water-rich vapour: Experimental data from 5 to 30 kbar. Am. Mineral., 64, 274-287.

Norrish, K. and Chappell, B.W. (1977) X-ray fluorescence spectrometry IN Physical Methods of Determinative Mineralogy, Zussman, J. (editor), Academic Press, London, 201-272.

Pearce, J.A. and Cann, J.R. (1973) Tectonic setting of basic volcanic rocks determined using trace element analyses. Earth Planet. Sci. Letters, 19, 290-300.

Peirce, H.W.; Damon, P.E. and Shafiqullah, M. (1979) An Oligocene (?) Colorado Plateau edge in Arizona. Tectonophys., 61, 1-24.

Perfit, M.R.; Gust, D.A.; Bence, A.E.; Arculus, R.J. and Taylor, S.R. (1980) Chemical characteristics of island-arc basalts: implications for mantle sources. Chem. Geol., 30, 227-256.

Ringwood, A.E. (1966) The chemical composition and origin of the Earth IN Advances in Earth Science, Hurley, P.M. (editor) MIT Press, Cambridge, Mass. 287-356.

Sato, H. (1977) Nickel content of basaltic magma: identification of primary magmas and a measure of the degree of olivine fractionation. Lithos, 10, 113-120.

Schwarzer, R.R. and Rogers, J.J.W. (1974) A worldwide comparison of alkali olivine basalts and their differentiation trends. Earth and Planet. Sci. Letters, 23, 286-296.

Seward, T.M. (1971) The distribution of transition elements in the system $CaMgSi_2O_6$ - $Na_2Si_2O_5$ - H_2O at 1000 bars pressure. Chem. Geol. 7= 73-95.

Stoeser, D.B. (1973) Mafic and ultramafic xenoliths of cumulus origin San Francisco volcanic field, Arizona. unpublished Ph. D. Dissertation, Univ. Oregon, 260 p.

Sun, S.-S. (1980) Lead isotopic study of young volcanic rocks from mid-ocean ridges, ocean islands and island arcs. Phil. Trans. R. Soc. Lond. (in press).

Takahashi, E. (1980) Melting relations of an alkali-olivine basalt to 30 kbar, and their bearing on the origin of alkali basalt magmas. Carn. Inst. Wash. Yb. 79, 271-276.

Taylor, S.R. and McLennan, S.M. (1981) The composition and evolution of the continental crust: rare earth element evidence from sedimentary rocks. Phil Trans. R. Soc. Lond. A., 301, 381-399.

Watson, E.B. (1980) Apatite and phosphorus in mantle source regions: an experimental study of apatite/melt equilibria at pressures to 25 kbar. Earth and Planet. Sci. Letters, 51, 322-335.

Wass, S.Y. (1979) Multiple origins of clinopyroxenes in alkali basaltic rocks. Lithos, 12, 115-132.

Wass, Suzanne Y. (1980) Geochemistry and origin of xenolith-bearing and related alkali basaltic rocks from the Southern Highlands, New South Wales, Australia. Amer. J. Sci., 280-A, 639-666.

Wood, D.A. (1979) A variably veined suboceanic upper mantle--Genetic significance for mid-ocean ridge basalts from geochemical evidence. Geology, 7, 499-503.

Wood, D.A.; Joron, J-L.; Treuil, M.; Norry, M. and Tarney, J. (1979) Elemental and Sr isotope variations in basic lavas from Iceland and the surrounding ocean floor. Contrib. Mineral. Petrol., 70, 319-339.

Wright, T.L. and Doherty, P.C. (1970) A linear programming and least-squares computer method for solving petrologic mixing problems. Bull. Geol. Soc. Am., 81, 1995-2008.

Yoder, H.S. and Tilley, C.E. (1962) Origin of basalts: an experimental study of natural and synthetic rock systems. J. Petrol., 3, 342-532.

APPENDIX 8

SUMMARY OF THE PETROLOGY AND GEOCHEMISTRY OF LOWER CRUSTAL NODULES FROM THE COLORADO PLATEAU NEAR WILLIAMS, ARIZONA

A study of a suite of lower crustal nodules from two localities near Williams, Arizona, is currently underway in conjuction with R.J. Arculus. The suite consists of coarse-grained cumulate 'amphibolites', two-pyroxene granulites and assorted 'granitoids'. A summary of the major petrologic features of the nodules examined so far is given in Table A8-1. Tables A8-2 and A8-3 present the major element analyses and trace element analyses respectively of selected samples. The chondrite-normalized rare earth element patterns (determined by spark source mass spectrometry, courtesy of S.R. Taylor and M.R. Perfit) are shown in Figure A8-1. The variety in rare earth abundances, in addition to the variety in major element and other trace element compositions, indicate that the lower crust of the Colorado Plateau is heterogeneous.

The coexistance of clinopyroxene and orthopyroxene in most nodules provides information on the temperatures of their equilibration. These temperatures (Table A8-4) suggest that the lower crust of the Colorado Plateau is relatively hot (880°C - 970°C), considerably above a normal geotherm predicted for continental regions (Clark and Ringwood, 1964).

The coarse-grained cumulate amphibolites possibly are fragments of a basaltic magma which stagnated in the crust and crystallized under hydrous conditions at high pressures. This suggestion is supported, in part, by the cryptic variation observed between the phase chemistry of various nodules. Support for a relatively recent petrogenesis is provided by a young K/Ar date (∿4 m.y.) (T.M. Harrison, analyst) on an amphibole separated from sample SW-1.

TABLE A8-1: Summary of Petrologic Characteristics of Lower Crustal Nodules from Williams, Arizona

Code No.	PLAG	CPX	OPX	OLIV	AMPH	OPAQUE PHASES	GLASS	MISCELLANEOUS PHASES
					TiO_2 Wt. %			
SW-1	AN 66-82	Salite	-	-	4.5	Al-rich Titmt	-	-
SW-2	AN 57-77	Salite	-	-	4.5	Al-rich Titmt	-	-
SW-3	AN 67-79	Salite	-	-	4.0	Sp; Mt; Titmt	-	Sulfide
SW-4	AN 68-87	Salite	-	Fo75	4.6	Sp; Mt; Titmt	-	-
SW-5	AN 29-32	Augite	EN60	-	1.8	Titmt	-	Apatite
SW-6	AN 57-75	Salite	EN75	-	-	Sp	-	-
SW-7	AN 67-79	Salite	EN72	-	-	Sp	-	Sulfide
SW-8	AN 32-38	Salite	EN70	-	5.0	-	-	Apatite
SW-9	AB25OR75	-	-	-	-	Titmt	Rhyolite	Kyanite; Zircon
SW-10	AN 26-38	Augite	EN58	-	-	Mt; Titmt	-	Apatite
SW-11	AN 41-52	Salite	EN65	Fo75	-	Sp; Ilm; Titmt	Basaltic	Sulfide
SW-12	AN 29-33	-	EN55-60	-	-	Mt; Titmt	Rhyolitic	-
SW-13	AN 46-59	Augite	EN70	-	-	Titmt	-	-
NW-2	AN 18-24 AB40OR60	-	-	-	-	Ilm; Mt	Rhyolitic	-
NW-1	An 60-77	Salite	EN73	-	-	Sp	-	-

TABLE A8-2: Major Element Analyses and CIPW Normative Mineralogies of Lower Crustal Nodules from Williams, Arizona

	SW-1	SW-6	SW-10	SW-12	NW-1
SiO_2	41.52	49.57	56.61	64.39	48.77
TiO_2	3.60	0.05	0.71	0.25	0.44
Al_2O_3	17.17	23.12	19.13	18.77	20.59
FeO	11.54	4.98	6.00	4.75	6.90
MgO	10.39	8.55	4.05	2.03	10.30
CaO	12.89	10.67	6.73	4.00	10.56
Na_2O	2.42	2.99	5.84	4.08	2.41
K_2O	0.47	0.06	0.93	1.67	0.11
CIPW-Norm.					
QTZ	-	-	-	19.75	-
OR	2.77	0.35	5.49	9.87	0.65
AB	1.03	25.28	49.34	34.45	20.33
AN	34.53	49.44	23.22	19.81	45.00
NE	10.52	-	-	-	-
DI	23.56	2.77	8.29	-	5.88
HY	-	.5.31	4.04	11.51	9.98
OL	17.98	15.55	6.82	-	15.68
MT	2.79	1.20	1.45	1.15	1.65
IL	6.83	0.09	1.35	0.48	0.83
CO	-	-	-	2.99	-
Mg #[1]	65.4	78.3	58.6	47.3	76.0

[1] FeO adjusted to .85 Σ FeO.

TABLE A8-3: Trace Element Abundances in Granulite Nodules from Williams, Arizona

	SW-6	SW-10	SW-12	NW-1
La	2.08	37.88	17.67	5.14
Ce	3.30	92.24	34.80	9.48
Pr	0.36	11.74	4.00	1.26
Nd	1.48	48.49	14.59	5.21
Sm	0.37	9.00	2.19	1.28
Eu	0.30	2.00	0.67	0.54
Gd	0.33	6.61	1.50	1.25
Tb	-	0.87	0.21	0.21
Dy	-	4.63	1.00	-
Ho	-	0.81	0.17	0.22
Er	0.19	2.04	0.50	0.60
Tm	-	-	-	-
Yb	0.20	2.01	0.52	0.55
Rb	0.5	-	-	-
Ba	95	740	620	110
Sr	-	-	-	-
Cs	0.06	0.04	0.29	0.09
Pb	0.22	5.8	7.50	1.80
U	-	0.25	0.27	0.14
Th	-	0.77	3.04	0.51
Zr	5.5	82.0	79.0	28.0
Hf	0.10	2.45	2.57	0.74
Y	2.05	23.00	6.00	6.00
Nb	1.58	12.70	8.80	5.00

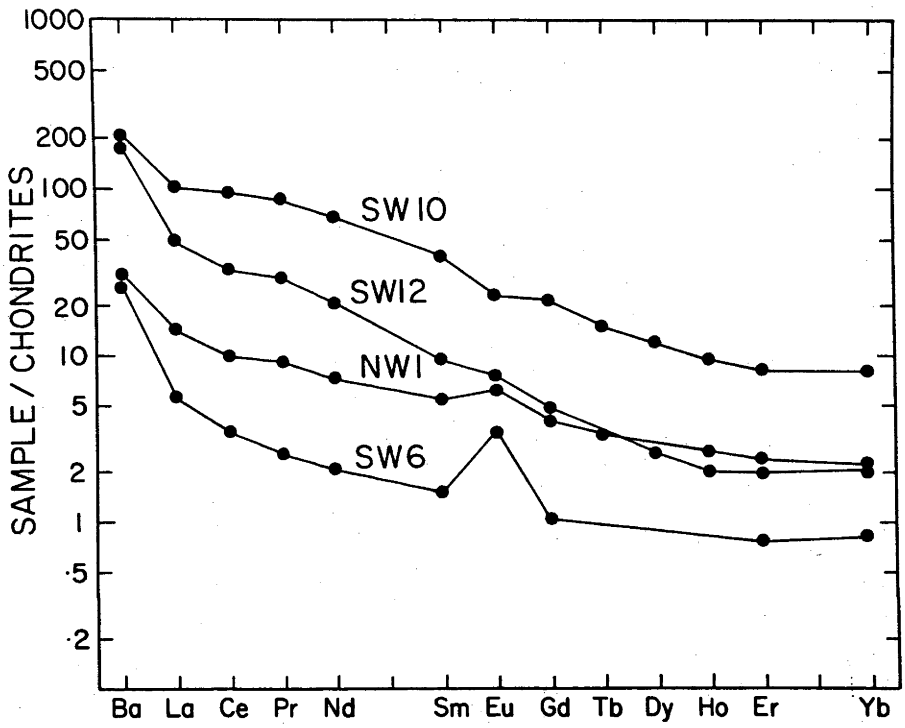

Figure A3 - 1. Chondrite-normalized rare earth abundances of lower crustal nodules from the Colorado Plateau near Williams, Arizona. Normalization values are those of Taylor and Gorton (1977).

TABLE A8-4: Clinopyroxene/Orthopyroxene Geothermometry of Lower Crustal Nodules from Williams, Arizona

Code No.	T, °C (Wood and Banno, 1973)	T, °C (Wells, 1977)
SW-5	867	901
SW-6	913	883
SW-7	910	902
SW-8 (c)	930	943
SW-8 (r)	880	872
SW-10	880	924
SW-13	960	973
NW-1	960	907

c-core; r-rim

REFERENCES

Clark, S.P. and Ringwood, A.E. (1964) Density distribution and constitution of the mantle. Rev. Geophys., 2,35-88.

Taylor, S.R. and Gorton, M.P. (1977) Geochemical application of spark source mass spectrography-III. Element sensitivity, precision, and accuracy. Geochim. Cosmochim. Acta, 41,1375-1380.

Wells, P.R.A. (1977) Pyroxene thermometry in simple and complex systems. Contrib. Mineral. Petrol., 62, 129-139.

Wood, B.J. and Banno, S. (1973) Garnet-orthopyroxene and orthopyroxene-clinopyroxene relationships in simple and complex systems. Contrib. Mineral. Petrol., 42, 109-124.

APPENDIX 9

ABSTRACTS OF JOINT STUDIES ON OTHER ASPECTS OF ARC VOLCANISM

Arculus, R.J. and Gust, D.A. (1981) The intrinsic oxygen fugacity of peridotites from Itinome-gata, Japan and megacryst ilmenite from alnoitic breccia of Malaita, Solomon Islands. IN 1981 IAVCEI Symposium - Arc Volcanism, Abstracts (Japan).

Gust, D.A. and Arculus, R.J. (1979) The origin of the "intraplate" calc-alkaline suite of the San Francisco Peaks - Mormon Mt. volcanics, Arizona : Primary basalt and melted crust? IN Hawaii Symposium on Intraplate Volcanism and Submarine Volcanism, Abstracts (Hawaii).

Perfit, M.R. and Gust, D.A. (1981) Petrochemistry and experimental crystallization of basalt from the Aleutian Islands, Alaska. IN 1981 IAVCEI Symposium - Arc Volcanism, Abstracts (Japan).

The intrinsic oxygen fugacity of peridotites from Itinome-gata, Japan, and megacryst ilmenite from the alnöitic breccia of Malaita, Solomon Islands.

Richard J. Arculus and David A. Gust, Research School of Earth Sciences, Australian National University, Canberra, A.C.T. 2600, Australia.

Introduction: The oxidation state of the upper mantle is an important parameter with respect to conditions of magma genesis, mineral and volatile stabilities as well as the long term evolution of the core and mantle system (Sato, 1972; Arculus and Delano, 1981). Direct measurement of the intrinsic oxygen fugacities (fO_2's) of samples from the upper mantle have been made for a variety of localities (e.g. Australia, W. Germany and the U.S.A.) and all of the results indicate equilibration in the vicinity of the iron-wüstite (IW) buffer. The hypothesis of shallow-level H_2-less seems to be the best explanation for the contrast between the oxidation state prevailing in the upper mantle compared with values determined for erupted basalts and more silicic rocks (Sato, 1972). Some rare magma types characterised by high carbonate content, e.g. kimberlites and alnöites, appear typically to be more oxidized than other basaltic associations. It is important to determine whether these magmas are derived from an oxidized source in the upper mantle. It also appears that island arc volcanics may be consistently, if slightly oxidized with respect to other tectonic environments (i.e. equilibrated at or above the Ni-NiO buffer cf. SiO_2-Fe_2SiO_4-Fe_3O_4 (QFM) for most non-arc basaltic rocks (Haggerty, 1978). This may be due to greater initial H_2O content in island arc basalts and consequent greater relative oxidation attendant on H_2-loss. Alternatively, potential upper-mantle source regions of island arc magmas may be oxidized by metasomatic fluxes released from subducted slabs. In this account, intrinsic fO_2 measurements are reported for samples which may have a bearing on the resolution of some of these problems. Unfortunately, mantle-derived peridotites are not abundant in island arcs being reported only from Japan, Kamchatka and Grenada (Lesser Antilles). Peridotites from Itinome-gata were studied here, together with a megacryst ilmenite from the alnöitic breccia on Malaita in the Solomon Islands. Although the latter occurrence is within an island arc, the source region appears to be the deeper portions of the Ontong Java Plateau (Nixon and Boyd, 1979).

Techniques: The experimental techniques of Sato (1972) and Arculus and Delano (1981) were employed to measure intrinsic fO_2's using oxygen ion-specific electrolytes (stabilized ZrO_2). Pure argon was used as a purge gas in the sample-bearing sensor and this may account for the relatively poor reversibility of one of the peridotite samples. Comparison of the Ar vs. CO_2-CO reversal purging technique (Arculus and Delano, 1981) shows that depending on sample type, slightly more oxidized fO_2 values, and slightly poorer reversal characteristics are experienced with pure Ar. However, the use of Ar speeds the data acquisition considerably. Whole-rock samples were finely ground in an agate ball mill. At no stage during preparation were organic liquids allowed to come into contact with the samples. At any given temperature, the samples were held for up to 50 hours to ensure a stable emf signal and to check for any auto-reduction.

Results: The fO_2 vs. 1/T data for the peridotite and ilmenite samples are displayed in Figure 1. The important points to note are a) the reduced character of the Itinome-gata samples in the vicinity of the IW buffer; b) the spread of fO_2 values at any given T for the peridotites indicative of either a slightly heterogeneous upper mantle in terms of oxidation state, or contrasted histories of alteration following eruption; c) the oxidized state (close to Ni-NiO) of the megacryst ilmenite; d) the absence of any auto-reduction at temperatures >1120°C indicative of the presence of carbon.

Discussion: The fO_2 data indicate that the upper mantle beneath Itinome-gata (N.E. Honshu) is generally similar in terms of oxidation state to that beneath Victoria (S.E. Australia), southern West Germany and the southwestern U.S.A. There is no sign of pervasive oxidation of this portion of the Japanese upper mantle. In addition, there is no prospect that erupted basaltic and andesitic volcanics with oxidation states close to Ni-NiO could be equilibrium melts of such peridotite samples, unless oxidation following separation of the magmas from a peridotite source has occurred.

However, isotopic dissimilarities between host basalts and andesites and included peridotites also preclude a close genetic relationship (Zashu et al., 1980).

The oxidized character of the ilmenite megacryst stands in strong contrast to the peridotite data. The generally accepted hypothesis for the origin of such megacrysts is that they represent high-pressure, equilibrium crystallization products of the host magma. The implication is that the alnöitic host was oxidized at depth (>10 kbar) and not as a result of low-P H_2-loss. There is a possibility that the event that triggered the eruption of the alnöitic host on the margins of the Ontong Java Plateau was, in part, an oxidizing metasomatic flux. The ultimate origin and genesis of such a flux remains obscure.

References

Arculus, R.J. and Delano, J.W. (1981) Geochim. Cosmochim. Acta, in press.
Haggerty, S.E. (1978) Geophys. Res. Lett. 5, 443-446.
Nixon, P.H. and Boyd, F.R. (1979) Proc. 2nd Int. Kimberlite Conf. Amer. Geophys. Union, 304-323.
Sato, M. (1972) Geol. Soc. Am. Mem. 135, 289-307.
Zashu, S. Kaneoka, I., Aoki, K-I (1980) Geochem. J. 14, 123-128.

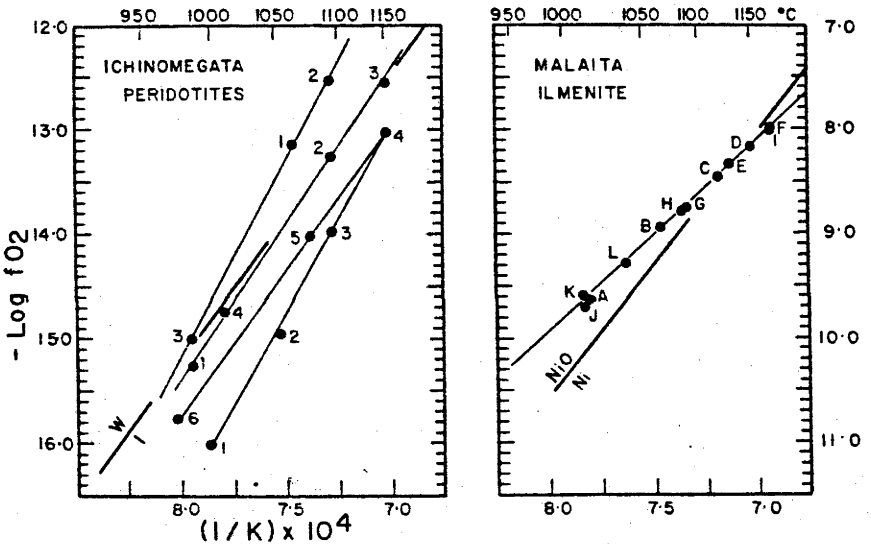

Fig. 1. Variation of fO_2 with respect to T, numbered or lettered in the order in which a specific datum was collected. For the peridotites, sample numbers corresponding to increasingly reduced fO_2 vs. 1/T lines are HK64081210, HK66031501 and HK50061804g.

The origin of the "intraplate" calc-alkaline suite of the San Francisco Peaks - Mormon Mt. volcanics, Arizona: Primary basalt and melted crust?

D.A. Gust and R.J. Arculus, Research School of Earth Sciences, Australian National University, Canberra, A.C.T., 2600, Australia.

The Cenozoic volcanism of the southwestern United States (Basin and Range - Colorado Plateau) is enigmatic and not easily related to a simple tectonic model. Elston (1976) has divided this volcanism into 3 overlapping episodes: 1) an early calc-alkaline phase 2) rhyolitic phase and 3) a late basaltic phase in which calc-alkaline volcanism is rare. Two notable exceptions to this pattern are the Quaternary calc-alkaline centers of Mt. Taylor, New Mexico and San Francisco Peaks - Mormon Mt. (SFP-MM), Arizona. Both volcanic fields occur near the edges of the Colorado Plateau where lower crust thins from ≳ 40 km to 20 km. The absence of subducted lithosphere beneath the SFP-MM area for ≳ the last 15 m.y., the present lack of intermediate and deep earthquakes, and the absence of an offshore trench suggest that the volcanism is not related to Andean or island arc type subduction zone magmatism. We are examining the SFP-MM area, in conjunction with the U.S.G.S., Flagstaff, Arizona, to develop a petrogenetic history for this example of intraplate volcanism.

The volcanic suite of the area is divisible into three distinctive groups: 1) transitional alkalic-tholeiitic basalts 2) calc-alkaline basaltic andesites - rhyodacites and 3) rhyolites. These groups are contemporaneous (L. Miocene - Recent) although the basalts constitute a majority of extruded material. The basalts, generally erupted from structurally controlled fissures, are similar to Basin and Range basalts. Hundreds of cinder cones, some with basalt flows, some with fractionated plugs and some containing ultramafic and crustal xenoliths are scattered through the volcanic field. The basalts range from basanatoid to hypersthene-normative tholeiite with $100Mg/Mg+Fe^{2+}$ from 69 to 55. Olivine and clinopyroxene (with spinel inclusions) are common phenocrysts. Plagioclase-phyric basalts, distinguished by high Al contents, are uncommon. The calc-alkaline suite appears to have little relation to these basalts. Dominantly andesitic, the calc-alkaline centers range from basaltic andesite to rhyodacite. Several sequences of basaltic andesite - rhyodacite are observed in San Francisco Peak. Clinopyroxene, orthopyroxene, oxyhornblende and plagioclase are major phenocryst phases in this group. The rhyolites ($Na \geq K$) occur as domes throughout the field. They have a diversity of mineral phases containing many of the following: ilmenite, magnetite, apatite, plagioclase, alkali feldspar, quartz, fayalite, Mn-rich fayalite, annite, riebeckite, zircon, spinel, rutile and a REE phase (polycrase?). Trace element geochemistry is distinctive from the remainder of the suite.

Tentative petrogenetic interpretations suggest different mechanisms for origin of each group in the suite: a) basalts formed by combination of variable % partial melting of upper mantle (50-70 km depth) plus fractional crystallization b) calc-alkaline suite derived by fractional crystallization of tholeiitic basalts or lower crustal melts c) rhyolites are melts of LIL-enriched lower crust. A high geothermal gradient (cause unknown) is required in this intraplate environment.

PETROCHEMISTRY AND EXPERIMENTAL CRYSTALLIZATION OF BASALTS FROM THE ALEUTIAN ISLANDS, ALASKA

M.R. Perfit and D.A. Gust, Research School of Earth Sciences, Australian National University, Canberra, A.C.T. 2600, Australia.

Volcanic rocks from the Aleutian Islands can be classified as part of the tholeiitic or calcalkaline series on the basis of their relative iron-enrichment trends. Alkalic rocks, such as those erupted on Bogoslof Island behind the main arc, are rare and clearly distinguished by their high K_2O and large ion lithophile element (LIL) abundances. Chemical differences between the three groups are subtle and none can be equated with so-called island arc tholeiites or shoshonites. Furthermore, there are no temporal relationships among the different rock types and both tholeiitic and calcalkaline lavas may be erupted from a single volcanic center. The chemical similarities between groups are exemplified by the comparable chondrite-normalized rare earth element (REE) patterns of basalts from Akutan, Umnak, Segula (all tholeiitic) Unalaska, Kiska (calcalkaline) and Bogoslof (alkaline) (see Fig. 1). Basalts have slightly fractionated REE abundances (La_N/Yb_N = 1.29-5.58) and high ratios of LIL to light-REE (e.g. Ba_N/La_N = 2.97-11.2). Incompatible element ratios (e.g. Zr/Nb, Th/U, Zr/Hf) and isotopic ratios ($^{87}Sr/^{86}Sr$, $^{143}Nd/^{144}Nd$) are similar in basalts from each suite suggesting they were derived from similar sources. In general, more evolved tholeiitic volcanics develop higher Rb/Sr ratios and Ba contents at given K_2O levels compared to calcalkaline rocks. Tholeiites also have higher TiO contents than calcalkaline volcanics at equivalent Mg-numbers.

On Unalaska Island, some of the most primitive calcalkaline basalts (Mg#$\sim$70) contain phenocrysts of magnesian olivine (Fo_{91-81}) and high-Al clinopyroxene. Cr-Al spinels are typically enclosed in olivine and become more iron- and titanium-rich in the groundmass. Xenoliths of wehrlite or gabbro are present in a number of basalts and are believed to represent cognate inclusions. In more differentiated basalts and basaltic andesites the phenocryst assemblage is dominated by calcic plagioclase, clinopyroxene and titanomagnetite with lesser amounts of hypersthene ± olivine. Calculated temperatures of equilibration, based on two-pyroxene geothermometers, suggest that crystallization occurred between 1100° and 990°. Hornblende appears as a phenocryst phase only in some high-silica andesites which may not be genetically related to the basalts.

Tholeiitic basalts on Akutan Island range in composition from slightly nepheline-normative to quartz-normative but all have low K_2O contents (<1.0 wt.%). The most mafic basalts contain abundant phenocrysts of calcic clinopyroxene ($Wo_{47}En_{47}Fs_6$) which have extensive Ca-Tschermak's substitution and commonly enclose aluminous spinels (Fig. 2). Rare pargasitic amphibole relicts are also enclosed in clinopyroxene megacrysts. The phase chemistry of these basalts is similar to that reported in "alkalic" basalts from Kanaga Island in the western Aleutians (DeLong et al. 1975). However, the trace element composition of these basalts is similar to the mafic calcalkaline basalts. More evolved tholeiitic basalts contain phenocrysts of calcic plagioclase, low-Ca clinopyroxene, hypersthene and/or olivine. Amphibole phenocrysts + orthopyroxene occur only in high silica andesites as in the calcalkaline suite.

Least-squares mixing calculations suggest that high-alumina basalts could be derived from the mafic basalts by the fractional crystallization of olivine + clinopyroxene ± spinel. Basaltic andesites are produced by the further crystallization of plagioclase + clinopyroxene ± olivine ± titanomagnetite as the liquid evolves. Rapid depletions in Cr and Ni contents with falling CaO/Al_2O_3 and Mg-number attest to the strong olivine + clinopyroxene ± spinel control on the liquid line of descent. Higher TiO_2 contents and greater iron enrichment in tholeiites compared to calcalkaline basalts is due to the late crystallization of titanomagnetite in the tholeiitic series. This may be due to relatively lower partial pressure of oxygen in tholeiitic centers.

Experimental crystallization of a high-Mg basalt (MgO = 9.64) in graphite capsules have been carried out under dry conditions between 1 atm and 20 kb. The results indicate that olivine ± Al-spinel are the liquidus phases below 12 kb. At sub-liquidus

temperatures plagioclase + clinopyroxene crystallize after olivine and the near solidus assemblage is clinopyroxene + orthopyroxene + plagioclase. Above 12 kb clinopyroxene is the liquidus phase followed by plagioclase and finally orthopyroxene. Low fO_2 conditions probably inhibited the crystallization of titanomagnetite at any temperature or pressure. The observed phenocryst relations, and chemical trends in Aleutian basalts are in agreement with experimental crystallization trends between 5 and 12 kb. The fractionation of predominantly olivine and clinopyroxene from mafic parental basalts in crustal magma chambers is a viable mechanism for producing the voluminous high-alumina basalts and basaltic andesites in the Aleutian Islands.

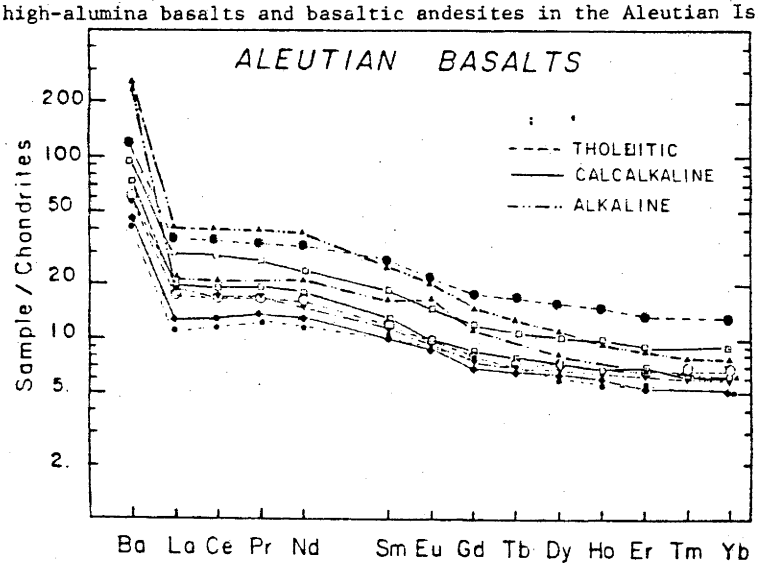

Fig. 1.

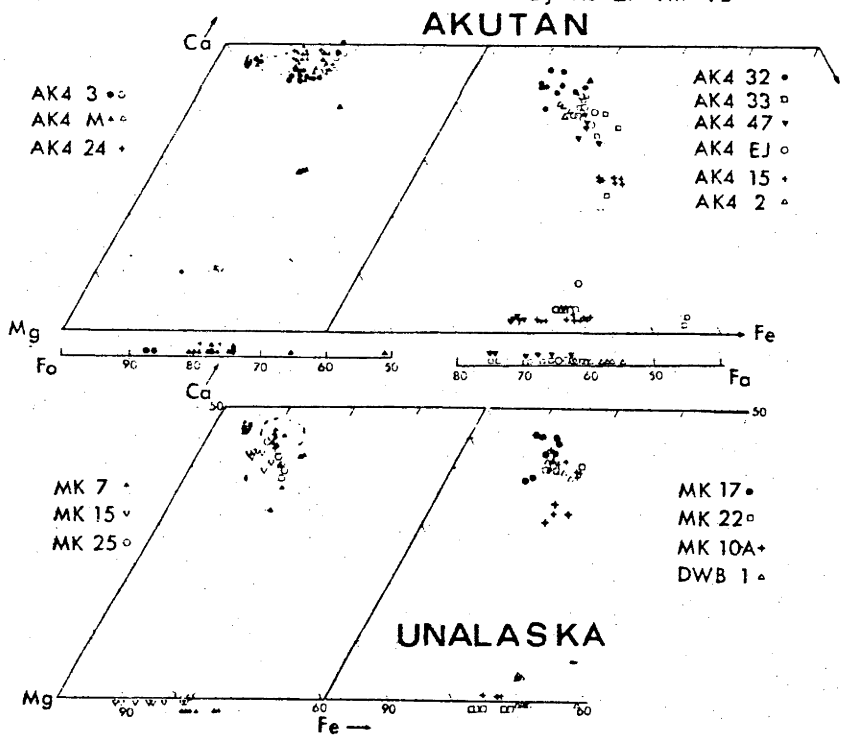

Fig. 2.